E301937 (12)

DNA-1948H-Rev 9

AD-A165 923

DEFENSE NUCLEAR AGENCY REACTION RATE HANDBOOK SECOND EDITION

Revision No. 9

Editors-in-Chief:

Dr. M.H. Bortner

Dr. T. Baurer

9 June 1983

Project Officer: Peter W. Lunn

Approved for public release; distribution is unlimited.

THIS WORK WAS SPONSORED BY THE DEFENSE NUCLEAR AGENCY UNDER RDT&E RMSS CODE B337083466 P99QAXDC00010 H2590D.

Prepared by DASIAC
DoD Nuclear Information and Analysis Center
Kaman Tempo
Santa Barbara, California

Under:
CONTRACT No. DNA 001-82-C-0274

UNCLASSIFIED
SECURITY CLASSIFICATION OF THIS PAGE

AD-A165923

REPORT DOCUMENTATION PAGE

Form Approved
OMB No. 0704-0188
Exp. Date: Jun 30, 1986

1a. REPORT SECURITY CLASSIFICATION UNCLASSIFIED	1b. RESTRICTIVE MARKINGS
2a. SECURITY CLASSIFICATION AUTHORITY	3. DISTRIBUTION/AVAILABILITY OF REPORT Approved for public release; distribution is unlimited.
2b. DECLASSIFICATION/DOWNGRADING SCHEDULE N/A since UNCLASSIFIED	
4. PERFORMING ORGANIZATION REPORT NUMBER(S)	5. MONITORING ORGANIZATION REPORT NUMBER(S) DNA-1948H-Rev 9
6a. NAME OF PERFORMING ORGANIZATION Kaman Tempo-DASIAC 6b. OFFICE SYMBOL (If applicable)	7a. NAME OF MONITORING ORGANIZATION Director Defense Nuclear Agency
6c. ADDRESS (City, State, and ZIP Code) 816 State Street (Drawer QQ) Santa Barbara, CA 93101-3207	7b. ADDRESS (City, State, and ZIP Code) Washington, DC 20305-1000
8a. NAME OF FUNDING/SPONSORING ORGANIZATION 8b. OFFICE SYMBOL (If applicable)	9. PROCUREMENT INSTRUMENT IDENTIFICATION NUMBER DNA 001-82-C-0274
8c. ADDRESS (City, State, and ZIP Code)	10. SOURCE OF FUNDING NUMBERS

PROGRAM ELEMENT NO	PROJECT NO	TASK NO	WORK UNIT ACCESSION NO.
62715H	P99QAXD	C	DH006635

11. TITLE (Include Security Classification)
DEFENSE NUCLEAR AGENCY REACTION RATE HANDBOOK, SECOND EDITION, REVISION No. C.

12. PERSONAL AUTHOR(S)
T. Baurer and M.H. Bortner (Eds)

13a. TYPE OF REPORT	13b. TIME COVERED	14. DATE OF REPORT (Year, Month, Day)	15. PAGE COUNT
Handbook	FROM 830301 TO 830601	1983, June 9	210

16. SUPPLEMENTARY NOTATION
This work was sponsored by the Defense Nuclear Agency under RDT&E RMSS Code B337083466 P99QAXDC00010 H2590D.

17. COSATI CODES			18. SUBJECT TERMS (Continue on reverse if necessary and identify by block number)	
FIELD	GROUP	SUB-GROUP		
4	1		Atmospheric Chemistry	Electromagnetic Propagation
20	14		Atmospheric Physics	Photoionization
			Atomic and Molecular Collisions	Photodetachment

19. ABSTRACT (Continue on reverse if necessary and identify by block number)

The 26 chapters of this handbook are concerned with atmospheric and ionospheric physical and chemical processes under both natural and disturbed conditions and the effects of disturbances on electromagnetic transmission. Topics covered are the structure, fluid mechanics and aeronomy, and ionospheric energy balance of the natural atmosphere; chemical kinetics of the naturally and nuclear perturbed atmosphere; data gathering methods based on laboratory experimentation, theoretical analysis, and atmospheric measurements; basic energy-level and equilibrium data; infrared kinetics of atmospheric radiative processes; cross-section data, solar photoionization rate constants, ultraviolet intensities, and solar dissociation of photochemical processes; low-energy electron and high-energy heavy-particle collision kinetics; charged particle recombination processes; electron attachment-detachment processes; thermal and non thermal ion-neutral reactions; excitation-deexitation processes; radiofrequency absorption; and computer modeling of deionization processes. Each chapter contains numerous references.

20. DISTRIBUTION/AVAILABILITY OF ABSTRACT	21. ABSTRACT SECURITY CLASSIFICATION
☐ UNCLASSIFIED/UNLIMITED ☒ SAME AS RPT ☐ DTIC USERS	UNCLASSIFIED

22a. NAME OF RESPONSIBLE INDIVIDUAL	22b. TELEPHONE (Include Area Code)	22c. OFFICE SYMBOL
Betty L. Fox	(202) 325-7042	STTI

DD FORM 1473, 84 MAR — 83 APR edition may be used until exhausted. All other editions are obsolete.

SECURITY CLASSIFICATION OF THIS PAGE
UNCLASSIFIED

18. SUBJECT TERMS (Continued)

Nuclear Atmospheric Effects
Atmospheric Reaction Rates
Radiative Processes
Atmospheric Dissociative Recombination
Ionospheric Disturbances

DNA 1948H
Rev 9

MEMORANDUM

To: All Recipients of the DNA Reaction Rate Handbook (DNA 1948H)

From: The Editors

Subject: Revision Number 9

Enclosed herewith you will find a copy of Revision Number 9 to the Handbook. It comprises completely revised and updated versions of the Title Page, DD Form 1473, Table of Contents, List of Illustrations, List of Tables, and Chapters 11 and 20 as well as the addition of Chapter 13B.

You should immediately discard the previous versions of Pages xv through xxxvi and Chapters 11 and 20 and replace them with the enclosed, and add Chapter 13B. Pen and ink changes should be made to the existing Chapter 13 to redesignate it as Chapter 13A. You should also enter on page iii in front of your Handbook the following information: Revision Number 9; Date of Issue - June 1983; Date of Receipt - whatever day you receive this; and sign your name in the last column.

TABLE OF CONTENTS

GROUP D -- CHAPTERS ON DATA APPLICATION

THIS PAGE IS INTENTIONALLY LEFT BLANK.

LIST OF ILLUSTRATIONS

THIS PAGE IS INTENTIONALLY LEFT BLANK.

LIST OF TABLES

THIS PAGE IS INTENTIONALLY LEFT BLANK.

11. THE KINETICS OF ATMOSPHERIC RADIATIVE PROCESSES IN THE INFRARED

J.P. Kennealy and F.P. Del Greco, Air Force Cambridge Research Laboratories (Latest Revision June 1983, T.L. Stephens, Ed., Physical Research, Inc.).

11.1 INTRODUCTION

In the normal atmosphere, stable molecular species such as water vapor, ozone, carbon dioxide and nitrous oxide are recognized sources of infrared radiation. Figure 11-1 (Reference 11-1) is a composite emission spectrum of the atmosphere obtained looking vertically from an aircraft at an altitude above most of the water vapor. In disturbed atmospheres, wide ranging and persistent perturbations of the infrared radiation from naturally occurring species are to be expected. If the perturbing source is a nuclear detonation, the new species generated by weapon/air interactions may also give rise to radiation as shown in Figures 11-2 and 11-3 (Reference 11-2).

The radiation shown in Figure 11-1 arises because infrared active molecules are held in local thermodynamic equilibrium (LTE) at low altitudes in the atmosphere; the features are seen as emission against the cold, black background of space. Figures 11-4 and 11-5 (Reference 11-3) are the complementary view from space where the earth's black body radiance is modified by the absorption/emission of the intervening atmosphere at a lower temperature. Interpretation of spectra such as these is an active field of research, including the remote sounding of the atmospheric composition and altitude profiles by rocket probes and satellites. Just as the atmosphere obscures the earth in Figures 11-4 and 11-5, it can also reduce the visibility of an objector phenomenon of interest. It is not sufficient to treat the atmosphere as an LTE radiator; nonequilibrium radiation generated high in the atmosphere must be accounted for. Subsequent sections of this chapter will discuss the important mechanisms of vibrational excitation, both collisional and radiative, which give rise to the vibration-rotation IR emissions in the atmosphere.

11.2 THERMAL RADIATION PROCESSES

The LTE radiation shown in Figure 11-1 arises from the thermal or collisional excitation of infrared active molecules. In LTE, the emission from the atmosphere is quantitatively related to the absorptivity of the atmospheric gases. According to the Kirchoff radiation law, the spectral radiance of an isothermal column of gas at temperature T is

$$N_\lambda = A_\lambda B_\lambda(T) \quad (W\ cm^{-2} sr^{-1} \mu m^{-1}) \qquad (11\text{-}1)$$

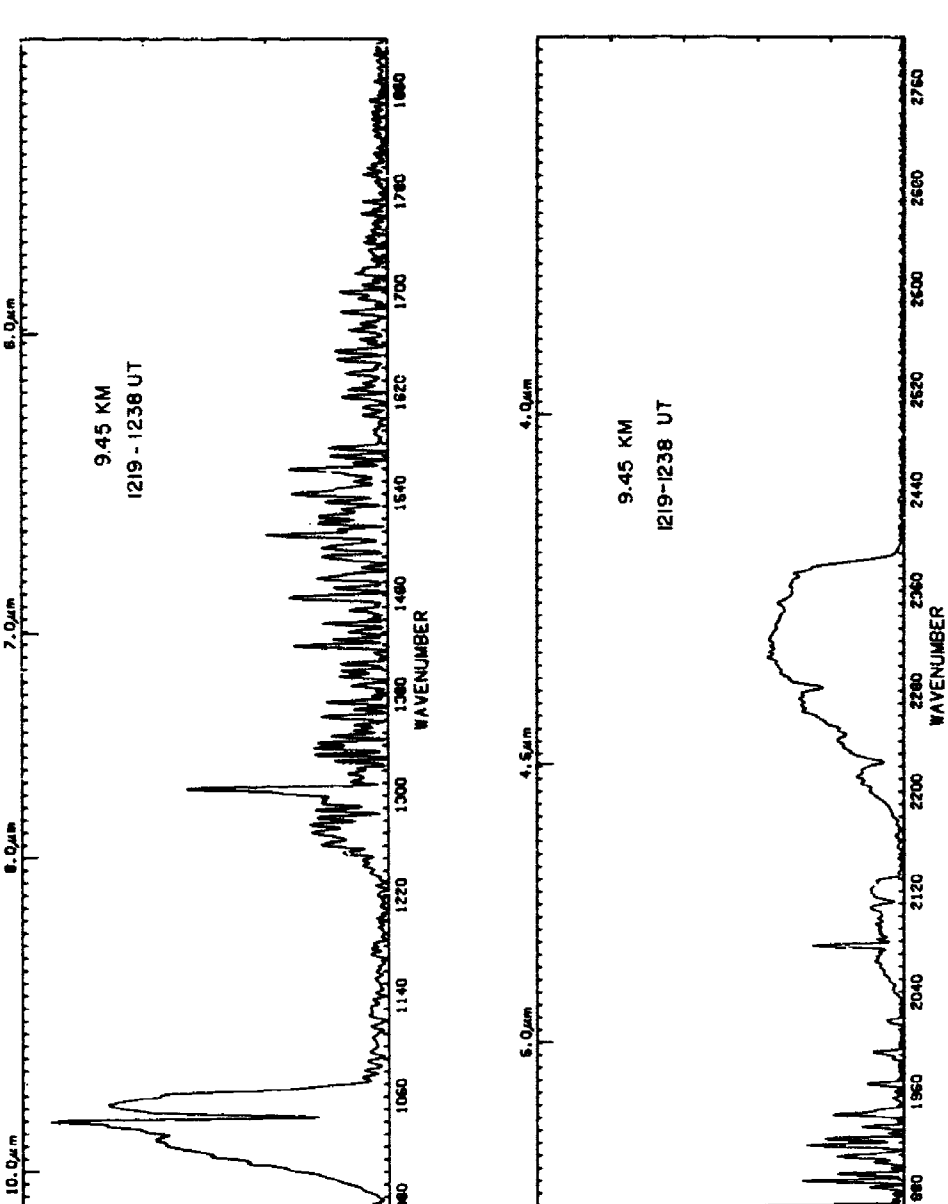

Figure 11-1. Normal airglow spectrum obtained near Hawaii, 19 April 1970 (Reference 11-1).

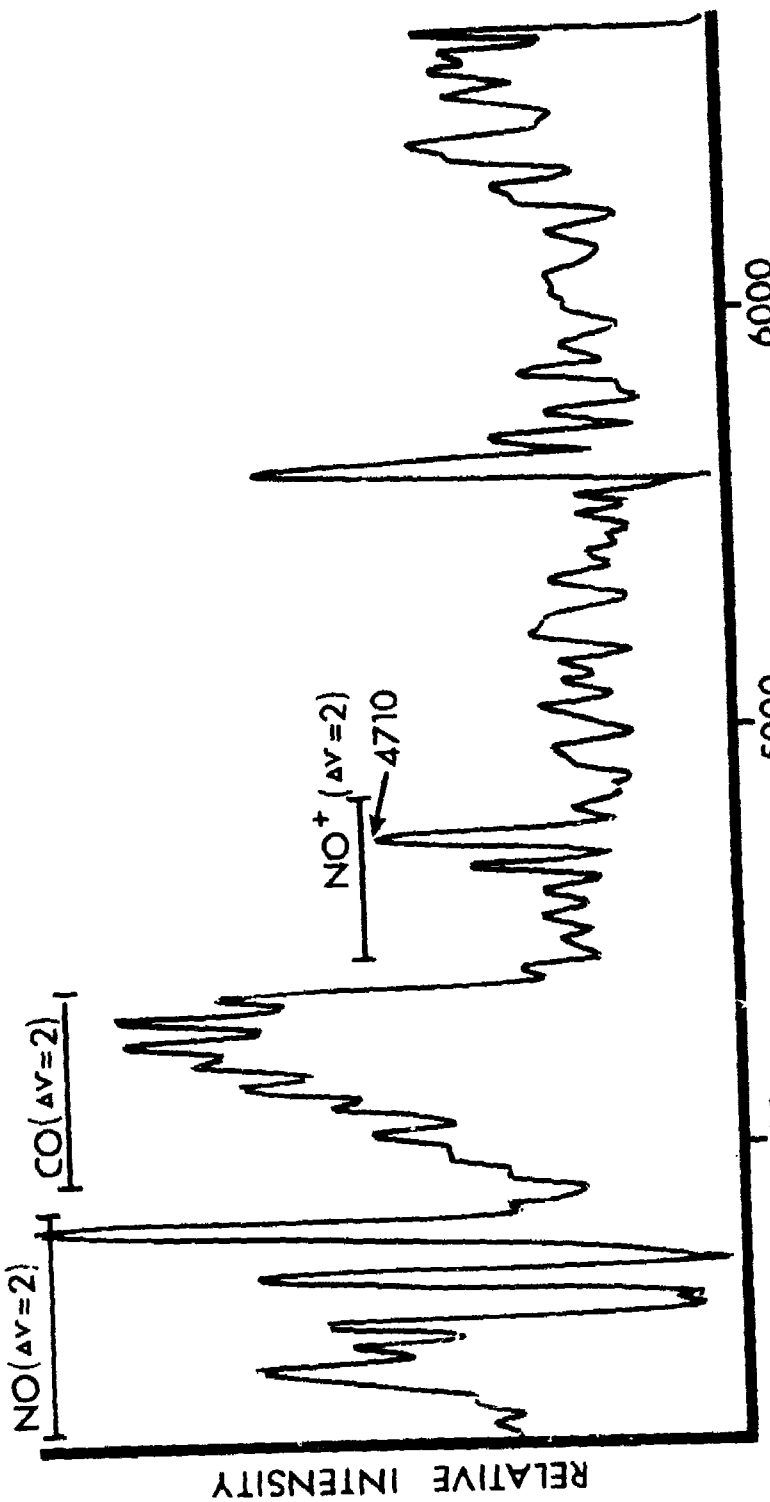

Figure 11-2. Infrared spectrum of a high-altitude nuclear detonation in the 1.5-3 micron region (Reference 11-2).

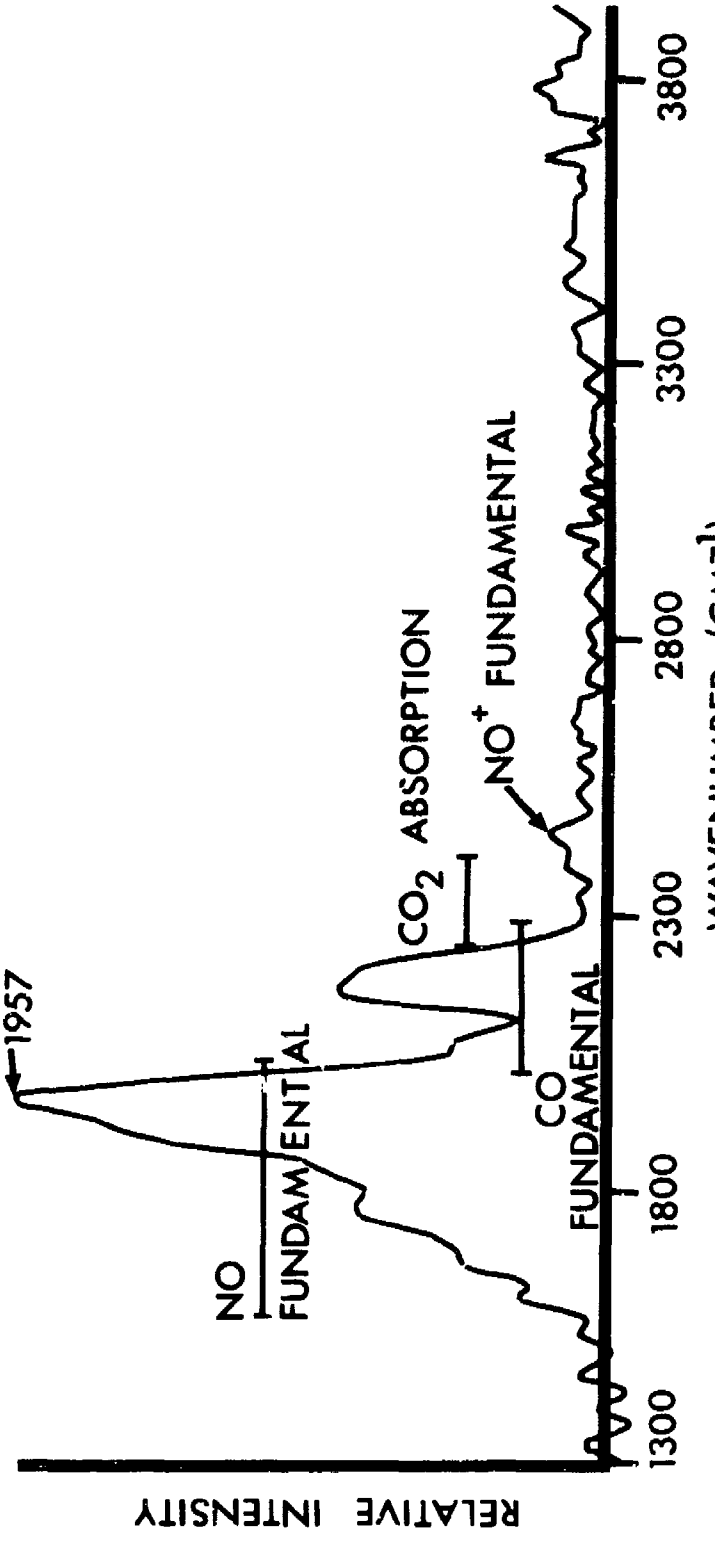

Figure 11-3. Infrared spectrum of a high-altitude nuclear detonation in the 3-6 micron region (Reference 11-2).

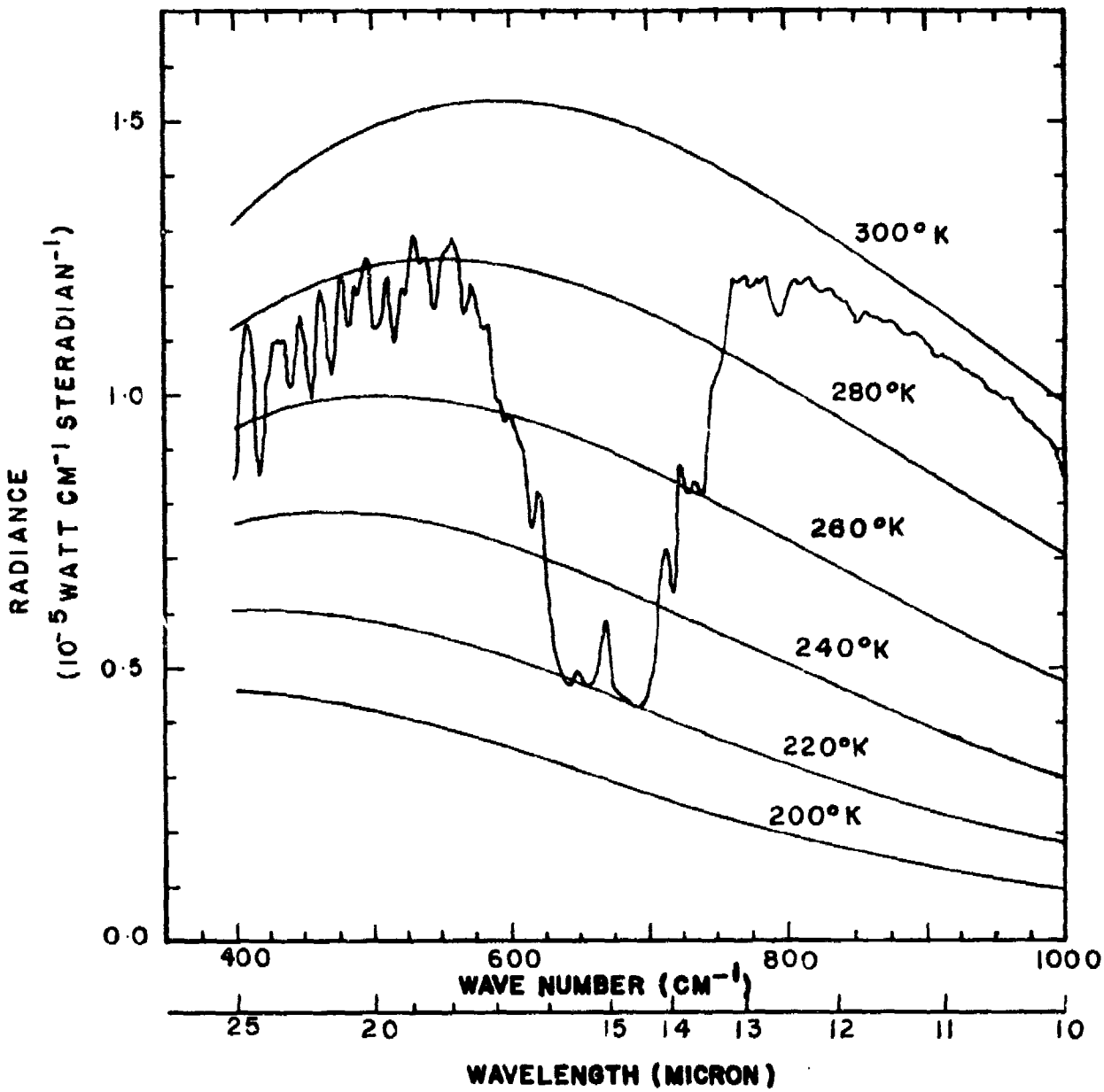

Figure 11-4. Earthshine in the 400-1000 cm^{-1} region (Reference 11-3).

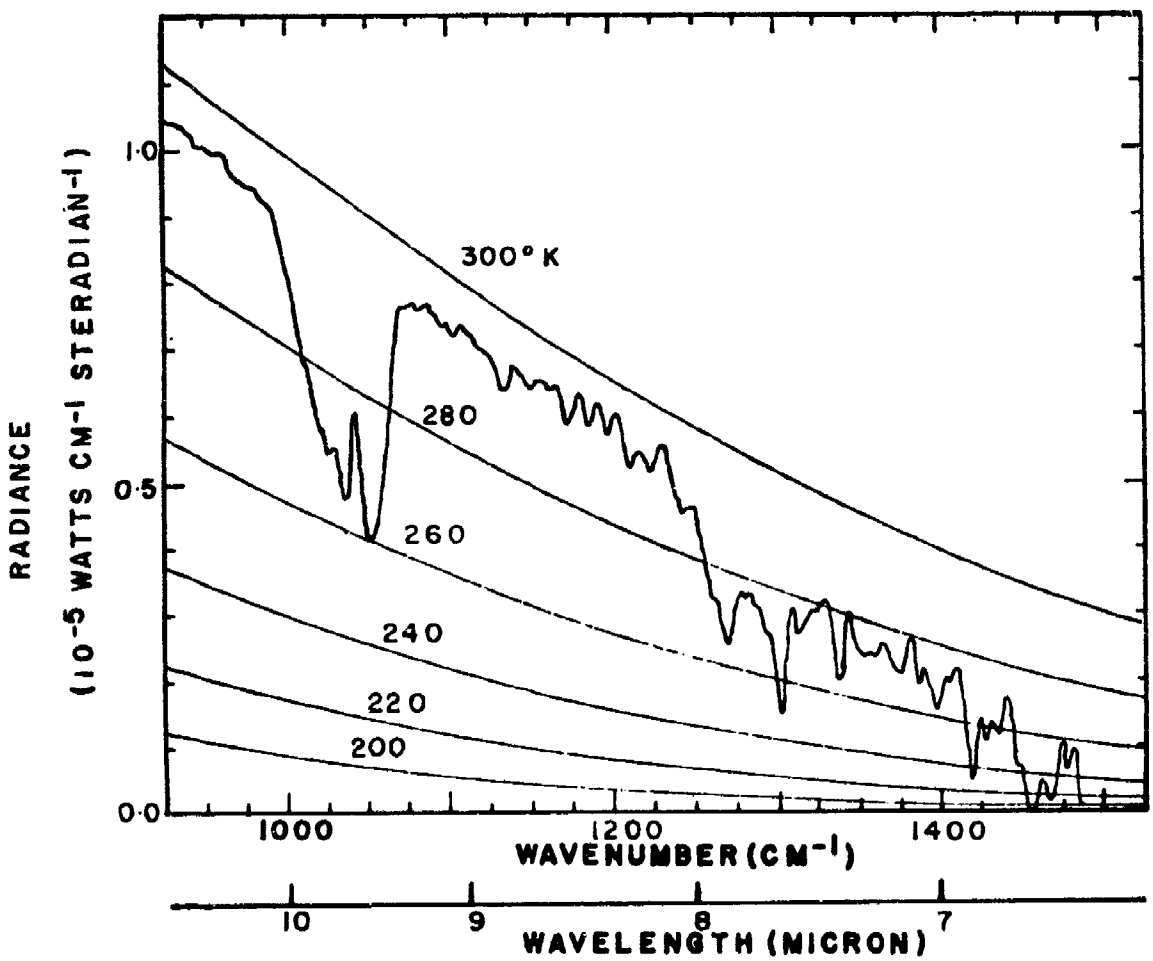

Figure 11-5. Earthshine in the 1000-1450 cm-1 region (Reference 11-3).

where

A_λ = the absorption of the column of gas at wavelength λ

$B_\lambda(T)$ = the Planck blackbody spectral emission function at temperature T and wavelength λ.

Infrared molecular absorption bands are composed of hundreds of individual absorption lines, each associated with the transition of the absorbing molecule between a pair of vibration-rotation levels.

The absorption coefficient $k(\nu)$ which describes the attenuation of a beam of light by an individual absorption line has a maximum at the central wavenumber ν_o and decreases as the distance from line center increases. If $k_\ell(\nu_o)$ is the absorption coefficient at line center, the absorption coefficient at some other wave number ν is, for Lorentz-shaped lines (typical of atmospheric gases at low altitudes):

$$k_\ell(\nu) = \frac{S_\ell \gamma_L}{\pi\,(\nu-\nu_o)^2 + \gamma_L^2} = \frac{k_\ell(\nu_o)\gamma_L^2}{\left[(\nu-\nu_o^2 + \gamma_L^2)\right]} \quad . \tag{11-2}$$

and for Doppler-shaped lines (typical of altitudes above about 30 km:

$$k_\ell(\nu) = \frac{S_\ell}{\gamma_D}\,\frac{\sqrt{\ell n 2}}{\pi}\,\exp\left[-\left(\frac{\nu-\nu_o}{\gamma_D}\right)^2 \ell n 2\right] \quad . \tag{11-3}$$

In these expressions, S_ℓ is the integrated line strength, which is expressed in units of wave numbers and is given by

$$S_\ell = \int_{-\infty}^{\infty} k_\ell(\nu)d\nu \quad . \tag{11-4}$$

The halfwidths γ_L and γ_D in the above expressions are defined as one-half of the total width of the line between the points where $k_\ell(\nu)$ is equal to one-half the value it has at the central wave number.

For pressure-broadened spectral lines, the Lorentz half-width is given by:

$$\gamma_L = \sum_i \gamma_i^o P_i \quad , \tag{11-5}$$

where P_i is the pressure in atmospheres of the i'th gas of a mixture and γ_i^o is the broadening coefficient for that particular gas in cm^{-1}/atm.

The Doppler width in cm^{-1} can be calculated from the expression:

$$\gamma_D = \sqrt{\frac{2kT\ell n2}{mc^2}}\ \nu_o = 3.58 \times 10^{-7} \sqrt{\frac{T}{M}}\ \nu_o \ . \qquad (11\text{-}6)$$

T is in degrees Kelvin and M is the mass of the emitter in atomic mass units, or molecular weight.

For an absorption band, the integrated band strength S is the sum of all the line strengths S_ℓ, or equivalently,

$$S = \int_{-\infty}^{\infty} \sum_{\ell} k_\ell(n)dn = \int_{-\infty}^{\infty} k(\nu)d\nu \ ,$$

where $k(\nu)$ is the absorption coefficient summed over all contributing molecular lines.

Band strengths S for a number of gas species of atmospheric interest are shown in Table 11-1. In the gas phase it is customary to relate band strengths to the column density of absorbers measured in atm-cm; hence the dimensions for S are $cm^{-1}(atm\text{-}cm)^{-1}$, often are written confusingly as $cm^{-2}atm^{-1}$. The atm-cm unit is based on the conventional standard temperature and pressure (STP) gas at 273 K and one atmosphere pressure. An equivalent unit for the integrated band strength is $cm^{-1}(Amagat\text{-}cm)^{-1}$ where an Amagat has Loschmidt's number of absorbers cm^{-3}. The integrated band strength S is related to the Einstein spontaneous transition probability A by the expression

$$S = 0.357\lambda_\mu^2 A,$$

where λ_μ is in microns, and to oscillator strength f by the relation

$$S = 2.38 \times 10^7 f \ .$$

In practice, calculating the radiance of a gas sample and predicting its spectrum after transmission through an atmospheric path can become a highly involved line-by-line exercise in which the spacing, broadening, overlap, and optical depth of the individual rotational lines of the same, or different, molecules must be taken into account. Penner's book (Reference 11-4), although old, is a good starting reference. Performing such calculations can be expensive. Some tools that can make the problem less burdensome are discussed below.

The LOWTRAN transmission code now exists in a LOWTRAN 5 (Reference 11-5) version which is more flexible than previous versions and provides atmospheric radiance as well as transmission. LOWTRAN is limited to 20 cm^{-1} resolution and ambient or near ambient atmospheres.

Table 11-1. Molecular band data for species of atmospheric interest.[a]

Species	Rotational Constant	Transition	Band Origin		Band Strength	Einstein Coefficient
			$\nu_o(cm^{-1})$	$\lambda_o(\mu m)$	$(cm^{-2}atm^{-1})$	(sec^{-1})
AlO	0.635	1-0	965	10.4	777	19.7
CO	1.923	1-0	2143	4.67	260	33.4
		2-0	4260	2.35	2.06	1.05
		3-0	6350	1.58	0.132	0.15
FeO	0.5108	1-0	871	11.5	450	9.58
NO	1.699	1-0	1876	5.33	135	13.3
		2-0	3724	2.69	2.11	0.82
		3-0	5544	1.80	4.85	0.042
NO^+	1.992	1-0	2344	4.27	99.2	13.6
		2-0	4656	2.15	0.6	0.36
OH	18.86	1-0	3569.6	2.80	51.34	18.37
		2-0	6973.6	1.43	10.13	13.82
UO		1-0	820	12.2		
UO_2		ν_1	756	13.1		
		ν_2	?	?		
		ν_3	776	12.9		
UO_2^+		ν_1	880	11.4		
		ν_2	?	?		
		ν_3	780	12.8		
CO_2	0.39021	02^00-01^10	618.0	16.18	4.69	0.86
		02^20-01^10	667.8	14.98	33.0	7.10
		01^10-000	667.4	14.98	213.0	2.66
		$100-01^10$	720.8	13.87	4.98(-2)	1.25
		001-100	961.0	10.40	1.59(-2)	0.63
		$001-02^00$	1063.8	9.40	1.8(-2)	0.51
		001-000	2349.2	4.26	2706.0	420
		101-100	2326.6	4.30		
		02^01-02^00	2327.4	4.30		
		02^01-000	3612.8	2.77	37.4	13.7
		10^1-000	3714.7	2.69	47.0	18.1

[a]References used in preparing this table are listed at its end, as are supplementary sources of useful data that have not been included in the table.

(continued)

Table 11-1. Molecular band data for species of atmospheric interest (continued).

Species	Rotational Constant	Transition	Band Origin		Band Strength	Einstein Coefficient
			$\nu_0(cm^{-1})$	$\lambda_0(\mu m)$	$(cm^{-2}atm^{-1})$	(sec^{-1})
H_2O	27.877	020-010	1556.9	6.42	0.17*	43.2
	14.512	010-000	1594.7	6.27	317.0	22.6
	9.285	020-000	3151.6	3.19	1.8	0.5
		100-000	3657.1	2.73	22.0	8.3
		001-000	3755.6	2.66	214.0	84.7
		110-000	5234.9	1.91	0.479	0.37
		011-000	5331.2	1.88	24.61	19.5
NO_2	8.0012	010-000	750	13.33		
	0.43364	100-000	1320	7.57		
	0.41040	001-000	1617	6.18	2248.0	164.0
		101-000	2908	3.44	66.0	15.6
O_3	3.55368	010-000	701	14.2	18.0	0.25
	0.445281	001-000	1042	9.60	350.0	10.7
	0.39457	100-000	1103	9.07	10.4	0.35
		020-000	1400	7.14		
		011-000	1728	5.79	1.35	0.11
		110-000	1792	5.59	0.54	0.05
		002-000	2043	4.85		
		101-000	2110	4.73	32.0	4.0
		111-000	2779	3.60	0.66	0.14
		003-000	3042	3.29	3.0	0.78
		102-000	3076	3.25		
		201-000	3181	3.14	0.33	0.094
NH_3	9.4443	ν_2	951	10.52	605.0	15.3
	6.196	ν_4	1628	6.14	110.0	8.23
		ν_1	3336	3.0	20.0	6.2
		ν_4	3443	2.90	13.0	4.3
		$\nu_1+\nu_2$	4307	2.32	3.2	1.7
		$\nu_1+\nu_3$	4426	2.26	21.5	11.8

(continued)

Table 11-1. Molecular band data for species of atmospheric interest (continued).

Species	Rotational Constant	Transition	Band Origin		Band Strength	Einstein Coefficient
			$\nu_0(cm^{-1})$	$\lambda_0(\mu m)$	$(cm^{-2}atm^{-1})$	(sec^{-1})
CH_4	5.240	0001-0000	1306	7.66	190.0	9.09
		0100-000	1533	6.52	2.03	0.13
		1000-000	2916	3.43	inactive	
		0010-000	3019	3.31	324.0	82.7
		0020-000	6006	1.67	1.76	1.78
HNO_3		ν_5	879	11.38	667.0	14.4
		ν_4	1325	7.55	1290.0	63.5
		ν_2	1712	5.84	1388.0	114.0
N_2O	0.419011	010-000	588.8	16.99	33.0	0.32
		02^00-000	1168.1	8.56	11.0	0.42
		100-000	1284.9	7.78	265.0	12.2
		11^10-000	1880.3	5.32	0.41	0.04
		001-000	2223.8	4.49	1846	256.0
		12^00-000	2462.0	4.06	10.4	1.77
		200-000	2563.3	3.90	44.0	8.1
		01^11-000	2798.3	3.57	2.42	0.53
		02^01-000	3365.0	2.97	1.91	0.61
		11^11-01^10	3473.2	2.88	4.68	1.58
		101-000	3480.8	2.87	40.4	13.7
		002-000	4417.4	2.26	1.70	0.93
		201-000	4730.8	2.11	0.098	0.062

Metal Oxides (AlO, FeO, UO, UO_2)

Abramowitz, S., N. Acquista, and K.R. Thompson, "The Infrared Spectrum of Matric Isolated Uranium Monoxide" J. Phys. Chem. 75, 2283 (1971).

Barrow, R.F., and M. Senior, "Ground State of Gaseous FeO" Nature 223, 1359 (1959).

Fissan, H., and K.G.P. Sulzmann, "Absorption Coefficients for the Infrared Vibration-Rotation Spectrum of FeO". J.Q.S.R.T. 12, 979 (1972).

Sulzmann, K.G.P., "Relative Spectral Absorption Coefficients for the Fundamental Rotation-Vibration Bands at AlO". J.Q.S.R.T. 13, 931 (1973).

(continued)

Table 11-1. Molecular band data for species of atmospheric interest (continued).

Sulzmann, K.G.P., "Shock Tube Measurements of the f-number for the Fundamental Vibration-Rotation Bands of AlO in the $X^2\Sigma^+$ Electronic Ground State" J.Q.S.R.T. 15, 313 (1975).

Von Rosenberg, C.W., Jr. and K.L. Wray, "Shock Tube Studies on $Fe(Co)_5 + O_2$: 11μ FeO Emission and Kinetics. J.Q.S.R.T. 12, 531 (1972).

Carbon Monoxide (CO)

Bouanich, Jean-Pierre, and C. Haeusler, "Linewidths of Carbon Monoxide Self-Broadening and Broadened by Argon and Nitrogen," J.Q.S.R.T. 12, 695 (1972).

Bouanich, J., and C. Brodbeck, "Mesure des Largeurs et des Desplacements des Raies de la Bande 0-2 de CO Autoperturbe et Perturbe par N_2, O_2, H_2, HCl, NO et CO_2," J.Q.S.R.T. 13, 1 (1973).

Draegert, D.A., and D. Williams, "Collisional Broadening of CO Absorption Lines by Foreign Gases," J. Opt. Soc. Amer. 58, 1399 (1968).

Korb, C.C., R.H. Hunt, and E.K. Plyler, "Measurement of Line Strengths at Low Pressure -- Application to the 2-0 Band of CO," J. Chem. Phys. 48, 4252, (1968).

Kostkowski, H.J., and A.M. Bass, "Direct Measurement of Line Intensi- ties and Widths in the First Overtone Band of CO," J.Q.S.R.T. 1, 177 (1961).

Rank, D.H., A.G. St. Pierre, and T.A. Wiggins, "Rotational and Vibrational Constants of CO," J. Mol. Spect. 18, 418 (1965).

Toth, R.A., R.H. Hunt, and E.K. Plyler, "Line Intensities in the 3-0 Band of CO and Dipole Moment Matrix Elements for the CO Molecule," J. Mol. Spect. 32, 85 (1969).

Varanasi, P., "Line Width Measurements of CO in an Atmosphere of CO_2," J.Q.S.R.T. 11, 249 (1971).

Weinberg, J.M., E.S. Fishburne, and K.N. Rao, "'Hot' Bands of CO at 4.7 Microns Measured to High J Values," J. Mol. Spect. 18, 428 (1965)

Nitric Oxide (NO)

Abels, L.L., and J.H. Shaw, "Widths and Strengths of Vibration-Rotation Lines in the Fundamental Band of Nitric Oxide," J. Mol. Spect. 20, 11 (1966).

Table 11-1. Molecular band data for species of atmospheric interest (continued).

Goldman, A., and S.C. Schmidt, "Infrared Spectral Line Parameters and Absorbance Calculations of NO at Atmospheric and Elevated Temperatures for the Bands Region," J.Q.S.R.T. 15, 127 (1975).

James, T.C., "Intensity of the Forbidden $^2\pi_{3/2} - {}^2\pi_{1/2}$ Satellite Bands in the Infrared Spectrum of Nitric Oxide," J. Chem. Phys. 40, 762 (1964).

James, T.C., and R.J. Thibault, "Spin-Orbit Constant of Nitric Oxide. Determination from Fundamental and Satellite Band Origins," J. Chem. Phys. 41, 2806 (1964).

King, W.T., and B. Crawford, "The Integrated Intensity of the Nitric Oxide Fundamental Band," J.Q.S.R.T. 12, 443 (1972).

Olman, M.D., M.D. McNelis, and D.C. Hause, "Molecular Constants of Nitric Oxide from the Near Infrared Spectrum," J.Mol. Spect. 14, 62 (1964).

Nitric Oxide Ion (NO^+)

Billingsley, F.P., II, "Calculation of the Absolute Infrared Intensities for the 0-1, 0-2, and 1-2 Vibration-Rotation Transition in the Ground State of NO^+," Chem. Phys. Lett. 23, 160 (1973).

Miescher, E., "Fine Structure of NO^+ and NO Emission Spectra in the Schuman Region," Can. J. Phys. 33, 355 (1955).

Hydroxl Radical (OH)

Bass, A.M., and D. Garvin, "Analysis of the Hydroxyl Radical Vibration-Rotation Spectra, Between 3900 Å and 11 500 Å," J. Mol. Spect. 9, 114 (1962).

Dieke, G.H. and H.M. Crosswhite, "The Ultraviolet Bands of OH," J.Q.S.R.T. 2, 97 (1962).

d'Incan, J., C. Effantin, and F. Roux, "Intensities Abolues et Forces D'Oscillateurs de Quelques Raies des Bandes de Vibration-Rotation 1-0 et 2-0 du Radical OH," J.Q.S.R.T. 11, 1215 (1971).

Krassovsky, V.I., N.N. Shefov, and V.I. Yarin, "Atlas of the Airglow Spectra, 3000-12 400 Å," Planet. Space Sci. 9, 883 (1962).

Mies, F.H., "Calculated Vibrational Transition Probabilities of OH ($X^2\pi$)," J. Mol. Spect. 53, 150 (1974).

Murphy, R., "Infrared Emission of OH in the Fundamental and First Overtone Bands," J. Chem. Phys. 54, 4852 (1971).

Table 11-1. Molecular band data for species of atmospheric interest (continued).

Roux, F., J. d'Incan, and D. Carny, "Experimental Oscillator Strengths in the Infrared Vibration-Rotation Spectrum of the Hydroxyl Radical," Astrophysics Journ. 186, 1141 (1973).

Carbon Dioxide (CO_2)

Amat, G., and M. Pimbert, "On Fermi Resonance in Carbon Dioxide," J. Mol. Spect. 16, 278 (1965).

Boese, R.W., J.H. Miller, and E.C.Y. Inn, "Intensity Measurements in the 1 Micron CO_2 Bands," J.Q.S.R.T. 6, 717 (1966).

Boese, R.W., J.H. Miller, E.C.Y. Inn, and L.P. Giver, "Intensity of the 1.6 Micron Bands of CO_2," J.Q.S.R.T. 8, 1001 (1968).

Calfee, R.F., and W.S. Benedict, "Carbon Dioxide Spectral Line Positions and Intensities Calculated for the 2.05 and 2.7 Micron Region," NBS Tech. Note, 332, March 1966.

Courtoy, C.P., "Le Spectre de CO_2 Entre 3500 et 8000 cm^{-1} et les Constantes Moleculaires de Cette Molecule," Can. J. Phys. 35, 608 (1957).

Gordon, H.R., and T.K. McCubbin, Jr., "The 15 Micron Bands of CO_2," J. Mol. Spect. 18, 73 (1965).

Gray, L.D., and J.E. Selvidge, "Relative Intensity Calculations for Carbon Dioxide," J.Q.S.R.T. 5, 291 (1965).

Hahn, Y.H., and T.K. McCubbin, Jr., "Bands of Carbon Dioxide in the Region of 4.3 Microns," J. Mol. Spect. 25, 138 (1968).

Madden, R.P., "A High Resolution Study of CO_2 Absorption Spectra Between 15 and 18 Microns," J.Chem. Phys. 35, 2083 (1961).

McClatchey, R.A., et al., "AFCRL Atmospheric Absorption Line Parameters Compilation," AFCRL-TR-73-0096, 26 January 1973.

McCubbin, T.K., and T.R. Mooney, "A Study of the Strengths and Widths of Lines in the 9.4 and 10.4 Micron CO_2 Bands," J.Q.S.R.T. 8, 1255 (1968).

Water Vapor (H_2O)

Benedict, W.S., and R.F. Calfee, "Line Parameters for the 1.9 and 6.3 Micron Water Vapor Bands," ESSA Professional Paper 2, June 1967.

Table 11-1. Molecular band data for species of atmospheric interest (continued).

Gates, G.M., R.F. Calfee, D.W. Hansen, and W.S. Benedict, "Line Parameters and Computed Spectra for Water Vapor Bands at 2.7μ," NBS Monograph 71, Aug. 1964.

Ludwig, C.B., C.C. Ferriso, and C.N. Abeyto, "Spectral Emissivities and Integrated Intensities of the 6.3μ Fundamental Band of H_2O," J.Q.S.R.T. 5, 281 (1965).

McClatchey, R.A., et al., "AFCRL Atmospheric Absorption Line Parameters Compilation," AFCRL-TR-73-0096, 26 January 1973.

Patch, R.W., "Absolute Intensity Measurements for the 2.7μ Band of Water Vapor in a Shock Tube," J.Q.S.R.T. 5, 137 (1965).

Nitrogen Dioxide (NO_2)

Arakawa, E.T., and A.H. Nelsen, "Infrared Spectra and Molecular Constants of $^{14}NO_2$ and $^{15}NO_2$," J. Mol. Spect. 2, 413 (1958).

Goldman, A., F.S. Bonomo, W.J. Williams, D.G. Murcray, and D.E. Snider, "Absolute Integrated Intensity and Individual Line Parameters for the 6.2 Band of NO_2," J.Q.S.R.T. 15, 107 (1975).

Guttman, A., "Absolute Infrared Intensity Measurements on Nitrogen Dioxide and Dinitrogen Tetroxide," J.Q.S.R.T. 2, 1 (1962).

Hurlock, S.C., W.J. Lafferty, and K.N. Rao, "Analysis of the ν2 Band of NO_2," J. Mol. Spect. 50, 246 (1974).

Olman, M.D., and C.D. Hause, "Molecular Constants of Nitrogen Dioxide from the Near Infrafed Spectrum," J. Mol. Spect. 26, 241 (1968).

Ozone (O_3)

Gora, E.K., "The Rotational Spectrum of Ozone," J. Mol. Spect. 3, 78 (1959).

Kaplan, L.D., M.V. Migeotte, and L. Neven, "9.6 Micron Band of Telluric Ozone and Its Rotational Analysis," J.Chem. Phys. 24, 1183 (1956).

McCaa, D.J., and J.H. Shaw, "The Infrared Spectrum of Ozone," J. Mol. Spect. 25, 374 (1968).

Trajmar, S., and D.J. McCaa, "The (ν1+ν3) Combination Band of Ozone," J. Mol. Spect. 14, 244 (1964).

Table 11-1. Molecular band data for species of atmospheric interest (continued).

Ammonia (NH_3)

Allario, F., and R.K. Seals, Jr., "Measurements of NH_3 Absorption Coefficients with a $C^{13}O_2^{16}$ Laser," App. Optics 14, 2229 (1975).

Benedict, W.S., E.K. Plyler, and E.D. Tidwell, "Vibration Rotation Bands of Ammonia, I. The Combination Bands $\nu_2 + (\nu_1, \nu_3)$," J. Res. Nat. Bur. Stds. 61, 123 (1958).

Benedict, W.S., and E.K. Plyler, "Vibration Rotation Bands of Ammonia, II. The Molecular Dimensions and Harmonic Frequencies of Ammonia and Generated Ammonia," Can. J. Phys. 35, 1235 (1957).

Benedict, W.S., and E.K. Plyler, "Vibration Rotation Bands of Ammonia, III. The Region 3.2 - 4.3 Missions," J. Chem. Phys. 29, 829 (1959).

Benedict, W.S., E.K. Plyler, and E.D. Tidwell, "Vibration-Rotation Bands of Ammonia, IV. The Stretching Fundamentals and Associated Bands near 3μ," J. Chem. Phys. 32, 32 (1960).

Dowling, J.M., "The Rotation-Inversion Spectrum of Ammonia," J. Mol. Spect. 27, 527 (1968).

Garing, J.S., H.H. Nielsen, and K.N. Rao, "The Low Frequency Vibration-Rotation Bands of the Ammonia Molecule" J. Mol. Spect. 3, 496 (1959).

Giver, L.P., J.H. Miller, and R.W. Boese, "A Laboratory Atlas of the $5\nu NH_3$ Absorption Band at 6475Å with Applications to Jupiter and Saturn," Icarus 25, 34 (1975).

Legan, R.L., J.A. Roberts, E.A. Rinehard, and C.C. Lin, "Linewidths of the Microwave Inversion Spectrum of Ammonia," J. Chem. Phys. 43, 4337 (1975).

McBride, J., and R.W. Nicholls, "The Vibration-Rotation Spectrum of Ammonia Gas I," J. Phys. 5, 408 (1972).

Taylor, F.W., "Spectral Data for the ν_2 Bands of Ammonia with Applications to Radiative Transfer in the Atmosphere of Jupiter," J.Q.S.R.T. 13, 1181 (1973).

Varanasi, P., "Shapes and Widths of Ammonia Lines Collision Broadened by Hydrogen" J.Q.S.R.T. 12, 1283 (1973).

Walker, R.E., and B.F. Hochheimer, "Inversion-Rotation Emission Spectrum of Thermally Excited NH_3 in the 60-200 cm^{-1} Region". J. Mol. Spect. 34, 500 (1970).

Table 11-1. Molecular band data for species of atmospheric interest (continued).

Methane (CH_4)

Armstrong, R.L., and H.L. Welsh, "The Absolute Intensities of the Infrared Fundamentals of Methane," Spectrochimica Acta 16, 840 (1960).

Botineau, J., "Infrared Absorption of Methane at High Resolution Between 1225 cm^{-1} and 1400 cm^{-1}," J. Mol. Spect. 41, 182 (1972).

Burgess, J.S., E.E. Bell, and H.H. Nielsen, "The Forbidden Transition ν_2 in the Infrared Spectrum of Methane, "J. Opt. Soc. Amer. 43, 1058 (1953).

Childs, W.H.J., and H.A. Jahn, "A New Coriolis Perturbation in the Methane Spectrum. III Intensities and Optical Spectrum," Proc. Roy. Soc. A169, 451 (1939).

Darnton, L., and J.S. Margolis, "The Temperature Dependence of the Half Widths of Some Self and Foreign Gas Broadened Lines of Methane," J.Q.S.R.T. 13, 969 (1973).

Finkman, E., A. Goldman, and U.P. Oppenheim, "Integrated Intensity of the 3.3μ Band of Methane," J. Opt. Soc. Amer. 57, 1130 (1967).

Goldberg, L., O.C. Mohler, and R.E. Donovan, "Experimental Determination of Absolute f-Values for Methane," J. Opt. Soc. Am. 42, 1 (1952).

Hecht, K.T., "Vibration-Rotation Energies of Tetrahedral XY_4 Molecules Part II. The ν_3 of CH_4," J. Mol. Spect. 5, 390 (1960).

Henry, L., N. Husson, R. Andia and A. Valentin, "Infrared Absorption Spectrum of Methane from 2884 cm^{-1} to 3141 cm^{-1}," J. Mol. Spect. 36, 511 (1973).

Herranz, J.H., J. Morcillo, and A. Gomez, "The ν_2 Infrared Band of CH_4 and CD_4," J. Mol. Spect. 19, 266 (1966).

Kyle, T.G., R.D. Blatherwich, and F.S. Bonomo, "ν_4 Band of $^{13}CH_4$," J. Chem. Phys. 53, 2800 (1970).

Margolis, J.S., "Line Strength Measurements of the $2\nu_3$ Band of Methane," J.Q.S.R.T. 13, 1097 (1973).

McDowell, R.S., "The ν_3 Infrared Bands of $C^{12}H_4$ and $C^{13}H_4$," J. Mol. Spect. 21, 280 (1966).

Pine, A.S., "Doppler Limited Spectra of the ν_3 Vibration of $^{12}CH_4$ and $^{13}CH_4$," J. Mol. Spect. 54, 132 (1975).

Table 11-1. Molecular band data for species of atmospheric interest (continued).

Plyler, E.K., E.D. Tidwell, and L.R. Blaine, "Infrared Absorption Spectrum of Methane from 2470 to 3200 cm^{-1}," J. Res. Nat. Bur. Stds. 64A, 201 (1960).

Pugh, L.A., T. Owen, and K.N. Rao, "$3\nu_3$ Band of $^{12}CH_4$ at 1.1μ," J. Chem. Phys. 59, 1243 (1973).

Rank, D.H., D.P. Eastman, G. Skorinko, and T.A. Wiggins, "Fine Structure in the Lines of the $2\nu_3$ Band of Methane," J. Mol. Spect. 5, 78 (1960).

Sarangi, S., and P. Varanasi, "Measurements of Intensities of Multiplets in the $2\nu_3$ Band of Methane at Low Temperatures," J.Q.S.R.T. 14, 365 (1974).

Nitric Acid (HNO_3)

Goldman, A., T.G. Kyle, and F.S. Bonomo, "Statistical Band Model Parameters and Integrated Intensities for the 5.9μ, 7.5μ, and 11.3μ Bands of HNO_3 Vapor," App. Opt. 10, 65 (1971).

McGraw, G.E., D.L. Bernitt, and I.C. Hisatsume, "Vibrational Spectra of Isotopic Nitric Acids," J. Chem. Phys. 42, 237 (1965).

Nitrous Oxide (N_2O)

Amiot, C., and Guelachvili, "Vibration Rotation Bands of N_2O 1.2 Micron -3.3 Micron Region," J. Mol. Spect. 51, 475 (1974).

Fraley, P.E., W.W. Brim, and K.N. Rao, "Vibration-Rotation Bands of N_2O at 4.5 μm" J. Mol. Spect. 9, 487 (1962).

Griggs, J.L., K.N. Rao, L.H. Jones, and R.M. Potter, "ν^3 Bands of $^{15}N_2{}^{18}O$," J. Mol. Spect. 18, 212 (1965).

Griggs, J.L., K.N. Rao, L.H. Jones, and R.M. Potter, "Vibration Rotation Bands of $^{15}N_2{}^{18}O$," J. Mol. Spect. 25, 34 (1968).

Krell, J.M., and R.L. Sams, "Vibration-Rotation Bands of Nitrous Oxide: 4.1 Micron Region," J. Mol. Spect. 51 (1974).

Lowler, J.E., "Band Intensity and Line Half-Width Measurements in N_2O near 4.5 Micron," J.Q.S.R.T. 12, 873 (1972).

Margolis, J.S., "Intensity and Half Width Measurements of the (00^02-00^00) Band of N_2O," J.Q.S.R.T. 12, 751 (1972).

Table 11-1. Molecular band data for species of atmospheric interest (concluded).

Pliva, J., "Some Near Infrared Bands of Nitrous Oxide," J. Mol. Spect. 25, 62 (1968).

Pliva, J., "Molecular Constants of Nitrous Oxide $^{14}N_2{}^{16}O$," J. Mol. Spect. 27, 461 (1968).

Pliva, J., "Infrared Spectra of Isotopic Nitrous Oxides," J. Mol. Spect. 12, 360 (1961).

Tidwell, E.D., E.K. Plyler, and W.S. Benedict, "Vibration Rotation Bands of N_2O," J. Opt. Soc. Amer. 50, 1243 (1960).

Rank, D.H., D.P. Eastman, B.S. Rao, and T.A. Wiggins, "Highly Precise Wavelengths in the Infrared II. HCN, N_2O, and CO," J. Opt. Soc. Amer. 51, 929 (1961).

Tien, C.L., M.F. Modest, and C.R. McCreight, "Infrared Radiation Properties of Nitrous Oxide," J.Q.S.R.T. 12, 267 (1972).

Young, L.D. Gray, "Relative Intensity Calculations for Nitrous Oxide," J.Q.S.R.T. 12, 307 (1972).

The AFGL atmospheric absorption line parameters compilation is constantly reviewed and updated. A new and growing compilation of evaluated data for "trace" gases, also available on tape, includes NO, SO_2, NO_2, NH_3, HCl, HF, OH, and HNO_3 (Reference 11-6). Finally, an efficient line-by-line algorithm has been implemented in the FASCODE (Fast Atmospheric Signature Code). It calculates transmittance and radiance to any desired degree of resolution and is ten times faster than previous HITRAN methods (Reference 11-7).

The molecular band model in the DNA ROSCOE/NORSE code provides a moderate resolution (5 to 20 cm^{-1}) transmission and radiance calculation for heated air with altered chemical species concentrations.

LTE conditions dominate so long as the collisional processes exciting and deexciting a vibrational mode dominate the radiative loss. In general, the numbers of collisions required for translational, rotational, and vibrational relaxations are of the order of <10, <100, and 10^3 to 10^6, respectively (References 11-8, 11-9). For polyatomic species having more than one vibrational mode, the effective mechanism for translational-vibrational (T-V) coupling into the molecule generally involves the mode of lowest frequency, which then couples intramolecularly with the other modes.

For a vibrational mode of species X, simplifying to a two-level model and neglecting absorption of radiation:

$$\frac{d[X(1)]}{dt} = K_{01}[X(0)] - (K_{10} + A_{10})[X(1)], \qquad (11\text{-}7)$$

and in the steady state:

$$\frac{[X(1)]}{[X(0)]} = \frac{K_{01}}{(K_{10} + A_{10})} \; . \qquad (11\text{-}8)$$

Here, $K_{01}(sec^{-1})$ and $K_{10}(sec^{-1})$ are the collisional excitation and deexcitation rates, respectively, [X(i)] is the number density (cm^{-3}) of species X in vibrational state i, and A_{10} (sec^{-1}) is the Einstein spontaneous emission coefficient for the transition (see Table 11-1). If Z_{ij} is the number of collisions required to bring about one transition from state i to state j, and N is the number of collisions per second experienced by a molecule at a given altitude, then $K_{ij} = N/Z_{ij}$. For the example given,

$$K_{10} = N/Z >> A_{10}$$

is the condition to be met if radiative loss is not to disrupt LTE. In that case the two vibrational levels are related by the Boltzmann factor:

$$[X(1)]/[X(0)] = \exp(-\theta/T), \qquad (11\text{-}9)$$

where T is the kinetic temperature and θ is the characteristic temperature $h\nu_0/k$ of the mode. When $T << \theta$, the reciprocal of K_{10} is a good approximation to the relaxation time for the system; it applies about as well for a system of many harmonic oscillators (Reference 11-8).

As altitude increases, collision rates in the atmosphere decrease, while A_{10} remains constant. Failure of K_{10} to dominate A_{10} implies

$$[X(1)]/[X(0)] < \exp(-\theta/T), \qquad (11\text{-}10)$$

so that the effective vibrational temperature of X falls below the kinetic temperature T. Therefore, a condition arises where the volume emission rate in an optically thin atmosphere is less than the LTE value; this is called collision-limiting. For most species this condition has its onset somewhere above 70 km; the actual altitude depends on where in the atmosphere $N/Z_{10} \sim A_{10}$. Values of Z_{10} for CO_2 and H_2O are listed in Table 11-2.

Oxygen atoms have been shown to accelerate the vibrational relaxation of both molecular nitrogen (Reference 11-11) and molecular oxygen (Reference 11-12). In the E-region and above, atomic oxygen is a major species and could in principle aid in maintaining LTE in radiative species in the atmosphere. Unless the kinetic temperature has been greatly increased by some perturbation, the practical importance of any such relaxation as a means of aiding the T-V energy-transfer process is likely to be minimal. It may, however, be effective in quenching emissions from molecules that have been vibrationally excited by alternative mechanisms. Degges (Reference 11-13) has pointed out the special circumstances that may allow oxygen atoms to excite NO via atom interchange.

11.3 VIBRATIONAL-VIBRATIONAL ENERGY TRANSFER

The exchange of vibrational quanta between molecules during collisions (V-V coupling), in the fashion:

$$X(v=1) + Y(v=0) \rightarrow X(v=0) + Y(v=1), \qquad (11\text{-}11)$$

is a process which, in disturbed atmospheric situations, plays an important role in the emission of infrared radiation. This occurs because the major atmospheric species N_2 and O_2, being homonuclear diatomic molecules, are both infrared-inactive and generally resistant to V-T deexcitation. Vibrationally excited nitrogen is particularly likely to remain excited and so to provide a persistent energy reservoir. (See Chapter 20 for a much fuller discussion of the dynamics of vibrationally excited nitrogen.) In addition, an important quenching process for vibrationally excited NO may be V-V energy transfer to O_2. The energy-transfer process of Equation 11-11 is known to be most efficient when species X and Y have nearly equal vibrational frequencies, such as N_2 and CO_2.

Table 11-2. Collisional excitation parameters.

Originally Excited Species	Bank Origin Wave Number, ν_o (cm^{-1})	Characteristic Temperature, $\theta = \frac{h\nu_o}{k}$ (K)	No. of Collisions Required to Bring About V-V Exchange: Z_{01}^{10}[a]	With Collision Partner	No. of Collisions Required to Bring About T-V Exchange: Z_{10}[a]	With Collision Partner	Reference[b]
CO_2	667	959	--	--	4 x 10^5	N_2	11-11
CO_2	2349	3380	7 x 10^2	N_2	--	--	11-11
H_2O	1595	2295	~5 x 10^3	O_2	2 x 19^4	Air	11-11
NO	1876	2700	5 x 10^5	N_2	--	--	11-10
NO(A)	2341	3371	7.9 x 10^2	N_2	--	--	11-10
CO	2143	3080	4.5 x 10^6	O_2	--	--	11-10
O_2	1556	2228	--	--	--	--	11-10
N_2	2331	3336	--	--	--	--	11-9

Notes:

[a] The Z-values relate to ~300 K.

[b] Reference 11-8 derives the theoretical basis for calculating relaxation rates at other temperatures and References 11-9 and 11-10 compile much of the pertinent data.

In the normal atmosphere, the effective nitrogen vibrational temperature in the E-region has been believed to be greater than the local kinetic temperature, i.e., $T_{vib} > T_{kin}$, but the altitude profile of T_{vib} and its response to auroral or other pertubations remained conjectural. O'Neil et al. (Reference 11-14) have reported on the result of a direct probing by electron beam luminescence of the nitrogen vibrational temperature in an IBC Class II aurora over Fort Churchill. Within experimental uncertainty the inferred vibrational population ratio $\{N_2\ (v=1)\}/\{N_2(v=0)\}$ was not recognizably greater than model atmosphere kinetic temperatures appropriate for the time of the flight. Figure 11-6 shows the upper limit nitrogen vibrational temperature consistent with their data.

At altitudes below 125 km the principal sink for nitrogen vibrational energy is probably the near-resonant transfer to CO_2, with an energy deficiency of only 19 cm^{-1} (see Chapter 10):

$$N_2(1) + CO_2(000) \xrightarrow{k} N_2(0) + CO_2(001), \qquad (11\text{-}12)$$

where $k \sim 7 \times 10^{-13}$ $cm^3 sec^{-1}$. The process of Reaction 11-12 is followed by radiation in the infrared of the energy just transferred, i.e.:

$$CO_2(001) \xrightarrow{A} CO_2(000) + h\nu\ (2349\ cm^{-1}), \qquad (11\text{-}13)$$

for which A = 400 sec^{-1} (Table 11-1).

One type of measurement conducted in the DNA HAES series of experiments has been a vertical probe of CO_2 4.3-micron radiance. Attempts have been made to model the radiation (Reference 11-15) and it has been found necessary to include, in addition to earthshine scatter, contributions from N_2 excited by auroral energy input and, in addition, in the vicinity of 85 km, a contribution from N_2 excited by

$$N_2\ (v=0) + OH\ (v') \rightarrow N_2(v>0) + OH\ (v<v'). \qquad (11\text{-}14)$$

The actual importance of V-V exchange in generating infrared backgrounds in a disturbed atmosphere depends primarily upon the effective vibrational temperature achieved by the excited nitrogen, and also upon the mixing ratio of emitter species introduced into the same region. Furthermore, the temperature dependence of V-V exchange processes is rather uncertain, especially at low kinetic temperatures (Reference 11-10).

Values of Z_{01}^{10}, the number of collisions required to bring about V-V exchange, are listed for several pairs of interacting partners in Table 11-2. Reference 11-10 provides a critical summary of rate constants.

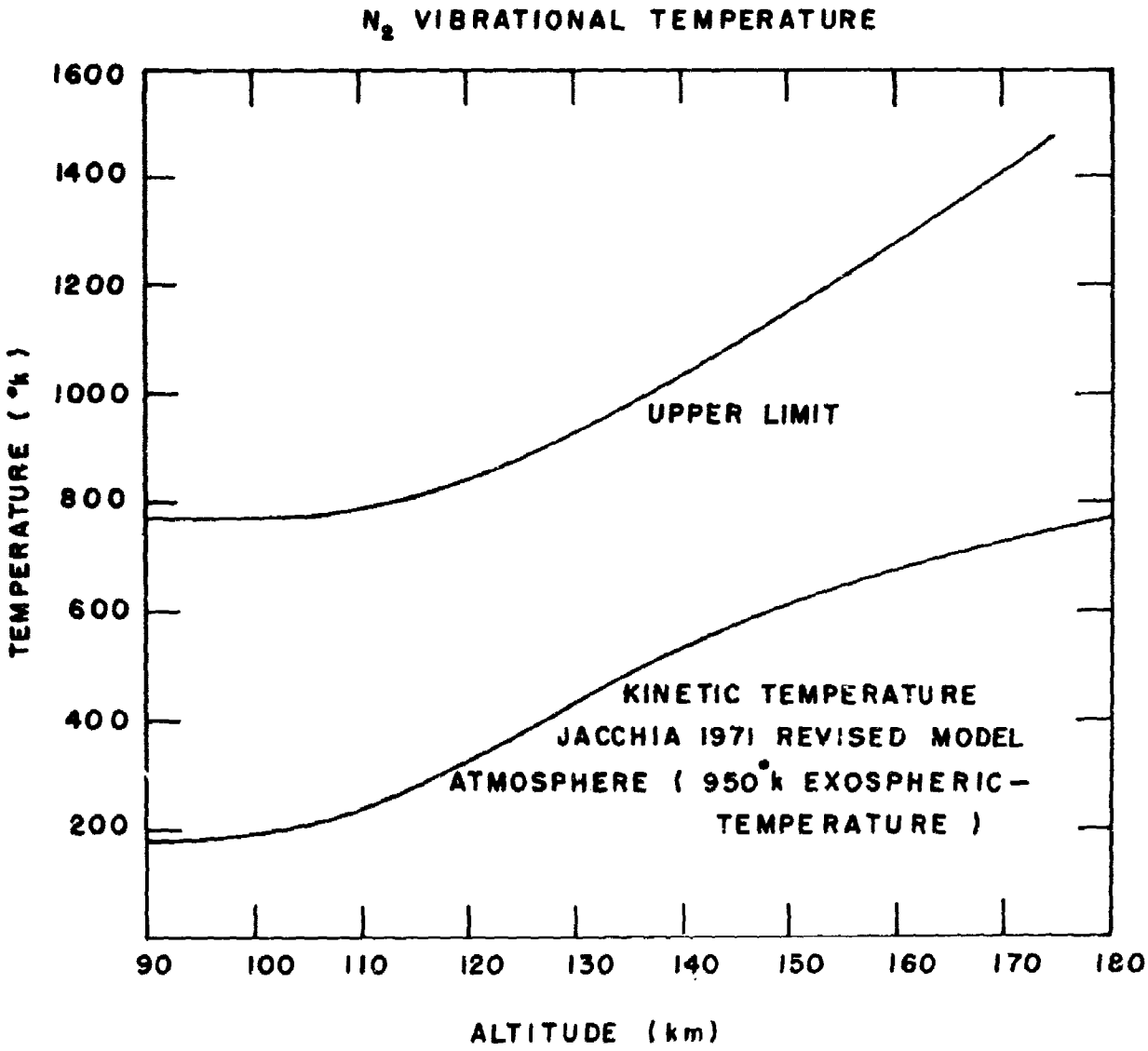

Figure 11-6. Nitrogen vibrational temperature derived from an electron-induced fluorescence probe in an IBC class II aurora (Reference 11-14).

11.4 CHEMIEXCITATION PROCESSES

Part or all of the energy output of exothermic interactions may be distributed into the available vibrational degrees of freedom of one or more reaction products. The number of reactions for which this is known to be true is large and growing, with special impetus in this area coming from the field of chemical lasers. Following a nuclear or other disturbance, chemical reactions take place for prolonged periods of time over large volumes of the atmosphere. It is thus inherently plausible that chemiexcitation should be an important source of infrared background radiation. In the paragraphs that follow, some of the chemiexcitation reaction products that are known or thought to be important within this context are discussed specifically. A fairly comprehensive review of infrared atmospheric emission processes has appeared in Reference 11-16.

11.4.1 Vibrationally Excited Hydroxyl ($OH^{\ddagger}$)

One of the brightest features of the airglow is the Meinel band emission of hydroxyl (Reference 11-17). This has been studied extensively: ground based measurements of high overtone bands in the visible and near infrared are most numerous and there is a growing body of infrared data from airborne and rocket-borne instruments carried out under the DNA HAES program. The night airglow radiation from hydroxyl peaks near 90 km and there is agreement that the process

$$H + O_3 \rightarrow O_2 + OH^{\ddagger} \quad (v \leq 9) \qquad (11\text{-}15)$$

is the dominant chemical source of the radiation, as well as a most important sink for the reactants. Shefov (Reference 11-18) has summarized and collated a large body of the data on atmospheric hydroxyl emissions, much of it done in the Soviet Union, relating observed intensities and apparent vibrational and rotational distributions to time of day, season, geomagnetic activity, etc.

It has not seemed possible to account for some of the large excursions in intensity and apparent vibrational distribution solely on the basis of the consequences of Reaction 11-15 and it has been suggested that the additional process

$$O + HO_2 \rightarrow O_2 + OH^{\ddagger} \quad (v \leq 6) \qquad (11\text{-}16)$$

has a role (Reference 11-19). Detailed kinetic information about Reaction 11-15 is lacking and its product vibrational distribution is still conjectural. At least now the electronic spectrum of HO_2 is well known (Reference 11-20) and it should be possible to study its kinetic behavior more confidently in the future.

Unlike Reaction 11-16, $H + O_3$ (Reaction 11-15) has been studied in some detail. Polanyi (Reference 11-21) and his collaborators at

Toronto first obtained spectra of OH from Reaction 11-15 reflecting the initial vibrational distribution. Their results, and the more recent results of Streit and Johnston (Reference 11-22), differ in detail but agree in assigning most of the product OH into v=9 with progressively lesser amounts in lower levels (Figure 11-7).* Distributions of this sort, using only radiative relaxation, yield adequate first order approximations to the observed hydroxyl airglow intensity distribution (Reference 11-25).

Since the reaction $O + OH \rightarrow O_2 + H$ is fast and atomic oxygen is abundant at airglow heights, the effect of reactive quenching of $OH^{\ddagger}$ by O must be accounted for in the analysis. Until recently, however, it has not been thought necessary to consider collisional quenching (by O_2 and N_2), although Fiocco and Visconti (Reference 11-26) did include that effect. Quenching rate constants for N_2 and O_2 had previously been reported as 0.36 and 1.0×10^{-14}, respectively, which should make them relatively unimportant quenching partners at airglow altitudes. However, the data shown in Table 11-3 indicate rate constants $> 5 \times 10^{-13}$ for O_2 and N_2 with OH (v>5) and these latter results have serious consequences for hydroxyl radiation modeling if they can be substantiated.

A simplified sample analysis involving Reaction 11-15 will serve to demonstrate some of the complexities of the problem. For each vibrational level v of the product OH, considering the radiative and collisional transitions only between nearest-neighbor levels:

$$\frac{d[OH(v)]}{dt} = k(v)\,[H]\,[O_3] + K_Q(v+1)\,[OH(v+1)] + A(v+1)[OH(v+1)] - K_Q(v)\,[OH(v)] - A(v)\,[OH(v)] - K_R(v)\,[OH(v)] \quad . \tag{11-17}$$

Here, k(v) is the rate constant for formation of OH in vibrational level v, $K_Q(v)$ is the quenching rate for level v at a given total density and composition of quenching species, A(v) is the Einstein coefficient for the vibrational transition v→v-1, and $K_R(v)$ is the chemical destruction rate (primarily from $O + OH \rightarrow O_2 + H$).

For the two highest levels of OH (v=9,8), the steady-state solutions are:

$$[OH(9)]_{ss} = \frac{k(9)\,[H]\,[O_3]}{K_Q(9) + K_R(9) + A(9)} \quad , \tag{11-18}$$

*Both groups used the relative Einstein coefficients of J.K. Cashion (Reference 11-23) to obtain their relative k_v values. Reinterpretations using the more recent calculations of F.H. Mies (Reference 11-24) would be desirable.

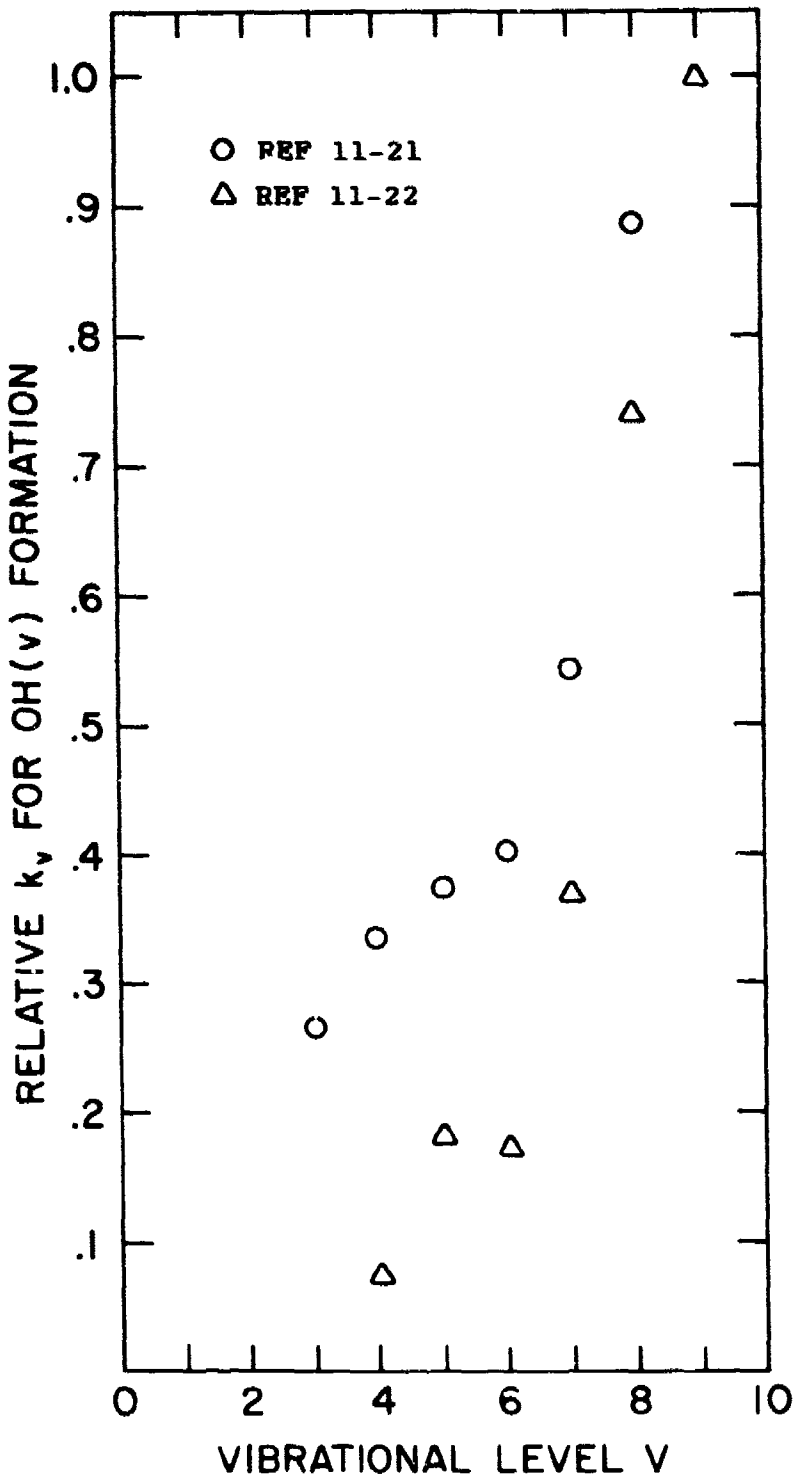

Figure 11-7. Relative rates of formation of OH in vibrational level v from the reaction $H + O_3 \rightarrow O_2 + OH$.

Table 11-3. Quenching rate constants for OH(v) + M, K_Q (cm^3/mol-sec) in units of 10^{-13}.

V/M	N_2	O_2	Ar	H_2O	CO_2
9	0.036[a]	0.10[b]		2.0[a]	0.24[a]
9	4.4	3.5	1.1		
8	3.7	5.4	1.1		
7	5.5	7.8	2.2		
6	5.0	7.3	2.9		
5	2.1	3.2	1.5		
4	0.78	1.4	0.079		

Note:

[a]S.D. Worley et al. (Reference 11-27).

[b]S.D. Worley et al. (Reference 11-28).

Remainder of data from Reference 11-22.

and

$$[OH(8)]_{ss} = \frac{k(8)\,[H]\,[O_3] + (K(9) + A(9))[OH(9)]}{K_Q(8) + K_R(8) + A(8)} \quad . \quad (11\text{-}19)$$

At an altitude of about 100 km, K_R is about 10 sec^{-1}, K_Q for OH(v) is 5 sec^{-1} (using the larger rate constants of Table 11-3) and A(1) is about 20 sec^{-1}. With the A's, K_R and K_Q all of comparable magnitude, it would not be appropriate to drop the quenching terms.

Some recent measurements of hydroxyl airglow altitude profiles have sought to record simultaneously both high and lowlevel vibrational bands to aid in assessing the relative importance of Reactions 11-15 and 11-16 as sources of hydroxyl. (References 11-29, 11-30). The results are difficult to interpret at best and have only been applied to determining an oxygen atom profile from the hydroxyl profile, assuming that oxygen atoms provided the only nonradiative loss term for OH(v). It remains to be seen if the larger rate constants for quenching by O_2 and N_2 are consistent with airglow data.

Hydroxyl airglow measurements from the ground in recent years have been providing believable evidence of short-term variations in brightness and apparent rotational temperature. Some instances are described simply as patchiness; other times large-scale wave motions

are associated with the observed intensity enhancements and temperature changes. (Reference 11-31). Attempts to correlate band intensity changes and rotational temperature changes have not always led to consistent conclusions. The rotational temperatures are generally deduced from the intensity ratio of pairs of low quantum number P-branch lines in a given band, assuming a Boltzmann distribution. The individual temperatures so derived appear credible on the whole and the rotational levels seem coupled to the local kinetic temperature in most instances.

There is some evidence (Reference 11-32) of systematic overpopulation of successively higher rotational levels relative to the lowest. It is as if the rotational distribution observed is incompletely relaxed from a much hotter rotational distribution. Dick and Krassovsky (Reference 11-33) discuss this point and provide leading references. The available evidence suggests that the altitude regime where airglow hydroxyl is generated could provide an environment where such an effect would occur. The Toronto group (Reference 11-21) observed very hot and even grossly non-Boltzmann rotational distributions at their lowest background pressures (up to 0.5 mtorr). They were careful to point out that the design of their experiment had reactants mixing together at considerably higher pressure before flowing into the observation region. Remarkably, the lower resolution data of Reference 11-22 all seem to be fit best by a 1500 K rotational temperature at all pressures; this may reflect a rapid freezing in by quenching of the rotational distribution in their experiment.

Deducing local kinetic temperatures from airglow observations and interpreting airglow brightness changes involves either unfolding or ignoring the finite depth of the emitting layer, which need not be uniform in temperature or composition. Rapid fluctuations or even slow changes in the brightness of individual lines or complete bands may not have simple explanations if vibrational relaxation turns out to be "fast" and rotational relaxation "slow". In view of the expected participation of rotational excitation in the relaxation of vibrational energy in molecules like hydroxyl (Reference 11-10), such an outcome is easy to accept.

11.4.2 Vibrationally Excited Nitric Oxide ($NO^{\ddagger}$)

Emissions from both $NO^{\ddagger}$ and $NO^{+\ddagger}$ have been observed in the spectrum of hot air resulting from an atmospheric nuclear detonation (Reference 11-2). Following atmospheric disturbances, both species play important roles in the complex chain of deionization reactions, and act in addition as potential sources of infrared radiation from chemiluminescent reactions. Two of the reactions leading to nitric oxide formation have been studied in detail to determine the individual rate constants of formation of NO into the energy accessible vibrational levels:

$$N\ (^4S) + O_2 \rightarrow O + NO\ (v \leq 7) \qquad (11\text{-}20)$$

and

$$N\ (^2D) + O_2 \rightarrow O + NO\ (v \leq 18). \qquad (11\text{-}21)$$

Rahbee et al. (Reference 11-34) and Whitson et al. (Reference 11-35) have both studied the reaction involving ground state $N(^4S)$ atoms in a room temperature integrating sphere reactor. There is some disagreement in the details of the product vibrational distribution as deduced by the two groups, but the results of Reference 11-34 are based on relatively high-resolution spectra and are to be preferred. A graphical presentation of their results is given in Figure 11-8. They conclude that no more than 8 percent of the exothermicity of the reaction is directed into NO ($v \geq 2$). Figure 11-9, taken mostly from Reference 11-35, summarizes available quenching rate constant data for NO.*

Reaction 11-21 has been studied in the COCHISE facility constructed at AFGL with DNA support. In these latter experiments all complications resulting from quenching collisions and wall effects are eliminated by operation in a low pressure (millitorr) short contact time (millisecond) cryopumped cryogenic chamber. Results from that study are shown in Figure 11-10. With $N(^2D)$ as the reactant atom, about 25 percent of the exothermicity appears in NO ($v>0$); fully 90 percent of the product NO is in states $v<9$ and the energetics will allow $O(^1D)$ as the atomic product. Table 11-4 shows the calculated chemiluminescent emission efficiency of the $N(^2D) + O_2$ mechanism of nitric oxide formation. The results for the overtone are preliminary. There has been encouraging agreement in accounting for aurorally and artificially enhanced nitric oxide radiation observed in the DNA HAES program and predictions based on these experimental results.

11.4.3 Vibrationally Excited Ozone ($O_3^\ddagger$)

Another potentially important source of chemiluminescent infrared radiation in a disturbed atmosphere is $O_3^\ddagger$. The probable formation reaction is the three body process

$$O + O_2 + M \rightarrow O_3^\ddagger + M\ . \qquad (11\text{-}22)$$

An "ozone precursor" has been identified by ultraviolet absorption ~3000Å) in oxygen subjected to pulse radiolysis. A number of investigators (References 11-38 through 11-41 have observed solar attenuation at broadly the same wavelength region at altitudes above 40 km. Noxon (Reference 11-42) presents arguments that none of the oxygen

---

*K. Glanzer and J. Troe (J. Chem. Phys. 63, 4352 (1975) report a rate constant of 3.8×10^{-11} for deactivation of NO(v=1,2) by atomic oxygen at 2700 K.

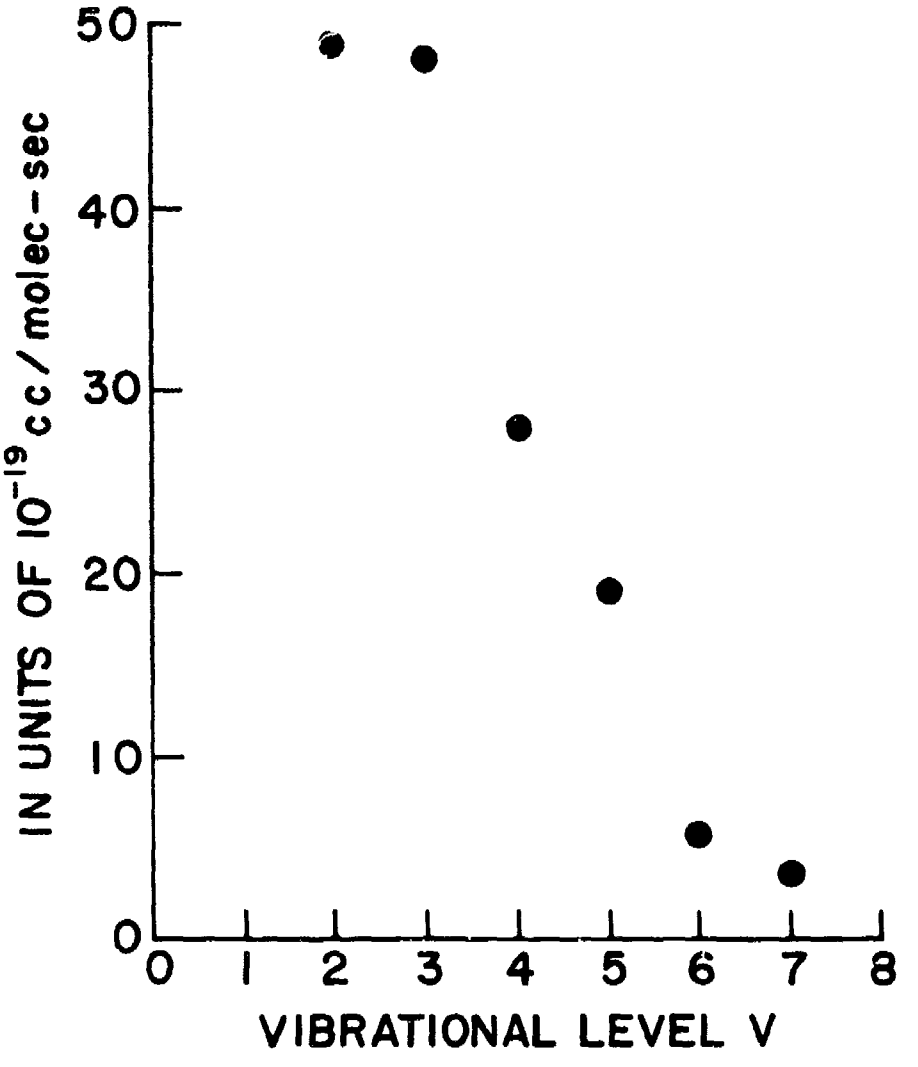

Figure 11-8. Individual rate constants for formation of NO in vibrational level v from the reaction $N(^4S) + O_2 \rightarrow O + NO$ (Reference 11-34).

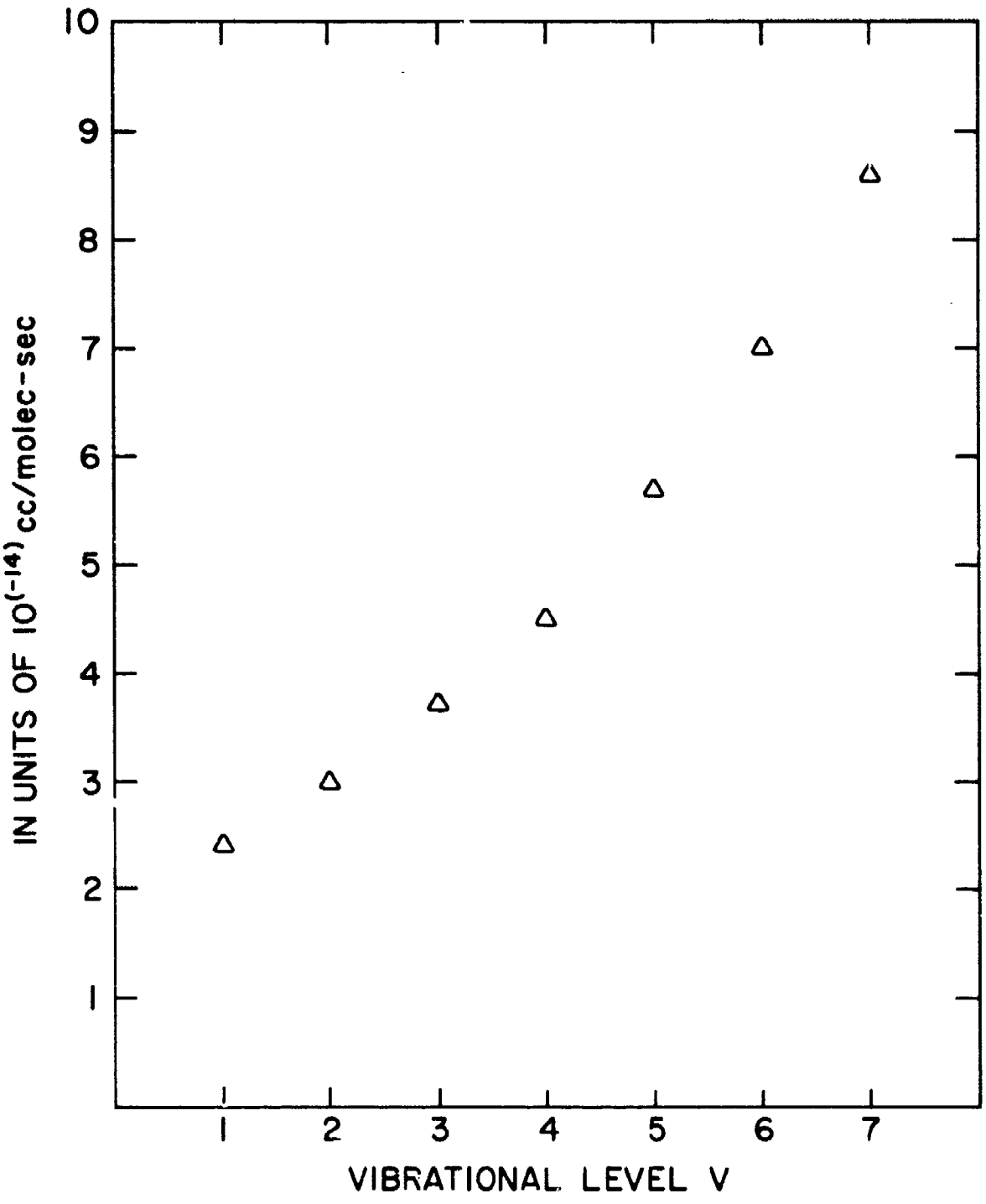

Figure 11-9. Rate constants for quenching of NO (v) by O_2 as a function of vibrational level v (References 11-35 and 11-36.

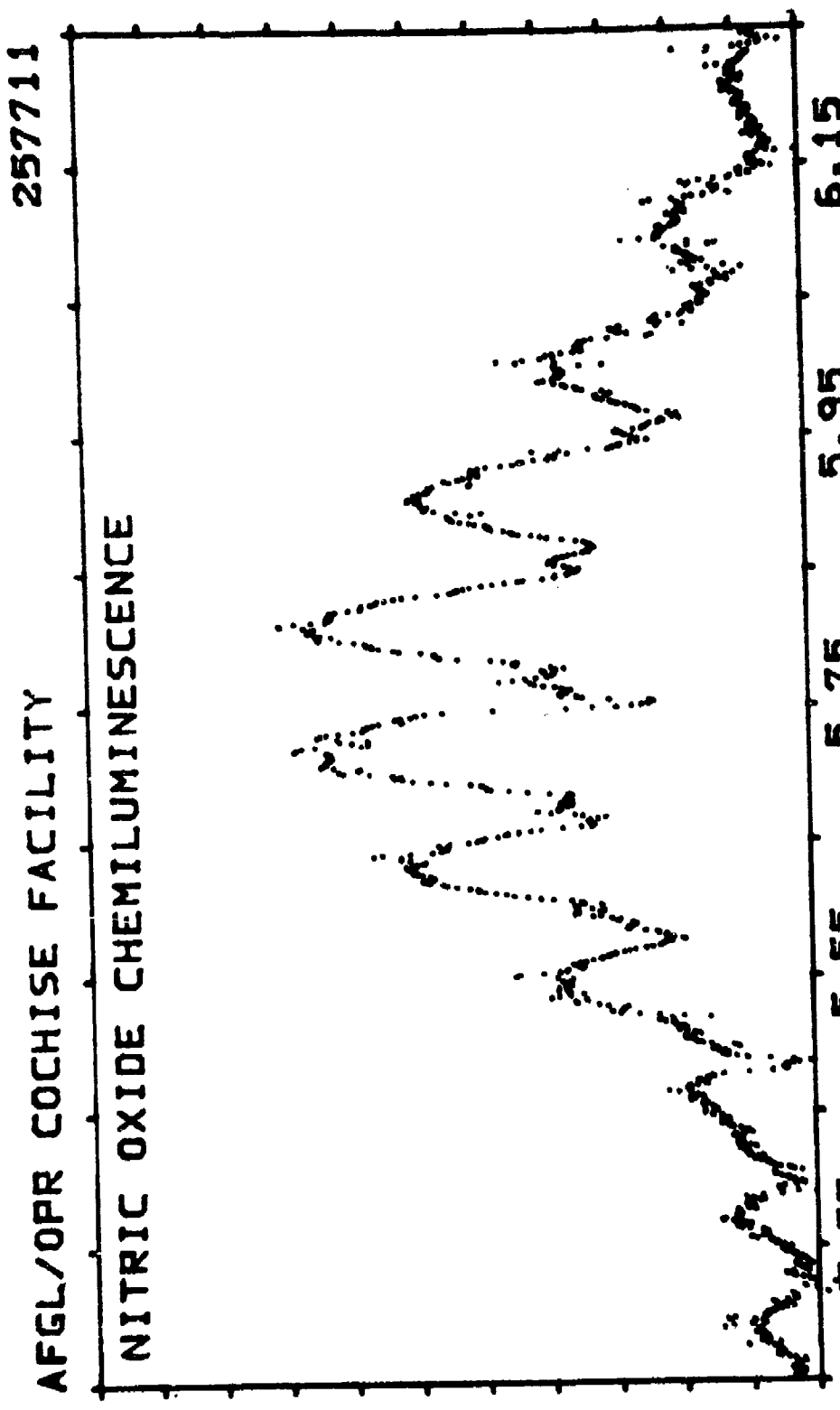

Figure 11-10. Observed spectrum of NO from the reaction of metastable nitrogen atoms and molecular oxygen under arrested relaxation conditions (Reference 11-37).

Table 11-4. Nitric oxide atmospheric emission photons radiated per molecule produced by $N(^2D)$.[a]

	Altitude (km)					
	75	80	85	90	95	100
$\Delta v=1$	1.70	2.52	3.21	3.64	3.84	3.92
$\Delta v=2$	0.15	0.21	0.25	0.28	0.29	0.30

Note:

[a]Calculation based on results of COCHISE experiments.

species $b^1\Sigma_g^+$, $a^1\Delta_g$, or $X^3\Sigma_g^-$ ($v\sim11$) can account for the atmospheric data, and either ground state $O_3^{\ddagger}$ or some low-lying electronically excited ozone species are prime candidates.

Von Rosenberg and Trainor (Reference 11-43) have flash photolyzed oxygen-ozone mixtures and studied the kinetics of the resulting infrared radiation in selected bands. They conclude that up to 50 percent of the 1.04 eV exothermicity of the $O + O_2 + M$ recombination is distributed in vibrational modes of the ozone formed, with, on the average, 1.6 quanta in $\nu_1 + \nu_3$ and 3.7 quanta in ν_2. Their data indicate excitation into high vibrational levels of all modes, and in addition, they observed radiation near 6.6 microns and 8.0 microns that may be associated with electronically excited states of ozone.

Further definition of the ozone radiation can be expected from the COCHISE facility. Figure 11-11 is a sample of very preliminary data showing for the first time the spectral extent of the ν_3 radiation. The COCHISE data seem to indicate a preference for O_3 formation in the ν_3 mode, in contrast to the results of von Rosenberg mentioned above. Table 11-5 summarizes some of the available data on ozone deactivation.

11.5 VIBRATIONALLY EXCITED METAL OXIDES ($MeO_x^{\ddagger}$)

The debris of nuclear detonations includes metallic matter that originates in the structures of both the nuclear devices and their carriers. If exothermic reactions take place between such that substances and ambient atmospheric species, then the likelihood of chemiluminescent processes is enhanced. Assuming the debris species to be primarily atomic metals (Me), reactions of two types,

$$Me_2 + O \rightarrow MeO + O \qquad (11\text{-}23)$$

and

Figure 11-11. Chemiluminescent ozone radiation from the $O + O_2 + M$ radiation (Reference 11-37).

Table 11-5. Vibrational relaxation of ozone for T = 298 K.

Process	Partner	Units of 10^{-14} k (c^3/mol-sec)	Reference
(100,010,001) → (000)	O_3	11.1	11-36
	O_3	5.86	11-44
	CO_2	9.70	11-36
	H_2	71.0	11-36
	O_2	1.93	11-36
	N_2	2.00	11-36
	Ar	0.385	11-44
(001,100) → (010)	O_3	17.2	11-44
	Ar	1.08	11-44
(010) → (000)	O_3	8.79	11-44
(001) ↔ (100)	O_2, N_2	>490	11-36
(001)+(100) → (101)+(000)	CO_2, O_3		

$$Me + O_2 + M \rightarrow MeO_2 + M, \qquad (11\text{-}24)$$

are expected to participate in the formation of metal monoxides and dioxides, respectively. These oxides may be formed with vibrational excitation, to a degree depending partially on the exothermicity of Reactions 11-23 and 11-24 for specific metals. It is noteworthy that even the endothermic oxide-forming reaction

$$Fe + O_2 \rightarrow FeO + O, \qquad (11\text{-}25)$$

the only such case for which data are available, evidently has a pre-exponential factor close to the gas kinetic cross-section, and an activation energy approximating the endothermicity of the reaction (Reference 11-24). Tables 11-6 and 11-7 summarize reaction rate data for some of the more significant metal oxide species.

11.5.1 Direct Infrared Radiative Excitation

For the earth to be in radiative equilibrium with the sun it must radiate at the same rate as a 250 K blackbody. The spectra shown in Figures 11-4 and 11-5 indicate that, as sensed at high altitude, the effective radiating temperature is spectrally dependent. Valleys occur in its spectral emission pattern wherever the stronger absorption

Table 11-6. Metal oxide rate constants at 300 K.

$Fe + O_2 \rightarrow FeO + O$	$\sim 1.0 \times 10^{-16}$ a
$FeO + O \rightarrow Fe + O_2$	3.3×10^{-11} a
$Fe^+ + O_2 + X \rightarrow FeO_2^+ + X$	$\sim 1.0 \times 10^{-30}$ b
$Mg^+ + O_2 + X \rightarrow MgO_2^+ + X$	$\sim 2.5 \times 10^{-30}$ b
$MgO^+ + O \rightarrow Mg^+ + O_2$	$\sim 1.0 \times 10^{-10}$ a
$Si^+ + O_2 \rightarrow SiO^+ + O$	8.0×10^{-6} a
$SiO^+ + O \rightarrow Si^+ + O_2$	$\sim 2.0 \times 10^{-10}$ a
$Th^+ + O_2 \rightarrow ThO^+ + O$	6.0×10^{-10} a
$Ti^+ + O_2 \rightarrow TiO^+ + O$	5.0×10^{-10} a
$U^+ + O_2 \rightarrow UO^+ + O$	8.5×10^{-10} a
$UO^+ + O_2 \rightarrow UO_2^+ + O$	2.0×10^{-9} a
$Al + O_2 \rightarrow AlO + O$	$\sim 1.0 \times 10^{-13}$ a

Notes:

[a] units $ml/mol\text{-}sec$

[b] units $ml^2/mol^2\text{-}sec$

Abstracted from Reference 11-46.

Table 11-7. Metal oxide cross sections at 300 K (cm^2).

$U + O \rightarrow UO^+ + e$	1.6×10^{-15}
$Th + O \rightarrow ThO^+ + e$	1.0×10^{-15}
$Ti + O \rightarrow TiO^+ + e$	4.5×10^{-15}
$U + O_2 \rightarrow UO_2^+ + e$	1.7×10^{-17}
$U + O_3 \rightarrow UO^+ + e + O_2$	2.0×10^{-16}
$Th + O_3 \rightarrow ThO^+ + e + O_2$	4.0×10^{-16}

Abstracted from Reference 11-47.

bands of infrared-active atmospheric gases occur. The spectral distribution of blackbody isothermals between 200 and 300 K are also indicated in Figures 11-4 and 11-5. Figure 11-12 compares the irradiance of the quiet sun at the top of the atmosphere with that of 250 and 300 K blackbodies. From approximately the vicinity of 5 μm to longer wavelengths the earthshine appears to be the more important source for pumping vibrational excitation. Among the entries in Table 11-1, the metal oxides are most susceptible to this source of excitation, since their fundamentals tend to fall near the peak of the earthshine irradiance spectrum.

In an irradiated volume of the atmosphere, the fraction of optically active molecules that are excited per second is (Reference 11-4):

$$F = \frac{N_{ex}}{N} \simeq 1.87 \times 10^{-5} \lambda^3 R_\lambda S, \qquad (11\text{-}26)$$

where

λ = the wavelength

R_λ = irradiance incident upon the volume of the vibrational absorption band; i.e., earthshine (watts $cm^{-2}\mu m^{-1}$),

S = integrated band strength of the transition ($cm^{-2}atm^{-1}$).

Assuming the entire volume to be optically thin to the incident radiation, the excitation rate along a line of sight through an atmospheric volume is FN_{col} excitations sec^{-1} cm^{-2}, where N_{col} is column density (cm^{-2}) of the molecular species under consideration.

Since the Einstein coefficient A of typical metal oxides is of the order of 5-10 sec^{-1} (Table 11-1), the rate constant for a quenching process such as

$$MeO(v=1) + M \rightarrow MeO(v=0) + M \qquad (11\text{-}27)$$

would have to be of the order of 10^{-12} cm^3 sec^{-1} for collisional quenching to be competitive with spontaneous radiation at altitudes about 100 km. However, quenching rate constants of this magnitude are not expected; therefore the radiative excitation rate is generally likely to be the emitted radiation rate.

11.5.2 Fluorescence Excitation

It appears that for many metal monoxides significant rates of vibrational excitation can be achieved by solar-induced fluorescence. The typical MeO has an accessible upper electronic state MeO(A), such that the wavelengths of the $\Delta v=0, +1, +2$ sequence in the MeO(A) $\leftrightarrow$

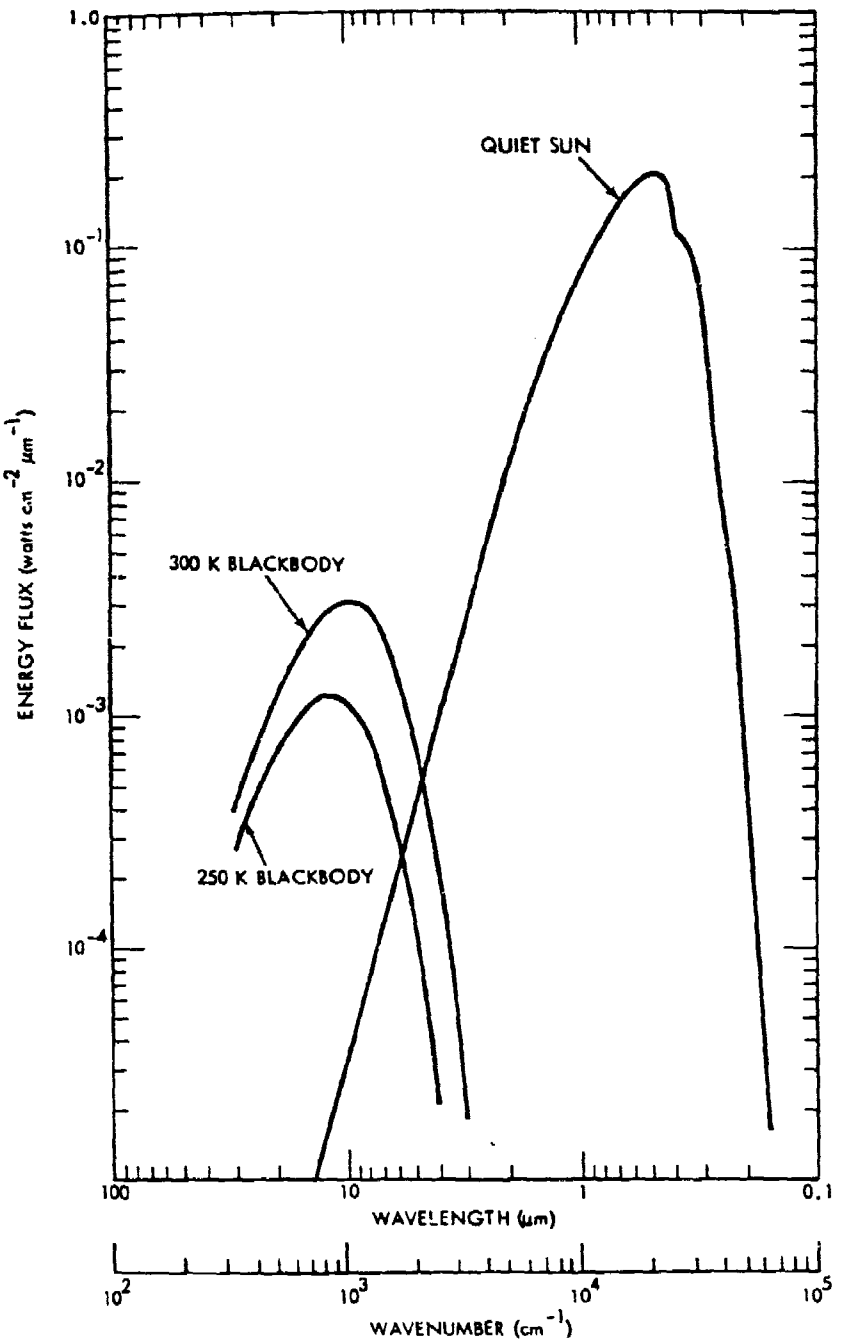

Figure 11-12. Irradiance at the top of the atmosphere, for quiet sun and two blackbody sources.

MeO(X) transition occur at or near the broad maximum of the solar continuum, viz., 3500-7500 Å. Groups of transitions of the following types:

$$MeO(X,v''=0) + h\nu \rightarrow MeO(A,v') \; ; \tag{11-28}$$

$$MeO(A,v') \rightarrow MeO(X,v''>1) + h\nu_f, \; (\nu_f > \nu_s); \tag{11-29}$$

where

s = solar

f = fluorescence,

are effective in populating upper vibrational levels in ground electronic state MeO(X). The normalized rate of MeO(X)→MeO(A) transitions in this case is

$$\frac{d\,[MeO(A)]\,/dt}{[MeO]} = 1.87 \times 10^{-5}\, R\lambda_e S_e\, \lambda^3 \; sec^{-1}, \tag{11-30}$$

where λ_e is the "center wavelength" (μm) of the MeO(A)↔MeO(X) electronic transition, S_e is the integrated intensity ($cm^{-2}atm^{-1}$) of the same transition, and $R\lambda_e$ is the solar irradiance (watts $cm^{-2}\mu m^{-1}$) upon the atmosphere at λ_e. Relationship 11-30 is an approximate one because, for simplicity, all v'↔v" transitions are treated together in this calculation. In reality, λ_e, S_e, and $R\lambda_e$ all depend to some extent on the exact vibrational transition involved. With a careful choice of λ_e, the foregoing calculation is good to better than a factor of two.

In order for this process to be important, MeO(A) ↔ MeO(X) must be an allowed transition; then the radiative lifetime of MeO(A) is small enough that collisional quenching can be ignored at the altitudes of interst.

To a first appoximation, the mean number of vibrational quanta excited in MeO(X) by the fluorescence process is simply a function of the Franck-Condon factors $q_{v'v''}$ governing the electronic transition:

$$\bar{v}'' = \sum_{v'} q_{v'o} \sum_{v''} q_{v'v''}v''. \tag{11-31}$$

Neglecting collisional quenching, the normalized rate of infrared emission due to solar fluorescence is

$$\frac{d[hn(1,0)]/dt}{\{MeO\}} = 1.87 \times 10^{-5}\, \lambda_e^3 S_e R\lambda_e \sum_{v'} q_{v',O} \sum_{v''} q_{v'v''}v'' \tag{11-32}$$

and in the case of AℓO,

$$\frac{d[h\nu(1.04\ \mu m]/dt}{AlO} = 0.06\ sec^{-1}\ . \qquad (11\text{-}33)$$

The numerical result of Equation 11-33 is based on an f-value of 0.014 for the AlO(B)↔AlO(X) transition. DNA is currently supporting research directed toward establishing comparable quantities for UO^+ and UO_2^+.

Metal oxides are not the only species of interest that can achieve significant excitation rates through fluorescence mechanisms. Bortner et al. (Reference 11-48) have compared various radiative and collisional excitation mechanisms involving atmospheric nitric oxide, and have described in detail the calculation of solar infrared, solar electronic, and earthshine infrared radiation rates for that species. A further example may be found in Reference 11-49 where, to account for the daytime 4.3-micron CO_2 limb radiance, the contribution of Δv_3=1 transitions originating in levels (101) and (021) had to be considered. The respective upper states are populated by absorption of solar infrared at 2.70 and 2.77 microns.

11.6 THE MARKOV PHENOMENON

A group consisting of M.N. Markov and various collaborators in the Lebedev Institute over the years has reported observation of "layers" of unaccountably bright infrared emission at altitudes up to 400 km (Reference 11-50). As time progressed, their instrumentation improved from extremely broad band radiometers to a rapid scanning prism-based spectrometer flown on Salyut 4. The latter results are troubled by frost absorption effects and a large "null" signal, but taken at face value they are evidence of a fairly narrow emission feature (approximately 0.25 micron), centered near 5.2 microns, in the sunlit atmosphere above 140 km. They are inclined to attribute the signal to nitric oxide radiation. In Reference 11-51 they discuss multiquantum rotational relaxation with specific application to nitric oxide formed in the $N(^2D) + O_2$ reaction. If the spectral results of Markov et al. are correct, then the known (Table 11-4) radiative consequences of the named reaction cannot account for their observation, which is severely deficient at longer wavelengths; i.e., where NO(v>1) would radiate. The Salyut 4 results presented relate only to measurements made on a single orbital pass and it is not known, for instance, what might have been observed from the unilluminated atmosphere by their instrument, or how often that instrument was exercised.

When discussing their results, the Lebedev group has also mentioned the isotopic species $N^{14}N^{15}$ as a potential radiator in the 4.3-micron region (in addition to NO^+ and CO); the suggestion is an interesting one and should be looked into.

11.7 RADIATIVE PROCESSES IN LOW-DENSITY PLASMAS*

For atmospheric plasmas of low density ($<10^{11}$ cm^{-3}) and moderate temperature (<10,000 K), basically four processes exist that need to be considered in computing the emissivity for wavelengths comparable to or longer than those in the visible region of the spectrum, viz., ion and neutral Bremsstrahlung, and radiative and collisional-radiative recombination. The present discussion is limited to theoretical techniques used to evaluate the emissivities due to these processes.

Although omitted from consideration here, certain other processes may be important in specific instances. For example, in an oxygen plasma, electron attachment to the neutral atom to form O^- must be taken into consideration for wavelengths of the order of 7500 Å or shorter.

11.7.1 Ionic Bremsstrahlung and Radiative Recombination (Free-Free and Free-Bound Emission)

The rate of emission for both of these processes may be calculated exactly for electrons scattered by or recombining with hydrogenic ions (Reference 11-52). For practical calculations it is convenient to use the semiclassical expressions due to Kramers (Reference 11-53) for the emission rates for both processes, and to express deviations from the semiclassical results in terms of Gaunt factors which depend on the frequency of emission. A full treatment of the problem along these lines has been given by Griem (Reference 11-54) and the frequency dependence of the Gaunt factors has been studied by Karzas and Latter (Reference 11-55). In the spectral range considered here, the Gaunt factors can be taken as unity. With this assumption and a Maxwellian distribution of electron velocities the emission rate per unit frequency range for both processes is given by the simple frequency-independent expression (Reference 11-56):

$$\varepsilon\nu = \frac{32\pi^2 e^6}{c^3 (6\pi m)^{1.5}} \frac{n_e n_i}{(kT)^{0.5}}, \qquad (11\text{-}34)$$

or in practical units by:

$$\varepsilon_\lambda = \frac{1.63 \times 10^{-31} \, n_e n_i}{\lambda^2 T^{0.5}} \text{ watts cm}^{-3} \text{ ster}^{-1} \mu\text{m}^{-1}, \qquad (11\text{-}35)$$

where the wavelength λ is expressed in μm, the electron and ion densities n_e and n_i in cm^{-3}, and the temperature in K.

---

*The authors are indebted to J.W. Cooper of the National Bureau of Standards for this section.

Despite the simplicity of these relationships, they are expected to provide an adequate first-order treatment of emissivity for most plasmas in the range of wavelengths, temperatures, and electron densities considered here. Deviations from Equation 11-35 owing to the use of unit Gaunt factors are not expected to lead to serious errors for wavelengths longer than those in the visible region. For example, Anderson and Griem (Reference 11-57) have investigated the deviations to be expected for helium plasmas at 20,000 K and find less than 10 percent discrepancies for wavelengths longer than 5,000 Å. Equation 11-35, or the more complicated expressions including Gaunt factors given by Griem (Reference 11-54), can be corrected in the case of non-hydrogenic plasmas, by multiplying by a temperature and wavelength-dependent factor (Reference 11-58). Such computations have been carried out for rare-gas plasmas and for oxygen and nitrogen (References 11-54, 11-55). The results for argon (Reference 11-59) at 8,000 and 16,000 K show deviations of greater than a factor of two in the visible region of the spectrum and deviations of the order of 10 percent or less for 1-μm wavelengths.

At shorter wavelengths and/or at lower temperatures, Equation 11-35 may not be adequate if the detailed wavelength dependence is needed, since in these circumstances the equation smooths out the variations -- actually somewhat jagged -- caused by the discrete nature of the bound levels. In such cases the contribution of free-free transitions and of recombination to each bound level must be estimated separately (Reference 11-60). A systematic procedure for carrying out calculations of this type has been described by Griem (Reference 11-54). The emissivity for recombination into a particular level $n\ell$ at frequency ν (sec^{-1}) is expressed as:

$$\varepsilon_\nu = \frac{4\pi^{1.5}h^5\ {}^3\sigma_{n\ell}(\nu)}{(mec)^2}\ \frac{g_{n\ell}}{g_{ion}}\ n_e n_i\ \frac{(E_{n\ell} - h\nu)}{(kT)^{2.5}}\ ,\ (h\nu > E_{n\ell}), \quad (11\text{-}36)$$

where $g_{n\ell}$ and g_{ion} are the statistical weights of the recombining level $n\ell$ and the ionic ground state, respectively, and $E_{N\ell}$ is the binding energy of level $n\ell$. The quantity $\sigma_{n\ell}(\nu)$ is the cross-section for photoabsorption for an initial state $n\ell$, the inverse process of recombination. These cross-sections may be estimated by quantum-defect methods (D. Sappenfield, private communication). For most purposes it is adequate to do this for only the lowest excited states to which recombination is allowed and to use the relationship pertaining to hydrogenic species:

$$\sigma_{n\ell} = \frac{64\ e^2}{3^{1.5}\hbar c}\left(\frac{E_{Ryd}}{h\nu}\right)^3\ \frac{\pi a_o^2\ g_n(\nu)}{n^5} \quad (11\text{-}37)$$

for higher levels.

If Equation 11-36 is used for the free-bound emissivity, the free-free emissivity must be estimated separately. This is given by the Kramers relation (Reference 11-61):

$$\epsilon_{ff} = \frac{32\pi^2 e^6 n_e n_i \exp(-h\nu/kT)}{c^3(6\pi m)^{1.5}(kT)^{0.5}} \quad , \tag{11-38}$$

or alternatively in practical units as:

$$\epsilon_{ff} = \frac{1.63 \times 10^{-31} n_e n_i \exp(-1.44 \times 10^4/\lambda T)}{\lambda^2 T^{0.5}} \tag{11-39}$$

watts cm^{-3} $ster^{-1}$ μm^{-1}, by analogy with Equations 11-34 and 11-35, respectively. Using this approach, detailed calculations of the emissivities of oxygen plasmas have been carried out by Sappenfield (private communication). Some of his results, at three different temperatures, are presented in Figures 11-13 through 11-15. For wavelengths longer than 1 μm, Equation 11-35 is probably adequate for most practical applications.* For example, Sappenfield's results deviate no more than 10 percent from those calculated using Equation 11-35 for wavelengths of 10 μm in the 500-6,000 K temperature range.

1.7.2 Neutral Bremsstrahlung

Calculations of neutral Bremsstrahlung are generally more difficult to perform than the analogous calculations for ions, for two reasons. First, the simplest case, viz.:

$$e + H \rightarrow e + H + h\nu \quad , \tag{11-40}$$

involves a two-electron problem, so that an accurate analytic theory cannot be given as in the case of positive-ion Bremsstrahlung.

Second, since negative ions possess at most a few bound states, quantum-defect methods cannot be used to compute the recombination emissivity if negative-ion formation is possible.†

Quantum-mechanical calculations of neutral Bremsstrahlung or the related free-free absorption process for hydrogen have been carried out (References 11-62 through 11-64), and the results are reported in a study of the emissivity of LTE hydrogen plasma (Reference 11-65). Among the species important in air chemistry, detailed calculations have been carried for atomic nitrogen and oxygen by Mjolsness and Ruppel (Reference 11-66). Using the assumption that the emission rate is proportional to the final electron velocity, they derive an equation for the emissivity:

$$\epsilon_\lambda = 2.402 \times 10^{-31} \sigma_o n_e n_i \theta^{-3.5} (u+2)u^2 \exp(-u) \tag{11-41}$$

---

*Equations 11-34 and 11-35 are valid only for frequencies well above the plasma frequency. For a discussion of the problem for extremely long wavelengths, see Reference 11-52, pp. 121 ff.

†Recombination to form negative ions is not considered here.

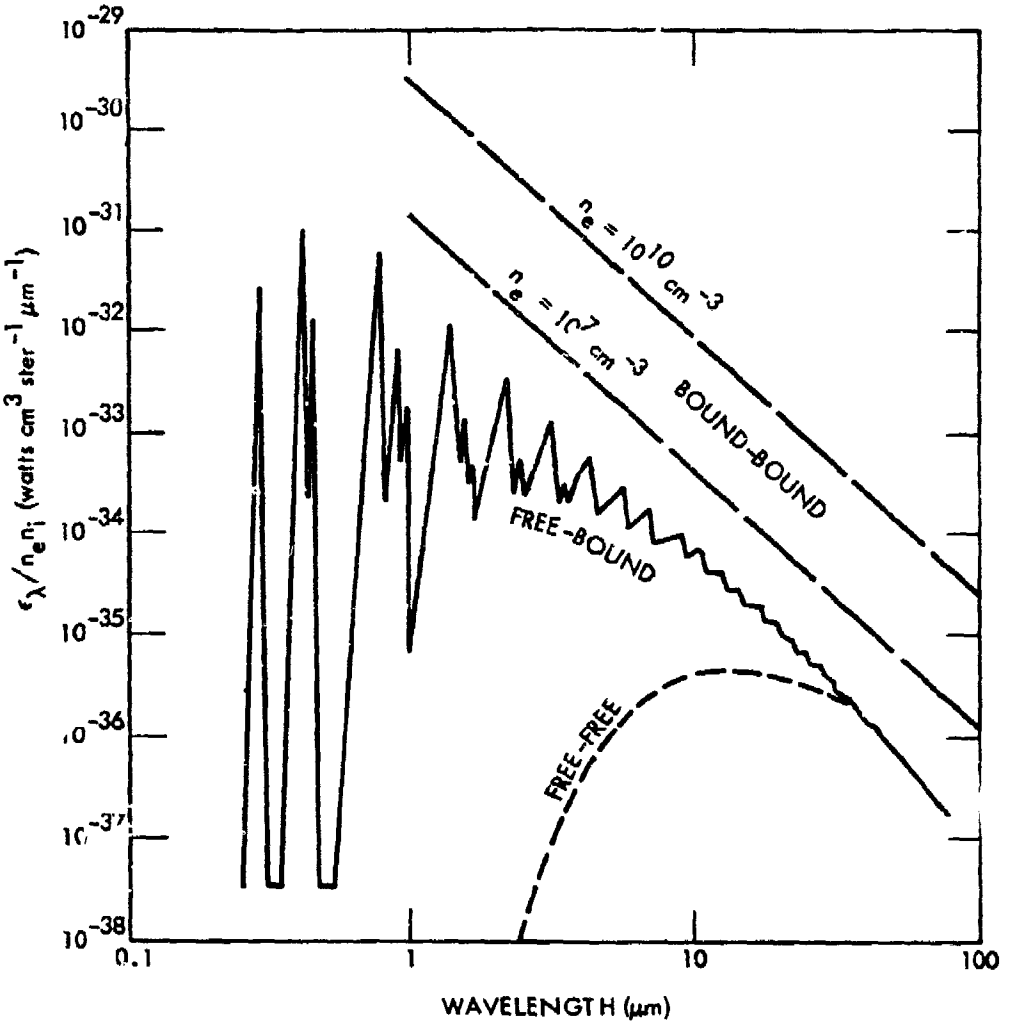

Figure 11-13. Calculated emissivities of oxygen plasma at 500 K (D. Sappenfield, private communication)

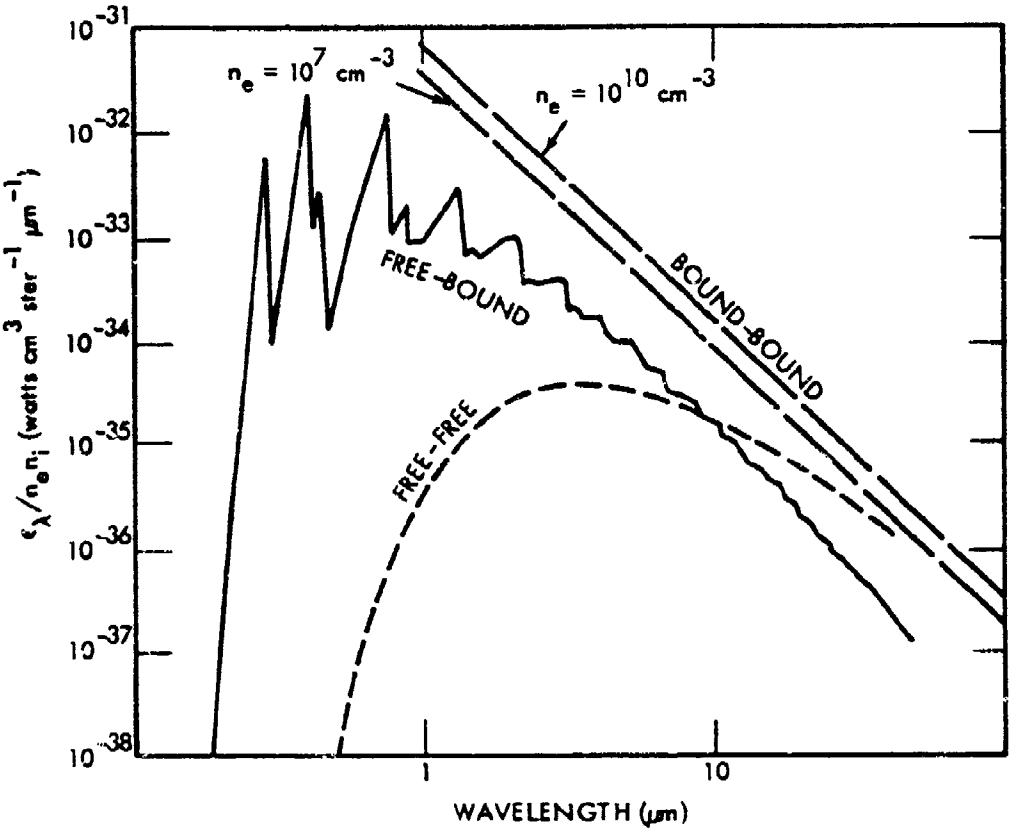

Figure 11-14. Calculated emissivities of oxygen plasma at 2,000 K (D. Sappenfield, private communication).

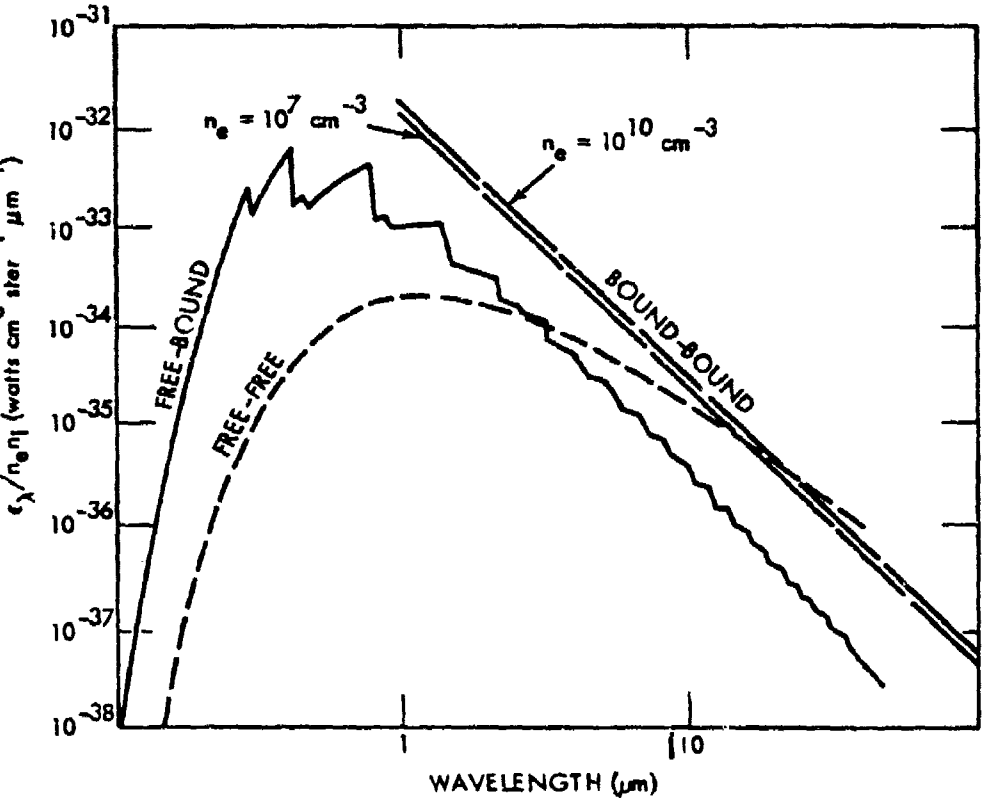

Figure 11-15. Calculated emissivities of oxygen plasma at 6,000 K (D. Sappenfield, private communication).

watts cm^{-3} $ster^{-1}\mu m^{-1}$, where $\theta=5,040/T$, $u=2.855\theta/\lambda$, and σ_o is a constant which for atomic oxygen and nitrogen has values of 7.1×10^{-7} and 8.0×10^{-7}, respectively. The accuracy of Equation 11-41 is difficult to assess since little work of comparable sophistication has been done for neutral low-energy Bremsstrahlung (see, however, Reference 67). Equation 11-38 is probably accurate to better than a factor of three for wavelengths shorter than 1 μm within the electron-energy and temperature ranges considered here, and should be more accurate at longer wavelengths. It should provide only order-of-magnitude estimates at shorter wavelengths and lower temperatures.

No calculations starting from first principles have been carried out for free-free emission involving molecules. A simplified expression relating the emission rate to the product of momentum-transfer cross-section times the initial electron energy has been derived semiclassically by Zel'dovich and Raizer (Reference 11-68) and has been used in the computation of emission from both atoms and molecules (References 11-66, 11-69, and private communication with D.H. Holland, M. Scheibe, C.H. Humphrey, D.R. Churchill, G. Gioumousis, and L.M. Tannenwald). The same result can be obtained through a consideration of the asymptotic representation of the quantum-mechanical expression for the Bremsstrahlung rate (Reference 11-70 and private communication with S. Geltman, Joint Institute for Laboratory Astrophysics). Such asymptotic representation shows further that the correct form for the Bremsstrahlung rate is:

$$\frac{dq}{d\upsilon} = \frac{4e^2}{3c^3}\left[E_i\sigma_m(E_f) + E_f\sigma_m(E_i)\right] \quad . \qquad (11\text{-}42)$$

which reduces to Zel'dovich and Raizer's result (Reference 11-68) when $E_i \approx E_f$) where E_i and E_f are, respectively, the initial and final electron energies, and σ_m is the momentum-transfer cross-section. Provided the Bremsstrahlung rate is not seriously affected by resonance effects,* the emissivity for all air species may be calculated using Equation 11-42, or its long-wavelength limit, from measured or calculated momentum-transfer cross-sections. This has been done by Kivel (Reference 11-69) for both atomic and molecular oxygen and nitrogen. The accuracy of this procedure was investigated experimentally by Taylor and Caledonia (Reference 11-71), who found agreement within a factor of about ten.

11.7.3 Collisional-Radiative Recombination

In a recombining plasma, the rate of recombination is determined by radiative recombination (free-bound processes) only if the electron density is sufficiently low that electron-atom collision processes can be neglected. In the range of temperatures and electron

*Resonance effects greatly enhance the probability of vibrational excitation by electron impact at electron energies below three electron volts for both N_2 and O_2. See Reference 11-74. The effect on emissivities has not been explored.

densities considered here, the rate of recombination is considerably enhanced owing to the effect of such collisions. The emissivity of a recombining plasma is also enhanced, since in the recombination process a quasi-equilibrium distribution of excited atomic states occurs that emits via decay to lower states (bound-bound emission). Calculations of the emissivity due to this process therefore depend on estimates of the population of excited states in the recombining plasma. A procedure for estimating the excited-state population has been given by Bates, Kingston, and McWhirter (References 11-72, 11-73). This procedure consists of setting up rate equations to describe the population changes among neutral atomic levels that occur as a result of electron excitation or deexcitation and radiative decay. Three assumptions are made in the solution of these equations: the populations of highly excited levels above some large principal quantum number are assumed to be in Saha equilibrium with the plasma; either all the radiation emitted in the decay process is assumed to escape from the plasma or it is assumed optically thick in strong (resonance-line) transitions; and neutral collision processes are neglected.

Detailed calculations of emissivities due to bound-bound transitions in recombining plasmas have been carried out only for hydrogen (D. Sappenfield, private communication), oxygen and nitrogen (D. Sappenfield, private communication), and helium plasmas (Reference 11-75). The results for oxygen, illustrated in Figures 11-13 through 11-15, indicate that at low temperatures (<6000 K) the bound-bound emission is probably the most intense type of radiation in a recombining plasma.

The accuracy of calculations of bound-bound emissivities cannot be estimated easily, since the coefficients of the rate equations that determine the excited neutral populations are obtained from theoretical calculations of uncertain accuracy. Indirect evidence of the validity of the calculations for oxygen and helium plasmas has been obtained by comparing the results with experimentally determined level populations. M. Peck and D. Sappenfield (private communication) have compared level populations computed for an oxygen plasma with those obtained from visible observations of a nuclear event. They found good agreement in the relative populations obtained by both methods. Johnson and Hinnov (Reference 11-75) have applied the same procedure to a helium plasma and compared calculated results with the observed level populations obtained by emission of light in a helium afterglow. They found it necessary to modify considerably the classical electron collision cross-sections in order to obtain agreement with the level populations determined experimentally.

Among the foregoing three assumptions, that relating to Saha equilibrium was checked by varying the quantum-number level above which it was assumed that Saha equilibrium prevails. No appreciable error was noted thereby. In addition, alternative calculations were carried out, assuming the plasma to be either transparent or opaque to resonance radiation (References 11-72, 11-73). Considerable

deviations in the populations of low-lying states occurred as a result of these alternative treatments. Finally, the effect of neutral collisions on emissivity has been studied theoretically by Collins (Reference 11-76), but has not been investigated experimentally.

11.8 CONCLUSIONS

Atmospheric radiative processes are directly related to the overall chemistry, in both the normal and disturbed atmospheres. At low altitudes the mechanism of T-V energy transfer is fast enough to maintain LTE vibrational populations of ambient infrared-active species, and therefore thermal radiation is dominant. Thus for any given emitter the important unknown is the profile of its mixing ratio. Somewhere above 70 km the collision frequency drops to a value low enough that LTE is no longer preserved. At about the same altitude, other excitation processes besides T-V energy transfer become important. These include: V-V processes such as the excitation of CO_2 by N_2^+ (Equation 11-12); a wide variety of possible chemiluminescent reactions; and fluorescence due to sunshine or earthshine.

In low-density plasmas, the important processes include neutral and ionic Bremsstrahlung (free-free emission), radiative recombination (free-bound emission), and line emission (bound-bound emission) due to collisional-radiative recombination. In atmospheric plasmas below 6000 K the bound-bound emission probably dominates.

Much remains to be done, both to understand the phenomenology of normal and perturbed atmospheric radiative processes, and to develop soundly based and accurate methods for calculating the emissivity of low-density plasmas.

APPENDIX I: BAND SHAPES AND BAND WIDTHS

The shape and width of a given band depend on its rotational temperature, which is usually related in turn to the local kinetic temperature. The number of bands contributing radiation depends on the effective vibrational temperature. These points are illustrated in Figures 11-16 through 11-19, for the spectrum of CO, in the range 4.30-5.30 μm. A rough approximation to the width of a particular emission band may be taken as the distance between the peaks of the P and R branches. It can be shown that the width thus defined is:

$$\Delta\nu \simeq 2.35(BT_{rot})^{0.5}\text{cm}^{-1}, \qquad (11\text{-}43)$$

where B is the rotational constant of the emitting state and T_{rot} the rotational temperature. The band origin of the (1-0) transition as given in Table 11-1 is at:

$$\nu_o = \omega_e - 2\omega_e x_e \text{cm}^{-1}\ , \qquad (11\text{-}44)$$

where ω_e and $\omega_e x_e$ are, respectively, the vibrational constant and the first anharmonic correction term. Succeeding band origins of (2-1), (3-2), etc., are displaced by $v(2\omega_e x_e)$ cm^{-1} where v is the vibrational quantum number of the lower state. The ν_o and B data in Table 11-1 are adequate for rough calculations of both band location and band width. For polyatomic species, which have more than one rotational constant, the one given in Table 11-1 is the largest value for the species.

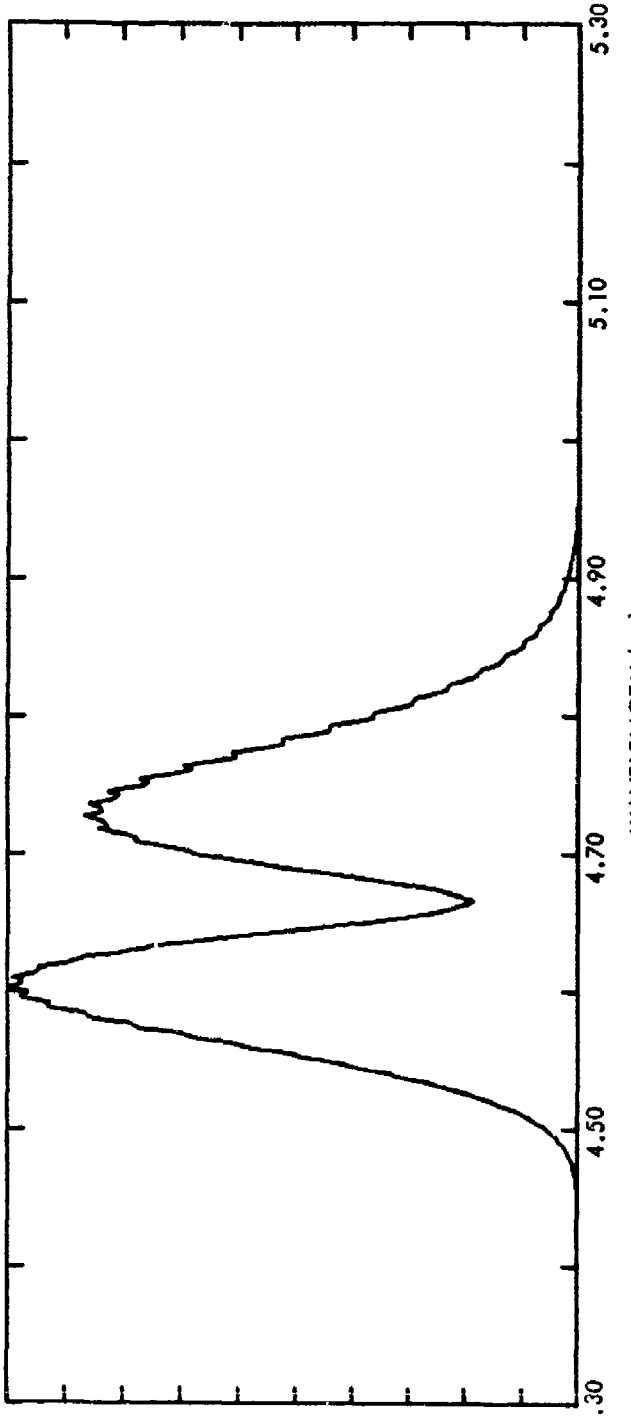

Figure 11-16. CO spectral band shapes in the 4.30-5.30 μm range (vibrational temperature = 300 K; rotational temperature = 300 K).

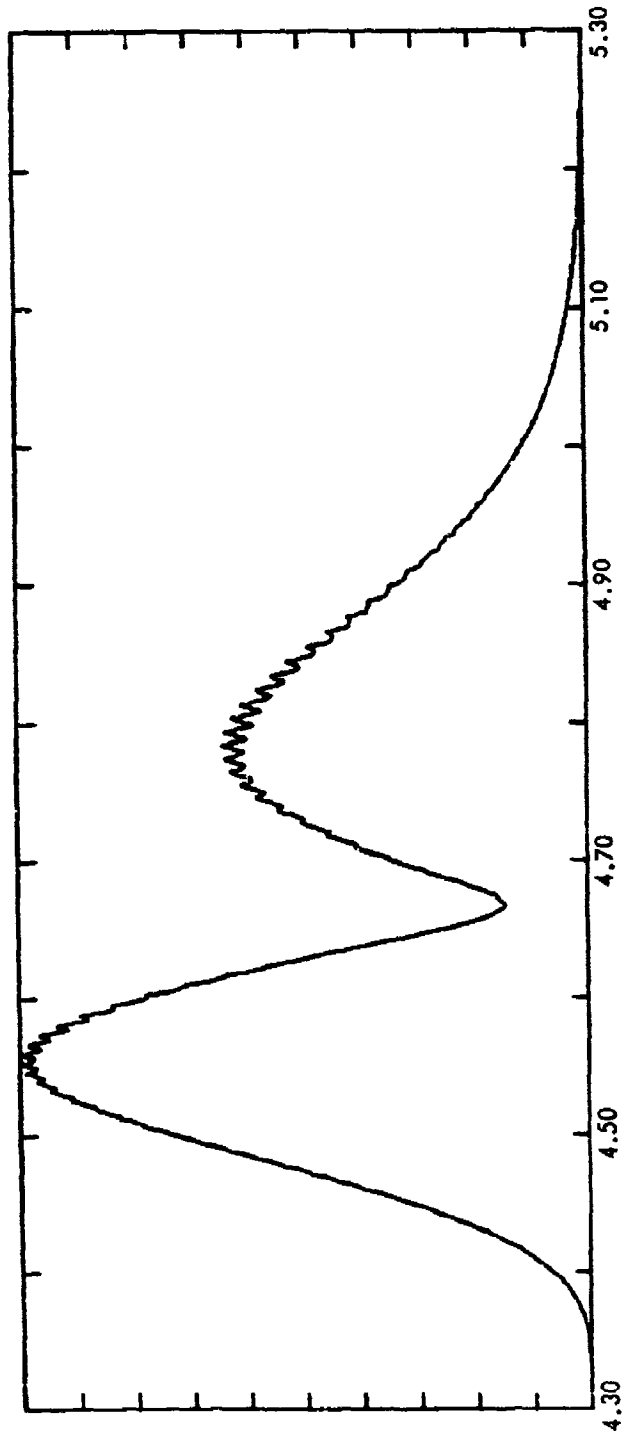

Figure 11-17. CO spectral band shapes in the 4.30-5.30 μm range (vibrational temperature = 1000 K; rotational temperature = 1000 K).

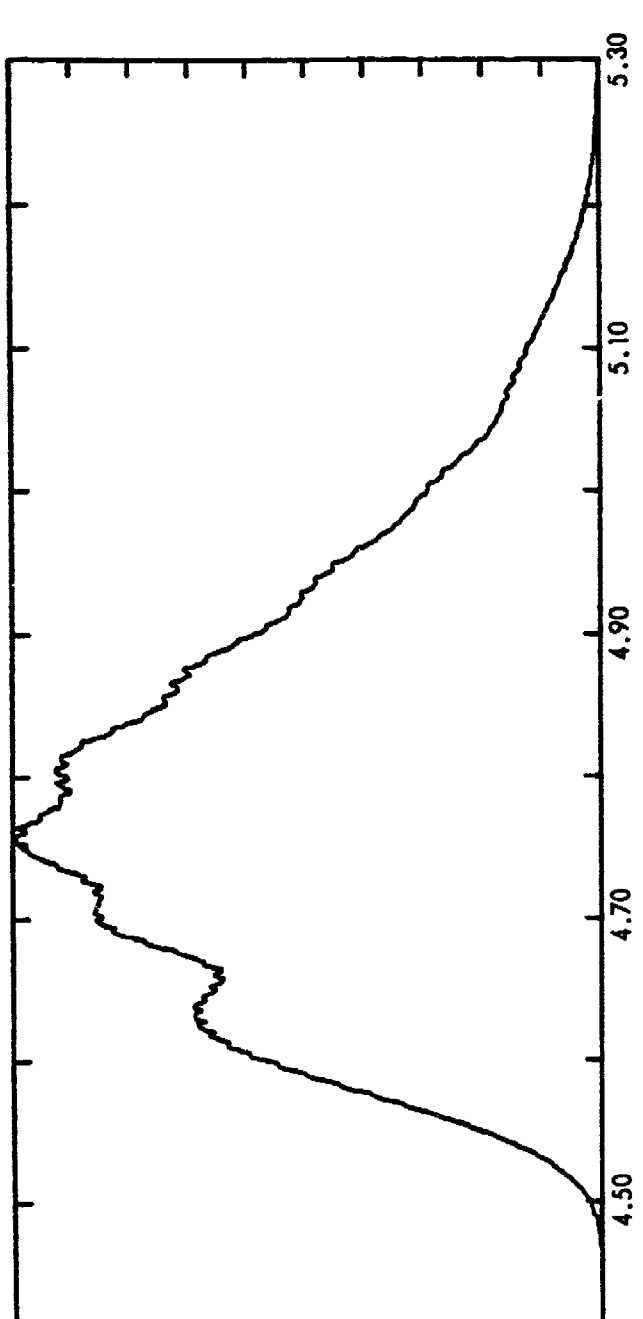

Figure 11-18. CO spectral band shapes in the 4.30-5.30 μm range (vibrational temperature = 5000 K; rotational temperature = 300 K).

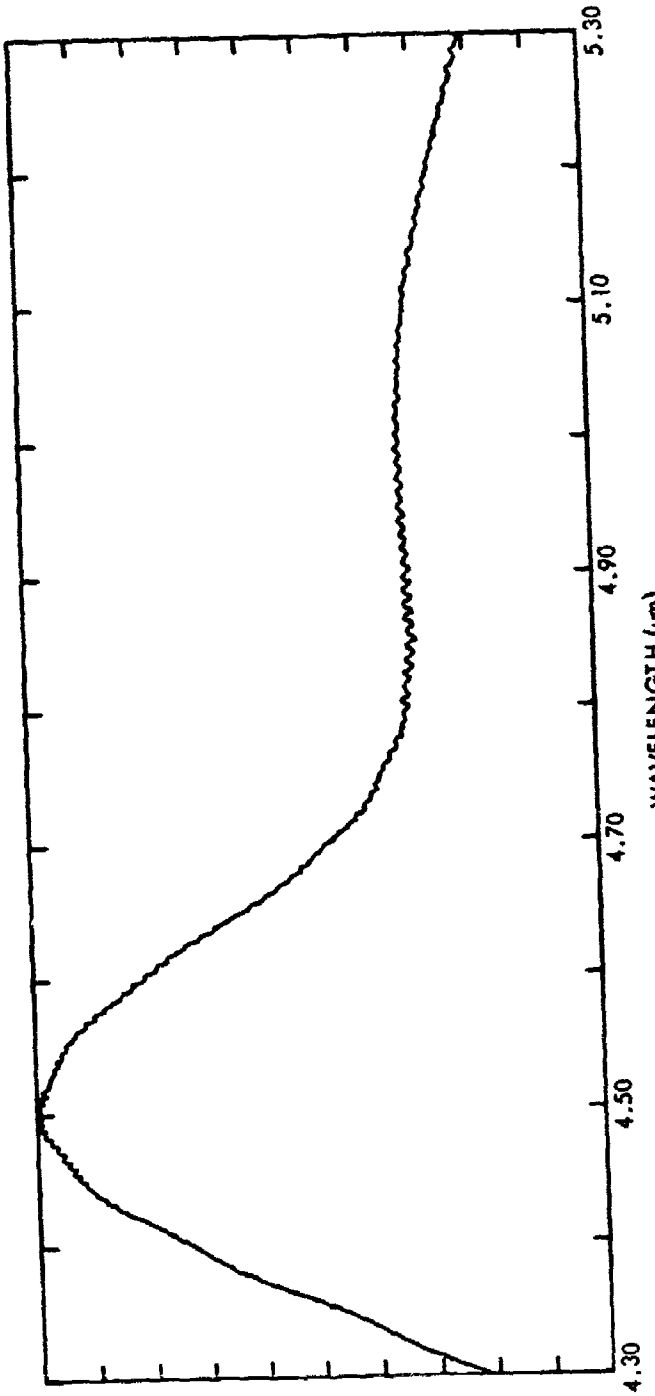

Figure 11-19. CO spectral band shapes in the 4.30-5.30 μm range (vibrational temperature = 5000 K; rotational temperature = 5000 K).

APPENDIX II: INFRARED EMISSION RELATIONSHIPS

Following are definitions, equations, and conversion factors and constants that are useful in calculating infrared emission rates of gases:

A. Definitions

S (cm^{-2} atm^{-1})	Integrated bandstrength of a transition
S_e (cm^{-2} atm^{-1})	Bandstrength of an electronic transition
f	Oscillator strength or "f-value" of a transition
N_{col}(cm^{-2})	Column density of a radiating species
λ_μ(μm)	Wavelength of a transition
A (sec^{-1})	Einstein spontaneous radiative transition probability
B (watts cm^{-2} $ster^{-1}$ μm^{-1})	Surface brightness of a radiating volume
$R_{\lambda\mu}$ or $R_{\lambda\mu e}$(watts $cm^{-2}\mu m^{-1}$)	Irradiance falling upon a surface from either earthshine or sunshine, respectively.
F	Fraction of molecules in an irradiated column excited per second under the influence of sunshine irradiance

B. Equations

$$S = 0.357\ \lambda_\mu^2 A = 2.38 \times 10^7 f$$

$$h\nu = 1.98 \times 10^{-19}\ \lambda_\mu^{-1}\ \text{watt-sec photon}^{-1}$$

$$F = 1.87 \times 10^{-5}\ \lambda_\mu^3\ R_{\lambda\mu e}\ S$$

$$F \times N_{col} = \text{excitation rate along a line of sight}$$

$$B = F\, N_{col}\, h\nu/4\pi = 2.94 \times 10^{-25} \lambda_{\mu}^{2}\, R_{\lambda\mu e}\, S\, N_{col},$$

in the absence of quenching

C. Conversion Factors and Constants

$$\lambda(\mu m) = 10^{4}/\tilde{\nu}(cm^{-1})$$

$$\tilde{\nu}\ (cm^{-1}) = 10^{4}/\lambda\ (\mu m)$$

$$\Delta\lambda\ (\mu m) = 10^{4}\ \Delta\tilde{\nu}\ (cm^{-1})/(\tilde{\nu}\ cm^{-1})^{2}$$
$$= 10^{-4}\ \lambda^{2}\ (\mu m)\ \Delta\tilde{\nu}\ (cm^{-1})$$

$$\Delta\tilde{\nu}\ (cm^{-1} = 10^{4}\ \Delta\lambda\ (\mu m)/(\lambda(\mu m))^{2}$$

$$1 \text{ erg} = 1.986 \times 10^{-16}\ cm^{-1}$$

$$[\text{photons/sec}] \times \frac{1.986 \times 10^{-19}}{\lambda(\mu m)} = \text{watts}$$

$$\text{ergs/sec} \times 10^{-7} = \text{watts}$$

$$\text{Loschmidt's No.} = 2.687 \times 10^{19}\ cm^{-3}$$

$$\text{Boltzmann's constant} = 1.380 \times 10^{-16}\ \text{ergs/K}$$
$$= 0.695\ cm^{-1}/K$$

$$1\ cm^{-1} = 2.998 \times 10^{10}\ Hz$$

$$\text{Planck's constant} = 6.626 \times 10^{-27}\ \text{erg-sec}$$

REFERENCES

11-1. Huppi, E.R., J.W. Rogers, and A.T. Stair, Jr., Appl. Optics 13, 1466 (1974).

11-2. Stair, A.T., Jr., and H.P. Gauvin, in Aurora and Airglow, B.M. McCormac, Ed., Reinhold, New York, p 365 (1967).

11-3. Conrath, B.J., R.A. Hanel, V.G. Kunde, and C.J. Prabhakara, Geophys. Res. 75, 5831 (1970).

11-4. Penner, S.S., Quantitative molecular spectroscopy and Gas Emissivities, Addition-Wesley Publishing Co., Reading, Mass. (1959).

11-5. Kneizys, F.X., et al., "Atmospheric Transmittance/Radiance: Computer Code LOWTRAN 5," AFGL-TR-80-0067 (1980).

11-6. McClatchey, R.A., et al., "AFCRL Atmospheric Absorption Line Parameters Compilation", AFCRL-TR-73-0096 (1973), L.S. Rothman, et al., Appl. Optics 17, 507 (1978); L.S. Rothman, Applied Optics, in press.

11-7. Smith, H.J.P., et al., "Fascode -- Fast Atmospheric Signature Code", AFGL TR-78-0081.

11-8. Herzfeld, K.F., and T.A. Litovitz, Absorption and Dispersion of Ultrasonic Waves, Academic Press, New York (1959)

11-9. Callear, A.B., and J.D. Lambert, in Comprehensive Chemical Kinetics, C.H. Bamford and C.F.H. Tepper, Eds., Elsevier, New York (1969).

11-10. Taylor, R.L., and S. Bitterman, Rev. Mod. Phys. 41, 26 (1969); Taylor, R.L., Can. J. Chem., 52, 1436 (1974).

11-11. Breshears, W.D., and R. Bird, J. Chem. Phys. 48, 4768 (1968).

11-12. Kieffer, J.H., and R.W. Lutz, in Eleventh Symp. (Int'l) on Combustion Berkeley Ca, 1966, the Combustion Institute, Pittsburgh Pa, p 67 (1967) .

11-13. Degges, T.C., Appl. Optics 10, 1856 (1971).

11-14. O'Neil, R.R., W.R. Pendleton, Jr., A.M. Hart, and A.T. Stair, Jr., J. Geophys. Res. 79, 1942 (1974).

11-15. Kumer, J.B., HAES Report No. 57, DNA 4260F and references therein (October 1976).

11-16. Ogawa, T., Planet. Space Sci. 24, 749 (1976).

11-17. Chamberlain, J.W., Physics of the Aurora and the Airglow, Academic Press, New York (1961).

11-18. Shefov, N.N., Planet. Space Sci. 17, 797, 1629 (1969); Ibid. 19, 129 (1971).

11-19. Breig, E.L., Planet. Space Sci. 18, 1271 (1970); Krassovski, V.I., Ann. Geophys. 27, 211 (1971); Nicolet, M., Ann. Geophys. 26, 531 (1970).

11-20. Freedman, P.A., and W.J. Jones, J. Chem. Soc. Far. Trans. II 72, 207 (1976).

11-21. Anlauf, K.G., R.G. MacDonald, and J.C. Polanyi, Chem. Phys. Letts. 1, 619 (1968); Charters, P.E., R.G. MacDonald, and J.C. Polanyi, Appl. Optics, 10, 1747 (1971); Polanyi, J.C. and J.J. Sloan, Int. J. Chem. Kinetics Symposium No. 1, 1975.

11-22. Streit, G.E. and H.S. Johnston, J. Chem. Phys. 64, 95 (1976).

11-23. Cashion, J.K., J. Mol. Spect. 10, 182 (1963).

11-24. Mies, J.H., J. Mol. Spect. 53, 150 (1974).

11-25. Heaps, H.S., and G.Z. Herzberg, Physic 133, 48 (1952).

11-26. Fiocco, G., and G. Visconti, J. Atm. Ten. Phys. 36, 583 (1974).

11-27. Worley, S.D., R.M. Coltharp, and A.E. Potter, Jr., J. Phys. Chem. 76, 1511 (1972).

11-28. Worley, S.D., R.M. Coltharp, and A.E. Potter, Jr., J. Chem. Phys. 55, 2608 (1971).

11-29. Rogers, J.W., R.E. Murphy, A.T. Stair, Jr., J.C. Ulwick, K.D. Baker, and L.L. Jensen, J. Geophys. Res. 78, 7023 (1973).

11-30. Good, R.E., Planet. Space Sci. 24, 389 (1976).

11-31. Moreels, G., and M. Herse, Planet. Space Sci. 25 265 and references therein (1977).

11-32. Harrison, A.W., W.F. Evans, and E.J. Llewellyn, Can J. Phys. 49, 2509 (1971).

11-33. Dick, K.A., Planet. Space Sci. 25, 595 (1977) and V.I. Krassovsky et al., Planet. Space Sci. 25 596 (1977).

11-34. Rahbee, A., and J. Gibson, in press.

11-35. Whitson, M.E., L.A. Darnton, and R.J. McNeal, Chem. Phys. Lett. 41, 552 (1976).

11-36. Rosen, D.I., and T.I., Cool, J. Chem. Phys. 59, 6097 (1973); ibid., 62, 466 (1975).

11-37. Unpublished data, AFGL COCHISE facility.

11-38. Hochanadel, C.J., J.A. Ghormley, and J.W. Boyle, J. Chem. Phys. 48, 2416 (1968).

11-39. Riley, J.F., and R.W. Cahill, J. Chem. Phys. 52 3297 (1970).

11-40. Bevan, P.L.T., and G.R.A. Johnson, J. Chem. Soc. for Trans. I. 69, 216 (1968).

11-41. Kreuger, A.J., Science 166, 998 (1969).

11-42. Noxon, J.F., Science 168, 1120 (1970).

11-43. Von Rosenberg, C.W., Jr., and D.W. Trainor, J. Chem. Phys. 61, 2442 (1974); ibid, 63 5348 (1975).

11-44. Hui, K.K., D.I. Rosen, and T.I. Cool, Chem. Phys. Lett. 32, 141 (1975).

11-45. Von Rosenberg, C.W., Jr., and K.L. Wray, Avco Everett Research Laboratory, Report AFCRL-70-0597 (AD 716493) (1970).

11-46. Murad, E., AFGL TR-77-0235.

11-47. Fite, W.L., T.A. Patterson, and M.A. Siegel, AFGL TR-77-0030.

11-48. Bortner, M.H., R.A. Carabetta, and R.H. Kummler, General Electric Co., Report DASA 2560 (1970).

11-49. James, T.C., and J.B. Kumer, J. Geophys. Res. 78, 832 (1973).

11-50. Markov, M.N., Appl. Optics 8, 887 (1969); M.N. Markov, G.M. Grechko, and A.A. Gukarov, Preprint No. 8, Lebedev Physical Institute, retranslated by I.L. Kofsky, Photometrics HAES Memorandum PIC-72.

11-51. Gordiets, B.F., M.N. Markov, and L.A. Saburova, Opt. Spect. 41, 554 (1976).

11-52. Bethe, H.A., and E.E. Salpeter, Quantum Mechanics of One and Two Electron Systems, Section 78, Academic Press, New York (1957).

11-53. Kramers, H.A., Phil. Mag. 46, 836 (1923).

11-54. Griem, H.R., Plasma Spectroscopy, Chapter 5, especially Equations 5 through 26, McGraw-Hill, New York (1964).

11-55. Karzas, W.J., and R. Latter, Astrophys. J., Suppl. 55, 167 (1961).

11-56. Finkelnberg, W., and T. Peters, in Handbuch der Physik 28, p 97, S. Flugge, Ed., Springer-Verlag, Berlin (1957).

11-57. Anderson, A.D., and H.R. Griem, Proc. Sixth Int'l. Conf. Ionization Phenomena Gases, Vol. 3, p 293, North Holland Publishing Co., Amsterdam (1963).

11-58. Biberman, L.M., and G.E. Norman, Opt. i Spektrosk. 8, 230 (1960).

11-59. Richter, J., in Plasma Diagnostics, pp 36 ff, W. Lochte-Holtgreven, Ed., North Holland Publishing Co., Amsterdam (1968).

11-60. Schlüter, D.Z., Z. Astrophys. 61, 67 (1964).

11-61. Burgess, A., and M.J. Seaton, Monthly Notices Roy. Astron. Soc. 120, 121 (1961).

11-62. Geltman, S., Astrophys. J. 141, 376 (1965).

11-63. Doughty, N.A., P.A. Frazier, and R.P. McEachron, Monthly Notices Roy. Astron. Soc. 132, 255 (1966).

11-64. John, T.L., Monthly Notices Roy. Astron. Soc. 131, 315 (1966).

11-65. Roberts, J.R., and P.A. Voigt, J. Res. Natl. Bur. Stds. 75A, 89 (1971).

11-66. Mjolsness, R.C., and H.M. Ruppel, Phys. Rev. 154, 98 (1967).

11-67. Kivel, B., J. Quant. Spectry. Radiative Transfer 7, 27 (1967).

11-68. Zel'dovich, Y.B., and Yu. P. Raizer, Physics of Shock Waves and High Temperature Hydrodynamic Phenomena, Vol. 1, pp 255 ff, Aca- demic Press, New York (1966).

11-69. Kivel, B., J. Quant. Spectry. Radiative Transfer 7, 51 (1967).

11-70. Frisov, O.B., and M.I. Chibisov, Sov. Phys. - JETP 12, 2235 (1961).

11-71. Taylor, R.L., and G. Caledonia, J. Quant. Spectry. Radiative Transfer 9, 681 (1969).

11-72. Bates, D.R., E. Kingston, and R.W.P. McWhirter, Proc. Phys. Soc. A267, 297 (1962); Ibid A270, 155 (1962).

11-73. Bates D.R., and E. Kingston, Planet. Space Sci. 11, 1 (1963).

11-74. Bardsley, J.N. and F. Mandl, Repts. Prog. Phys. 31, 471 (1968).

11-75. Johnson, L.C., and E. Hinnov, Phys. Rev. 187, 143 (1969).

11-76. Collins, C.B., Phys. Rev. 177, 254 (1969); Ibid 186, (1969).

13B. SOLAR PHOTODISSOCIATION IN THE ATMOSPHERE

R.P. Turco, R&D Associates
R.E. Huffman, Air Force Geophysics Laboratory
(Latest Revision 15 June 1979)

13B.1 INTRODUCTION

A comprehensive description of the chemical interactions of solar radiation with the earth's atmosphere necessarily includes consideration of photodissociation processes as well as photoionization processes, which are discussed in Chapter 13 (now Chapter 13A).

The basic photodissociation event involves the absorption of a photon by a molecule, resulting in the rupture of a chemical bond. This produces neutral fragments having generally greater chemical reactivity than the original molecule. A few general comments will serve to further differentiate photodissociation from photoionization in the earth's atmosphere. The important altitudes for photodissociation are from ground level to about 200 km, which are lower than for photoionization. Also, the important wavelengths are longer, since dissociation energies are almost always less than ionization energies. The wavelength region of interest extends from the intense hydrogen Lyman-alpha line at 121.6 nm through the ultraviolet and the visible to about 750 nm. Since the solar flux available between 100 and 300 nm at altitudes below 150 km is controlled largely by the atmospheric absorption due to molecular oxygen and ozone, this absorption must be treated in some detail.

The wavelength region below 100 nm has usually been neglected in discussions of photodissociation, and will be neglected here. The photolysis of molecular nitrogen at these wavelengths, however, now appears to be an important source of nitrogen atoms (Reference 13B-1). The rate for the dissociation process

$$N_2 + h\nu \rightarrow N + N$$

at the top of the atmosphere is reported in Reference 13B-1 as $1.90 \times 10^{-8} sec^{-1}$. An unknown fraction of the products is thought to be in the excited $N(^2D)$ state.

One final distinction between photodissociation and photoionization effects within the context of the earth's atmosphere is that chemical models of atmospheric composition must generally include many more photodissociation than photoionization processes.

This chapter provides information on molecular photodissociation rates in the atmosphere at solar zenith angles of 30, 60, and 75 degrees. In order to calculate these rates, it is first necessary to specify the photodissociation cross-sections, incident solar fluxes, and an atmospheric model for light attenuation and scattering.

These subjects are discussed in Sections 13B.2, 13B.3, and 13B.4, respectively. Photodissociation rate parameters are given in Section 13B.5. Although only the photodissociations of neutral molecules are dealt with here, photodissociations of positive and negative ions, both simple and clustered, are also of aeronomic importance. Calculations for these species may be added in some future revision of this chapter, when sufficient cross-section data are available.

13B.2 CROSS-SECTIONS FOR INDIVIDUAL ABSORBING SPECIES

Table 13B-1 summarizes the literature sources of available photodissociation data (cross-sections σ and quantum yields γ) for 18 gaseous species of interest.

Table 13B-1. Photodissociation data sources for gaseous species.

Initial Species	References for: σ	γ	Initial Species	References for: σ	γ
O_2	13B-2	------	H_2O_2	13B-5	------
O_3	13B-2	13B-2	HNO_2	13B-3	------
NO	13B-2	------	HNO_3	13B-2	------
NO_2	13B-2	------	CO_2	13B-2	13B-6
NO_3	13B-3	------	CH_4	13B-2	13B-2
N_2O	13B-4	------	HCHO	13B-2	13B-2
N_2O_5	13B-3	------	SO_2	13B-2	------
HO_2	13B-2	------	H_2S	13B-2	------
H_2O	13B-2	------	OCS	13B-7	------

The cross-sections have generally been determined to within 10-20% uncertainties in regions of strong molecular absorption, e.g., for O_2 in the Schumann-Runge (S-R) continuum, and for O_3, NO_2, NO_3, N_2O_5, and HNO_3. In weaker absorption regions, the cross-section uncertainty can be as large as 50% or more, e.g., for O_2 in the Herzberg continuum, and for N_2O, H_2O, H_2O_2, CO_2, CH_4, and OCS.

Several species display considerable band structure in their absorption spectra, and the measured cross-sections are dependent upon experimental gas pressure and wavelength resolution. Because of band structure, the cross-sections for HNO_2, CO_2, HCHO, and SO_2 are uncertain by 30-50% at many wavelengths. (The O_2(S-R) and NO(delta) absorptions are discussed in Section 13B-4.) The absorptions of two species (HO_2 and H_2S) have been measured only once at important wavelengths; the observed cross-sections are therefore tentatively assigned a 50% uncertainty pending verification by additional measurements. At the solar Lyman-alpha line, the absorption cross-section of O_2 is known to better than 5%, and those of H_2O and CH_4 to better than 20%; for other dissociating species Lyman-alpha absorption is not significant.

The absorption cross-sections of O_2, NO_2, N_2O, CO_2, and OCS are temperature-sensitive (References 13B-2 through 13B-4 and 13B-7). In carrying out calculations ancillary to the preparation of this chapter (see Section 13B.5), cross-sections were adjusted to a typical upper-atmospheric temperature of 230K.

Uncertainties in photodissociation quantum yields are often larger than those in the corresponding total absorption cross-sections. Discussions of quantum yield data relevant to this chapter are available (References 13B-2, 13B-3). The quantum yields for O_3 photolysis in terms of alternative sets of products are well established. The cutoff wavelength for $O(^1D)$ production, lies at about 310 ± 5 nm. The direct formation of O_2 ($^1\Sigma_g^+$) by ozone photolysis below 266 nm is insignificant, and is not taken into account in the calculations mentioned above. The total photodissociation efficiency adopted for CO_2 is unity at all wavelengths (Reference 13B-6), although quantum efficiencies as low as 0.5 have been measured in the range 150-166 nm (Reference 13B-8). Below 166 nm CO_2 photolysis is assumed to produce exclusively $O(^1D)$, while above this wavelength only ground-state oxygen atoms are generated. The branching ratio for CH_4 photolysis to produce either atomic or molecular hydrogen is uncertain by a factor of two. The quantum yields for HCHO photolysis to form either molecular products (H_2 + CO) or radicals (H + CHO) are uncertain by roughly 50% above 320 nm, and 30% below this wavelength. The photodissociation products and quantum yields have not yet been determined for N_2O_5; unit quantum yield is assumed (Reference 13B-3) for the process:

$$N_2O_5 + h\nu \rightarrow N_2O_4 + O \equiv 2NO_2 + O.$$

13B.3 THE SOLAR FLUX ABOVE THE ATMOSPHERE

The solar flux incident at the top of the atmosphere, and the attenuated solar flux for 10-km altitude intervals from 10 to 170 km, are shown for zenith angles of 30, 60, and 75 degrees in Figures 13B-1a, b, and c, respectively. (Scattered and reflected radiation are not included in these figures.)

The solar fluxes indicated for the wavelength region 140-330 nm and at the Lyman-alpha line (121.6 nm) for average solar conditions are based upon compiled and evaluated observational data (Reference 13B-9). In the O_2 Schumann-Runge band region (178-198 nm) the attenuated fluxes only at altitudes of 30, 50, 70, and 90 km are shown for clarity. Beyond 330 nm, the solar fluxes have been averaged from a relatively recent tabulation (Reference 13B-10), replacing values recommended previously (Reference 13B-11).

Wavelengths below 140 nm must be considered in order to take account of CO_2 photodissociation. Accordingly, the CO_2 dissociations in the highly absorbing regions 127.5-137.5 nm and 110-115 nm have been included by using standard solar fluxes (Reference 13B-9) and measured cross-sections for CO_2 and O_2 (Reference 13B-2). (O_2 is the major atmospheric absorber at these wavelengths.)

Detailed assessments are available describing the uncertainty and variability of solar fluxes above the atmosphere (References 13B-3, 13B-9, 13B-11, 13B-12). Briefly, for the range 140-300 nm the measured fluxes are about 10-30% uncertain at any given time and have a 27-day solar-rotation variation of about 10% at 140 nm, decreasing to less than 1% at 240 nm, with possibly an 11-year solar-cycle variation of up to 50% at 140 nm, decreasing to about 5-10% at 300 nm. Above 300 nm, the solar-flux uncertainty and variability are less than about 10-15% overall. At the Lyman-alpha line (121.6 nm) there are about a 30% uncertainty and a 30-60% variability.

In the mesosphere and lower thermosphere, solar variability has been shown theoretically to cause variations in the O and O_3 densities through O_2 and H_2O photodissociations (References 13B-13, 13B-14). Hence solar variability may be important to consider in aeronomic investigations of the oxygen and hydrogen constituents in the upper atmosphere.

13B.4 ATMOSPHERIC ATTENTUATION AND SCATTERING OF SOLAR RADIATION

For solar radiation to dissociate the molecular constituents of the atmosphere, it must first propagate through an overlying layer of air. Photons in transit may be absorbed or scattered, thereby attenuating the direct solar beam. Moreover, light may be reflected

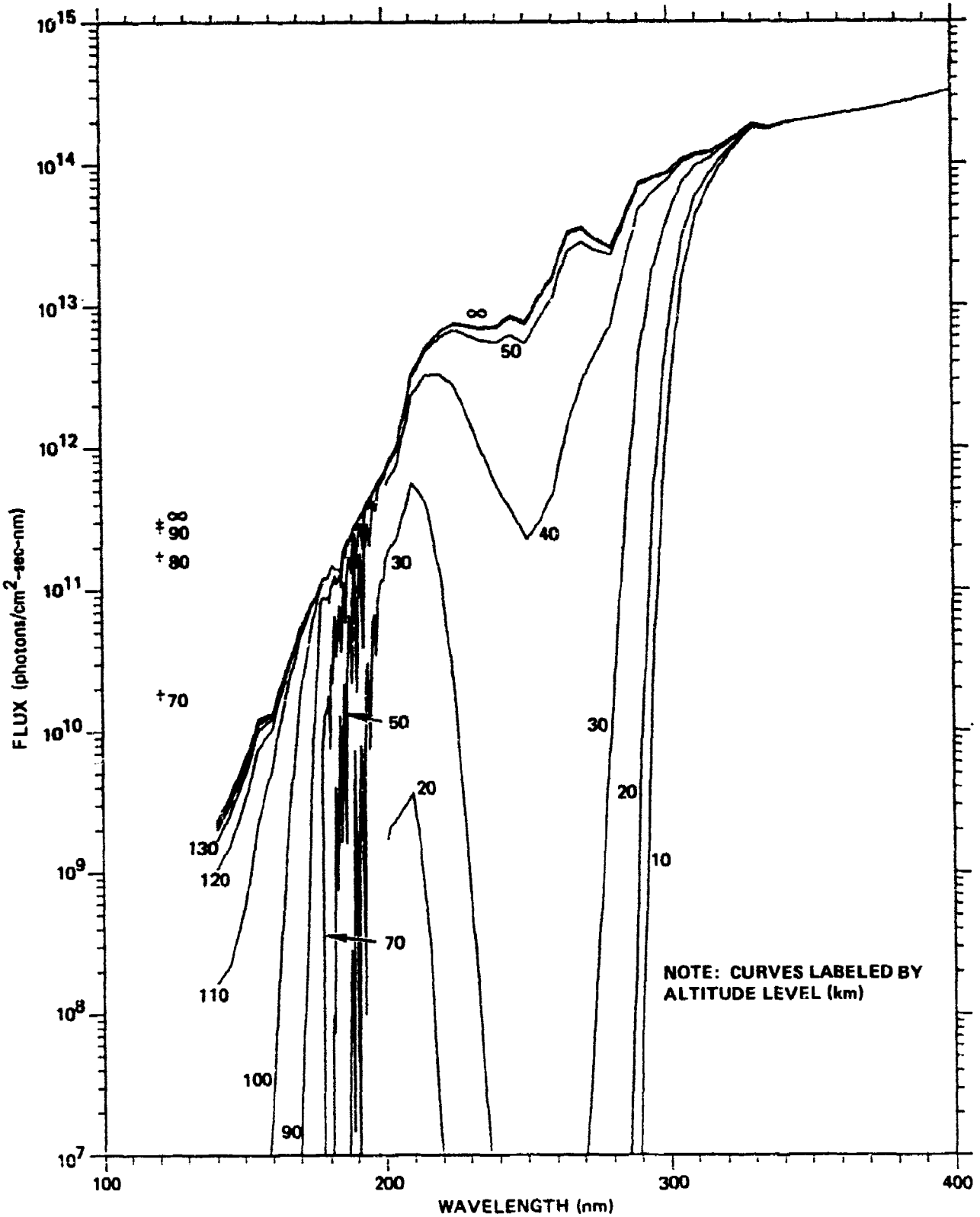

Figure 13B-1a. Solar irradiances in the atmosphere for a zenith angle of 30 degrees.

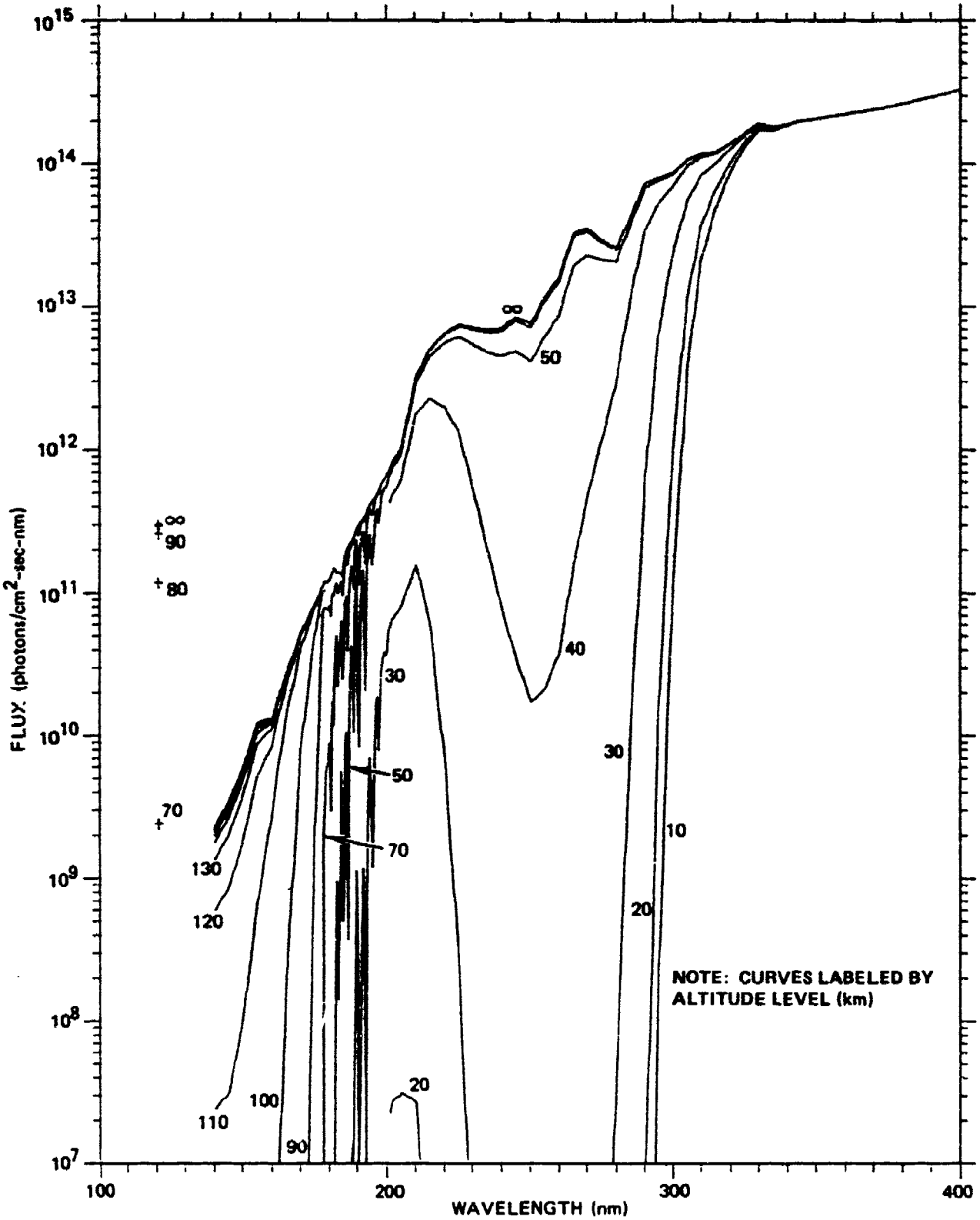

Figure 13B-1b. Solar irradiances in the atmosphere for a zenith angle of 60 degrees.

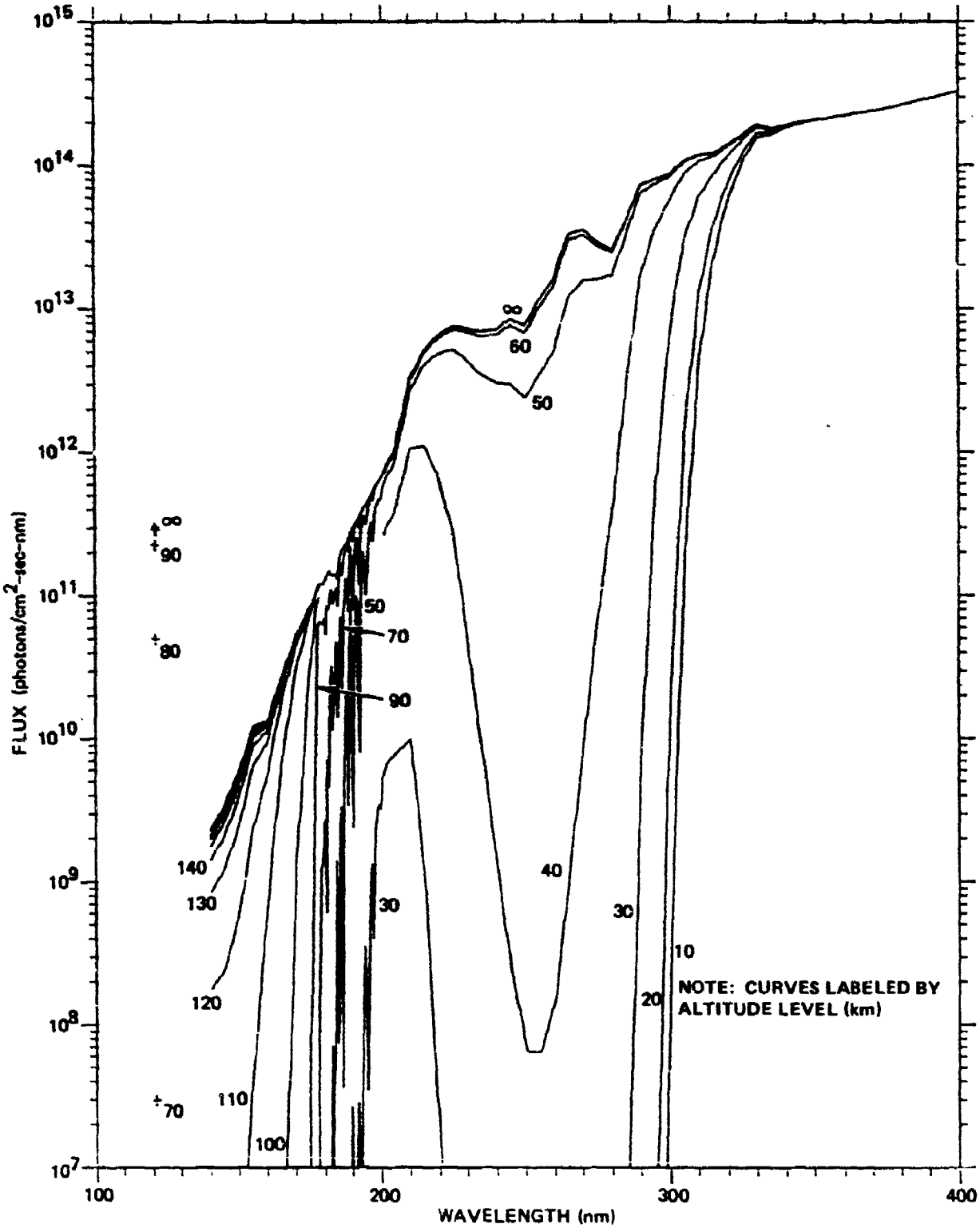

Figure 13B-1c. Solar irradiances in the atmosphere for a zenith angle of 75 degrees.

or scattered into otherwise shadowed regions, enhancing flux intensities there.

13B.4.1 Atmospheric Absorption

The absorption law governing the direct transmission of radiation through the atmosphere is:

$$T(\lambda) = \exp\left[-\tau(\lambda)\right] , \qquad (13B\text{-}1)$$

where $T(\lambda)$ is the transmission at wavelength λ. The optical depth $\tau(\lambda)$ is determined by:

$$\tau(\lambda) = \sum_i \sigma_i(\lambda) N_i , \qquad (13B\text{-}2)$$

where σ_i is the total absorption cross-section of the i'th constituent in cm^2 and N_i is its column density in molecules per cm^2-column along the absorption path.

These relationships hold strictly for a single wavelength, but they are assumed to be satisfactory as well over wavelength intervals of moderate extent, where the absorption cross-section and the incident solar flux are relatively constant. For several cases important in atmospheric photodissociation, this assumption is not valid owing to the presence of absorption bands consisting of many narrow lines. The O_2(S-R) bands and several NO band systems are examples. In such cases, band models or other more elaborate treatments are necessary.

Absorption in the O_2(S-R) band system between 175 and 200 nm can be determined accurately using a high-resolution cross-section incorporating thousands of individual rotational lines with explicitly specified strengths and shapes. For convenience of application, such a detailed cross-section is usually employed to calculate effective O_2 transmission factors and dissociation rates in a set of finite wavelength intervals (usually corresponding to the O_2(S-R) vibrational bands) as functions of the O_2 column density and local air temperature. The effective absorption parameters so obtained are fitted with appropriate polynomials or interpolation constants and tabulated for general use (References 13B-15 through 13B-18). The accuracy of the detailed absorption-model calculations is related to the accuracy of the line widths and line strengths upon which they are based, and is probably about 20% overall.

A simpler method for treating the O_2(S-R) bands has been used in calculations ancillary to the preparation of this chapter (Section 13B.5). This method utilizes a band absorption model for small wavelength intervals (0.1 nm) over the S-R band region (Reference 13B-2). In the band model adopted for this purpose, the optical depth is proportional to the O_2 column density for weak absorption, and to the square root of the column density for both moderate and strong absorptions. The square-root law has been verified experimentally

for moderate absorption in the O_2(S-R) bands (Reference 13B-19). This law is less valid for strong absorption, but in the application considered here the contribution to atmospheric photodissociation from the spectral intervals suffering strong O_2(S-R) band absorption can be neglected (Reference 13B-2). The uncertainty in O_2(S-R) band absorption determined with the band model is about 30% (Reference 13B-2).

The dissociation rate of NO in the (0,0) and (1,0) delta bands is calculated using the results of a detailed line-by-line computation (Reference 13B-20), but with the overall rate lowered by a factor of 2.3 to account for revised values of the oscillator strengths (Reference 13B-21). Considering the uncertainty in the estimated absorption of the NO lines by the O_2 rotational spectrum, however, the accuracy of the results obtained in these calculations is probably only about 50%.

13B.4.2 Distributions of Light-Attenuating Species

The only important upper-atmospheric light-attenuating species in the wavelength range 100-1000 nm are O_2 and O_3. The vertical profile of O_2 used for the photodissociation rate calculations described in Section 13B.5 is the mean reference profile presented in Chapter 2A of this Handbook. The O_3 profile adopted in this same computational context is taken from an empirical model for midlatitude O_3 concentrations at altitudes to 75 km (Reference 13B-22); above 75 km absorption due to O_3 may be neglected.

Concentrations of O_2 vary with location, season, and (for altitudes above 100 km) with solar activity (Reference 13B-23). Below 100 km, however, these variations are usually only of the order of 10-20% and are relatively well defined by season and latitude. In the altitude range 100-150 km, the variations range up to 50%, but are generally associated with such ascertainable geophysical conditions as, e.g., the exospheric temperature.

The attenuation of sunlight by O_3 begins near 55 km and increases rapidly with decreasing altitude down to about 15 km. Above 50 km, the O_3 concentration oscillates diurnally, but this phenomenon can usually be ignored in photodissociation calculations.

The variability of O_3 density is a topic of intensive study. Locally, the total O_3 column density may vary by up to 30-40% from day to day (References 13B-24, 13B-25). For altitudes in the range 20-55 km, the O_3 concentration typically varies by 10-20% (Reference 13B-22). Larger, as much as twofold, variations in O_3 that occur below 20 km are probably associated with meteorological variations (References 13B-22, 13B-24, 13B-25).

The global average O_3 vertical column density is about (8-9) x 10^{18} molecules per cm^2. Averaged yearly, roughly 50% more O_3 occurs

at the poles than at the equator (References 13B-24, 13B-25). A seasonal variation in O_3 density also exists, with the abundance in winter and spring generally exceeding that in summer and fall by about 50% at high latitudes, but less than 10% at low latitudes (References 13B-24, 13B-25).

When averaged from year to year, the total O_3 column density at a given location usually varies by about 5%, the largest variability being associated with higher latitudes (References 13B-3, 13B-26, 13B-27). The quasi-biennial variation in total O_3 is about 2% with little latitude dependence observed (Reference 13B-26). The 11-year total O_3 variation (apparently related to the sunspot cycle) is characteristically less than 5% at high latitudes and less than 2% at low latitudes (References 13B-26, 13B-27).

13B.4.3 Scattered Radiation

The consideration of photodissociation processes at wavelengths not strongly absorbed in the lower atmosphere must take account of the reflection and scattering of sunlight by the earth's surface and by air molecules and particulates, including clouds. Scattering can either attenuate or enhance the radiation received at a given observation point, depending upon the location of that point with respect to the sun and the scattering region. Above a reflecting layer, molecular photodissociation rates are enhanced by an amount related to both the reflection spectrum of the layer and the absorption spectrum of the species being dissociated.

The intensities of scattered and reflected sunlight in the atmosphere have been calculated, using a model for radiation transport in a scattering, absorbing atmosphere over a partially reflecting surface (Reference 13B-28). The results of this calculation can be interpreted quite simply as indicating that for an average surface and cloud albedo of about 0.30, light intensities at altitudes above 10 km for wavelengths longer than 310 nm are enhanced by about 40% due to scattering and reflection. Other calculations suggest that this enhancement is nearly independent of solar elevation for zenith angles less than 80 degrees (Reference 13B-29). Upon closer inspection it may be seen from the results of the sunlight intensity calculations (Reference 13B-28) that scattered and reflected light intensities are nearly zero at 305 nm and increase rapidly to about 40% of the incident intensity at 320 nm. Therefore, for purposes of the photodissociation rate computation of Section 13B.5, a linear increase has been adopted over the wavelength range 305-320 nm.

At shorter wavelengths, i.e., 200-300 nm, large relative photon-flux enhancements can occur in the stratosphere because of scattering. These enhancements have little aeronomic consequence, however, since the absolute fluxes involved are extremely small (Reference 13B-28).

The average global surface albedo of 0.30 comprises about half cloud albedo, averaging 0.50, and half ocean albedo, averaging 0.10 (Reference 13B-30). The cloud albedo spectrum is relatively flat throughout the visible and near-ultraviolet regions, while the spectrum for natural water surfaces peaks in the visible and falls off by about 30% in the near ultraviolet (Reference 13B-30).

Because the local surface and cloud albedos can range from less than 0.10 to more than 0.60, scattered and reflected light intensities vary widely with geographic location and meteorological conditions (Reference 13B-30). At large solar zenith angles (i.e., exceeding 75 degrees), scattered light intensities are difficult to calculate, and the approximate model used in Section 13B.5 is inapplicable. Thus, while the global average scattered and reflected light fluxes assumed in Section 13B.5 are probably accurate to within 30% at wavelengths longer than 310 nm, they could vary approximately two-fold locally, and by still greater factors at large zenith angles.

13B.5 MOLECULAR PHOTODISSOCIATION IN THE ATMOSPHERE

Given the fundamental information contained in the preceding three sections, rates of photodissociation of gaseous species in the atmosphere may be calculated for a variety of conditions. Moreover, the limitations of application of these rates, owing to uncertainties associated with the basic data, may also be specified.

13B.5.1 Calculated Photodissociation Rates

The rate of occurrence of photodissociation of molecules of the i'th gaseous species at a given location in the atmosphere is given by:

$$S_i(cm^{-3}sec^{-1}) = n_i \int \sigma_i(\lambda)\ I(\lambda)\ d\lambda = n_i J_i \quad , \qquad (13B\text{-}3)$$

where n_i is the local number density (cm^{-3}) of the dissociating molecule, $\sigma_i(\lambda)$ is the photodissociation cross-section in cm^2 at wavelength λ, and $I(\lambda)$ is the local solar flux intensity (photons $cm^{-2}sec^{-1}$) per unit wavelength.

The photodissociation rates $J_i(sec^{-1})$ for 23 processes involving 17 of the 18 species listed in Table 13B-1 (omitting NO_3) are presented in Figures 13B-2a, b, and c for solar zenith angles of 30, 60, and 75 degrees, respectively. The photodissociation processes shown are $O_2^{(1)} \rightarrow O + O$; $O_2^{(2)} \rightarrow O + O(^1D)$; $O_3^{(1)} \rightarrow O + O_2$; $O_3^{(2)} \rightarrow O + O_2(^1\Delta_g)$; $O_3^{(3)} \rightarrow O(^1D) + O_2(^1\Delta_g)$; $NO \rightarrow N + O$; $NO_2 \rightarrow NO + O$; $N_2O \rightarrow N_2 + O(^1D)$; $N_2O_5 \rightarrow NO_2 + NO_2 + O$; $HNO_2 \rightarrow OH + NO$; $HNO_3 \rightarrow OH + NO_2$;

$HO_2 \rightarrow OH + O$; $H_2O \rightarrow OH + H$; $H_2O_2 \rightarrow OH + OH$; $CO_2^{(1)} \rightarrow CO + O$; $CO_2^{(2)} \rightarrow CO + O(^1D)$; $CH_4^{(1)} \rightarrow CH_3 + H$; $CH_4^{(2)} \rightarrow CH_2 + H_2$; $HCHO^{(1)} \rightarrow CHO + H$; $HCHO^{(2)} \rightarrow CO + H_2$; $SO_2 \rightarrow SO + O$; $OCS \rightarrow CO + S(^1D)$; $H_2S \rightarrow HS + H$.

The J_i are given for altitudes between 10 and 170 km; they remain essentially constant above this range. Using Figures 13B-2a, b, and c to find the J_i appropriate to a given altitude and solar zenith angle, the value of S_i may readily be calculated for any concentration n_i of the i'th species, using Equation (13B-3).

Dissociation products have been indicated above wherever these are known. Where no electronic state is given, the process is either known or assumed to yield only ground-state products. In a few instances, however, possible excited states are ignored, e.g., in the CH_2 product of CH_4 photolysis. Also, excited states produced in wavelength regions of secondary importance to the overall dissociation process are neglected, e.g., in OH due to H_2O photolysis below 140 nm and in O due to SO_2 photolysis below 160 nm. In the calculations on which Figures 13B-2a, b, and c are based, predissociation and direct dissociation are combined whenever the products are the same. (See Chapter 12 of this Handbook for a discussion of photodissociation mechanisms.)

The photodissociation rate of NO_3 is essentially independent of altitude and zenith angle and is therefore not included in Figures 13B-2a, b, and c. Two photodissociation channels are thought to be involved (Reference 13B-3):

$$NO_3 + h\nu \rightarrow NO_2 + O \quad (J = 0.10 \text{ sec}^{-1}), \text{ and}$$

$$NO_3 + h\nu \rightarrow NO + O_2 \quad (J = 0.04 \text{ sec}^{-1}).$$

Photodissociation rates averaged over 24 hours are often used in photochemistry models to simulate the effect of diurnal variations on species concentrations. These rates can be found from the photodissociation coefficients at several different zenith angles by an appropriate quadrature. A simpler, less precise technique takes one-half the photorate value for an "average" solar zenith angle of about 60 degrees (Reference 13B-31). The latter approximation is probably accurate enough for most applications of the data included in this chapter.

For atmospheric considerations, molecules may be roughly categorized by the spectral region of their dominant absorption. Thus, molecules fragmented primarily by light at wavelengths longer than the O_3 Hartley-band cutoff near 300 nm (NO_2, NO_3, HNO_2, HCHO) comprise a class of long-wavelength absorbers whose dissociation rates are relatively insensitive to the O_2 and O_3 distributions. In the stratosphere, however, these molecules are still somewhat sensitive

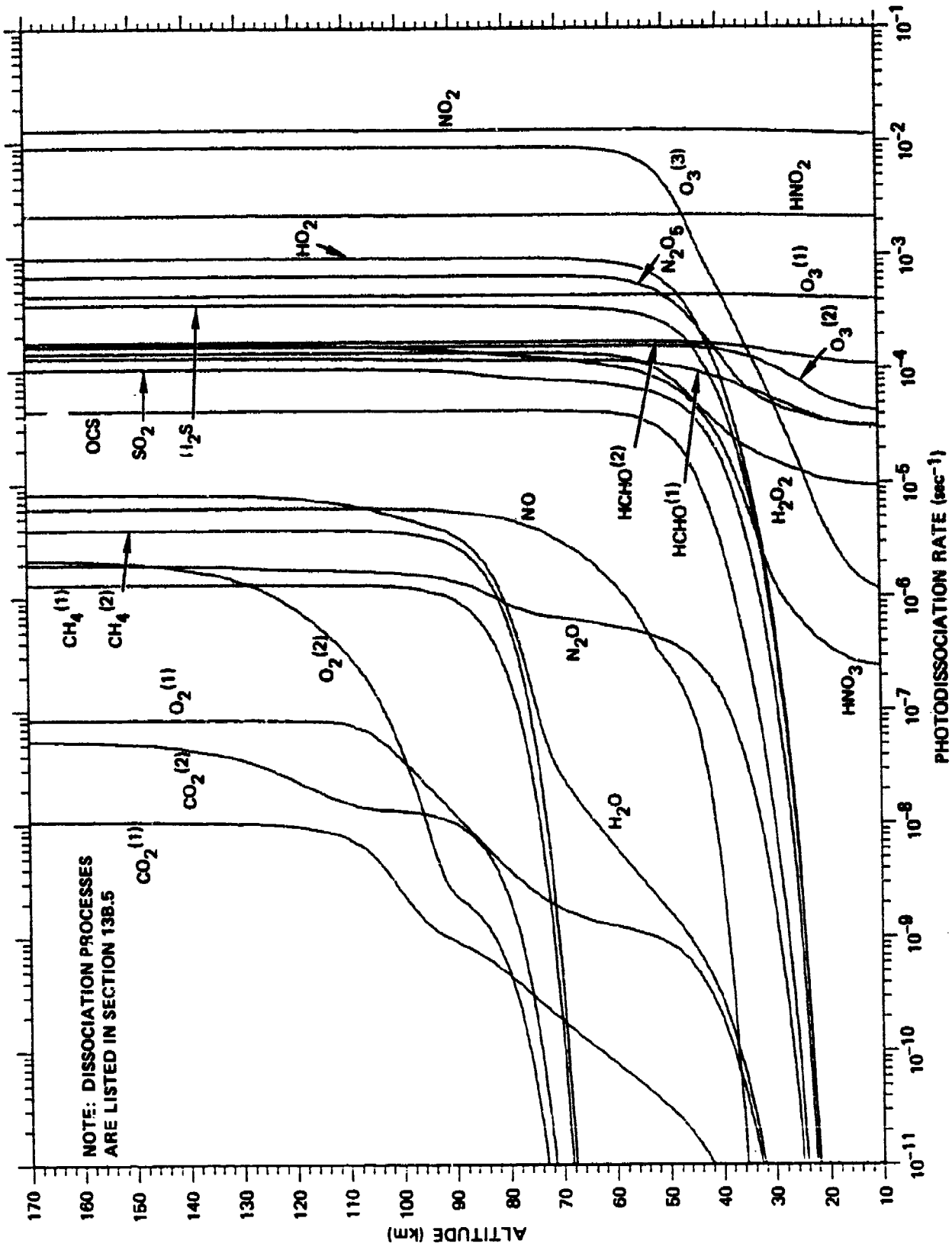

Figure 13B-2a. Atmospheric molecular photodissociation rates at a solar zenith angle of 30 degrees.

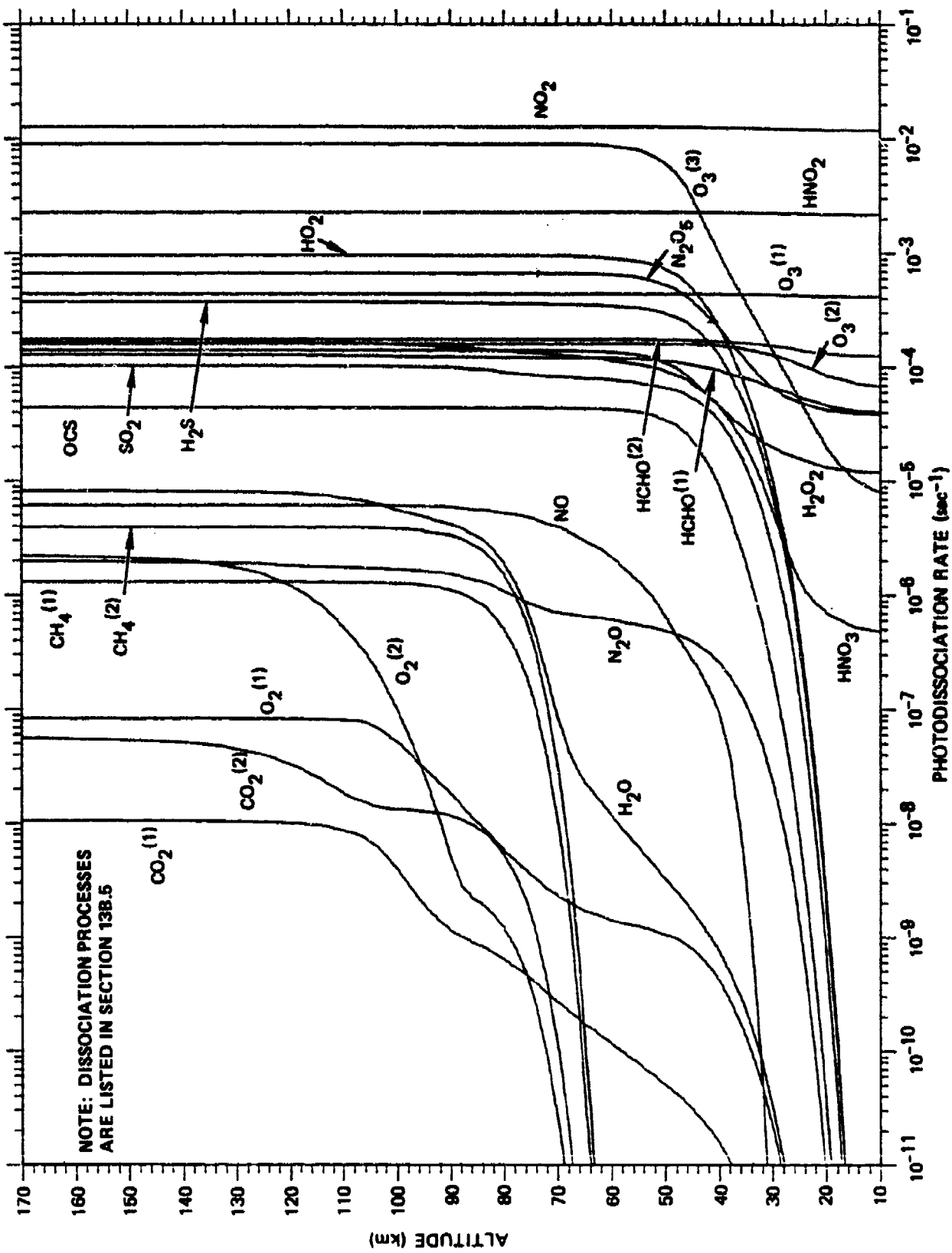

Figure 13B-2b. Atmospheric molecular photodissociation rates at a solar zenith angle of 60 degrees.

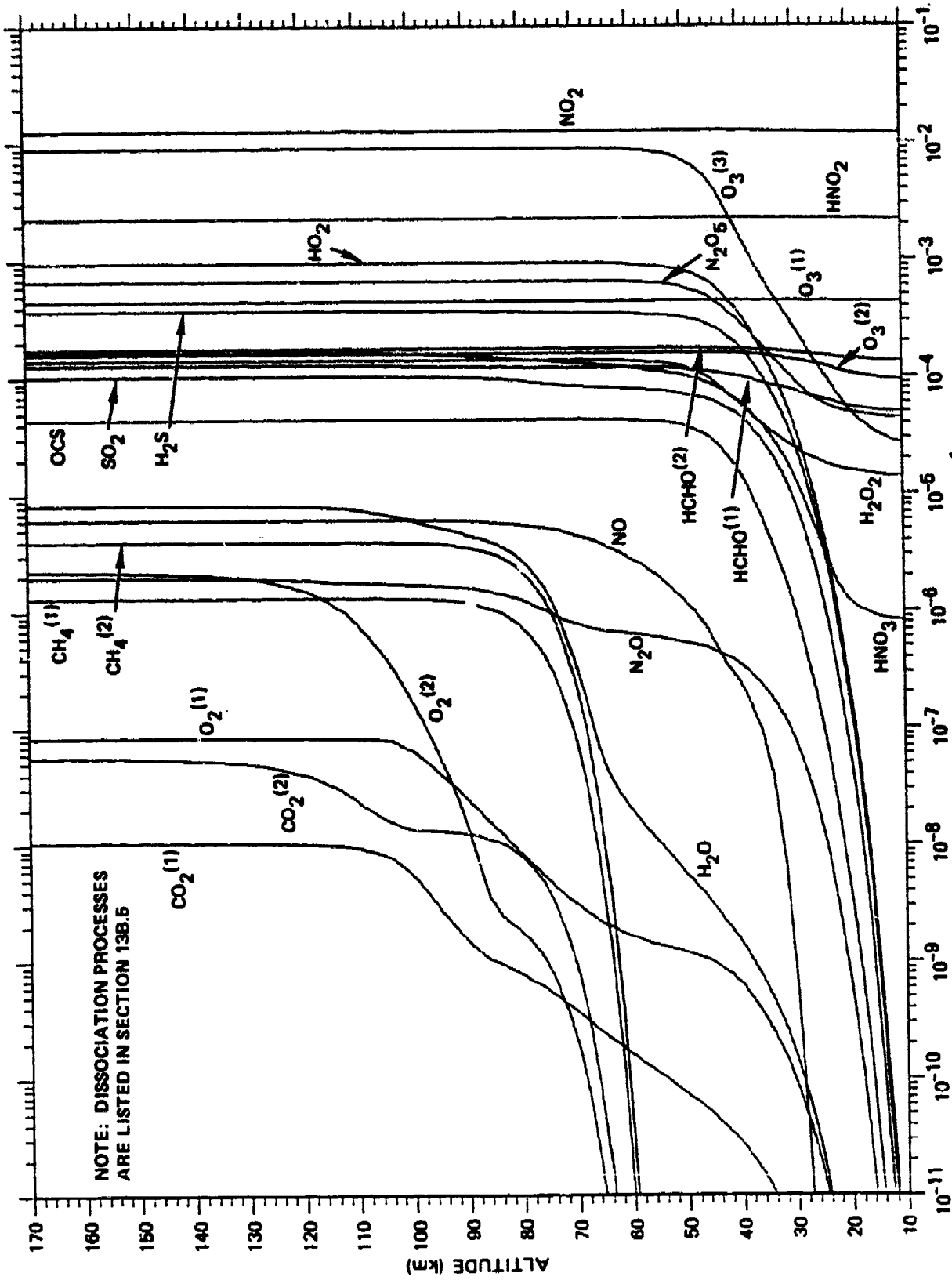

Figure 13B-2c. Atmospheric molecular photodissociation rates at a solar zenith angle of 75 degrees.

to the O_3 Huggins-band absorption between 300 and 330 nm (Reference 13B-28). Molecular absorbers in the long-wavelength category are also affected by scattered light.

Air constituents with large absorption coefficients between 200 and 300 nm (O_3, N_2O_5, HNO_3, HO_2, H_2O_2, H_2S, OCS) have photodissociation rates that are controlled primarily by O_3 absorption, while molecules having strong absorption features below 200 nm (O_2, NO, N_2O, H_2O, CO_2, CH_4, SO_2) have dissociation rates that are determined largely by the continuum and band absorption of O_2.

13B.5.2 Uncertainties in Photodissociation Rates

Uncertainties in the calculated atmospheric photodissociation rates are related to uncertainties and variabilities in those parameters (viz., absorption cross-sections, dissociation quantum yields, incident solar fluxes, scattered and reflected light intensities, molecular band absorptances, and O_2 and O_3 concentrations) on which the calculations are based. These sources of uncertainty have been discussed.

Scattered and reflected light is the primary source of uncertainty in the total photodissociation rates of long-wavelength absorbers (NO_2, NO_3, HNO_2, HCHO). This uncertainty amounts to about 20% for low-zenith-angle global average conditions, and up to 50% for more variable local situations. For extended solar elongations and in twilight, the relative magnitude of the scattering effect is less predictable, but large uncertainties, exceeding 50%, may be expected. Secondary sources of uncertainty for these photo rates are associated with the O_3 abundance due to Huggins-band absorption (10%) and the individual photodissociation cross-sections (10-20%).

Molecular species that are dissociated by light between 200 and 300 nm (O_2, N_2O_5, HNO_3, HO_2, H_2O_2, H_2S, OCS) are most sensitive to O_3 absorption. In the stratosphere, O_3 variability can introduce uncertainties of 50% into these rates. The O_3 variability at each wavelength is amplified exponentially in terms of light transmission (Equation (13B-1).) Even though the variability in the total O_3 abundance above a given altitude tends to decrease with decreasing altitude down to about 20 km, the exponential amplification acts to increase the over-all photorate uncertainty. Other sources of uncertainty in these photodissociation rates arise in connection with absorption cross-sections and solar fluxes. The O_3 dependence of these photo-rates should be kept in mind when applying the data given in this chapter, always being sure to associate the tabulated rates with the adopted O_3 distribution (Reference 13B-22).

Photodissociation rates that depend upon radiation at wavelengths below 200 nm, including the Lyman-alpha line, (O_2, NO, N_2O, H_2O, CO_2 CH_4, SO_2) are most sensitive to O_2 absorption. Variability in O_2 concentrations and uncertainty in O_2 S-R band absorptances can lead to a 30-40% uncertainty in these photorates. Above 70 km altitude,

both H_2O and CH_4 are dissociated primarily by Lyman-alpha radiation; the photodissociation rates are therefore sensitive to the variabilities in O_2 abundance (20%) and Lyman-alpha flux (30-60%). For all the molecules in this category, uncertainties in the photodissociation rate include contributions due to the variability and uncertainty in solar fluxes below 200 nm (30-40%), and due to the uncertainties in cross sections as well.

Several species (O_3, N_2O, SO_2, H_2S, OCS) are dissociated at high altitudes by radiation of wavelengths shorter than 200 nm, and at low altitudes by middle-wavelength radiation (200-300 nm). Hence for different altitude regions the primary determinants of the dissociation rate uncertainty among the different contributing parameters may themselves differ. To some extent, this is also true for species (O_3, H_2O_2, HNO_3, N_2O_5) that absorb both middle- and long-wavelength radiation.

For certain photodissociating species (NO_3, CH_4, HCHO), the uncertainties in dissociation quantum yields contribute a substantial uncertainty to the computed dissociation rates. This gives rise to a 50% uncertainty in the photodissociation branching ratios for these molecules.

Above a certain altitude (roughly 10, 60, and 120 km for long-, middle-, and short-wavelength absorbers, respectively) each photodissociation rate depends mainly upon the incident (and reflected) solar flux and the dissociation cross-section. For each photodissociation process treated in this chapter, the corresponding "zero optical depth" uncertainty in the dissociation rate is given in the appropriate part of Table 24-1 in Chapter 24 of this Handbook.

REFERENCES

13B-1. Ogawa, T., and T.Shimazaki, J. Geophys. Res. 80, 3945 (1975); Ogawa, T., and Y. Kondo, Planet. Space Sci. 25, 735 (1977).

13B-2. Turco, R.P., Geophys. Surveys 2, 153 (1975).

13B-3. Hudson, R.D., Ed., Chlorofluoromethanes and the Stratosphere, NASA Reference Publ. 1010 (1977).

13B-4. Selwyn, G., J. Podolske, and H.S. Johnston, Geophys. Res. Letts. 4, 427 (1977).

13B-5. Molina, L.T., S.D. Schinke, and M.J. Molina, Geophys. Res. Letts. 4, 580 (1977).

13B-6. Slanger, T.G., and G. Black, J. Chem. Phys. 68, 1844 (1978).

13B-7. Chou, C.C., H.V. Ruiz, K. Moe, and F.S. Rowland, unpublished data, Dept. of Chemistry, Univ. of California, Irvine (1976).

13B-8. Inn, E.C.Y., J. Geophys. Res. 77, 1991 (1972).

13B-9. Delaboudiniere, J.P., et al, COSPAR Tech. Manual No. 7 (1978)

13B-10. White, O.R., Ed., The Solar Output and Its Variation, Colorado Associated Univ. Press, Boulder (1977).

13B-11. Ackerman, M., in Mesospheric Models and Related Experiments, G. Fiocco, Ed., D. Reidel Publishing Co. (1971); p. 149.

13B-12. Simon, P.C., Aeronomica Acta No. 183, Institut d'Aeronomie Spatiale de Belgique, Brussels (1977).

13B-13. Frederick, J.E., Planet. Space Sci. 25, 1 (1977).

13B-14. Breig, E.L., J. Geophys. Res. 78, 5718 (1973).

13B-15. Kockarts, G., Planet. Space Sci. 24, 589 (1976).

13B-16. Fang, T.M., S.C. Wofsy, and A. Dalgarno, Planet. Space Sci. 22, 413 (1974).

13B-17. Blake, A.J., J. Geophys. Res. 84, 3272 (1979).

13B-18. Hudson, R.D., and S.H. Mahle, J. Geophys. Res. 77, 2902 (1972).

13B-19. Blake, A.J., J.G. Carver, and G.N. Haddad, J. Quant. Spectry. Radiative Transfer 6, 451 (1967).

13B-20. Cieslik, S., and M. Nicolet, Planet. Space Sci. 21, 925 (1973).

13B-21. Mandelman, M., and T. Carrington, J. Quant. Spectry. Radiative Transfer 14, 509 (1974).

13B-22. Krueger, A.J., and R.A. Minzer, J. Geophys. Res. 81, 4477 (1976).

13B-23. U.S. Standard Atmosphere Supplements (1966).

13B-24. Dütsch, H.U., J. Geophys. Res. 75, 1707 (1970).

13B-25. Nicolet, M., Revs. Geophys. Space Phys. 13, 593 (1975).

13B-26. Angell, J.K., and J. Korshover, Monthly Weather Rev. 101, 426 (1973).

13B-27. Angell, J.K., and J. Korshover, Monthly Weather Rev. 104, 63 (1976).

13B-28. Luther, F.M., and R.J. Gelinas, J. Geophys. Res. 81, 1125 (1976).

13B-29 Isaaksen, I.A., K.H. Midtbo, J. Sunde, and P.J. Crutzen, Geophys. Norveg. 36, 11 (1977).

13B-30. Kondratyev, K.Ya., Radiation Characteristics of the Atmosphere and the Earth's Surface, Amerind Publishing Co., New Delhi, India (1973).

13B-31. Cogley, A.C., and W.J. Borucki, J. Atmos. Sci. 33, 1347 (1976).

20. EXCITATION AND DEEXCITATION PROCESSES

A.W. Ali, Naval Research Laboratory
F.R. Gilmore, R&D Associates
R.H. Kummler, Wayne State University
J.W. McGowan, University of Western Ontario
(Latest Revision 2 July 1979)

20.1 INTRODUCTION

The many physical and chemical interactions that occur virtually continuously at altitudes between sea level and about 1000 km comprise a response of the atmosphere to its absorption of both solar and anthropogenic energy under either quiescent or disturbed conditions. Atmospheric disturbances arise in nature by virtue of solar flares, electron and proton precipitations, volcanic activity and the like, to all of which mankind adds the debris of combustion, pollution, explosions, and other products of his civilization. Energy absorption by atmospheric constituents of all kinds is manifest in several ways, including in particular the generation of large numbers of excited species. These may be unstable with respect to radiative deexcitation (characterized by short lifetimes), or they may be metastable. Moreover, such excited species may be either electrically neutral or ionic, and either atomic or molecular in composition. They all play an important role in the atmosphere, in ultimately dispersing the energy absorbed. Excited metastable species play significant secondary roles in the physics and chemistry of the atmosphere, i.e., by way of energy-transfer interactions with ground-state species.

This chapter deals with the excitation and deexcitation of atmospheric species first by discussing the relevant excitation mechanisms (Section 20.2) and the characteristics of excited states (Section 20.3). In addition, the chapter presents detailed information on the excitation and deexcitation of particularly important excited species (Section 20.4), and reaction rate coefficients appropriate to the relevant energy-transfer interactions (Section 20.5). The emphasis, therefore, is on the characteristics of both the excited states of important species and their chemical reactions in both quiescent and disturbed atmospheric media.

At one time the role of excited-state reactions in the laboratory as well as in the atmosphere were considered to be of minor consequence relative to that of ground-state reactions. It is now recognized, however, that in any ambience small numbers of metastably excited species may have disproportionately large effects on the overall chemical phenomenology, and that consequently they may significantly affect both steady-state conditions and the relaxation of highly disturbed gas-phase systems of all kinds.

The roles of specific excited species in both quiescent and disturbed atmospheric systems as well as laboratory systems have been reported extensively (References 20-1 through 20-16). Excited species and the transfer of their energy of excitation to other species have attracted particular attention with the advent of lasers (Reference 20-17). Other studies have focused upon the role of excited species in specific portions of the atmosphere, e.g., the stratosphere (Reference 20-18) and the quiescent ionosphere (Reference 20-19). More general considerations of the role of excited species in the atmosphere as a whole under varying conditions of ambience have also appeared (Reference 20-20).

20.2 EXCITATION AND DEEXCITATION MECHANISMS

The elevation of species from lower energy levels, e.g., ground state, to either radiative or metastable excited states may proceed via photoabsorption, charged particle impact, charge exchange and charged rearrangement processes, collisions among neutral species with and without rearrangement, and dissociative recombinations. These processes are briefly described in this section.*

In general, each excitation process is matched by a corresponding inverse deexcitation mechanism, such that the rate coefficient for the latter is derivable from that for the former by application of the principle of detailed balance.

20.2.1 Photoabsorption

Within the context of this chapter, the term "photoabsorption" broadly includes the photo-induced dissociation (cf. Chapter 13B), dissociative ionization, and ionization (cf. Chapter 13; now 13A) of molecules, as well as absorption of light-producing electronic and vibrational excitation. These types of interactions are represented, respectively, by Reactions (20-1) through (20-5):

$$O_2 + h\nu \rightarrow O + O^* \qquad (20\text{-}1)$$

$$O_2 + h\nu \rightarrow O^+ + e + O^* \qquad (20\text{-}2)$$

$$N_2 + h\nu \rightarrow N_2^+ (X,A,B) + e \qquad (20\text{-}3)$$

$$O(^3P) + h\nu \rightarrow O(^3S) \qquad (20\text{-}4)$$

$$NO + h\nu \rightarrow NO^{\ddagger}. \qquad (20\text{-}5)$$

---

* Throughout this chapter, electronically or vibrationally excited species are indicated by the asterisk(*) or the double-cross (‡), respectively, whenever the state is not otherwise specifically identified. The absence of any symbolism accompanying the chemical formula for a species implies the ground state (electronic, vibrational, or both).

20.2.2 Charged Particle Impact

A group of reactions analogous respectively to Reactions (20-1) through (20-5), but initiated by energetic collisions with charged particles (e.g., electrons) rather than photons, is set forth here as Reactions (20-6) through (20-10). Although the colliding species indicated in these reactions is the electron, any other charged particles (e.g., protons) may have the same effects.*

$$O_2 + e \rightarrow O + O^* + e \qquad (20\text{-}6)$$

$$O_2 + e \rightarrow O^+ + 2e + O^* \qquad (20\text{-}7)$$

$$N_2 + e \rightarrow N_2^+(X,A,B) + 2e \qquad (20\text{-}8)$$

$$N(^4S) + e \rightarrow N(^4P) + e \qquad (20\text{-}9)$$

$$N_2 + e \rightarrow N_2^\ddagger + e \quad . \qquad (20\text{-}10)$$

20.2.3 Charge-Exchange and Ion-Molecule Rearrangement

The exothermicity of certain charge-exchange reactions may be manifest as kinetic energy, or as internal degrees of freedom (e.g., vibrational, electronic modes) of the product species. In the latter types of energy redistribution, the reaction products are in appropriately excited states, as in the following examples of resonant and nonresonant (respectively), asymmetric interactions:

$$O^+(^2D) + N_2 \rightarrow N_2^+(A)^\ddagger + O \qquad (20\text{-}11)$$

$$N_2^+ + N \rightarrow N^+ + N_2^\ddagger \quad . \qquad (20\text{-}12)$$

Likewise, the excess energy of exothermic ion-molecule rearrangements, e.g.:

$$O^+ + N_2 \rightarrow NO^+ + N + 1.1 \text{ eV} \qquad (20\text{-}13)$$

may be partitioned into internal degrees of freedom of the reaction products, such as to yield appropriately excited species.

20.2.4 Neutral Species Interactions

Endothermic collisions among neutral species may result in excitation owing to the conversion of translational energy into vibrational or electronic modes of the collision products, e.g.:

---

* In addition, particularized aspects of the atmospheric effects of proton precipitation are described separately in subsection 20.4.8.

$$O + N_2 + 0.289v \text{ eV} \rightarrow N_2^{\ddagger} + O \qquad (20\text{-}14)$$

where v = the vibrational level of the product $N_2^{\ddagger}$.

Similarly, exothermic collisons involving excited neutral reactants may yield excited products through transfer of internal energy modes among the species upon collision, e.g.:

$$O(^1D) + N_2 \rightarrow N_2^{\ddagger} + O(^3P) \qquad (20\text{-}15)$$

$$O(^1D) + O_2 \rightarrow O_2(b^1\Sigma_g^+, v \leq 2) + O(^3P) \qquad (20\text{-}16)$$

Such interactions may also be characterized by atom rearrangements as well as excitation of the products, e.g.:

$$N(^2D) + O_2 \rightarrow NO^{\ddagger} + O \quad . \qquad (20\text{-}17)$$

20.2.5 Dissociative Recombination

In addition to their direct excitation effects upon impact with neutrals (discussed in subsection 20.2.2), energetic electrons (and thermal) colliding with common atmospheric molecular ions may produce atomic species in both electronically excited and ground states by dissociative recombination, e.g.:

$$O_2^+ + e \rightarrow O(^3P) + 0.9\ O(^1D) + 0.1\ O(^1S) \qquad (20\text{-}18)$$

$$N_2^+ + e \rightarrow 0.92\ N(^4S) + 1.08\ N(^2D) \qquad (20\text{-}19)$$

$$NO^+ + e \rightarrow N(^2D) + O(^3P) \quad . \qquad (20\text{-}20)$$

20.3 GENERAL CHARACTERISTICS OF EXCITED STATES AND THEIR ROLE IN THE DISTURBED ATMOSPHERE

The dominant neutral species in the quiescent atmosphere are N_2, O_2, and O. The more important minor species include CO_2, O_3, H_2O, OH, NO, and NO_2. Ionized species are present as well, and their densities are enhanced under disturbed conditions, depending on altitude, energy deposition, and strength of the initiating disturbance. In addition, large numbers of excited-state species present under both disturbed and quiescent conditions (but especially the former) act as a temporary repository of at least part of the energy introduced into the atmosphere by the disturbing phenomenon. This energy is ultimately either radiated in whatever wavelength regions happen to be characteristic of the species, or collisionally transferred into alternative degrees of freedom as the disturbed atmosphere "cools", or "relaxes."

To more fully understand and deal with this role of excited states as a medium of energy storage in the atmosphere, it is first necessary to distinguish between the effective lifetime τ_e, which allows for collisional deexcitation, and the collision-free radiative lifetime τ_o. The reciprocals of these two lifetimes, i.e., the corresponding frequencies, are related through the reactive collision frequencies for all the excited species involved. The latter term is simply the product, summed over all excited species, of the individual rate constants k_i ($cm^3 sec^{-1}$) for inelastic scattering with other species, and the number density n_i (cm^{-3}):

$$1/\tau_e = 1/\tau_o + \sum_i k_i n_i \quad . \tag{20-21}$$

Much of what is known about the excitation energies, principal transitions, and radiative lifetimes of the longer-lived electronically excited states of most of the important atmospheric species is summarized in Table 20-1. Table 20-2 presents similar data pertaining to relevant vibrational modes associated with important atmospheric species. In addition, Grotrian energy-level diagrams of some atmospheric species of interest are shown in Figures 20-1 and 20-2, and Chapter 10 contains yet more energy-related information.

Finally, in considering energy-transfer phenomena, resonance or near-resonance reactions may play significant roles, depending upon the details of the potential-energy surfaces associated with specific interactions being examined in this context (References 20-13, 20-21 through 20-24).

20.4 THE EXCITATION AND DEEXCITATION OF SPECIFIC STATES

This section presents detailed data from relevant literature pertaining to the dynamics of specific excited atoms, ions, and molecules in quiescent and disturbed atmospheres and in the laboratory. References 20-1 through 20-5, 20-9 through 20-13, and 20-15 through 20-17 have more general coverage of this subject area.

20.4.1 Neutral Molecular Nitrogen, N_2

20.4.1.1 Vibrational Excitation-Deexcitation of the Ground Electronic State, $N_2(X) \rightleftarrows N_2(X)^{\ddagger}$

An appreciable portion of the energy deposited in the atmosphere is stored as vibrational excitation of ground-state nitrogen. This result may arise through any one of several physical and chemical processes, as follows:

(a) Radiative transitions from high-lying excited states (Reference 20-62):

$$N_2(A^3\Sigma_u, v'') \rightarrow N_2(X^1\Sigma_g^+, v') + h\nu; \tag{20-22}$$

Table 20-1. Radiative lifetimes and transitions for electronically excited states of principal atmospheric species.

Species and State	Mean Radiative Lifetime (sec)	Principal Transition; λ (nm); Name of Transition	Approx ΔE_{if} (eV)[a]	References
Atoms and Atomic Ions				
$C(^3P)$	Ground state			
(^1D)	3.2×10^3	$^3P \leftarrow {}^1D$; 982.3, 985.0	1.26	20-25
(^1S)	2.0	$^1D \leftarrow {}^1S$; 872.7	1.42	20-25
$(2p^3\ {}^5S^o)$	0.03	$^3P \leftarrow {}^5S$; 296.5, 296.7	4.18	20-25
$C^+(^2P^o)$	Ground state			
(^4P)	Moderately long	$^2P^o \leftarrow {}^4P$; ~233	5.35	20-25
$N(^4S^o)$	Ground state			
$(^2D^o_{3/2})$	6.1×10^4	$^4S^o \leftarrow {}^2D^o_{3/2}$; 520 (nebular)	2.38	20-25
$(^2D^o_{1/2})$	1.4×10^5	$^4S^o \leftarrow {}^2D^o_{5/2}$; 520.1	2.38	20-25
$(^2P^o)$	13	$^2D^o \leftarrow {}^2P^o$; 1039.6, 1040.4	1.19	20-25
$(^3s\ ^4P)$	2.5×10^{-9}	$^4S^o \leftarrow {}^4P$; 120.0, 120.1	10.31	20-25, 20-26
$N^+(^3P)$	Ground state			
(^1D)	250	$^3P \leftarrow {}^1D$; 658.4, 654.8	1.89	20-25
(^1S)	0.90	$^1D \leftarrow {}^1S$; 575.5	2.15	20-25
$O(^3P)$	Ground state			
(^1D)	148	$^3P \leftarrow {}^1D$; 630, 636.4 (red lines)	1.96	20-25, 20-27, 20-28

Noces: Refer to end of table.

(continued)

Table 20-1. Radiative lifetimes and transitions for electronically excited states of principal atmospheric species (continued).

Species and State	Mean Radiative Lifetime (sec)	Principal Transition; λ (nm); Name of Transition	Approx ΔE_{if} (eV)[a]	References
Atoms and Atomic Ions (continued)				
$O(^1S)$	0.80	$^1D \leftarrow {}^1S$; 557.7 (green line)	2.22	20-25, 20-29
$(3_s\ ^5S^o)$	0.0006	$^3P \leftarrow {}^5S^o$; 135.6, 135.9	9.13	20-25
$(3s\ ^3S^o)$	1.8×10^{-9}	$^3P \leftarrow {}^3S^o$; 130.2, 130.5, 130.6	9.51	20-25, 20-30, 20-31
$O^+(^4S^o)$	Ground state			
$(^2D^o_{3/2})$	5.9×10^3	$^4S^o \leftarrow {}^2D^o_{3/2}$; 372.6 (nebular)	3.33	20-25
$(^2D^o_{5/2})$	2.1×10^4	$^4S^o \leftarrow {}^2D^o_{5/2}$; 372.9	3.32	20-25
$(^2P^o_{1/2})$	5.4	$^2D^o \leftarrow {}^2P^o_{1/2}$; 731.9, 733.0 (auroral)	1.69	20-25
$(^2P^o_{3/2})$	4.2	$^2D^o \leftarrow {}^2P^o_{3/2}$; 731.9, 733.0	1.69	20-25
Diatomic Molecules and Molecular Ions[b]				
$N_2(X^1\Sigma_g^+)$	Ground state			
$(A^3\Sigma_u^+)$	1.3 (F_2); 2.7 (F_1, F_3)	A → X (Vegard-Kaplan)	6.2	20-32 thru 20-34
$(B^3\Pi_g^+)$	8.0×10^{-6}	B → A; 1051 (first positive)	1.2	20-34 thru 20-36
$(W^3\Delta_u)$	1.0×10^{-3} (v=2)	W → X W → B	7.4 0.003	20-37, 20-38
$(B'\ ^3\Sigma_u^-)$	10^{-5} est.	B' → B (Y bands)	0.8	20-39

(continued)

Table 20-1. Radiative lifetimes and transitions for electronically excited states of principal atmospheric species (continued).

Species and State	Mean Radiative Lifetime (sec)	Principal Transition: λ (nm); Name of Transition	Approx ΔE_{if} (eV)[a]	References
Diatomic Molecules and Molecular Ions (continued)				
$N_2(a'\ ^1\Sigma_u^-)$	≥0.04	a' → X (Wilkinson)	8.4	
$(a\ ^1\Pi_g)$	1.4×10^{-4} $(1.15 \pm 0.20) \times 10^{-4}$	a → X; 145.0 (Lyman-Birge-Hopfield)	8.6	20-40, 20-41
$(w\ ^1\Delta_u)$	10^{-4} est.	w → a; 3640	0.3	20-39
$(C^3\Pi_u)$	4.0×10^{-8}	C → B; 337.1 (second positive)	3.7	20-42 thru 20-45
$(E^3\Sigma_g^+)$	2.0×10^{-4}	E → A,C	5.7, 0.8	20-41, 20-46
$N_2^+(X^2\Sigma_g^+)$	Ground state			
$(A^2\Pi_u)$	1.7×10^{-5}(v=3)	A → X; 1103.6 (Meinel)	1.0	20-36, 20-45, 20-47 thru 20-49
$(B^2\Sigma_u^+)$	5.9×10^{-8}	B → X; 391.4 (first negative)	3.2	20-43 thru 20-45
$(^4\Sigma_u^+)$	Moderately long	$^4\Sigma_u^+ \rightarrow X$	~6	20-39, 20-50
$NO(X^2\Pi)$	Ground state			
$(a^4\Pi)$	156, 93, 35 msec ~0.16 (Ω = 5/2)	a → X	4.7	20-51, 20-52
$(A^2\Sigma^+)$	2.0×10^{-7}	A → X; 226.5 (γ bands)	5.5	20-53 thru 20-55
$(B^2\Pi)$	3.6×10^{-6}	B → X; (β bands)	5.6	20-53 thru 20-56

(continued)

Table 20-1. Radiative lifetimes and transitions for electronically excited states of principal atmospheric species (continued).

Species and State	Mean Radiative Lifetime (sec)	Principal Transition: λ (nm); Name of Transition	Approx $\Delta\mathcal{E}_{if}$ (eV)[a]	References
Diatomic Molecules and Molecular Ions (continued)				
$NO^+(X^1\Sigma^+)$	Ground state			
$(a^3\Sigma^+)$	Long	a → X	6.4	20-57, 20-58
$(b^3\Pi)$	1.4×10^{-4}	b → a	0.9	20-59
$(w^3\Delta)$	$\sim 10^{-4}$ est.	w → b	0.3	20-39
$NO_2(^2B_1)$[c]	5.5×10^{-5} to 9.0×10^{-5}	$A\ ^2B_1 \rightarrow X\ ^2A_1$		20-60, 20-61
$O_2(X^3\Sigma_g^-)$	Ground state			
$(a^1\Delta_g)$	3.9×10^3	a → X; 1268 (infrared atmospheric)	0.98	20,28, 20-62 20-63
$(b^1\Sigma_g^+)$	12	b → X; 761.9 (atmospheric)	1.63	20-62, 20-64, 20-65
$(c^1\Sigma_u^-)$	Long	c → X; 285.6 (Herzberg II)	4.0	20-66
$(C^3\Delta_u)$	Long	C → X (Herzberg III) C → a	~4.2	20-39
$(A^3\Sigma_u^+)$	0.03	A → X; 285.6 (Herzberg I) A → b; 458.6 (Broida-Gaydon)	4.3	20-67
$(B^3\Sigma_u^-)$	4.2×10^{-8}	B → X; 203.0 (Schumann Runge)	6.1	20-62
$O_2^+(X^2\Pi_g)$	Ground			
$(a^4\Pi_u)$	Long	a → X; 602.6	4.0	20-39

(continued)

Table 20-1. Radiative lifetimes and transitions for electronically excited states of principal atmospheric species (continued).

Species and State	Mean Radiative Lifetime (sec)	Principal Transition; λ (nm); Name of Transition	Approx ΔE_{if} (eV)[a]	References
Diatomic Molecules and Molecular Ions (continued)				
$O_2^+(A^2\Pi_u)$	7×10^{-7}	A → X (second negative)[d]	5.0	20-68, 20-69
$(b^4\Sigma_g^-)$	1.1×10^{-6}	b → a; 602.6 (first negative)	2.1	20-68, 20-69 20-71
$CO(X^1\Sigma^+)$	Ground state			
$(a^3\Pi)$	$\sim 10^{-2}$ (dep. on J)	a → X (Cameron bands)	6.0	20-72, 20-73
$(a'^3\Sigma^+)$	10^{-5} (v=4)	a' → a (Asundi bands) a' → X (Birge-Hopfield)	~0.9 ~6.9	20-74, 20-75
$(d^3\Delta)$	6.0×10^{-6}	d → a (triplet bands)	1.5	20-74
$CO^+(X^2\Sigma^+)$	Ground state			
$(A^2\Pi)$	3.8×10^{-6}	A → X (comet tail)	2.6	20-47, 20-69
$CH(X^2\Pi)$	Ground state			
$(A^2\Delta)$	5×10^{-7}	A → X	2.9	20-76, 20-77
$(B^2\Sigma)$	4×10^{-7}	B → X	3.2	20-77
$CN(X\Sigma^+)$	Ground state			
$(A^2\Pi)$	7×10^{-6} (v=1)	A → X (red bands)	1.1	20-78
$(B^2\Sigma^+)$	8×10^{-8}	B → X; 388.3 (violet bands)	3.2	20-79, 20-80

[a]Radiant energy at intermediate frequency in the transitional energy range.

[b]The quoted lifetime is for the v=0 level and the wavelength and energy are for the (0,0) transition unless otherwise noted.

[c]This triatomic molecule is included for the sake of continuity with the NO and NO^+ species preceding.

[d]The much shorter lifetime reported in Reference 20-70 has been disregarded since it would yield an unreasonably large transition moment (Reference 20-39).

Table 20-2. Ground electronic state vibrational data for molecules (sources: Chapters 10 and 11 of this Handbook).

Molecule and Vibrational Spacing	Approximate Energy of Vibrational Interval (eV)	Transition to Ground State λ(μm)	Lifetime (sec)
N_2			
v=1	0.29		Long
O_2			
v=1	0.19		Long
NO			
v=1	0.23	5.3	8.3×10^{-2}
v=2	0.46	2.68	1.3
CO			
v=1	0.26	4.6	2.9×10^{-2}
v=2	0.52	2.35	1.0
OH			
v=1	0.44	2.8	8.2×10^{-2}
v=2	0.88	1.4	1.8×10^{-1}
O_3			
v=1	0.14	9.6	9.2×10^{-2}
v=2	0.09	14.0	3.7
v=3	0.13	9.0	8.0
CO_2			
v=1	0.17	---	---
v=2	0.08	15.0	3.6
v=3	0.29	4.26	2.5×10^{-3}

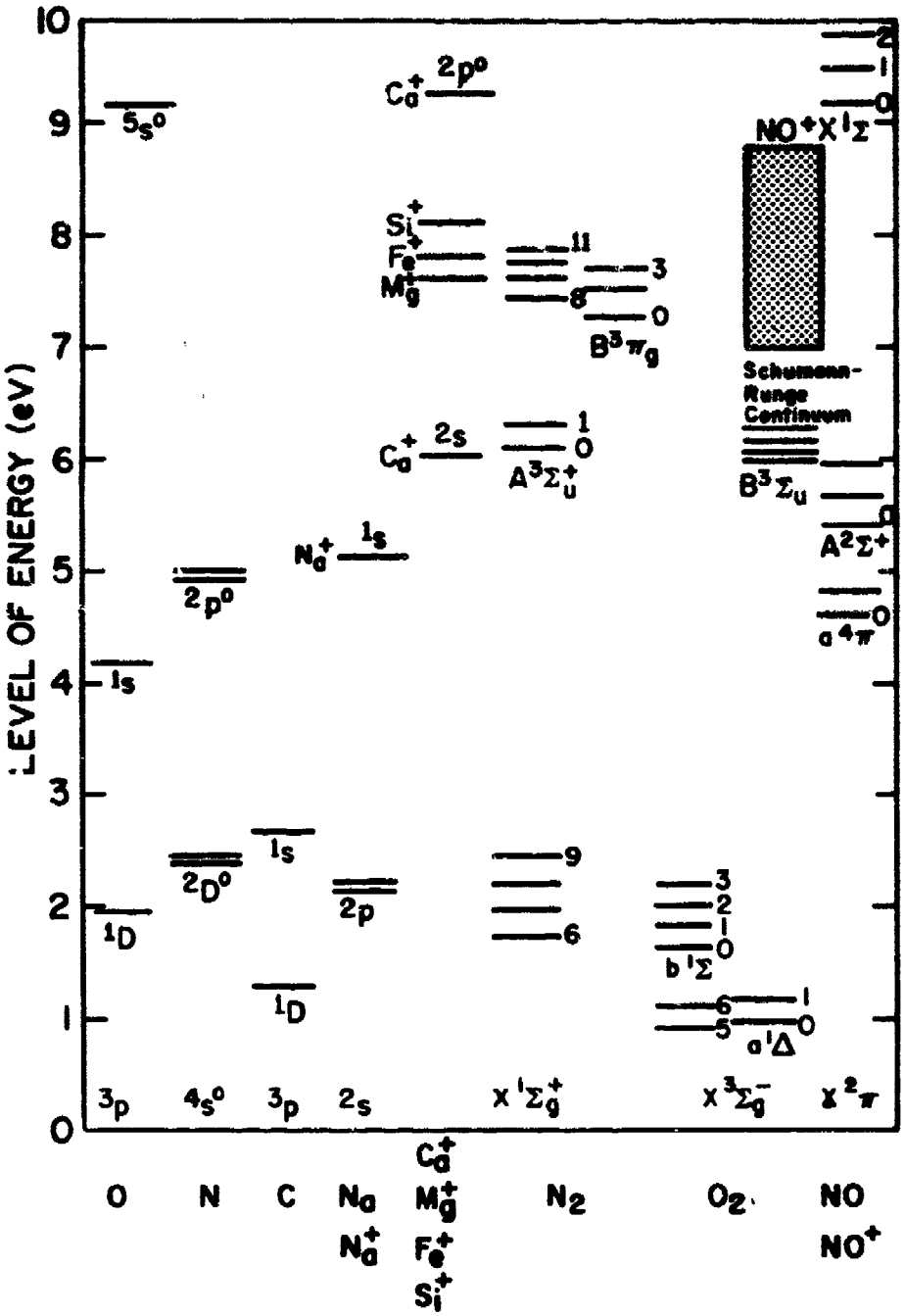

Figure 20-1. Energy levels of pertinent atoms, molecules, and ions.

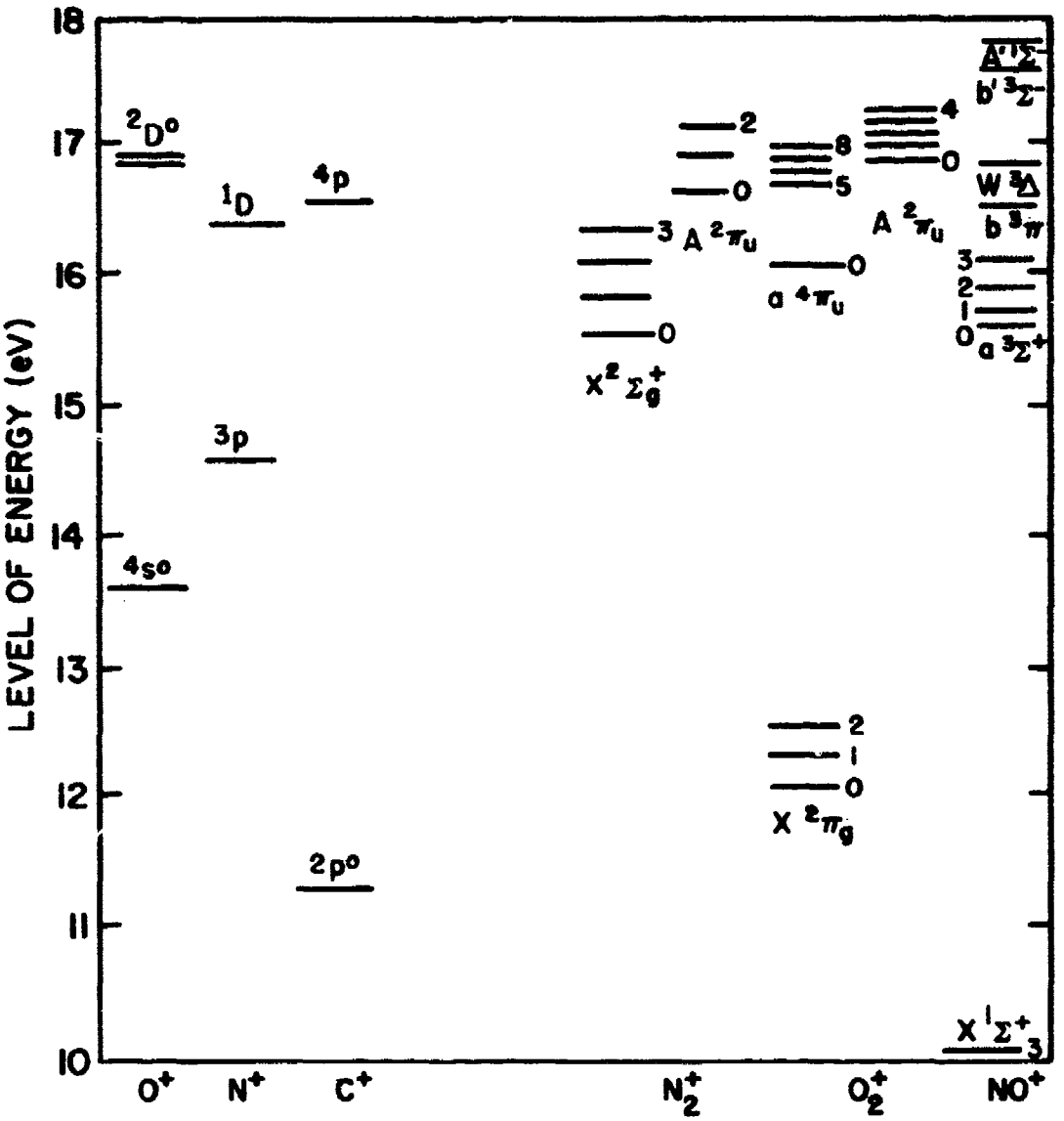

Figure 20-2. Energy levels of pertinent ions above those of the corresponding ground-state neutral species.

(b) Chemical reaction (References 20-6 through 20-8):

$$NO(X^2\Pi) + N(^4S^o) \rightarrow N_2(X^1\Sigma_g^+, v>0) + O(^3P); \qquad (20\text{-}23)$$

(c) Energy transfer (References 20-11, 20-81 through 20-86):

$$O(^1D) + N_2(X^1\Sigma_g^+, v=0) \rightarrow O(^3P) + N_2(X^1\Sigma_g^+, v>0); \qquad (20\text{-}24)$$

(d) Resonance excitation under electron impact (References 20-87 through 20-90):

$$N_2(X^1\Sigma_g^+, v=0) + e \rightarrow N_2^-(^2\Pi, v') \rightarrow N_2(X^1\Sigma_g^+, v>0) + e . \qquad (20\text{-}25)$$

Equation (20-25) represents a very efficient process, having a cross-section that approaches 6×10^{-16} cm^2 at its maximum (Reference 20-91). This reaction has been the subject of considerable experimental (References 20-87 through 20-90) and theoretical (References 20-92 through 20-95) attention, with satisfactory reproduction of the experimental results (Reference 20-96) in at least one of the calculations (Reference 20-95). The ground-state vibrational excitation arises through the intermediate ion (References 20-87 through 20-94), $N_2^-(^2\Pi)$, which in turn decays, primarily into eight individual vibrational states ($v=1\rightarrow8$) of the product. The corresponding individual cross-sections, excited by electron impacts, have been resolved experimentally (References 20-87 through 20-89), as functions of the energies of the incident electrons. Deexcitation of the vibrational levels by electrons, i.e., the reverse of Equation (20-25), has also been observed (Reference 20-97). Excitation rate coefficients have been obtained by integrating the electron impact cross-sections with the electron velocity over an electron Maxwellian velocity distribution (References 20-98, 20-99). The results are shown in Figure 20-3 and in Table 20-3. Similar values of the coefficients have been obtained by other workers (Reference 20-100). It ensues that greater accuracy is achieved in calculating the energy deposited by colliding electrons into the vibrational modes of $N_2(X)$ by considering the threshold energies for each individual level, than by basing the determination on the threshold energy for the intermediate negative ion, as suggested elsewhere (References 20-101, 20-102).

Of the numerous chemical reactions reported in which vibrationally excited products have been identified (References 20-14, 20-103 through 20-105), Reaction (20-23) is the only one thus far examined in detail (References 20-6 through 20-8, 20-85) for which N_2^+ is a product. It has been determined, moreover, that 25% of the exothermicity of Reaction (20-23) is converted into vibrational energy (Reference 20-85).

Regarding Reaction (20-24), it had been inferred (Reference 20-11) from the near coincidence of the electronic excitation energy of $O(^1D)$ and the vibrational excitation energy of $N_2(X, v=7)$ that a

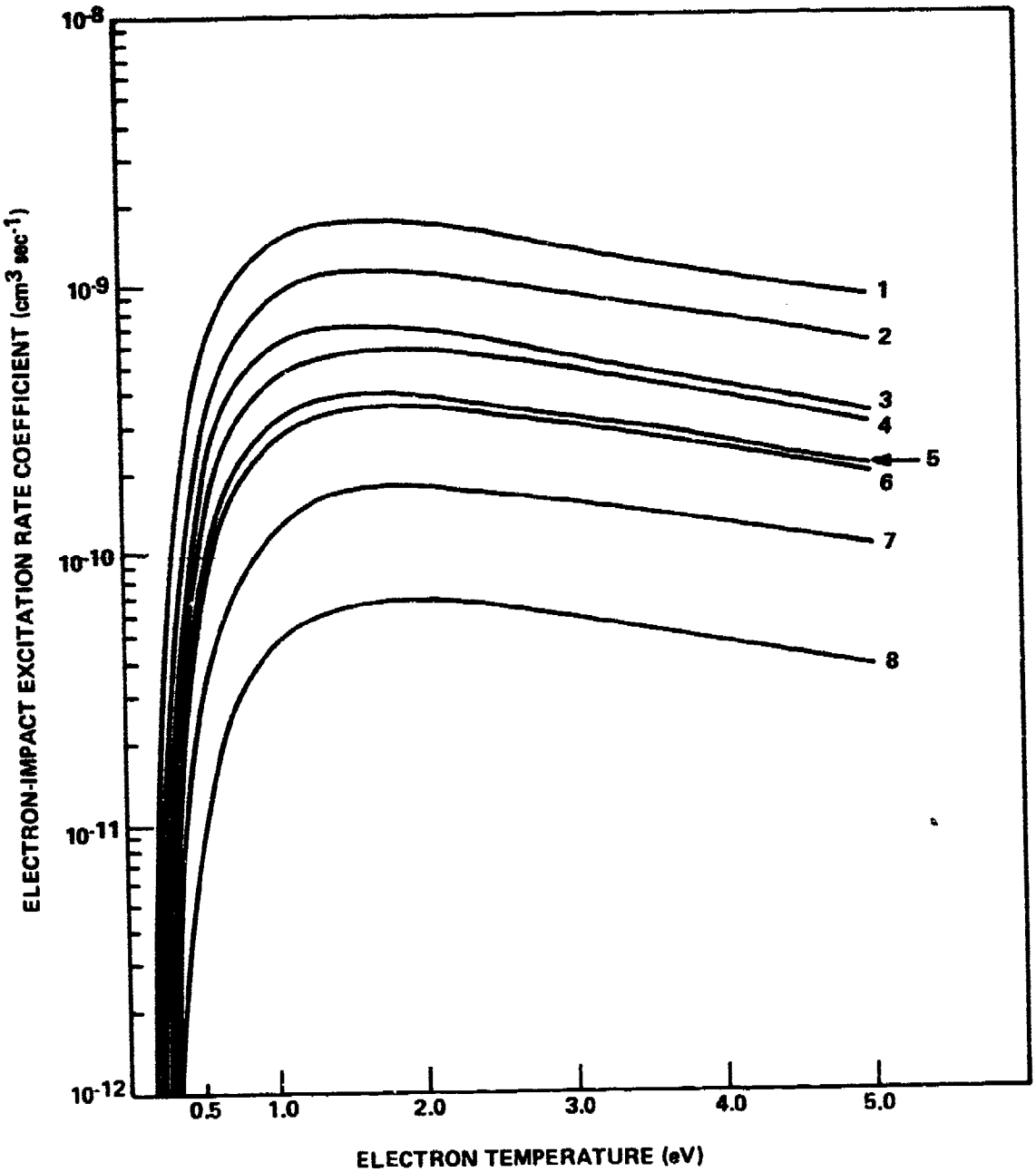

Figure 20-3. Electron-impact excitation rate coefficients of eight $N^2(X)$ vibrational levels as functions of the electron temperature (References 20-98, 20-99).

Table 20-3. Electron-impact excitation rate coefficients (cm^3sec^{-1}) for eight vibrational levels of $N_2(X)$ as a function of electron temperature T_e(eV) (References 20-98, 20-99).

T_e/X_v	X_1	X_2	X_3	X_4	X_5	X_6	X_7	X_8
0.1	1.98(-14)[a]	1.49(-16)[a]	6.28(-17)[a]	1.57(-17)[a]	5.58(-18)[a]	1.37(-18)[a]	2.27(-19)[a]	2.51(-20)[a]
0.2	4.01(-12)	1.48(-12)	8.81(-13)	4.16(-13)	2.16(-13)	1.14(-13)	3.28(-14)	7.81(-15)
0.3	5.63(-11)	2.83(-11)	1.83(-11)	1.05(-11)	6.20(-12)	4.13(-12)	1.45(-12)	4.31(-13)
0.4	2.08(-10)	1.14(-10)	7.59(-11)	4.76(-11)	3.02(-11)	2.24(-11)	8.71(-12)	2.85(-12)
0.5	4.38(-10)	2.52	1.68(-10)	1.11(-10)	7.33(-11)	5.77(-11)	2.39(-11)	8.26(-12)
0.6	6.96(-10)	4.11	2.74	1.88	1.27(-10)	1.04(-10)	4.47	1.60(-11)
0.7	9.43(-10)	5.66	3.77	2.65	1.82	1.52	6.76	2.47
0.8	1.16(-9)	7.04	4.67	3.35	2.32	1.98	9.00(-11)	3.33
0.9	1.34	8.20	5.41	3.96	2.75	2.38	1.10(-10)	4.12
1.0	1.48	9.12	5.99	4.45	3.11	2.72	1.27	4.80
1.1	1.58	9.84(-10)	6.43	4.85	3.38	2.99	1.42	5.37
1.2	1.66	1.04(-9)	6.75	5.15	3.60	3.20	1.53	5.83
1.3	1.71	1.08	6.96	5.39	3.75	3.37	1.62	6.19
1.4	1.74	1.10	7.09	5.56	3.86	3.48	1.69	6.46
1.5	1.76	1.12	7.16	5.67	3.93	3.57	1.74	6.65
1.6	1.77	1.12	7.17	5.75	3.96	3.62	1.77	6.78
1.7	1.76	1.12	7.15	5.79	3.97	3.65	1.79	6.86
1.8	1.75	1.12	7.09	5.81	3.96	3.66	1.80	6.89
1.9	1.73	1.11	7.00	5.80	3.94	3.65	1.80	6.89
2.5	1.56	1.02(-9)	6.26	5.51	3.61	3.45	1.71	6.46
3.0	1.39	9.21(-10)	5.57	5.15	3.36	3.20	1.58	5.88
3.5	1.24	8.29	4.93	4.77	2.93	2.95	1.44	5.29
4.0	1.11(-9)	7.47	4.38	4.43	2.64	2.73	1.32	4.74
4.5	9.95(-10)	6.74	3.90	4.12	2.38	2.55	1.21	4.24
5.0	8.96(-10)	6.11(-10)	3.49(-10)	3.84(-10)	2.16(-10)	2.39(-10)	1.12(-10)	3.80(-11)

Note:

[a] Numbers in parentheses indicate powers of 10 by which the entries are to be multiplied. Where no parentheses are given the entries are to be multiplied by the same power of 10 as the preceding entry or entries.

significant amount of energy transfer from the one to the other may occur. Following the utilization of this near-resonance concept in calculating the vibrational temperature of the ambient atmosphere (Reference 20-84), and in recognition of its possible significance in this context, Reaction (20-24) has been increasingly investigated (References 20-81, 20-82, 20-85, 20-86), the most recent such experimental effort (Reference 20-86) indicating that 30% of the internal energy of $O(^1D)$ is transferred by this process to N_2 as vibrational energy.

The formation of vibrationally excited $N_2(X)$ via radiative cascade as in Reaction (20-22) clearly depends on the prior excitation of the $N_2(A^3\Sigma)$ state and on the population densities of its vibrational levels, transitions from which to ground-state vibrational levels comprise a further factor in determining the vibrational energy of $N_2(X)$.

In principle, vibrational deexcitation processes might be expected to follow the reverse paths of the corresponding excitations. Thus, the rate coefficients of electron-impact deexcitations via superelastic collisions should be calculable from the respective excitation rate coefficients (Table 20-3) by applying the principle of detailed balance. However, vibrationally excited molecules may also transfer their energies either directly to the vibrational modes (vibration-vibration, or VV) or to kinetic energy (vibration-translation, or VT) of other species.

These (VV and VT) quenching processes are believed to be well understood (References 20-105 through 20-109). A typical VT transition at room temperature without chemical change, e.g., $N_2(v=1\rightarrow0)$, requires 10^{10} collisions (Reference 20-108), but this number is considerably reduced when the VT relaxation is achieved with atom exchange (References 20-110 through 20-113). Furthermore, the probability of vibrational energy transfer increases with increasing temperature and decreasing vibrational spacings. Usually the deexcitation of higher vibrational levels is a stepwise process. Thus, for most conditions $\Delta v=\pm1$, but for higher vibrational levels and/or high kinetic temperatures transitions can also occur for which $\Delta v > 1$ (References 20-114, 20-115).

A summary of VT data for many molecules is available (Reference 20-116). Such data are ordinarily presented as a relaxation time-pressure product $p\tau$, where τ is the e-folding time of the vibrational energy ϵ, according to:

$$d\epsilon/dt = \tau^{-1}(\epsilon_{equil}-\epsilon) \qquad (20\text{-}26)$$

at constant translational temperature and in the absence of sources. The rate constant can be readily obtained from the $p\tau$ product, i.e.,

$$K = (p\tau M)^{-1}, \qquad (20\text{-}27)$$

where M is the density of the deactivating agent at pressure p. Furthermore, the rate constant for the deexcitation of the first vibrational level k_{10} is:

$$k_{10} = \left[M\tau(1-e^{-h\nu/kT})\right]^{-1} \quad . \tag{20-28}$$

where $h\nu$ is the vibrational energy spacing and k in the exponential term is the Boltzmann constant. For higher vibrational level deexcitations, on the other hand, the following relation may be utilized:

$$k(v=n) = nk_{10} \quad . \tag{20-29}$$

Measurement of the quenching of vibrationally excited N_2 by atomic oxygen over a wide range of kinetic temperatures (References 20-117 through 20-119) has indicated that O is an effective quencher. Even at low kinetic temperatures, the measured deexcitation rate considerably exceeds the calculated rate (Reference 20-120). Similarly, high energy transfer rates have also been indicated as a result of recent VT measurements in N_2 (Reference 20-121).

The VV energy transfer processes to other atmospheric molecules are either nonresonant or near-resonant. While acting as a deexcitation mechansism for the vibrational energy of N_2, the process excites vibrational modes of other molecules. This transferred energy reappears as infrared radiation whenever the energy-acquiring molecule has a permanent dipole moment. The N_2 vibrational energy transfer to CO_2, for example, is well known from its application to the CO_2 laser (Reference 20-122). Both VT and VV energy transfer rate data pertaining to $N_2^{\ddagger}$ deexcitation are presented in Table 20-4.

Vibrational deexcitation through energy transfer into electronic excitation of atoms is another possibility. It has been argued (Reference 20-126) that the excitation of the sodium D-line in auroras below 100 km altitude is a likely result of energy transfer to the sodium from vibrationally excited nitrogen. This reaction has been observed in the laboratory (Reference 20-127), and its cross-section has been measured as 10^{-15} cm^2 (Reference 20-128). It is doubtful, however, that vibrationally excited nitrogen exists below the turbopause (References 20-82, 20-129 through 20-131), as would have to be the case for this postulate to be correct.

The emphasis placed on N_2 vibrational temperature stems from the fact that the degree of N_2 vibrational excitation significantly affects certain reactions, the most important of which is:

$$N_2^{\ddagger} + O^+(^4S) \rightarrow NO^+ + N(^4S) \quad . \tag{20-30}$$

This reaction depends upon both the N_2 vibrational temperature (References 20-132, 20-133) and the ion kinetic temperature (Reference 20-134). It plays an important role in the deionization processes of the quiescent and the disturbed ionosphere. It has been

Table 20-4. Energy transfer from $N_2(v=1)$.

Collision Partner	Probable Product	Rate Constant	Temperature Range(K)	References
N_2	Kinetic energy	$<<10^{-20}$	300	20-18, 20-123, 20-124
N_2	Kinetic energy	$8.5 \times 10^{-7} \exp(-273/T^{1/3})$	1000-5000	20-18, 20-123
N_2	$N_2^{\ddagger}$ (Resonant-VV)	3×10^{-13}	300	20-124
O_2	Kinetic energy	$<<10^{-20}$	300	20-18
O_2	Kinetic energy	$8.5 \times 10^{-7} \exp(-273/T^{1/3})$	1000-5000	20-18
O_2	$O_2^{\ddagger}$ (Nonresonant-VV)	$1.74 \times 10^{-10} \exp(-124/T^{1/3})$	200-5000	20-18
O	Kinetic energy	$1.2\ 10^{-13} \exp(-23/T^{1/3})$	300-5000	20-117 through 20-119, 20-125
CO_2	$CO_2^{\ddagger}$ (001)(Nonresonant-VV)	$1.71 \times 10^{-6} \exp(-175/T^{1/3})$ $6.0 \times 10^{-14} \exp(+15.3/T^{1/3})$	200-2000	20-18
NO	$NO^{\ddagger}$ (Nonresonant-VV)	1.5×10^{-16}	20-124	

suggested (Reference 20-132) that Reaction (20-30) would contribute to the loss of electrons in the ionosphere, owing to enhanced NO^+ formation. Several workers have shown that this is the case in the quiescent ionosphere auroral arcs (e.g., References 20-83, 20-84, 20-129, 20-130, 20-135, and 20-136) and atmospheres disturbed by nuclear bursts (Reference 20-137).

The N_2^+ loss processes discussed above, and also the diffusional loss, are illustrated as functions of altitude in Figure 20-4. The rates shown there were obtained (References 20-129, 20-130) using COSPAR atmospheric densities (Reference 20-138).

20.4.1.2 Electronic Excitation-Deexcitation: $N_2(X^1\Sigma_g^+) \rightleftarrows N_2(A^3\Sigma_u^+)$

Triplet-state nitrogen (e.g., $A^3\Sigma_u^+$, $B^3\Pi_g$, $C^3\Pi_u$, $E^3\Sigma_g^+$) may be formed by electron-impact excitation from the ground state (References 20-139 through 20-148). The (A) state at 6.17 eV is the lowest of these, and is metastable with two distinct substate lifetimes (a consequence of asymmetric transitions) of 1.27 and 2.5 sec (± about 20%), respectively (Reference 20-32). It emits in the well-known Vegard-Kaplan band system. In addition to electron impact from ground-state nitrogen, cascade from higher-lying triplet states, especially the (B) and (C) states, are alternative means for populating the (A) state.

Electron-impact excitation cross-sections of the triplet states have been calculated (References 20-149 through 20-151), and measured cross-sections exist for the (A) (References 20-143, 20-144), (B) (References 20-143 through 20-146), and (C) (References 20-143, 20-146 through 20-148) states. However, poor agreement exists among the reported shapes and peak values of these cross-sections, whether experimental or theorectical (Reference 20-152). A case in point is the peak cross-section of the (A) state, for which values have been published (in units of 10^{-17} cm^2) of 5.25 (Reference 20-144), 3.00 (Reference 20-143), 12.00 (Reference 20-151), and 15 (References 20-149, 20-150). A more recent calculation (Reference 20-153) provides a peak at 2×10^{-17} cm^2, which is shifted toward higher energies. Figure 20-5 presents the rate coefficient for electron-impact excitation of ground-state N_2 to the (A) state, using an average of the experimental cross-sections as a limit. This rate was obtained (Reference 20-154) using the earlier calculated cross-section of References 20-149 and 20-150, averaged with the electron velocity over a Maxwellian electron velocity distribution.

Vibrational excitation of the $N_2(A)$ state is important in auroral emissions, and has been suitably calculated for auroral conditions (Reference 20-155).

The significance of $N_2(A)$ becomes apparent in highly disturbed atmospheres and in auroral displays. Apart from the electron-impact excitation and cascade from higher N_2 triplet states, the following near-resonant charge-exchange reaction should also be considered as a mechanism for excitation of the (A) state:

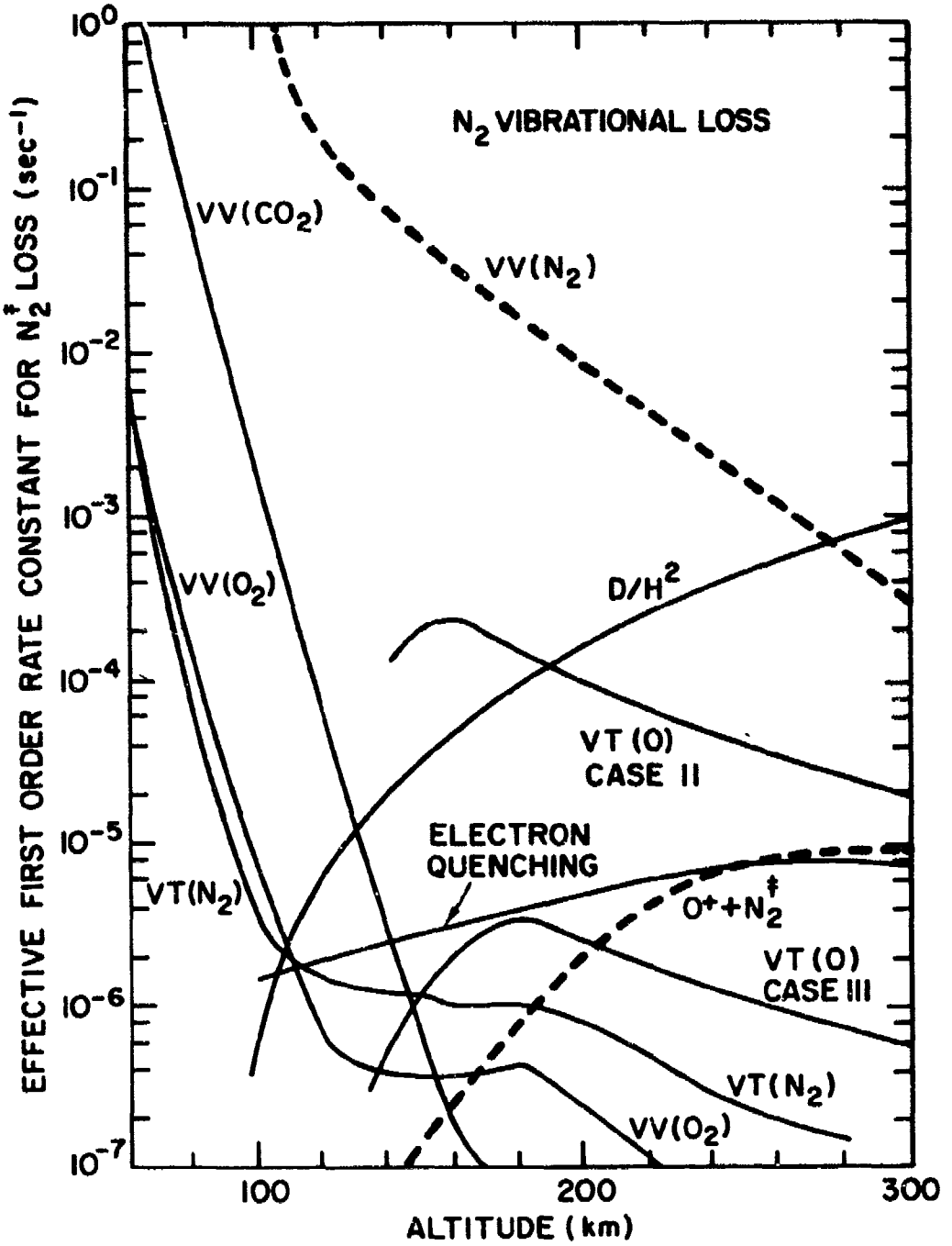

Figure 20-4. Loss rates for N_2 vibrational energy as functions of altitude (D/H^2 = diffusion coefficient divided by square of the scale height; cases II and III for VT(O) are described in the indicated references) (References 20-129, 20-130).

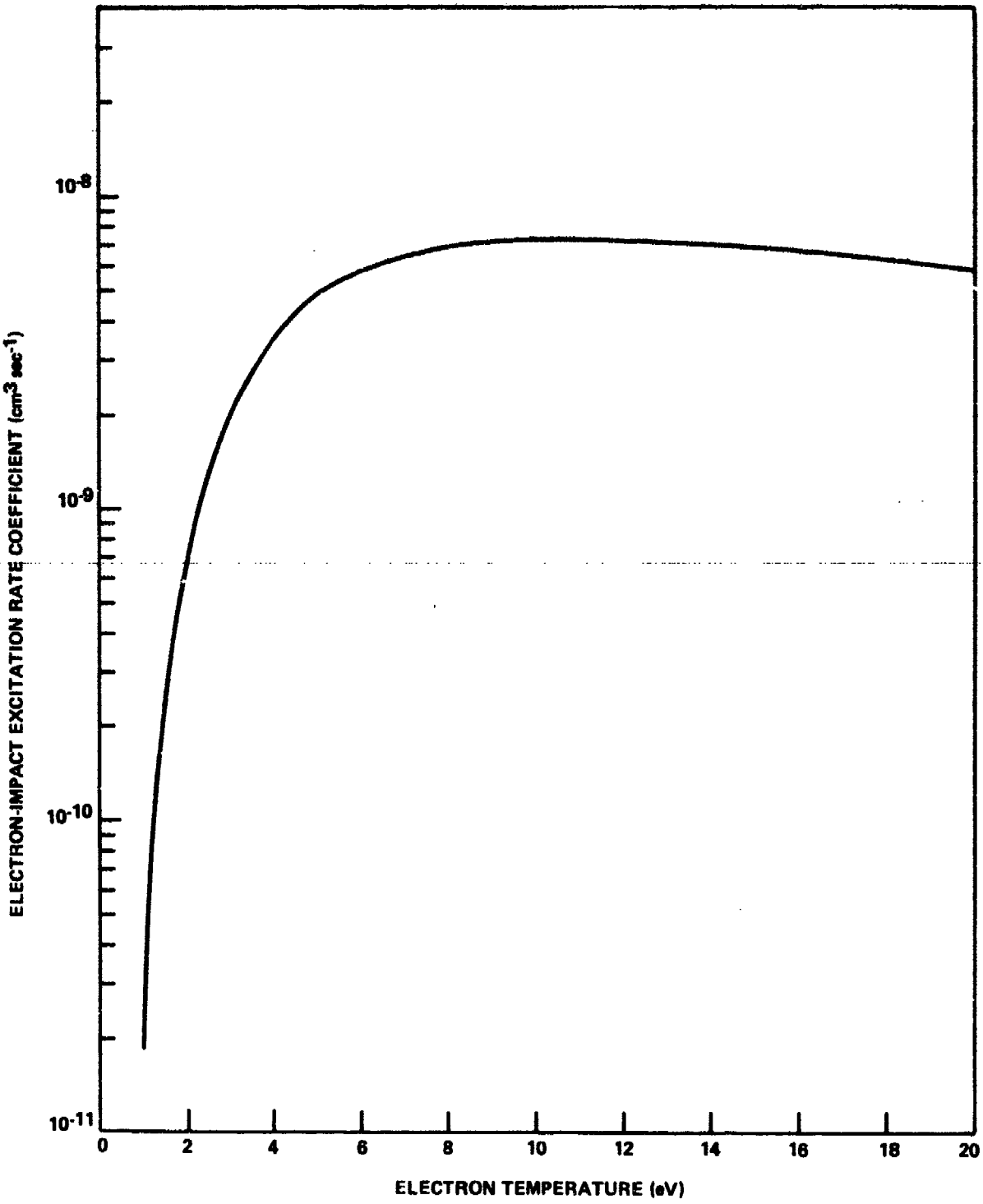

Figure 20-5. Electron-impact excitation rate coefficient of $N_2(A^3\Sigma_u^+)$ from the ground state, as a function of electron temperature (Reference 20-154).

$$N_2^+(X) + NO \rightarrow N_2(A) + NO^+ \quad . \qquad (20\text{-}31)$$

This reaction has a measured rate coefficient of 3.3×10^{-10} cm^3sec^{-1} (References 20-156 through 20-158).

Deexcitation of the (A) state proceeds through superelastic collisions with electrons, and via quenching collisions with atmospheric species. Quenching by ground-state nitrogen is only slightly effective (References 20-159, 20-160), but atomic nitrogen has been observed to be a relatively efficient quencher, by means of atom interchange (Reference 20-161):

$$N + N_2(A) \rightarrow N_2(X) + N \quad . \qquad (20\text{-}32)$$

Under atmospheric conditions, following an earlier report (Reference 20-11) of quenching by atomic oxygen, an overall rate coefficient for $N_2(A)$ in the (v=0) level has been obtained in the aurora (Reference 20-162), as 7.5×10^{-11} cm^3sec^{-1}, a portion of which (3×10^{-12} cm^3sec^{-1}) is due to formation of $O(^1S)$ among the products (Reference 20-163).

Metallic species, e.g., Na, Fe, Hg, Ba, are also effective quenchers of $N_2(A)$ via Penning ionization (References 20-12, 20-164, 20-165). Table 20-5 summarizes the available quenching data for $N_2(A)$ by several atmospheric species.

20.4.1.3 The $(a^1\Pi_g)$ State of Nitrogen

Of the many metastable states of nitrogen, only one other is treated here. The $(a^1\Pi_g)$ state, with a lifetime of 0.1 msec, has attracted some theoretical (Reference 20-151) and considerable experimental (References 10-143, 20-144, 20-170 through 20-173) attention concerning its excitation cross-section by electron impact. The most recent value (Reference 20-173) is in very good agreement with earlier findings (Reference 20-144) from threshold up to 40 eV incident electron energy. The excitation threshold for the state is 8.5 eV, coincident with a metastable state that has been observed elsewhere (Reference 20-174) to lead to associative ionization of the type:

$$N_2^* + NO \rightarrow N_2NO^+ + e \quad . \qquad (20\text{-}33)$$

However, the product N_2NO^+ has not as yet been identified in D-region mass-spectral observations.

20.4.2 Ionized Molecular Nitrogen, N_2^+

20.4.2.1 Electronic Excitation-Deexcitation: $N_2^+(B^2\Sigma_u^+)$

One of the strongest emissions in the aurora, twilight glow, dayglow, and highly disturbed atmospheres is the 391.4-nm band,

Table 20-5. Quenching data for $N_2(A^3\Sigma_u^+)$.

Quenchant	Rate Constant (cm^3 sec^{-1})	References
N_2	$<3 \times 10^{-19}$	20-159
	$\sim 10^{-19}$	20-15
O_2	2.5×10^{-12}	20-163, 20-166
O	$\leq 3 \times 10^{-11}$	20-11
	5×10^{-11}	20-15
	7.5×10^{-11}	20-162
N	5×10^{-11}	20-167
	5×10^{-12}	20-168
	5×10^{-11}	20-169
NO	7×10^{-11}	20-167

corresponding to the (0,0) transition of the first-negative band system ($B^2\Sigma_u^+ \rightarrow X^2\Sigma_g^+$) of N_2^+. The principal ionospheric formation processes for N_2^+ in the (B) state include solar photoionization of N_2 (Reference 20-175):

$$N_2 + h\nu(>18.7 \text{ eV}) \rightarrow N_2^+(B^2\Sigma_u^+) + e \quad , \tag{20-34}$$

energetic electron-impact ionization of N_2:

$$N_2 + e \rightarrow N_2^+(B^2\Sigma_u^+) + 2e \quad , \tag{20-35}$$

and photoexcitation by resonance scattering of solar radiation (Reference 20-176) at 391.4 nm off ambient N_2^+:

$$N_2^+(X^2\Sigma_g^+) + h\nu \rightarrow N_2^+(B^2\Sigma_u^+) \quad . \tag{20-36}$$

An additional mechanism that must be considered is electron-impact excitation from the ground state of the ion, especially by low-energy electrons (Reference 20-177):

$$N_2^+(X^2\Sigma_g^+) + e \rightleftarrows N_2^+(B^2\Sigma_u^+) + e \quad . \tag{20-37}$$

Only Reaction (20-35) is likely to be important in auroras. Indeed, the efficiency of converting incident electron energy into

the (0,0) transition in air via Reaction (20-35) is constant and has a value of about 5.2×10^{-3} (Reference 20-178), independent of the electron energy above 100 eV. This process plays an important role in determining the auroral strength. In highly disturbed atmospheres, on the other hand, Reactions (20-34) and (20-37) represent important excitation mechanisms in addition to Reaction (20-35). The electron-impact ionization cross-section leading to the formation of $N_2^+(B, v=0)$ as one of the few ionization continua of N_2^+ via Reaction (20-35) has been measured extensively (References 20-179 through 20-182) and is well established. Using the measured cross-section (Reference 20-180), averaged with the electron velocity over a Maxwellian electron velocity distribution, the electron-impact excitation rate coefficient for the (0,0) band has been obtained (Reference 20-154).

The excitation cross-section for the (0,0) band emission from the ground state of the ion, i.e., Reaction (20-37), has also been measured (References 20-177, 20-183, 20-184) and important disagreements have been found among the various determinations. For example, the peak cross-sections reported in References 20-177 and 20-183 are, respectively, 44 and 22 times as large as that obtained in Reference 20-184. However, a direct measurement of the rate coefficient for this reaction (Reference 20-185) indicates that the earlier cross-section determination of Reference 20-177 may have been too large by a factor of 40, which would suggest that the smaller value obtained in Reference 20-184 might be the most reliable.

Rate coefficients for both Reactions (20-35) and (20-37) are compared in Figure 20-6, where the data for the latter reaction (electron-impact excitation) have been obtained from the deexcitation rates of Reference 20-184.

An important deexcitation mechanism for $N_2^+(B, v=0)$ is collisional quenching by N_2, the cross-section for which has been measured (References 20-182, 20-186, 20-187). The corresponding rate coefficient for thermal temperatures is about 4.4×10^{-10} $cm^3 sec^{-1}$. In a highly ionized medium, however, superelastic collisions of $N_2^+(B)$ with electrons provides an additional deexcitation path. Comparison of the relative importance of the preceding reactions on the 391.4-nm emission in the quiescent ionosphere has shown (Reference 20-188) that at altitudes above 100-150 km, resonance scattering is the major source of 391.4-nm radiation. At higher densities, however, resonance charge-exchange reactions may be significant, e.g.:

$$N_2^+(B^2\Sigma_u^+) + O_2(X^3\Sigma_g^-) \rightarrow N_2(X^1\Sigma_g^+) + O_2^+(b^4\Sigma_g^-) \quad . \qquad (20\text{-}38)$$

Reactions of this type would produce additional $O_2^+(b \rightarrow a)$ first-negative band emission and $O_2^+(a^4\Pi_u)$ metastable ions. Because of the near-resonant nature of the reaction, it may proceed at a faster rate than the charge-exchange with N_2^+ in the ground state as one of the reactants. A relatively recent examination of the twilight airglow from rocket measurements has led to the conclusion that 90% of

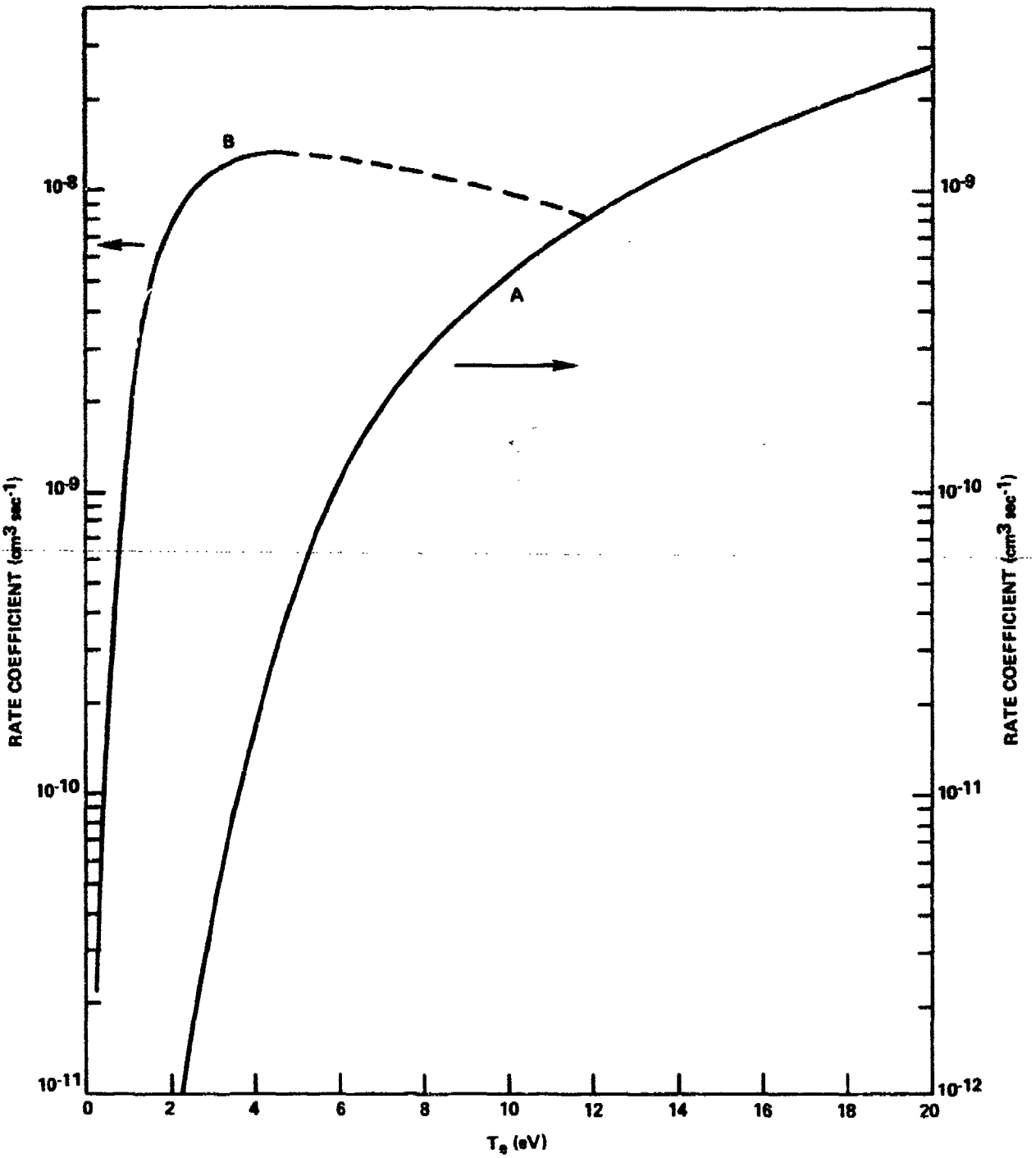

Figure 20-6. Rate coefficients as functions of electron temperature for Reactions (20-35) ($N_2 + e \rightarrow N_2^+(B,v=0) + 2e$) and (20-37) ($N_2^+(X) + e \rightarrow N_2^+(B,v=0) + e$) are indicated as curves A and B respectively; the dashed part of curve B is obtained from Reference 20-185, adjusted to the results of Reference 20-184.

the 391.4-nm emission is due to solar photon scattering off $N_2^+(X)$, while solar photoionization leading to the (B) state produces less than 10% of the emission (Reference 20-189).

20.4.2.2 Electronic Excitation-Deexcitation: $N_2^+(A^2\Pi_u)$

The formation of $N_2^+(A^2\Pi_u)$, which emits in the well-known Meinel (A→X) band system in the aurora and in the ambient and disturbed ionosphere, proceeds through mechanisms analogous to those that produce $N_2^+(B)$, i.e., Reactions (20-34) through (20-37). However, an additional source has been suggested, which proceeds via the near-resonant charge-exchange (Reference 20-190):

$$O^+(^2D) + N_2 \rightarrow N_2^+(A^2\Pi_u, v=1) + O(^3P). \qquad (20\text{-}39)$$

It has been observed (Reference 20-191) that the (1,0) and (1,2) bands of the Meinel system often exhibit anomalously high intensities in the aurora, which may be attributable to the preferential excitation of the first vibrational level according to Reaction (20-39). This is one of the important processes related to deionization in that it exchanges an atomic ion for a molecular one, which is then subject to dissociative recombination, a much faster process than the radiative recombination of atomic ions. The cross-section for Reaction (20-39) had been measured (Reference 20-192) for ion velocities of about 10^6 cm-sec^{-1} and found to be quite large, corresponding to a reaction rate coefficient of approximately 10^{-9} cm^{3}sec^{-1}. A more recent rate measurement (Reference 20-193) at thermal temperature gave a value of $k = 6 \times 10^{-10}$ cm^{3}sec^{-1}, in reasonable agreement with the earlier finding.

Observations of normal auroras indicate that the Meinel band system is one of the strongest emissions (References 20-194, 20-195), which has also been detected in dayglow (Reference 20-196). The cross-section for the electron-impact ionization reaction analogous to Reaction (20-35), but having $N_2^+(A)$ as its product, has been measured (Reference 20-197). In addition, the auroral emission of the Meinel band system relative to that of the first-negative band system has been calculated, using available data on excitation cross-sections, transitions, and quenching rates (Reference 20-198). Comparison of the results of these calculations with measured data exhibits reasonable agreement.

The electron-impact excitation of the Meinel bands from the ground state of the ion, i.e., the reaction analogous to Reaction (20-37), has not been measured. This process becomes important in the highly disturbed atmosphere as a cooling mechanism for electrons.

Deexcitation of the Meinel band system should proceed through superelastic collisons with low-energy electrons, and via quenching of N_2 and O_2. The quenching rates of $N_2^+(A)$ vibrational levels by N_2

and O_2 have been measured (References 20-197, 20-199, 20-200), but with poor agreement among the various results obtained. Average values (Reference 20-198) for quenching of the (v=1) level by N_2 and O_2 are 4.5 and 7.0 x 10^{-10} cm^3sec^{-1}, respectively.

The charge-transfer reaction:

$$N_2^+(A^2\Pi_u) + O_2 \rightarrow N_2 + O_2^+(a^4\Pi_u) \qquad (20\text{-}40)$$

may be another loss mechanism for the (A) state of N_2^+, since the reaction is in near-resonance.

Other excited states of N_2^+ have been observed, particularly $^4\Sigma$ and $^4\Delta$ metastables. These states have been found (References 20-50, 20-201) to form N_3^+ through the reaction:

$$N_2^+(^4\Sigma \text{ or } ^4\Delta) + N_2 \rightarrow N_3^+ + N \quad . \qquad (20\text{-}41)$$

Finally, the electron-impact ionizations of both N_2 and O_2 to the respective molecular ions in their ground electronic states fail to populate the vibrational levels of the products according to Franck-Condon predictions. Investigations near the respective ionization thresholds (References 20-202, 20-203) indicate that vibrational excitation is induced indirectly via autoionizing states. The importance of autoionization can be seen in the case of $N_2^+(X)$, where the Franck-Condon factors for transitions from $N_2(X, v=0)$ to $N_2^+(X,v)$ decrease by nearly an order of magnitude for each successive vibrational level of the ion produced, while for electrons with energies not far above the ionization potential it has been demonstrated (Reference 20-204) that the populations of the v=0,1 levels in the product are nearly equal.

20.4.3 Neutral Atomic Nitrogen, N

The nitrogen atom has two low-lying metastable states of interest, $N(^2D)$ and $N(^2P)$, for which several formation mechanisms exist. The $N(^2D)$ state, which is the upper level for the 520-nm dayglow, is produced by the dissociative recombination reactions:

$$N_2^+(X) + e \rightarrow N(^4S) + N(^2D) \qquad (20\text{-}42)$$

and

$$NO^+(X) + e \rightarrow N(^2D) + O \quad . \qquad (20\text{-}43)$$

Earlier calculations (Reference 20-205) of the branching ratios for these reactions have shown that the products of the NO^+ dissociative recombination, i.e., Reaction (20-43), are about 100% $N(^2D)$ and 100% $O(^3P)$. A more recent investigation (Reference 20-206) has indicated, however, that the actual yield of $N(^2D)$ is about 76%, the balance

being $N(^4S)$. In the N_2^+ dissociative recombination, i.e., Reaction (20-42), the yield is equal parts of $N(^2D)$ and $N(^4S)$ (Reference 20-207).

The two metastables, $N(^2D, ^2P)$, are also produced by electron impact from the ground state of the nitrogren atom, $N(^4S)$:

$$N(^4S) + e \rightarrow N(^2D, ^2P) + e \quad . \tag{20-44}$$

Among the calculated cross-sections for these excitations (References 20-208 through 20-212), the most recent (Reference 20-212) is also the most accurate in that it considers such relevant factors as target polarization, the higher-lying configurations, and so forth, which were neglected elsewhere. Using the cross-sections of Reference 20-212, the excitation rate coefficients for the low-lying levels of the nitrogen atom have been obtained (Reference 20-213) for a Maxwellian electron velocity distribution. These rate coefficients are presented in Figure 20-7 as functions of the electron temperature and are listed in Table 20-6 with the corresponding deexcitation rate coefficients.

Several charge-exchange and ion-atom interchange reactions, in ambient and highly disturbed ionospheres, also produce $N(^2D)$ and $N(^2P)$. Following are some examples taken from a large set of reactions (Reference 20-214), where only exothermic processes were considered and where conservation of total spin was observed:

$$N_2^+(X^2\Sigma_g^+) + O(^3P) \rightarrow NO^+(X^1\Sigma^+) + N(^2D, ^2P) \tag{20-45a}$$

$$N_2^+(X^2\Sigma_g^+) + O(^1D) \rightarrow NO^+(X^1\Sigma^+) + N(^2D, ^2P) \tag{20-45b}$$

$$N^+(^3P) + O_2(X^3\Sigma_g^-) \rightarrow O_2^+(X^2\Pi_g) + N(^2D) \tag{20-46}$$

$$N^+(^3P) + O(^1D) \rightarrow N(^2D) + O^+(^4S) \tag{20-47a}$$

$$N^+(^1D) + O(^3P) \rightarrow N(^2D) + O^+(^4S) \quad . \tag{20-47b}$$

...mination (Reference 20-215) of Atmospheric Explorer data showed Reaction (20-45a) to be the principal process for producing $N(^2D)$ in the normal ionosphere and the atomic reaction product to be 100% $N(^2D)$. The electron-impact dissociative ionization and dissociation of N_2 also produce $N(^2D)$, via the respective reactions:

$$N_2 + e \rightarrow N^+ + N(^2D) + 2e \tag{20-48}$$

and

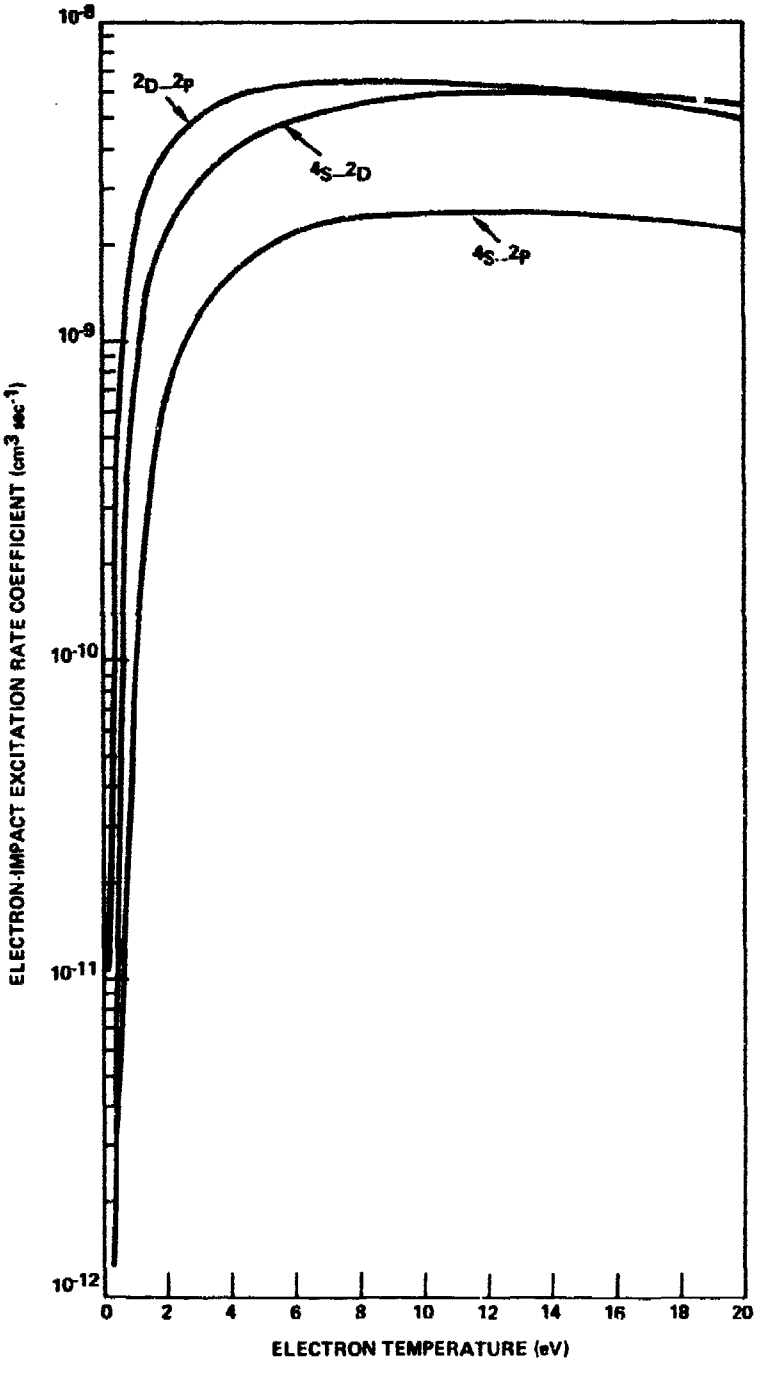

Figure 20-7. Electron-impact excitation rate coefficients for the low-lying states of atomic nitrogen as functions of the electron temperature (Reference 20-213).

Table 20-6. Electron-impact excitation and deexcitation rate coefficients for the low-lying states of the nitrogen atom (Reference 20-213).[a]

T_e(eV)	$^4S - ^2D$	$^4S - ^2P$	$^2D - ^2P$
0.1	8.0 (-20)[b]	2.6 (-25)	2.10 (-14)
	6.3 (-10)[c]	5.5 (-10)	5.7 (-9)
0.2	1.54 (-14)	2.03 (-17)	1.16 (-11)
	8.6 (-10)	7.5 (-10)	7.8 (-9)
0.3	1.25 (-12)	1.11 (-14)	9.78 (-11)
	1.35 (-9)	1.1 (-9)	8.9 (-9)
0.5	4.2 (-11)	1.47 (-12)	6.0 (-10)
	1.9 (-9)	1.2 (-9)	1.0 (-8)
0.7	1.98 (-10)	1.63 (-11)	1.16 (-9)
	2.34 (-9)	1.8 (-9)	1.0 (-8)
1.0	6.38 (-10)	8.91 (-11)	2.05 (-9)
	2.7 (-9)	2.1 (-9)	1.1 (-8)
1.2	1.08 (-9)	1.73 (-10)	2.56 (-9)
	3.1 (-9)	2.29 (-9)	1.16 (-8)
1.5	1.52 (-9)	3.38 (-10)	3.24 (-9)
	2.9 (-9)	2.4 (-9)	1.2 (-8)
2.0	2.27 (-9)	6.54 (-10)	4.1 (-9)
	2.9 (-9)	2.6 (-9)	1.2 (-8)
3.0	3.31 (-9)	1.23 (-9)	5.18 (-9)
	2.9 (-9)	2.7 (-9)	1.3 (-8)
5.0	4.50 (-9)	1.99 (-9)	6.2 (-9)
	2.90 (-9)	2.7 (-9)	1.3 (-8)
7.0	5.26 (-9)	2.36 (-9)	6.5 (-
	2.9 (-9)	2.6 (-9)	1.3 (-
10.0	5.85 (-9)	2.4 (-9)	6.5
	2.9 (-9)	2.3 (-9)	1.2 (
15.0	5.97 (-9)	2.49 (-9)	6.1 (-9)
	2.79 (-9)	2.1 (-9)	1.1 (-8)
20.0	4.96 (-9)	2.28 (-9)	5.47 (-9)
	2.2 (-9)	1.8 (-9)	9.7 (-9)

Notes:

[a] Numbers in parentheses indicate the power of 10 by which the entries are to be multiplied.

[b] Excitation rate coefficient.

[c] The corresponding deexcitation rate coefficient.

$$N_2 + e \rightarrow N + N(^2D) + e \quad . \qquad (20\text{-}49)$$

Despite numerous novel experimental approaches (References 20-216 through 20-218), exact branching ratios characterizing the production of $N(^2D)$ from Reactions (20-48) and (20-49) are not yet available.

Deexcitation of $N(^2D)$ and $N(^2P)$ proceeds by superelastic collisions with low-energy electrons. However, a major loss mechanism for $N(^2D)$, in daytime, aurora, and highly disturbed atmospheres, is via:

$$N(^2D) + O_2 \rightarrow NO + O \quad . \qquad (20\text{-}50)$$

The rate coefficient for Reaction (20-50) has been determined (References 20-219, 20-220) as: $k \sim 6 \times 10^{-12}$ $cm^3 sec^{-1}$. Another sink for $N(^2D)$ is:

$$N(^2D) + N_2O \rightarrow N_2 + NO \quad , \qquad (20\text{-}51)$$

for which the rate coefficient at room temperature is: $k = 1.6 \times 10^{-12}$ $cm^3 sec^{-1}$ (References 20-219, 20-221).

The quenching rate coefficient of $N(^2D)$ by atomic oxygen has been measured (Reference 20-222) as: $k = 1.8 \times 10^{-12}$ $cm^3 sec^{-1}$, which is three times as large as a value estimated from atmospheric data (Reference 20-223). Quenching rate coefficients of $N(^2D)$ by atmospheric species of interest are summarized in Table 20-7.

Table 20-7. Quenching of $N(^2D)$.

Quenching Species	Rate Constant (cm^3 sec^{-1})	Reference
O_2	6×10^{-12}	20-219, 20-220
N_2	1.6×10^{-14}	20-219
O	1.8×10^{-12}	20-221
	6×10^{-13}	20-222
NO	7.0×10^{-11}	20-219
e	See Table 20-6	20-213

20.4.4 Ionized Atomic Nitrogen, N^+

The atomic nitrogen ion has two low-lying metastable states, $N^+(^1D)$ and $N^+(^1S)$, which are important in highly ionized atmospheres. These are formed from the neutral metastables $N(^2D)$ and $N(^2P)$ by photoionization, the cross-sections for which have been calculated (Reference 20-224).

The same metastable ions, $N^+(^1D, ^1S)$, are also produced by electron-impact excitaton of the ground state of the ion, $N^+(^3P)$, where the relevant near-threshold collision strengths have also been calcu'ated (References 20-210, 20-225). These collison strengths are in good agreement and have been utilized (Reference 20-213) to obtain the corresponding deexcitation rate coefficients for a Maxwellian electron velocity distribution, as listed in Table 20-8. The corresponding excitation rate coefficients are obtainable through application of the principle of detailed balancing.

Table 20-8. Electron-impact deexcitation rate coefficients for the low-lying metastable states of N^+ (T_e in units of eV) (Reference 20-213).

Transition	Deexcitation Rate Coefficients ($cm^3\ sec^{-1}$)
$^1D - ^3P$	$4.8 \times 10^{-8}\ (T_e)^{-1/2}$
$^1S - ^3P$	$3.2 \times 10^{-8}\ (T_e)^{-1/2}$
$^1S - ^1D$	$3.3 \times 10^{-8}\ (T_e)^{-1/2}$

In addition to the above processes, $N^+(^1D)$ and $N^+(^1S)$ are generated in the electron-impact dissociative ionization of N_2, and probably in such charge-exchange processes (Reference 20-214) as:

$$N_2^+(X^2\Sigma_g^+) + N(^2D) \rightarrow N_2(X^1\Sigma_g^+) + N^+(^1D) \qquad (20\text{-}52)$$

and

$$N_2^+(X^2\Sigma_g^+) + N(^2P) \rightarrow N_2(X^1\Sigma_g^+) + N^+(^1S) \quad . \qquad (20\text{-}53)$$

The deexcitation and loss processes of $N^+(^1D, ^1S)$ include superelastic collisons with electrons and such charge-exchange and ion-atom interchange reactions, in addition to Reaction (20-47b), as:

$$N^+(^1D) + O_2(X^3\Sigma_g^-) \rightarrow O_2^+(a^4\Pi_u) + N(^4S) \qquad (20\text{-}54)$$

$$N^+(^1S) + NO(X^2\Pi_r) \rightarrow NO^+(a^3\Sigma^+) + N(^2P) \quad . \qquad (20\text{-}55)$$

No quantitive measurements are available, however, relating to Reactions (20-52) through (20-55).

20.4.5 Neutral Molecular Oxygen, O_2

20.4.5.1 Vibrational Excitation-Deexcitation of the Ground Electronic State, $O_2(X) \rightleftarrows O_2(X)^{\ddagger}$

During the years since the classical reviews (References 20-11, 20-111, 20-226) of the vibrational excitation of ground-state oxygen in the atmosphere were published, additional interactions, e.g.,:

$$O + O_3 \rightarrow O_2(a^1\Delta_g) + O_2(X^3\Sigma_g^-)^{\ddagger} \quad , \tag{20-56}$$

have been found (Reference 20-227) to comprise efficient means of generating the higher vibrational levels of $O_2(X)^{\ddagger}$. Vibrational excitation by electron impact with $O_2(X)$ (References 20-228, 20-229) is also an important process, for which the cross-sections are, however, generally both narrower and of lesser magnitude than the comparable processes in $N_2(X)$. Electron-impact excitation rate coefficients obtained (Reference 20-230) from the measured cross-sections are presented in Figure 20-8 for a Maxwellian electron velocity distribution. (It may be useful to compare, in this context, the curves of Figure 20-8 with the corresponding material relating to $N_2(X)$, in Figure 20-3.)

In addition, high-energy ($\geq$10 eV) ions are found (Reference 20-231) to generate vibrationally excited oxygen via:

$$O^+ + O_2(X) \rightarrow O^+ + O_2(X)^{\ddagger} \quad . \tag{20-57}$$

The signficance of vibrationally excited $O_2(X)$ arises from its role in enhancing the rates of such processes as:

$$O_2(X) + e \rightarrow O^- + O \quad , \tag{20-58}$$

where it is found that the cross-section for Reaction (20-58) depends strongly on the $O_2(X)$ internal temperature (References 20-203, 20-232, 20-233). As the equlibrium temperature of $O_2(X)$ increases from 300 K to 2100 K, the energy levels of both the maximum cross-section and the threshold for Reaction (20-58) shift downward. These results have been interpreted (Reference 20-234) as being due to the vibrational excitation of $O_2(X)$, but it has also been shown (Reference 20-235) that rotational excitation must be important as well.

Vibrationally excited $O_2(X)^{\ddagger}$ is quenched by several atmospheric species; quenching coefficients for various collision partners are summarized in Table 20-9. Using these data in conjunction with atmospheric densities and temperatures (Reference 20-138), the effective first-order deactivation rate coefficients for $O_2(X,v=1)$ are shown in Figure 20-9 as functions of altitude.

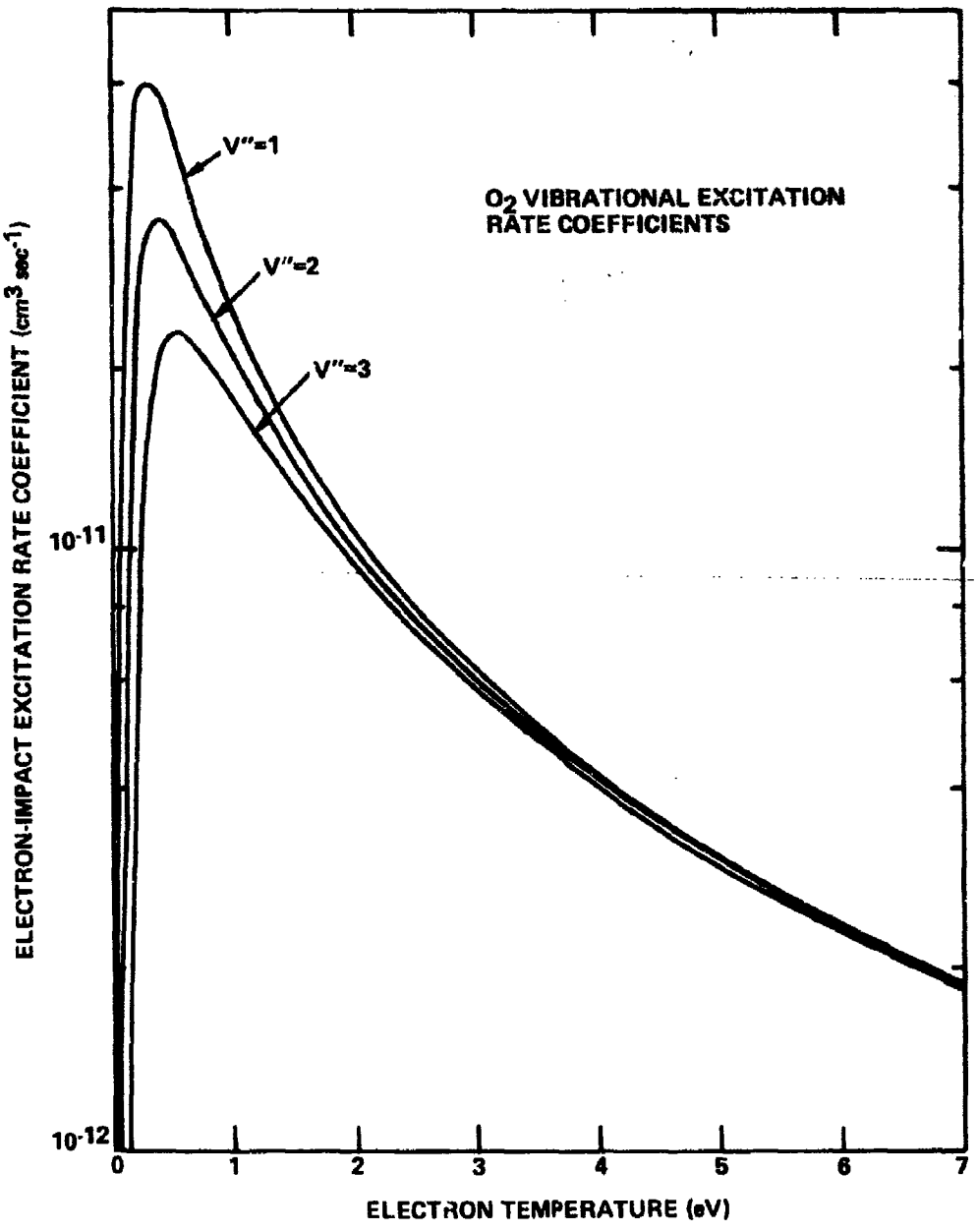

Figure 20-8. Electron-impact excitation rate coefficients of three $O_2(X)$ vibrational levels as functions of the electron temperature (Reference 20-230).

Table 20-9. Deactivation of $O_2(v=1)$ by quenching via several collision partners.

Reaction	Rate Coefficient (cm^3 sec^{-1})	Temperature Range (K)	References
$O_2^{\ddagger} + M \rightarrow O_2 + M$ (VT)	$4.81 \times 10^{-8} \exp(-170/T^{1/3})$	200-5000	20-18, 20-116 20-123, 20-236
M = N_2 or O_2			
$O_2^{\ddagger} + O \rightarrow O_2 + O$ (VT)	$6.88 \times 10^{-9} \exp(-76.75/T^{1/3})$	200-2000	20-18, 20-237
	$1.7 \times 10^{-10} \exp(-4000/T)$	2000-4000	20-238
$O_2^{\ddagger} + H_2O \rightarrow O_2 + H_2O^{\ddagger}$ (VV)	$3.6 \times 10^{-10} \exp(-60.69/T^{1/3})$	200-5000	20-18, 20-123

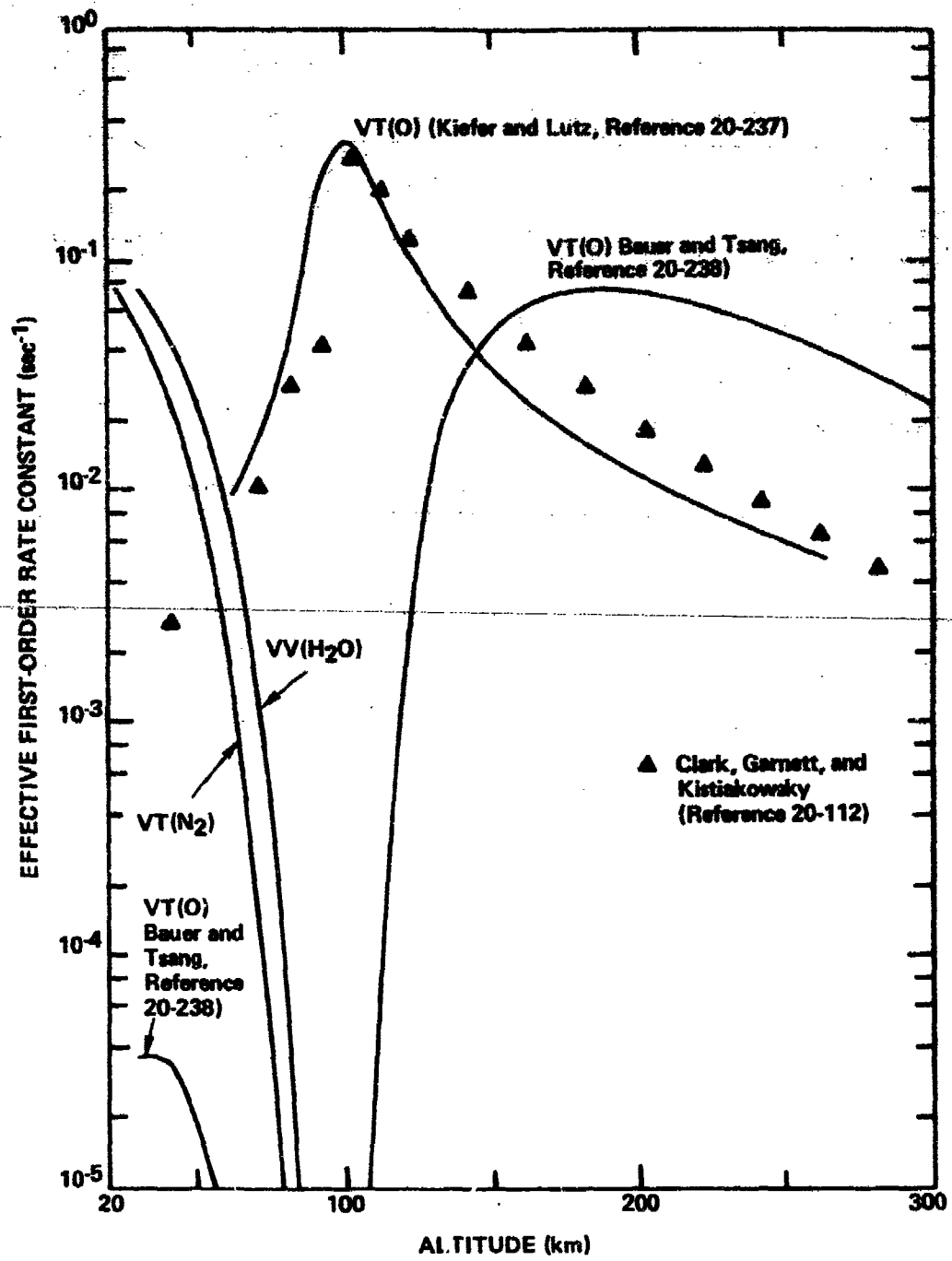

Figure 20-9. Deactivations of $O_2(v=1)$ by various processes as functions of altitude (Reference 20-138).

20.4.5.2 Electronic Excitation-Deexcitation: $O_2(X^3\Sigma_g^-) \rightleftarrows O_2(a^1\Delta_g)$

Among the most abundant metastable states found in the upper atmosphere is the $(a^1\Delta_g)$ state of the oxygen molecule. This state is the upper level from which the (0,0) transition band to the ground electronic state gives rise to the infrared atmospheric emission at 1.27 μm. Its daytime density (References 20-239, 20-240) at 50 km altitude is about 10^{10} cm^{-3}, and its abundance is attributed to the photodissociation of ozone by solar radiation in the Hartley continuum (References 20-239, 20-241):

$$O_3 + h\nu \text{ (Hartley continuum)} \rightarrow O + O_2(a^1\Delta_g) \quad . \qquad (20\text{-}59)$$

Table 20-10 (Reference 20-242) lists the quantum yields for various photolytic processes, including Reaction (20-59), for a range of wavelengths in the visible and ultraviolet regions.

Table 20-10. Summary of evaluated photochemical data (Reference 20-242).

Photolytic Process	Quantum Yield	Wave-Length (nm)	Wavelength Range (nm) for Absorption Coefficients
$O_3 + h\nu$ (vis) $\rightarrow O + O_2$	1	450-750	440-850
$O_3 + h\nu$ (uv) $\rightarrow O(^1D) + O_2(a^1\Delta_g)$	1 0	250-310 >310	200-360
$\rightarrow O(^1D) + O_2(X^3\Sigma_g^-)$	0	<350	
$\rightarrow O(^3P) + O_2$(singlet)	0 ~1	<310 310-350	
$\rightarrow O$ (total) $+ O_2$	1	250-350	
$\rightarrow O(^1D) + O_2(b^1\Sigma_g^+)$	0	250-350	
$\rightarrow O(^3P) + O_2(X^3\Sigma_g^-)$	0	250-350	

Other mechanisms producing $O_2(a^1\Delta_g)$ include the neutral rearrangement:

$$O(^3P) + O_3 \rightarrow O_2(X^3\Sigma_g^-) + O_2(a^1\Delta_g) \quad . \qquad (20\text{-}60)$$

with a rate coefficient (Reference 20-243) $k = 4.5 \times 10^{-15}$ cm^3sec^{-1}, and electron-impact excitation:

$$O_2(X^3\Sigma_g^-) + e \rightarrow O_2(a^1\Delta_g) + e \quad . \qquad (20\text{-}61)$$

The cross-section for Reaction (20-61) has been measured (Reference 20-244). It has also been calculated using the Born approximation (Reference 20-245). Rate coefficients for the electron-impact excitation of $O_2(a^1\Delta_g)$ from the ground state as functions of the electron temperature have been derived (and are listed in Table 20-11) from the measured cross-sections for low-energy electrons (Reference 20-246). It has been suggested (Reference 20-247) that the exothermic reaction:

Table 20-11. Electron-impact excitation rate coefficients (cm^3sec^{-1}) for the production of $O_2(a^1\Delta_g)$ and $O_2(b^1\Sigma_g^+)$ from $O_2(X^3\Sigma_g^-)$ (Reference 20-246).

Electron Temperature (eV)	$(a^1\Delta_g)$	$(b^1\Sigma_g^+)$
0.1	1.7(-15)	3.1(-18)
0.2	5.1(-13)	1.6(-14)
0.3	3.7(-12)	3.2(-13)
0.5	2.3(-11)	4.1(-12)
0.7	3.2(-11)	1.4(-11)
1.0	1.3(-10)	3.2(-11)
1.2	1.9(-10)	4.6(-11)
1.5	3.0(-10)	6.7(-11)
2.0	4.4(-10)	1.1(-10)
3.0	6.5(-10)	1.5(-10)
5.0	8.5(-10)	2.0(-10)

Note: Numbers in parentheses indicate the power of 10 by which the entries are to be multiplied.

$$O_2^+ + NO \rightarrow NO^+ + O_2(a^1\Delta_g) \qquad (20\text{-}62)$$

may be relevant to auroral phenomena.

The altitude profile of $O_2(a^1\Delta_g)$ obtained from rocket measurements of the 1.27-μm radiation (References 20-240, 20-248) is well understood in terms of its daytime production mechanism. The nighttime measurements, however (Reference 20-249), imply the importance of such additional reactions as:

$$O + O + M \rightarrow O_2(a^1\Delta_g) + M \qquad (20\text{-}63)$$

(M = third body) and

$$O + HO_2 \rightarrow O_2(a^1\Delta_g) + OH \quad . \qquad (20\text{-}64)$$

The latter mechanism has been suggested (Reference 20-250) as an additional source for nightglow.

The singlet metastable state, $O_2(a^1\Delta_g)$, is quite stable and its behavior has been documented in depth (Reference 20-251). It is quenched by atmospheric species, e.g., O_2, N_2, O, O_3, and in highly disturbed atmospheres by low-energy electrons. The quenching data are in excellent agreement (Reference 20-252). The most reliable values (excluding the data of Reference 20-253) are given in Table 20-12. It is evident from these data that molecular oxygen is the dominant quenching partner in the normal atmosphere, a conclusion confirmed by the interpretation of atmospheric $O_2(a^1\Delta_g)$ emission offered in Reference 20-240.

Other loss mechanisms for $O_2(a^1\Delta_g)$ have been suggested, such as:

$$O_2^- + O_2(a^1\Delta_g) \rightarrow O_2 + O_2 + e \quad . \qquad (20\text{-}65$$

occurring in polar-cap absorption events (Reference 20-259) and in the disturbed atmosphere (Reference 20-260). Further investigations have verified the rapidity of the reaction (References 20-261, 20-262) with a rate coefficient $k \sim 2 \times 10^{-10}$ cm^3sec^{-1}, and have indicated that:

$$O^- + O_2(a^1\Delta_g) \rightarrow O_3 + e \quad , \qquad (20\text{-}66)$$

is rapid as well, with a rate coefficient $k = 3 \times 10^{-10}$ cm^3sec^{-1}.

Deexcitation detachment reactions such as Reaction (20-65) are significant for disturbed atmospheres in which anomalously long,

Table 20-12. Quenching data for $O_2(a^1\Delta_g)$.

Quenching Species	Rate Constant ($cm^3\ sec^{-1}$)	References
O_2	2.4×10^{-18}	20-252
	2.2×10^{-18}	20-254
	2.2×10^{-18}	20-255
	2.0×10^{-18}	20-256
	$2.2 \left(\frac{T}{300}\right)^{0.8} \times 10^{-18}$	20-242
N_2	$<1.1 \times 10^{-19}$	20-240
CO_2	3.9×10^{-18}	20-252
H_2O	1.5×10^{-17}	20-252
Ar	$\leq 2.1 \times 10^{-19}$	20-252
O	$\leq 1.3 \times 10^{-16}$	20-257
N	$(2.8 \pm 2) \times 10^{-15}$	20-257
O_3	3×10^{-15}	20-258

e.g., 1.27 μm, emissions are found, presumably owing to the presence of $O_2(a^1\Delta_g)$ (References 20-263 through 20-265).

Still another channel by which $O_2(a^1\Delta_g)$ may be quenched is the radiative formation of O_2 dimer (References 20-251, 20-266):

$$2\ O_2(a^1\Delta_g) \rightleftarrows O_4^* \rightarrow 2\ O_2(X^3\Sigma_g^-) + h\nu(634,\ 703\ nm) \quad . \qquad (20\text{-}67)$$

The same interaction leads alternatively to the formation of $O_2(b^1\Sigma_g^+)$ (References 20-266, 20-267):

$$2\ O_2(a^1\Delta_g) \rightarrow O_2(b^1\Sigma_g^+) + O_2(X^3\Sigma_g^-) \quad . \qquad (20\text{-}68)$$

However, the rate coefficient (Reference 20-268) for Reaction (20-67) is $k = 2 \times 10^{-17}\ cm^3 sec^{-1}$, which indicates that both Reactions (20-67) and (20-68) are probably unimportant in the normal atmosphere.

20.4.5.3 Electronic Excitation-Deexcitation: $O_2(X^3\Sigma_g^-) \rightleftarrows O_2(b^1\Sigma_g^+)$

The metastable state $O_2(b^1\Sigma_g^+)$ is the upper level for the $O_2(b \rightarrow X)$ atmospheric band emission. It is formed similarly to $O_2(a^1\Delta_g)$, by electron-impact excitation from the ground state of the molecule:

$$O_2(X^3\Sigma_g^-) + e \rightarrow O_2(b^1\Sigma_g^+) + e \quad . \tag{20-69}$$

The cross-section has been measured (Reference 20-244), and excitation rate coefficients over a range of electron temperatures, which have been obtained (Reference 20-246) from the measured cross-sections for low-energy electron collisions, are compiled in Table 20-11.

Additional mechanisms for generating $O_2(b^1\Sigma_g^+)$ include solar photolysis of ozone:

$$O_3 + h\nu \rightarrow O_2(b^1\Sigma_g^+) + O \quad , \tag{20-70}$$

three-body formation:

$$O + O + M \rightarrow O_2(b^1\Sigma_g^+) + M \quad , \tag{20-71}$$

and neutral rearrangement:

$$O + O_3 \rightarrow O_2(b^1\Sigma_g^+) + O_2(X^3\Sigma_g^-) \quad . \tag{20-72}$$

Two additional production mechanisms are Reaction (20-68) and the energy-transfer reaction (References 20-269, 20-270):

$$O(^1D) + O_2(X^3\Sigma_g^-) \rightarrow O(^3P) + O_2(b^1\Sigma_g^+) \quad . \tag{20-73}$$

The measured rate coefficient for Reaction (20-73) (Reference 20-270) is $k = 9 \times 10^{-11}$ cm^3sec^{-1}, which may be important in auroras (Reference 20-271). Reaction (20-73) has been identified (Reference 20-272) as resonant with the (v=2) level of $O_2(b^1\Sigma_g^+)$. More recent observations (Reference 20-273), however, of the atmospheric band in auroras indicate emission from higher, i.e., ($v \geq 5$), vibrational levels. This suggests the existence of energy-transfer processes from $O(^1S)$, $N(^2D)$, and also $O(^1D)$ at high kinetic energies, such as to populate the ($v \geq 4$) levels (Reference 20-273).

The quenching of $O_2(b^1\Sigma_g^+)$ proceeds via low-energy electron collisions in both normal and highly disturbed atmospheres. Quenching also occurs by collision with N_2 and O_2, where $k = (1.5\text{-}2.5) \times 10^{-15}$ cm^3sec^{-1} (References 20-274, 20-275) and 1.5×10^{-16} cm^3sec^{-1} (References 20-15, 20-274), respectively.

20.4.5.4 Electronic Excitation-Deexcitation: $O_2(X^3\Sigma_g^-) \rightleftarrows O_2(A^3\Sigma_u^+)$

The $(A^3\Sigma_u^+)$ state of the oxygen molecule is metastable and is the upper level of the forbidden Herzberg band transitions. From observations in the normal atmosphere and from laboratory afterglow measurements, the dominant excitation of this state is believed to be due to the three-body process (References 20-276, 20-277):

$$O + O + M \rightarrow O_2(A^3\Sigma_u^+) + M \quad . \tag{20-74}$$

The rate coefficient for Reaction (20-74) has been measured (Reference 20-278) with $M = N_2$; it has a value $k \sim 10^{-37}$ cm^{6}sec^{-1} at low pressure, i.e., $n(N_2) < 10^{16}$ cm^{-3}. In highly disturbed atmospheres, electron impacts with $O_2(X)$ are expected to excite the $(A^3\Sigma_u^+)$ state. However, data exist for the cross-section for this process only at 20 and 45 eV electron energies (Reference 20-279). The quenching of $O_2(A^3\Sigma_u^+)$ by atmospheric species is not a well-known phenomenon.

20.4.6 Neutral Atomic Oxygen, O

The oxygen atom has two low-lying metastable states, $O(^1D)$ and $O(^1S)$, the upper levels for emissions at 630 and 557.7 nm, respectively. In addition, the resonance line at 130.4 nm has been of considerable interest in atmospheric ultraviolet emission. The (^1D) and (^1S) states are discussed in detail below.

20.4.6.1 Electronic Excitation-Deexcitation: $O(^3P) \rightleftarrows O(^1D)$

The (^1D) state of atomic oxygen emits two forbidden lines at 630 and 636.4 nm, which are prominent in the aurora, dayglow, nightglow, twilight, and in highly disturbed atmospheres. In the dayglow the major source of $O(^1D)$ is the O_2 photodissociation in the Schumann-Runge continuum (Reference 20-280):

$$O_2 + h\nu(>7.1 \text{ eV}) \rightarrow O(^3P) + O(^1D) \quad . \tag{20-75}$$

Below 80 km altitude, the photolysis of ozone contributes greatly to $O(^1D)$ production, via reactions listed in Table 20-10. At higher altitudes, $O(^1D)$ is produced by dissociative recombination:

$$O_2^+ + e \rightarrow O(^3P) + O(^1D) \tag{20-76}$$

and by electron-impact excitation of the ground state:

$$O(^3P) + e \rightarrow O(^1D) + e \quad . \tag{20-77}$$

Equations (20-76) and (20-77) are important $O(^1D)$ contributors in auroras and highly disturbed atmospheres as well as the normal atmosphere. The rate coefficient for Reaction (20-76) has been reliably

measured over a wide range of electron temperatures (Reference 20-281). At room temperature, $k = 2.2 \times 10^{-7}$ cm^3sec^{-1}. Afterglow measurements (References 20-282, 20-283) of the branching ratio among the products of Reaction (20-76) have shown the true products to be: 0.9 $O(^1D)$ + 0.1 $O(^1S)$ + 1.0 $O(^3P)$, with appropriate reaction rate coefficients at 300 K (as defined in terms of the individual species productions rather than disappearance of the reactant O_2^+) equal to 1.9×10^{-7}, 2.1×10^{-8}, and 2.1×10^{-17} cm^3sec^{-1}, respectively.

The electron-impact excitation cross-sections for the ground-state configuration, which includes $O(^1D)$ and $O(^1S)$, have been calculated (References 20-208 through 20-210, 20-284). The cross-sections obtained in the most recent and most accurate of these calculations (Reference 20-284) have been utilized to obtain (Reference 20-213) the relevant rate coefficients for excitation. These rates are presented as functions of the electron temperature in Figure 20-10. They are also listed in Table 20-13, along with the corresponding deexcitation rate coefficients, obtained by detailed-balance computations (Reference 20-213).

The (^1D) state also arises as a result of electron impacts with molecular oxygen via dissociation and dissociative ionization reactions. No quantitative data are available in this area, however. Data from flowing-afterglow experiments (Reference 20-278) suggest that the deactivation of $O(^1S)$ by $O(^3P)$ may also give rise to $O(^1D)$:

$$O(^1S) + O(^3P) \rightarrow O(^1D) + O(^1D) \qquad (20\text{-}78)$$

$$\rightarrow O(^3P) + O(^1D)$$

the importance of which in the nightglow has been noted elsewhere (Reference 20-11). This reaction and its kinetics are discussed further below.

The quenching of $O(^1D)$ by collisions with atmospheric species includes, in highly ionized atmospheres, superelastic collisions with low-energy electrons (see Table 20-13). It had earlier been concluded (Reference 20-11), on the basis of older quenching data, that molecular nitrogen is the most efficient quenching agent, having a rate coefficient for the process of $k \approx 8 \times 10^{-11}$ cm^3sec^{-1}. This value was supported at the time of its publication (References 20-285, 20-286), and in a later review (Reference 20-15). More recent findings (Reference 20-287, however, have determined the quenching rate coefficients of $O(^1D)$ by N_2 and O_2 to be 5.5 and 7.5×10^{-11} cm^3sec^{-1}, respectively, indicating that O_2 is the more efficient quencher, contrary to prior opinion (Reference 20-286).

In addition to collisional quenching, $O(^1D)$ undergoes depletion by chemical interactions with minor atmospheric species, especially in the stratosphere. The importance of these reactions has been demonstrated both in the D-region (Reference 20-288) and in the stratosphere (Reference 20-289). In the stratosphere, for example,

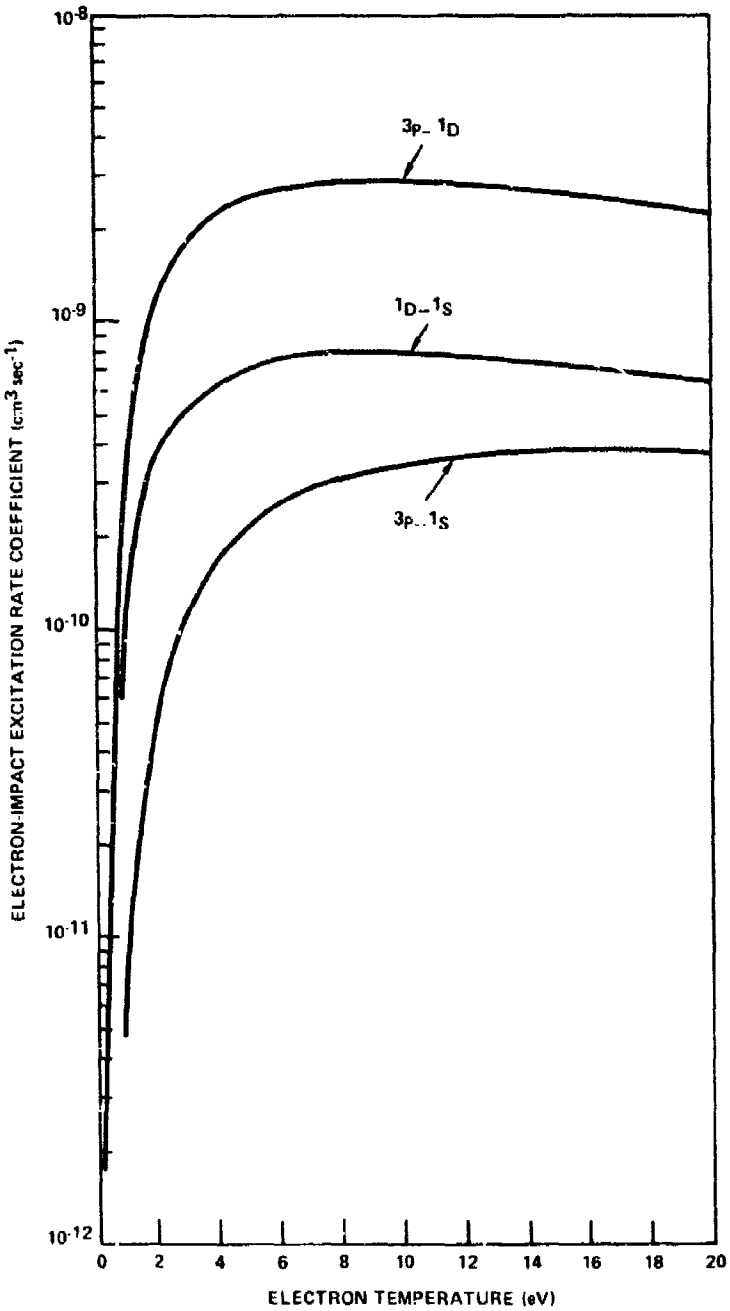

Figure 20-10. Electron-impact excitation rate coefficients for the low lying states of atomic oxygen as functions of the electron temperature (Reference 20-213).

Table 20-13. Electron impact excitation and deexcitation rate coefficients for the low-lying states of the oxygen atom (Reference 20-213).[a]

T_e(eV)	$^3P - {}^1D$	$^3P - {}^1S$	$^1D - {}^1S$
0.1	1.92 (-18)[b]	1.78 (-28)	2.25 (-19)
	1.1 (-9)[c]	2.1 (-9)	4.9 (-9)
0.2	5.28 (-14)	1.96 (-19)	1.76 (-14)
	1.7 (-9)	2.1 (-9)	5.8 (-9)
0.3	1.76 (-12)	2.10 (-16)	8.07 (-13)
	2.2 (-9)	2.1 (-9)	6.5 (-9)
0.5	3.28 (-11)	6.04 (-14)	1.52 (-11)
	2.9 (-9)	2.3 (-9)	6.4 (-9)
0.7	1.21 (-10)	7.25 (-13)	5.4 (-11)
	3.5 (-9)	2.5 (-9)	6.4 (-9)
1.0	3.43 (-10)	4.93 (-12)	1.38 (-10)
	4.4 (-9)	2.9 (-9)	6.3 (-9)
1.2	5.20 (-10)	1.06 (-11)	1.97 (-10)
	4.8 (-9)	3.1 (-9)	6.2 (-9)
1.5	7.94 (-10)	2.32 (-11)	2.76 (-10)
	5.2 (-9)	3.4 (-9)	6.0 (-9)
2.0	1.21 (-9)	5.15 (-11)	3.98 (-10)
	5.8 (-9)	3.7 (-9)	6.0 (-9)
3.0	1.84 (-9)	1.16 (-10)	5.30 (-10)
	6.3 (-9)	4.2 (-9)	5.5 (-9)
5.0	2.52 (-9)	2.21 (-10)	7.16 (-10)
	6.7 (-9)	4.6 (-9)	5.5 (-9)
7.0	2.73 (-9)	2.8 (-10)	7.76 (-10)
	6.5 (-9)	4.6 (-9)	5.3 (-9)
10.0	2.80 (-9)	3.3 (-10)	7.5 (-10)
	6.1 (-9)	4.5 (-9)	4.6 (-9)
15.0	2.58 (-9)	3.8 (-10)	6.9 (-10)
	5.3 (-9)	4.5 (-9)	4.0 (-9)
20.0	2.23 (-9)	3.7 (-10)	6.4 (-10)
	4.4 (-9)	4.1 (-9)	3.5 (-9)

Notes:

[a] Numbers in parentheses indicate the power of 10 by which the entries are to be multiplied.

[b] Excitation rate coefficient.

[c] The corresponding deexcitation rate coefficient.

the presence of OH and HO_2 free radicals is attributable solely to the reaction of $O(^1D)$ with water vapor:

$$O(^1D) + H_2O \rightarrow OH + OH, \quad (20\text{-}79)$$

for which $k = 6 \times 10^{-10}$ cm^3sec^{-1} (Reference 20-290), or 3.5×10^{-10} cm^3sec^{-1} (References 20-242, 20-291). It has been shown (Reference 20-288) that ozone concentrations in agreement with measured values may be computed only if several $O(^1D)$ reactions involving hydrogen and water are taken into consideration. These include Reaction (20-79) and also:

$$O(^1D) + H_2 \rightarrow OH + H \ , \quad (20\text{-}80)$$

for which $k = 3 \times 10^{-10}$ cm^3sec^{-1} (Reference 20-292). Thus if it were assumed that $k \sim 10^{-11}$ cm^3sec^{-1} for Reaction (20-80), $O(^1D)$ densities of 10^3-10^4 cm^{-3} between 40 and 100 km altitude are derived (Reference 20-288). This result is probably too large because of the assumed value for the rate coefficient of Reaction (20-80). However, the general conclusion that even small concentrations of $O(^1D)$ are extremely important persists even when turbulent transport is taken into account (References 20-293, 20-294). In addition to Reactions (20-79) and (20-80), other chemical reactions removing $O(^1D)$ from the stratosphere are:

$$O(^1D) + CH_4 \rightarrow CH_3 + OH \quad (20\text{-}81)$$

and

$$O(^1D) + N_2O \rightarrow N_2 + O_2$$
$$\rightarrow NO + NO \ , \quad (20\text{-}82)$$

for which $k = 3$ and 1×10^{-10} cm^3sec^{-1}, respectively (Reference 20-295).

These reactions demonstrate the importance of $O(^1D)$ in the stratosphere. Its role in the tropospheric chemistry has also been documented (References 20-296 through 20-298). Table 20-14 (Reference 20-299) summarizes the quenching reactions of $O(^1D)$ and the corresponding rate coefficients. In addition to these, the population density of $O(^1D)$ is also affected in highly ionized atmospheres by numerous charge-exchange and ion-atom interchange reactions (Reference 20-214), including such examples as:

$$N_2^+ + O(^1D) \rightarrow N_2(X^1\Sigma_g^+) + O^+(^2D) \quad (20\text{-}83)$$

and

$$N^+(^3P) + O(^1D) \rightarrow N(^2D) + O^+(^4S) \quad (20\text{-}84)$$

as depleting mechanisms, and:

Table 20-14. Reaction rate coefficients for $O(^1D)$ loss (Reference 20-299).

Reaction	Rate Constant (cm^3sec^{-1}) at 298 K
$O(^1D_2) + O_2 \rightarrow O_2\ (b^1\Sigma_g^+) + O(^3P)$	$(3.7 \pm 0.3) \times 10^{-11}$
$O(^1D_2) + O_3 \rightarrow O_2\ (X^3\Sigma_g^-) + O_2\ (?)$ (a) $\rightarrow O_2 + 2\ O(^3P)$ (b)	$(2.3 \pm 0.3) \times 10^{-10}$; Branching ratio ~0.5
$O(^1D_2) + NO \rightarrow NO + O(^3P)$	$(4 \pm 1) \times 10^{-11}$
$O(^1D_2) + NO_2 \rightarrow NO + O_2$	$(1.4 \pm 0.3) \times 10^{-10}$
$O(^1D_2) + N_2 \rightarrow N_2 + O(^3P)$	$(2.8 \pm 0.3) \times 10^{-11}$
$O(^1D_2) + N_2 + M \rightarrow N_2O + M$	2.8×10^{-36} cm^6sec^{-1} (Reference 20-287)
$O(^1D_2) + N_2O \rightarrow N_2 + O_2$ (a) $\rightarrow NO + NO$ (b)	$(1.20 \pm 0.15) \times 10^{-10}$; Branching ratio ~0.5
$O(^1D_2) + NH_3 \rightarrow NH_2 + OH$	$(2.7 \pm 0.4) \times 10^{-10}$
$O(^1D_2) + H_2 \rightarrow OH + H$	$(1.25 \pm 0.25) \times 10^{-10}$
$O(^1D_2) + H_2O \rightarrow OH + OH$	$(2.0 \pm 0.3) \times 10^{-10}$
$O(^1D_2) + H_2O_2 \rightarrow OH + HO_2$	$(2.8 \pm 1.0) \times 10^{-10}$
$O(^1D_2) + CO \rightarrow CO + O(^3P)$	$(3.6 \pm 0.5) \times 10^{-11}$
$O(^1D_2) + CO_2 \rightarrow CO_2 + O(^3P)$	$(1.0 \pm 0.2) \times 10^{-10}$
$O(^1D_2) + CH_4 \rightarrow CH_3 + OH$ (a) $\rightarrow CH_2O + H_2$ (b)	$(1.5 \pm 0.3) \times 10^{-10}$; Branching ratio ~0.5
$O(^1D_2) + C_2H_6 \rightarrow C_2H_5 + OH$ (a) $\rightarrow CH_3 + CH_2OH$ (b)	$(3.2 \pm 0.5) \times 10^{-10}$; Branching ratio ~0.5

$$N^+(^1S) + O_2(a^1\Delta_g) \rightarrow NO^+(A^1\Pi) + O(^1D) \qquad (20\text{-}85)$$

as a mechanism of formation of $O(^1D)$.

20.4.6.2 Electronic Excitation-Deexcitation: $O(^3P) \rightleftarrows O(^1S)$

It was suggested 50 years ago (Reference 20-300) that $O(^1S)$ may be formed in the nightglow by the reaction:

$$O(^3P) + O(^3P) + O(^3P) \rightarrow O(^1S) + O_2 \qquad (20\text{-}86)$$

where, among the collision partners available to O_2, only energy transfer to $O(^3P)$ could generate $O(^1S)$. This implicitly assumed an initial step in which the stabilized excited O_2 would have sufficient energy to excite an $O(^3P)$ atom to the $O(^1S)$ state. Such a mechanism was proposed some 30 years later (Reference 20-301):

$$O(^3P) + O(^3P) + M \rightarrow O_2^* + M \qquad (20\text{-}87)$$

$$O_2^* + O(^3P) \rightarrow O_2 + O(^1S) \quad . \qquad (20\text{-}88)$$

Still later, the validity of this two-step mechanism was disputed, and its abandonment was advocated (Reference 20-302), but more recently it has been supported (Reference 20-303) on the basis of new data on $O(^1S)$ production, combined with current altitude profiles of 557.7-nm intensities and $O(^3P)$ concentrations. It was suggested (Reference 20-303) that the excited intermediate molecular form of oxygen in Reactions (20-87) and (20-88) might be $O_2(A^3\Sigma_u^+)$. This interpretation has received fresh confirmation from recent experimental data (Reference 20-304). The measured total rate coefficient for the overall production of $O(^1S)$, i.e., for Reactions (20-87) and (20-88), has been determined (Reference 20-303) as a function of the kinetic temperature: $k_{Total} = 1.4 \times 10^{-30} \exp(-1300/RT)$ cm^6sec^{-1}. This should be compared with the three-body process, Reaction (20-86), for which $k = 4.8 \times 10^{-33}$ cm^6sec^{-1} at 300 K (Reference 20-305). Additional three-body reactions forming $O(^1S)$ include:

$$O(^3P) + O(^3P) + N(^4S) \rightarrow O(^1S) + NO \qquad (20\text{-}89)$$

and

$$N(^4S) + N(^4S) + O(^3P) \rightarrow N_2 + O(^1S) \quad , \qquad (20\text{-}90)$$

for which $k = 2.56 \times 10^{-31}$ and 1.3×10^{-30} cm^6sec^{-1}, respectively (Reference 20-305).

Formation of $O(^1S)$ also occurs via the dissociative recombination of O_2^+, i.e., Reaction (20-76). The rate coefficients describing the kinetics of electron-impact excitation of $O(^1S)$ from both $O(^3P)$ and $O(^1D)$ in highly ionized atmospheres are included in Figure 20-10 and Table 20-13.

The daytime photodissociation of O_2:

$$O_2 + h\nu(\lambda<133.2 \text{ nm}) \rightarrow O(^3P) + O(^1S) \qquad (20\text{-}91)$$

contributes appreciably (Reference 20-306) to the 557.7-nm emission below 150 km altitude, with the major contribution to $O(^1S)$ formation coming from the photodissociation of O_2 in the wavelength range 120.5-129.2 nm. It has been suggested (Reference 20-307), however, that absorption near the ionization threshold, $\lambda = 102.7$ nm, is primarily responsible for the photodissociation. Quantum yield measurements of $O(^1S)$ generation via the photodissociation of O_2 over a wavelength range 85-130 nm has led to the conclusion (Reference 20-308) that Reaction (20-91) is more efficient around 105 nm, and that the photodissociative excitation around the Lyman-β (102.57 nm) provides the major fraction of the $O(^1S)$ produced.

Quenching of $O(^1S)$ takes place via collision with atmospheric species and superelastic collisions with low-energy electrons in highly disturbed atmospheres. Early auroral measurements of the green lines (Reference 20-309) found the effective lifetime of the 557.7-nm emission to be shorter than its natural lifetime. This is attributable to the quenching of $O(^1S)$ by several atmospheric species, the corresponding rate coefficients of which, including temperature dependence in some instances, have been measured extensively. The previous value of the rate coefficient for quenching of $O(^1S)$ by $O(^3P)$, as set forth in Reaction (20-78), was $k = 1.38 \times 10^{-13}$ cm^3sec^{-1} (Reference 20-278). This has now been superseded by a much larger value, i.e, $k = 7.5 \times 10^{-12}$ cm^3sec^{-1} at 300 K (Reference 20-305), and $k = 5.0 \times 10^{-11} \exp(-610/RT)$ cm^3sec^{-1} (Reference 20-303). The quenching of $O(^1S)$ by O_2:

$$O(^1S) + O_2 \rightarrow O(^3P) + O_2 \quad , \qquad (20\text{-}92)$$

has been characterized by the following rate coefficients: $k = 4.0 \times 10^{-12} \exp(-1730/RT)$ cm^3sec^{-1} (Reference 20-310), and $k = 4.9 \times 10^{-12} \exp(-1700/RT)$ cm^3sec^{-1} (Reference 20-311). The latter value is smaller by 20% at room temperature than an earlier measurement (Reference 20-312). The quenching rate coefficient of $O(^1S)$ by N_2 is $k < 5 \times 10^{-17}$ cm^3sec^{-1} (Reference 20-311). Table 20-15 (Reference 20-299) summarizes the quenching rate coefficients of $O(^1S)$ by several major and minor atmospheric species.

20.4.7 Ionized Atomic Oxygen, O^+

The atomic oxygen ion has two low-lying metastable states, $O^+(^2D)$ and $O^+(^2P)$, which play important roles in the chemistry of both quiescent and disturbed atmospheres. They are produced in the dayglow through the direct photoionization of the oxygen atom:

$$O(^3P) + h\nu \rightarrow O^+(^4S, {}^2D, {}^2P) + e \quad . \qquad (20\text{-}93)$$

The photoionization cross-sections, especially the partial cross-sections leading to the individual states, have been calculated (References 20-224, 20-313). Chapter 12 of this Handbook presents partial photoionization cross-section results obtained from Reference 20-224.

Table 20-15. Reaction rate coefficients for $O(^1S)$ deactivation (Reference 20-299).

Reactants (All Products Unknown)	Temperature Range (K)	Rate Constant ($cm^3 sec^{-1}$)
$O(^1S) + O(^3P)$	200-370	$(5.0 \pm 2.5) \times 10^{-11} \exp(-300/T)$
$O(^1S) + O_2$	200-450	$(4.8 \pm 1.9) \times 10^{-12} \exp(-850/T)$
$O(^1S) + O_3$	298	$(5.8 \pm 1.2) \times 10^{-10}$
$O(^1S) + NO$	200-300	$(3.3 \pm 0.3) \times 10^{-11} (T^{0.5})$
$O(^1S) + NO_2$	298	$(5.0 \pm 2.5) \times 10^{-10}$
$O(^1S) + N_2$	200-380	$\leq 5 \times 10^{-17}$
$O(^1S) + N_2O$	200-370	$(3.8 \pm 0.8) \times 10^{-11} \exp(-420/T)$
$O(^1S) + NH_3$	298	$(5.0 \pm 2.5) \times 10^{-10}$
$O(^1S) + H_2O$	298	$\leq 1 \times 10^{-9}$
$O(^1S) + CO_2$	150-500	$(3.0 \pm 0.9) \times 10^{-11} \exp(-1320/T)$
$O(^1S) + CH_4$	298	$\leq 5.4 \times 10^{-14}$

The $O^+(^2D)$ and $O^+(^2P)$ states are also produced by collisions with energetic electrons, analogously to the photoionization:

$$O(^3P) + e \rightarrow O^+(^4S, {}^2D, {}^2P) + 2e \quad . \qquad (20\text{-}94)$$

Quantitative branching ratios for Reaction (20-94) are not available. These may be estimated, however, using the corresponding photoionization cross-sections as a guide. It has also been demonstrated (Reference 20-314) that 100-eV electrons impacting on O_2 in dissociative ionization produce a 25% yield of excited states among the O^+ ions generated.

In addition to these processes, $O^+(^2D)$ and $O^+(^2P)$ are formed by electron-impact excitation of the ground state:

$$O^+(^4S) + e \rightarrow O^+(^2D, {}^2P) + e \quad . \qquad (20\text{-}95)$$

Relevant near-threshold collision strengths for the constituent processes of Reaction (20-95) have been calculated (References 20-210, 20-315), and deexcitation rate coefficients have been calculated from them for a Maxwellian electron velocity distribution (Reference

20-213). Table 20-16 presents these coefficients. The corresponding excitation rates are obtainable via detailed-balance computations.

Table 20-16. Electron-impact deexcitation rate coefficients for the low-lying metastable states of O^+ (T_e in eV) (Reference 20-213).

Transition	Deexcitation Rate Coefficients ($cm^3\ sec^{-1}$)
$^2D - {}^4S$	$1.3 \times 10^{-8}\ (T_e)^{-1/2}$
$^2P - {}^4S$	$6.3 \times 10^{-9}\ (T_e)^{-1/2}$
$^2P - {}^2D$	$2.4 \times 10^{-8}\ (T_e)^{-1/2}$

Quenching of $O^+(^2D)$ (Table 20-16) proceeds through superelastic collisions, especially in highly ionized atmospheres. Additional important loss mechanisms for $O^+(^2D)$ are its near-resonant charge exchanges with N_2 and O_2:

$$O^+(^2D) + N_2 \rightarrow N_2^+(A^2\Pi_u, v=1) + O(^3P); \qquad (20\text{-}39)$$

$$O^+(^2D) + O_2 \rightarrow O_2^+(A^4\Pi_u, v=0) + O(^3P); \qquad (20\text{-}96)$$

$$\rightarrow O_2^+(A^2\Pi_u, v=0) + O(^3P) \quad . \qquad (20\text{-}97)$$

The rate coefficients for these processes are large; $k \sim 3 \times 10^{-10}$ $cm^3 sec^{-1}$ (References 20-192, 20-201). Reaction (20-39) may enhance infrared emissions in the Meinel bands (References 20-190, 20-191). However, Reaction (20-97) may result in visible radiation from the second-negative bands of O_2^+. Near-resonant Reactions (20-39) and (20-97) have been suggested as potential new laser sources (Reference 20-316).

The importance of Reactions (20-39), (20-96), and (20-97) for atmospheric deionization is apparent, in that atomic ions are thereby converted to molecular ions, for which the rates associated with dissociative recombination with free electrons are much faster than any of the recombination processes available to atomic ions.

The radiative decay of $O^+(^2P)$ to $O^+(^2D)$ is accompanied by emission at 731.9 nm. The $O^+(^2P)$ is also quenched by collision with low-energy electrons, as summarized in Table 20-16. Its quenching by other atmospheric species, however, is not well known. Dayglow measurements of the surface emission at 731.9 nm were analyzed in

the course of the Atmospheric Explorer C Satellite experiments (Reference 20-317). The results indicated that $O_3^+(^2P)$ quenching by N_2 may have a rate coefficient as large as $k = 5 \times 10^{-10}$ $cm^3 sec^{-1}$.

20.4.8 Proton-Impact Excitation

The precipitation into the atmosphere of energetic protons produces a kind of disturbance generally known as the proton aurora. Proton auroras are different from electron auroras both in their emissions and in the lesser extent of their vertical distribution, a function of the more limited energy ranges of ions than of electrons in the atmosphere.

Atomic hydrogen lines, H_α (656.4 nm) and H_β (486.1 nm), were first discovered in the auroral spectrum and were attributed to hydrogen or proton showers (Reference 20-318). The displacement of the H_β toward the blue was interpreted in terms of high-speed protons being neutralized upon collision with atmospheric atoms or molecules. Reviews of proton precipitation and hydrogen-line emission phenomena (Reference 20-319) indicate that typical protons have energies in the range 1-100 keV.

Hydrogen line emissions are excited by:

$$H^+ + M \rightarrow H(n\ell) + M^+ \quad . \qquad (20\text{-}98)$$

which leaves the hydrogen atom in either the ground state or an excited state. The hydrogen atoms thus created have very high velocities and travel in straight lines causing ionization and/or excitation:

$$H + M \rightarrow H^+ + M^* + e \qquad (20\text{-}99)$$

$$\rightarrow H(n\ell) + M^* \qquad (20\text{-}100)$$

$$\rightarrow H(n\ell) + M^+ + e \quad . \qquad (20\text{-}101)$$

Considerable experimental data exist (Reference 20-320) for hydrogen-line emissions due to collisions of protons with N_2. The measured emission cross-sections are basically for excited states where n=2, 3, and 4 with representative emissions of Lyman-α, H_α, and H_β.

In addition to hydrogen-line emissions in the proton aurora, the collisions of protons and hydrogen atoms with atmospheric atoms and molecules excite other well-known atomic and molecular emissions. Among the most prominent such excitations are the Meinel and first-negative bands of N_2^+, i.e.:

$$H^+ + N_2 \rightarrow H^* + N_2^+(A^2\Pi_u) \qquad (20\text{-}102)$$

$$\rightarrow H^* + N_2^+(B^2\Sigma_u^+) \quad . \qquad (20\text{-}103)$$

Measurements (Reference 20-321) of the cross-sections for excitation of the Meinel bands according to Reaction (20-102) by protons and hydrogen atoms impinging on N_2 in the energy range 0.5-25 keV, indicate that H and H^+ both make contributions of comparable magnitude to the generation of Meinel-band emission. The cross-sections for first-negative band emission by proton and hydrogen atom impacts on N_2 according to Reaction (20-103) have also been measured (References 20-322 through 20-324) for incident energies in the range 1-25 keV. For energies above 25 keV, measured cross-sections for Reaction (20-103) exist (References 20-325, 20-326) up to 100 keV. For proton impacts alone at energies exceeding 20 keV, the 391.4-nm emission has been measured (References 20-327, 20-328) to 1 MeV, however.

Laboratory investigations of the excitation of other electronic emissions in N_2 by proton impact have provided measurements for the $N_2(B \rightarrow A)$ first-positive (Reference 20-321) and $(C \rightarrow B)$ second-positive band (Reference 20-322) emissions.

Experimental data relating to excitations in O_2 are limited in terms of the energy range and electronic states. Some data exist for the excitation of the Schumann-Runge continuum (References 20-329, 20-330) and the O_2^+ $(b \rightarrow a)$ emission (Reference 20-331). Furthermore, the proton-impact dissociation of O_2,

$$H^+ + O_2 \rightarrow H^+ + O(^3P) + O(^1D) \qquad (20\text{-}104)$$

$$\rightarrow H^+ + O(^3P) + O(^3P) \quad , \qquad (20\text{-}105)$$

has been measured over a limited energy range (References 20-329, 20-330) where part of the dissociation process results in the excitation of the 630-nm oxygen red line. However, another investigation (Reference 20-332) based on the use of certain scaling laws yielded proton excitation cross-sections for O and O_2 from electron-impact excitations, in good agreement with some measured cross-sections (Reference 20-322).

20.4.9 Metallic Species

Alkali atoms such as Na, K, etc. are present in the atmosphere in small quantities, and are generally concentrated in the D- and E-regions. The measurement of emissions from Na and K in the twilight (Reference 20-333) has permitted the inference of altitude profiles of these species. Sodium ions have been measured (Reference 20-334) by rocket-borne spectrometry, and other metallic ions are also found to be present (References 20-335, 20-336) in the D- and E-regions. The densities of metallic ions like Mg^+ and Fe^+ are maintained by ablating meteoroids (Reference 20-337). Other metallic atoms and ions may be introducted into the atmosphere by such anthropogenic processes as nuclear detonations.

Alkali atoms are excited during daylight by absorption and resonant scattering of the solar radiation. At night their emission results from chemical reactions. The detailed chemistry of the alkali metals in their reactions with atomospheric species, however, is not yet well understood (Reference 20-338). Many of these metallic species may be in excited states, especially the energetic ions created as a result of nuclear events. For Na^+, Fe^+, Al^+, and a few other metallic ions it has been shown (References 20-339, 20-340) that excitation has a marked effect upon the cross-sections measured at kilovolt energies. Thus, it could be said that a large number of reaction rate parameters involving metallic atoms and their ions interacting with atmospheric species remain unknown. This includes reactions where the metallic species concerned are in ground states as well as in excited states.

20.5 REACTION RATES FOR REACTIONS INVOLVING EXCITED STATES

Table 20-17 summarizes reaction rate coefficients and cross-sections for reactions involving the excited states of species of interest and provides a considerable portion of the information available in this area. The emphasis is on atmospheric species. Temperatures at which measurements were made are listed, as well as the experimental techniques used to obtain the data, and appropriate references.

Table 20-17. Excitation and deexcitation rate coefficients or cross sections.

Reaction	(1) Reaction Coefficient ($cm^3 sec^{-1}$) or (2) Cross Section (cm^2)	Temperature or Energy	Type of Experiment	References
Electron-Impact Excitation and Deexcitation				
$e + H(^1S) \rightarrow e + H(^2P)$	(2) 7×10^{-17} (max)	10-50 eV	a	20-341 through 20-343
$\rightarrow e + H(^2S)$	(2) 1.4×10^{-17} (max)	12 eV	a	20-344 through 20-346
$e + Na(3^2S) \rightarrow e + Na(3^2P)$	(2) 2×10^{-15} (max)	10 eV	a	20 347
$e + He(1^1S) \rightarrow e + He(2^3S)$	(2) 3×10^{-18} (max)	20.6 eV	a	20 348
$\rightarrow e + He(2^1S)$	(2) 1×10^{-18}		a	20 348
$\rightarrow e + He(2^3P)$	(2) 3×10^{-18}			20 348
$e + He(2^1S) \rightarrow e + He(2^3S)$	(2) 3×10^{-14}	0.025 eV	Static afterglow	20-349, 20-350
$e + N(^2D) \rightleftarrows e + N(^4S)$	(1) See Table 20-6 for temperature-dependent rate coefficients		Theory	20 212, 20-213
$e + N(^2P) \rightarrow e + N(^4S)$	(1) See Table 20-6 for temperature-dependent rate coefficients		Theory	20 212, 20-213
$e + O(^1D) \rightarrow e + O(^3P)$	(1) See Table 20-13 for temperature-dependent rate coefficients		Theory	20 213, 20-284
$e + O(^1S) \rightarrow e + O(^3P)$	(1) See Table 20-13 for temperature-dependent rate coefficients		Theory	20-213, 20-284
$e + N_2 \rightarrow e + N_2^{\ddagger}$	(2) 5×10^{-16}	2.3 eV	a, Theory	20-87 through 20-89
	(1) See Table 20-3 for excitation rate coefficients			20-87 through 20-89

[a] Beams and fast-flowing systems.

(continued)

Table 20-17. Excitation and deexcitation rate coefficients or cross sections (continued).

Reaction	(1) Reaction Coefficient ($cm^3 sec^{-1}$) or (2) Cross Section (cm^2)	Temperature or Energy	Type of Experiment	References
Electron-Impact Excitation and Deexcitation (continued)				
$e + N_2 \rightarrow e + N_2 (A^3\Sigma_u^+)$	(2) See Figure 20-5 for excitation rate coefficients		a	20-143
$e + N_2 \rightarrow e + N_2(B^3\Pi_g)$	(2) 6.0×10^{-17} (max)	10 eV	a	20-144
$e + N_2 \rightarrow e + N_2(C^3\Pi_u)$	(2) 4.0×10^{-17} (max)	17 eV	a	20-143
$e + CO \rightarrow e + CO^{\ddagger}$	(2) 8×10^{-16} (max)	1.75 eV	a	20-87 through 20-89
$e + H_2 \rightarrow e + H_2^{\ddagger}$	(2) 6×10^{-17} (max)	2 eV	a	20-87 through 20-89
$e + N_2 \rightarrow 2e + N_2^+ (B)$	(2) 2×10^{-17} (max)	100 eV	a	20-180, 20-181
$e + N_2 O^{\ddagger} \rightarrow N_2 + O^-$	(2) 8.3×10^{-18}	2.3 eV	a	20-351
$e + N^+(^3P) \rightleftarrows e + N^+(^1D)$	(1) See Table 20-8 for temperature-dependent rate coefficients		Theory	20-213, 20-224 20-225
$e + N^+(^3P) \rightleftarrows e + N^+(^1S)$	(1) See Table 20-8 for temperature-dependent rate coefficients		Theory	20-213, 20-224 20-225
$e + N^+(^1D) \rightleftarrows e + N^+(^1S)$	(1) See Table 20-8 for temperature-dependent rate coefficients		Theory	20-213, 20-224 20-225
$e + O^+(^4S) \rightleftarrows e + O^+(^2D)$	(1) See Table 20-16 for temperature-dependent rate coefficients		Theory	20-213, 20-224, 20-315

[a] Beams and fast-flowing systems.

(continued)

Table 20-17. Excitation and deexcitation rate coefficients or cross sections (continued).

Reaction	(1) Reaction Coefficient ($cm^3 sec^{-1}$) or (2) Cross Section (cm^2)	Temperature or Energy	Type of Experiment	References
Electron-Impact Excitation and Deexcitation (continued)				
$e + O^+(^4S) \rightleftarrows e + O^+(^2P)$	(1) See Table 20-16 for temperature-dependent rate coefficients		Theory	20-213, 20-224, 20-315
$e + O^+(^2D) \rightleftarrows e + O^+(^2P)$	(1) See Table 20-16 for temperature-dependent rate coefficients		Theory	20-213, 20-224 20-315
Two-Body Reactions				
$O(^1S) + O(^3P) \rightarrow O(^1D) +$	(1) 7.5×10^{-12}	300 K	Flowing afterglow	20-305
$O(^1D \text{ or } ^3P)$	(1) $5.0 \times 10^{-11} \exp -\frac{610}{RT}$			20-303
$O(^1S) + N_2O \rightarrow O + N_2O$	(1) 1.4×10^{-11}	300 K	Flowing afterglow	20-352
$O(^1S) + O_2 \rightarrow O + O_2$	(1) $4.0 \times 10^{-13} \exp -\frac{1730}{RT}$		Flowing afterglow	20-310
$O(^1S) + CO_2 \rightarrow O + CO_2$ or $O_2 + CO$	(1) $3.1 \times 10^{-11} \exp -\frac{1320}{T}$	200-450 K	Flowing afterglow	20-352
$O(^1S) + N_2 \rightarrow O + N_2$	(1) $<5 \times 10^{-17}$	300 K	Flowing afterglow	20-352
$O(^1D) + N_2 \rightarrow O(^3P) + N_2$	(1) 5.6×10^{-11}	300 K	Atmospheric, flowing afterglow	20-287, 20-352
$O(^1D) + O_2 \rightarrow O(^3P) + O_2$	(1) 7.5×10^{-11}	300 K	Atmospheric, flowing afterglow	20-287, 20-352
$O^+(^2D) + N_2 \rightarrow O(^3P) + N_2^+$	(2) $\sim 3 \times 10^{-15}$	0.5 - 100 eV	a	20-192

[a] Beams and fast-flowing systems.

(continued)

Table 20-17. Excitation and deexcitation rate coefficients or cross sections (continued).

Reaction	(1) Reaction Coefficient ($cm^3 sec^{-1}$) or (2) Cross Section (cm^2)	Temperature or Energy	Type of Experiment	References
Two-Body Reactions (continued)				
$O^+(^2D) + O_2 \rightarrow O(^3P) + O_2^+$	(2) ~ 3×10^{-15}	0.5 - 100 eV	a	20-192
$O + O_3 \rightarrow O_2 + O_2(a^1\Delta_g)$	(1) $4.5 \times 10^{(-15\pm2)}$	300 K	Flowing afterglow	20-243
$O_2^+(X, v \geq 7) + O_3 \rightarrow 2O_2 + O(^1D)$	(1) Large	300 K	Flash photolysis	20-353
$O_2(a^1\Delta_g) + O_2 \rightarrow O_2(X) + O_2$	(1) 2.4×10^{-18}	300 K	Flowing afterglow	20-252 through 20-256
$O_2(a^1\Delta_g) + O_2^- \rightarrow 2O_2 + e$	(1) 2×10^{-10}	300 K	Flowing afterglow	20-261, 20-262
$O_2(a^1\Delta_g) + O^- \rightarrow O_3 + e$	(1) 3×10^{-10}	300 K	Flowing afterglow	20-261
$O_2(a^1\Delta_g) + N \rightarrow NO + O$	(1) $(2.8 \pm 2.0) \times 10^{-15}$	300 K	Flowing afterglow	20-256
$O_2(b^1\Sigma_g^+) + O_3 \rightarrow 2O_2 + O$	(1) 6×10^{-13}	300 K	Flowing afterglow	20-354
$O_2(b^1\Sigma_g^+) + N_2 \rightarrow O_2 + N_2$	(1) $(1.5\text{-}2.5) \times 10^{-15}$	300 K	Flowing afterglow	20-15, 20-274 20-275
$O_2(b^1\Sigma_g^+) + O_2 \rightarrow O_2 + O_2$	(1) (1.5×10^{-16})	300 K	Flowing afterglow	20-15, 20-274
$O_2^+ + e \rightarrow O^* + O^{**}$	(1) See discussion at Subsection 20.4.6.1 for temperature-dependent rate coefficients		Flowing afterglow	20-281, 20-283
$N(^2D) + O_2 \rightarrow NO + O$	(1) $4 \times 10^{-13} T^{1/2}$	236-365 K	Flash photolysis	20-220

[a] Beams and fast-flowing systems.

(continued)

Table 20-17. Excitation and deexcitation rate coefficients or cross sections (continued).

Reaction	(1) Reaction Coefficient ($cm^3 sec^{-1}$) or (2) Cross Section (cm^2)	Temperature or Energy	Type of Experiment	References
Two-Body Reactions (continued)				
$N + NO \rightarrow N_2^{\ddagger}(X, v\sim8) + O(^3P)$	(1) 2.2×10^{-11}	300 K	Flowing afterglow	20-159
$N + N_2(X) \rightarrow N + N_2(A)$	(1) $1.9 \times 10^{-6}\ T^{-3/2} \exp(-E_{XA}/kT)$		Shocks	20-169
$N_2 + N_2(X) \rightarrow N_2^* + N_2(A)$	(1) $k(N_2) \leq 0.01\ k(N)$		Active discharge, shocks	20-169
$A^{\ddagger} + B \rightarrow A + B^{\ddagger}$	Considerable literature is available on this type of reaction. The general agreement of vibrational energy transfer associated with lower vibrational levels is encouraging.		Flames, flash photolysis, shocks, theory	20-108, 20-109, 20-123
$A + BC^{\ddagger} \rightarrow AB + C$	Considerable literature on this subject of a nonatmospheric nature has been generated by Polanyi at the University of Toronto (cf the listed references).			20-355 through 20-357
$NO(A, v=x) + N_2(X, v=0) \rightarrow$ $NO(A, v=x-1) + N_2^{\ddagger}(X, v=1)$	(1) Very large	300 K	Flash photolysis, theory	20-108, 20-109
$N_2^{\ddagger}(X,v) + O^+ \rightarrow NO^+ + N$	(1) $3.1 \times 10^{-14}(T_a)^{-1.0}$	$T_a \leq 0.065$ eV	$T_a = T_{vib}$	20-133
	(1) $1.2 \times 10^{-10}(T_a)^{2.0}$	$0.065 \leq T_a \leq 0.67$		20-134
	(1) $8.5 \times 10^{-11}(T_a)^{1.2}$	$T_a > 0.67$ eV	Flowing afterglow	20-358
$N_2^{\ddagger}(X,v\geq7) + Na(3^2S) \rightarrow N_2 + Na^*$	(1) $\sim 10^{-10}$	300 K	Flowing afterglow	20-128
$N_2^{\ddagger}(X,v=1) + M \rightarrow N_2(X,v=0) + M$	(1) See Table 20-2	300 K	Flowing afterglow	See Table 20-2
$N_2(A) + N_2 \rightarrow N_2(X) + N_2$	(1) $<3 \times 10^{-19}$ $\sim 1 \times 10^{-19}$	300 K	High pressure chemical reactions	20-159, 20-15

(continued)

Table 20-17. Excitation and deexcitation rate coefficients or cross sections (continued).

Reaction	(1) Reaction Coefficient ($cm^3 sec^{-1}$) or (2) Cross Section (cm^2)	Temperature or Energy	Type of Experiment	References
Two-Body Reactions (continued)				
$N_2(A) + O_2 \rightarrow N_2 + (O_2 \text{ or } 2O)$	(1) 2.5×10^{-12}	~300 K	Atmospheric	20-163, 20-166
$N_2(A) + O \rightarrow N_2 + O$ or $NO + N$	(1) 3×10^{-11} (1) 5×10^{-11} (1) 7.5×10^{-11}	~300 K	Atmospheric	20-11 20-15 20-162
$N_2(A) + N \rightarrow N + N_2^{\ddagger}(X)$	(1) 5×10^{-11}	~300 K	Flowing afterglow	20-167, 20-169
$N_2(A) + NO \rightarrow N_2 + NO$	(1) 7×10^{-11}	300 K	Flowing afterglow	20-167
$N_2(a,v) + N_2 \rightarrow N_2(a,v^1<v) + N_2$	(1) Large	1000 K	Theory	20-114
$N_2 + Ba \rightarrow N_2(X) + Ba^+(6^2P_{3/2}) + e$	(1) Large	300 K	a, Static afterglow	20-164, 20-359, 20-360
$OH^{\ddagger}(X,v') + OH^{\ddagger}(X,v) \rightarrow OH(A) + OH(X)$	(1) $\sim 10^{-10}$	~300 K	Flames	20-361
$N_2^+(A^2\Pi_u) + O_2 \rightarrow N_2 + O_2^+$	(1) 7.0×10^{-10} for $\bar{v}=1$	300 K	a	20-197 through 20-200
$N_2^+(A) + N_2 \rightarrow N_2^+ + N_2$	(1) 4.5×10^{-10} for $\bar{v}=1$	300 K	a	20-197 through 20-200
$N_2^+(B) + N_2 \rightarrow N_2^+ + N_2$	(1) 4.4×10^{-10}	300 K	Static afterglow	20-182
$N_2^+(B) + O_2 \rightarrow N_2^+ + O_2$	(1) 7.0×10^{-10}	300 K	Static afterglow	20-182
$He(2^3S) + N_2 \rightarrow He(^1S) + N_2^+(B) + e$	(1) 1.4×10^{-10}	300 K	a, Flowing afterglow	20-127, 20-362
$He(2^3S) + O_2 \rightarrow He(^1S) + (O_2^+)^* + e$	(1) 5.0×10^{-10}		Flowing afterglow	20-362
$He^+ + N_2(X) \rightarrow He + N_2^+(C,v=3)$	(2) Large, 4×10^{-10}	300 K	a	20-133, 20-363

[a] Beams and fast-flowing systems.

(continued)

Table 20-17. Excitation and deexcitation rate coefficients or cross sections (continued).

Reaction	(2) Cross Section (cm^2) or (3) Reaction Coefficient ($cm^6 sec^{-1}$)	Temperature or Energy	Type of Experiment	References
Two-Body Reactions (continued)				
$H^+ + Cs \rightarrow H(^2P) + Cs^+$	(2) 6×10^{-15}	1 keV	a	20-364
Three-Body Reactions				
$N + N + N_2 \rightarrow N_2(B) + N_2$	(3) 1.4×10^{-33}	300 K	Flowing afterglow	20-278
$N + O + N_2 \rightarrow NO(B) + N_2$	(3) 1×10^{-34}	300 K	Flowing afterglow	20-278
$O + O + N_2 \rightarrow O_2(A) + N_2$	(3) 2.1×10^{-37}	300 K	Flowing afterglow	20-278
$O + O + N_2 \rightarrow O_2(B) + N_2$	(3) 1.7×10^{-37}	300 K	Flowing afterglow	20-278
$O + O + O_2 \rightarrow O_2(A, v=9,10) + O_2$	(3) 1×10^{-33} (v=9)	1000 K	Theory	20-365
	(3) 5.5×10^{-33} (v=10)	1000 K	Theory	20-365
$O + O + CN \rightarrow O_2 + CN(A)$	(3) 10^{-31}, $\sim 10^{-30}$	300 K	Flash photolysis	20-366
$O + O + Na \rightarrow O_2 + Na(^2P)$	(3) 1.5×10^{-29}	1250-1500 K	Flames	20-367
$H + H + Na \rightarrow H_2 + Na(^2P)$	(3) 5×10^{-31}	1250-1500 K	Flames	20-367
$N + N + O \rightarrow N_2 + O(^1S)$	(3) 1.3×10^{-30}	~300 K	Flowing afterglow	20-305
$N + O + O \rightarrow NO + O(^1S)$	(3) 2.5×10^{-31}	300 K	Flowing afterglow	20-305
$O + O + O \rightarrow O_2 + O(^1S)$	(3) 4.8×10^{-33}	300 K	Flowing afterglow	20-305
$O + O + O \rightarrow O_2 + O(^1D)$	(3) Large	300 K	Theory	20-368
$H + H_2 + O_2 \rightarrow H_2O + OH(A)$	(3) 5×10^{-37}	1000-1900 K	Static afterglow	20-369
$H^+ + e + e \rightarrow H(n) + e$	(3) $9.5 \times 10^{-29} \frac{n^4}{T_e^2}$ (T_e in eV)		Theory	20-370

REFERENCES

20-1. Armstrong, E.B., and A. Dalgarno, Eds., The Airglow and Aurorae, Pergamon Press, London (1956).

20-2. Zelikoff, M., Ed., The Threshold of Space, Pergamon Press, New York (1957).

20-3. Ratcliffe, J.A., Ed., Physics of the Upper Atmosphere, Academic Press, New York (1960).

20-4. Chamberlain, J.W., Physics of the Aurora and Airglow, Academic Press, New York (1961).

20-5. Cadle, R.D., Ed., Chemical Reactions in the Lower and Upper Atmosphere, Interscience Publishers, New York (1961).

20-6. Phillips, L.F., and H.I. Schiff, J. Chem. Phys. 36, 1509 (1962).

20-7. Phillips, L.F., and H.I. Schiff, J. Chem. Phys. 36, 3283 (1962).

20-8. Morgan, J.E., L.F., Phillips, and H.I. Schiff, Disc. Faraday Soc. 33, 118 (1962).

20-9. Bates, D.R., Disc. Faraday Soc. 37, 21 (1964).

20-10. Hines, C.O., et al., Eds., Physics of the Earth's Upper Atmosphere, Prentice-Hall, Englewood Cliffs, New Jersey (1965).

20-11. Hunten, D.M., and M.B. McElroy, Revs. Geophys. 4, 303 (1966).

20-12. Muschlitz, E.E., in Molecular Beams, J. Ross, Ed., Interscience Publishers, New York (1966); p. 171.

20-13. Wright, A., and C. Winkler, Active Nitrogen, Academic Press, New York (1968).

20-14. Gilmore, F.R., E. Bauer, and J.W. McGowan, J. Quant. Spectry. Radiative Transfer 9, 157 (1969).

20-15. Zipf, E.C., Jr., Can J. Chem. 47, 1863 (1969).

20-16. Donovan, R.J., and D. Husain, Chem. Revs. 70, 489 (1970).

20-17. Shuler, K.E., and W.R. Bennett, Eds., Appl. Opt., Suppl. 2: Chemical Lasers, Vol. 4 (1965).

20-18. Taylor, R.L., Can J. Chem. 52, 1436 (1974).

20-19. Vlasov, M.N., J. Atm. Terrestr. Phys. 38, 807 (1976).

20-20. McGowan, N.J., R.H. Kummler, and F.R. Gilmore, in The Excited State in Chemical Physics, J.W. McGowan, Ed., John Wiley and Sons, New York (1975); Chapter 6.

20-21. Laidler, K.J., Chemical Kinetics of Excited States, Oxford University Press, London (1965).

20-22. Bates, D.R., Ed., Atomic and Molecular Processes, Academic Press, New York (1962).

20-23. Ford, U., and W. Lichten, Phys. Rev. Letts. 14, 627 (1965).

20-24. Bauer, E., E.R. Fisher, and F.R. Gilmore, J. Chem. Phys. 51 4173 (1969).

20-25. Wiese, W.L., M. Smith, and B.M. Glennon, Atomic Transition Probabilities, Vol. I, National Standard Reference Data System, Report NSRDS-NBS-4 (1966).

20-26. Lawrence, G.M., and B.D. Savage, Phys. Rev. 141, 67 (1966).

20-27. Omholt, A., Planet. Space Sci. 2, 246 (1960).

20-28. Garstang, R.H., Mon. Not. Roy. Astron. Soc. 111, 115 (1951).

20-29. Nicolaides, C., O. Sinanoglu, and P. Westhaus, Phys. Rev. A4, 1400 (1971).

20-30. Lawrence, G.M., Can J. Chem. 47, 1856 (1969).

20-31. Lawrence, G.M., Phys. Rev. A2, 397 (1970).

20-32. Shemansky, D.E., J. Chem. Phys. 51, 689 (1969).

20-33. Shemansky, D.E., and N.P. Carleton, J. Chem. Phys. 51, 682 (1969).

20-34. Shemansky, D.E., and A.L. Broadfoot, J. Quant. Spectry. Radiative Transfer 11, 1385 (1971)

20-35. Jeunehomme, M., J. Chem. Phys. 45, 1805 (1966).

20-36. Hollstein, M., D.C. Lorents, R. Peterson, and J.R. Sheridan, Can J. Chem. 47, 1858 (1969).

20-37. Wu, F.L., and W. Benesch, Phys. Rev. 172, 31 (1968).

20-38. Covey, R., and W. Benesch, Bull. Am. Phys. Soc. 18, 575 (1973).

20-39. Gilmore, F.R., unpublished data (1971).

20-40. Shemansky, D.E., J. Chem. Phys. 51, 5487 (1969).

20-41. Borst, W.L., and E.C. Zipf, Phys. Rev. A3, 979 (1971).

20-42. Bennett, R.G., and F.W. Dalby, J. Chem. Phys. 31, 434 (1959).

20-43. Hesser, J.E., J. Chem. Phys. 48, 2518 (1968).

20-44. Johnson, A.W., and R.G. Fowler, J. Chem. Phys. 53, 65 (1970).

20-45. Lotchin, L.W., E.L. Chapp, and D.J. Pegg, J. Chem. Phys. 59 3960 (1973)

20-46. Freund, R.S., J. Chem. Phys. 50, 3734 (1969).

20-47. Holland, R.F., and W.B. Maier II, J. Chem. Phys. 56, 5229 (1972).

20-48. Peterson, J.R., and J.J. Mosely, J. Chem. Phys. 58, 172 (1973).

20-49. Cartwright, D.C., J. Chem. Phys. 58, 178 (1973).

20-50. McGowan, J.W., and L. Kerwin, Can. J. Chem. 43, 2086 (1964).

20-51. Frosch, R., and G. Robinson, J. Chem. Phys. 41, 367 (1964).

20-52. Lefebvre-Brion, H., and F. Guerin, J. Chem. Phys. 49, 1446 (1968).

20-53. Jeunehomme, M., J. Chem. Phys. 45, 4433 (1966).

20-54. Bubert, H., and F.W. Froben, Chem. Phys. Letts. 8, 242 (1971).

20-55. Weinstock, E.M., R.N. Zare, and L.A. Melton, J. Chem. Phys. 56, 3456 (1972).

20-56. Jeunehomme, M., and A.B.F. Duncan, J. Chem. Phys. 41, 1692 (1964).

20-57. Edqvist, O., et al., Ark. Fys. 40, 439 (1970).

20-58. Mathis, R.F., B.R. Turner, and J.A. Rutherford, J. Chem. Phys. 49, 2051 (1968).

20-59. Maier, W.B. II, and R.F. Holland, J. Chem. Phys. 54, 2693 (1971)

20-60. Schwartz, S., and H. Johnston, J. Chem. Phys. 51, 1286 (1969).

20-61. Keyser, L., S. Levine, and F. Kaufman, J. Chem. Phys. 54, 355 (1971).

20-62. Nicholls, R., Ann. Geophys. 20, 144 (1964).

20-63. Badger, R.M., A.C. Wright, and R.F. Whitlock, J. Chem. Phys. 43, 4345 (1965).

20-64. Miller, J.H., R.W. Boese, and L.P. Giver, J. Quant. Spectry. Radiative Transfer 9, 1507 (1969).

20-65. Childs, W., and R. Mecke, Zeits. Phys. 68, 344 (1931).

20-66. Degen, V., Can. J. Phys. 46, 783 (1968).

20-67. Jarmain, W.R., and R.W. Nicholls, Proc. Phys. Soc. 90, 545 (1967).

20-68. Jeunehomme, M., J. Chem. Phys. 44, 4253 (1966).

20-69. Fink, E.H., and K.H. Welge, Z. Naturforsch. 23a, 358 (1968).

20-70. Copeland, G.E., J. Chem. Phys. 54, 3482 (1971).

20-71. Fairbairn, H.R., J. Chem. Phys. 60, 521 (1974).

20-72. James, T.C., J. Chem. Phys. 55, 4118 (1971).

20-73. Johnson, C.E., and R.I. Van Dyke, Jr., J. Chem. Phys. 56, 1506 (1972).

20-74. Wentink, T., Jr., E.P. Marram, L. Isaacson, and R.J. Spindler, Report AFWL-TR-67-30 (1967).

20-75. Isaacson, L., E.P. Marram, and T. Wentink, Jr., Appl. Optics 8, 235 (1969).

20-76. Bennett, R.G., and F.W. Dalby, J. Chem. Phys. 32, 1716 1960).

20-77. Fink, E.H., and K.H. Welge, J. Chem. Phys. 42, 4086 (1965).

20-78. Jeunehomme, M., J. Chem. Phys. 42, 4086 (1965).

20-79. Bennett, R.G., and F.W. Dalby, J. Chem. Phys. 36, 399 (1962).

20-80. Moore, J.H., Jr., and D.W. Robinson, J. Chem. Phys. 48, 4870 (1968).

20-81. Fisher, E.R., and E. Bauer, J. Chem. Phys. 57, 1966 (1972).

20-82. Bauer, E., R.H. Kummler, and M.H. Bortner, Appl. Optics 10, 1861 (1971).

20-83. Walker, J., Planet. Space Sci. 16, 321 (1968).

20-84. Walker, J.C., R.S. Stolarski, and A.F. Nagy, Ann. Geophys. 25, 831 (1969).

20-85. Black, G., L. Sharpless, and T.G. Slanger, J. Chem. Phys. 58, 4792 (1973).

20-86. Slanger, T.G., and G. Black, J. Chem. Phys. 60, 468 (1974).

20-87. Schulz, G.J., Phys. Rev. 116, 114 (1959).

20-88. Schulz, G.J., Phys. Rev. 125, 229 (1962).

20-89. Schulz, G.J., Phys. Rev. 135, A988 (1964).

20-90. Ehrhardt, H., and K. Willman, Zeits. Phys. 204, 462 (1967).

20-91. Englehardt, A.G., A.V. Phelps, and C.G. Risk, Phys. Rev. 135, A1566 (1964).

20-92. Herzenberg, A., and F. Mandl, Proc. Roy. Soc. (London) A270, 48 (1962).

20-93. Chen, J.C.Y., J. Chem. Phys. 40, 3507 (1964).

20-94. Chen, J.C.Y., Phys. Rev. 146, 61 (1966).

20-95. Britwhistle, D.T., and A. Herzenberg, J. Phys. B4, 153 (1971).

20-96. Schulz, G.J., Revs. Mod. Phys. 45, 378 (1973).

20-97. Burrow, P.D., and P. Davidovitz, Phys. Rev. Letts. 21, 1789 (1968).

20-98. Ali, A.W., Naval Research Lab., Plasma Dynamics Tech. Note 24 (1970).

20-99. Ali, A.W., Naval Research Lab., Report 7578 (1973).

20-100. Abraham, G., and E.R. Fisher, J. Appl. Phys. 43, 4621 (1972).

20-101. Green, A.E.S., and C.A. Barth, J. Geophys. Res. 70, 1083 (1965).

20-102. Green, A.E.S., Ed., The Middle Ultraviolet, John Wiley and Sons, New York (1966); p. 165.

20-103. Shuler, K.E., T. Carrington, and J.C. Light, in Reference 20-17; p. 81.

20-104. Polanyi, J.C., J. Quant. Spectry. Radiative Transfer 3, 471 (1963).

20-105. Herschbach, D., in Reference 20-17; p. 128.

20-106. Herzfeld, K.F., and T.A. Litovitz, Absorption and Dispersion of Ultrasonic Waves, Academic Press, New York, (1959).

20-107. Rapp, D., and T.E. Sharp, J. Chem. Phys. 38, 2641 (1963).

20-108. Callear, A.B., in Reference 20-17; p. 145.

20-109. Takayanagi, K., in Advances in Atomic and Molecular Physics, Vol 1, D.R. Bates and I. Estermann, Eds., Academic Press, New York (1965); p. 149.

20-110. Bates, D.R., J. Atm. Terrestr. Phys. 6, 171 (1955).

20-111. Dalgarno, A., Planet. Space Sci. 10, 19 (1963).

20-112. Clark, T.C., S.H. Garnett, and G.B. Kistiakowsky, J. Chem. Phys. 52, 4694 (1970).

20-113. Garnett, S.H., G.B. Kistiakowsky, and B.V. O'Grady, J. Chem. Phys. 51, 84 (1969).

20-114. Bauer, E., and F.W. Cummings, J. Chem. Phys. 36, 618 (1962).

20-115. Treanor, C.E., J. Chem. Phys. 43, 532 (1965).

20-116. Millikan, R., and D. White, J. Chem. Phys. 39, 3209 (1963).

20-117. Breshears, W.D., and P.F. Bird, J. Chem. Phys. 48, 4768 (1968).

20-118. McNeal, R.J., M.E. Whitston, Jr., and G.R. Cook, Chem. Phys. Letts. 16, 507 (1972).

20-119. McNeal, R.J., M.E. Whitston, Jr., and G.R. Cook, J. Geophys. Res. 79, 1527 (1974).

20-120. Fisher, E.R., and E. Bauer, J. Chem. Phys. 57, 1966 (1972).

20-121. Baranov, V.Y., V.G. Nizen, and S.V. Pigulskii, Sov. J. Plasma Phys. 3, 769 (1977).

20-122. Patel, C.K.N., Phys. Rev. Letts. 12, 588 (1964).

20-123. Taylor, R., and S. Bitterman, Revs. Mod. Phys. 41, 26 (1969).

20-124. Fisher, E.R., and R.H. Kummler, J. Chem. Phys. 49, 1075 (1968).

20-125. Breig, E.L., M.E. Brenner, and R.J. McNeal, J. Geophys. Res. 78, 1225 (1973).

20-126. Hunten, D.M., J. Atm. Terrestr. Phys. 27, 583 (1965).

20-127. Starr, W.L., J. Chem. Phys. 43, 73 (1965).

20-128. Fite, W.L., W.R. Henderson, H.F. Krause, and J.E. Mentall, Fifth Intl. Conf. Phys. Electronic Atomic Collisions, Leningrad (1967).

20-129. Jamshidi, E., E.R. Fisher, and R.H. Kummler, J. Geophys. Res. 78, 6151 (1973).

20-130. Kummler, R.H., and M.H. Bortner, Space Res. 12, 711 (1972).

20-131. Kumer, J.B., and T.C. James, J. Geophys. Res 79, 638 (1974).

20-132. Schmeltekopf, A.L., F.C. Fehsenfeld, G.I. Gilman, and E.E. Ferguson, Planet. Space Sci. 15, 401 (1967).

20-133. Schmeltekopf, A.L., E.E. Ferguson, and F.C. Fehsenfeld, J. Chem. Phys. 48, 2966 (1968).

20-134. Johnsen, R., and M.A. Biondi, J. Chem. Phys. 59, 3504 (1973).

20-135. Thomas, L., and R.B. Norton, J. Geophys. Res. 72, 5552 (1967).

20-136. Newton, G.P., J.C.G. Walker, and P.H.E. Meijer, J. Geophys. Res. 79, 3807 (1974).

20-137. Whitten, R., and A. Dalgarno, Planet. Space Sci. 15, 1419 (1967).

20-138. COSPAR International Reference Atmosphere, North-Holland Publishing Co., Amsterdam (1965).

20-139. Lichten, W., Phys. Rev. 120, 848 (1960).

20-140. Olmstead, J., A.S. Norton, and K. Street, J. Chem. Phys. 42, 2321 (1965).

20-141. Foner, S.N., and R.L. Hudson, J. Chem. Phys. 37, 1662 (1962).

20-142. Winters, H.F., J. Chem. Phys. 43, 926 (1965).

20-143. Brinkmann, R.T., and S. Trajmar, Ann. Geophys. 26, 201 (1970).

20-144. Borst, W.L., Phys. Rev. A5, 648 (1972).

20-145. Stanton, P.N., and R.M. St. John, J. Opt. Soc. Am. 59, 252 (1969).

20-146. Shemansky, D.E., and A.L. Broadfoot, J. Quant. Spectry. Radiative Transfer 11, 1401 (1971).

20-147. Jobe, J.D., F.A. Sharpton, and R.M. St. John, J. Opt. Soc. Am. 57, 106 (1967).

20-148. Burns, D.J., F.R. Simpson, and J.W. McConkey, J. Phys. B2, 52 (1969).

20-149. Cartwright, D.C., Phys. Rev. A2, 1331 (1970).

20-150. Cartwright, D.C., Aerospace Report TR-0059 (9260-01)-6 (1970).

20-151. Chung, S., and C.C. Lin, Phys. Rev. A6, 988 (1972).

20-152. Ali, A.W., Naval Research Lab., Memo Report 2724 (1973).

20-153. Cartwright, D.C., S. Trajmar, A. Chutjian, and W. Williams, Phys. Rev. A16, 1041 (1977).

20-154. Ali, A.W., and A.D. Anderson, Naval Research Lab., Report 7432 (1972).

20-155. Cartwright, D.C., J. Geophys. Res. 83, 517 (1978).

20-156. Turner, B.R., J.A. Rutherford, and R.F. Stebbings, J. Geophys. Res. 71, 4521 (1966).

20-157. Goldan, P.O., et al., J. Chem. Phys. 44, 4095 (1966).

20-158. Fehsenfeld, F.C., D.B. Dunkin, and E.E. Ferguson, Planet. Space Sci. 18, 1267 (1970).

20-159. Noxon, J.F., J. Chem. Phys. 36, 926 (1962).

20-160. Zipf, E.C., Jr., Bull. Am. Phys. Soc. 9, 185 (1964).

20-161. Young, R.A., Can. J. Chem. 44, 1171 (1966).

20-162. Vallance Jones, A., and R.L. Gattinger, J. Geophys. Res. 81, 497 (1976).

20-163. Meyer, J.A., D.W. Setser, and D.H. Steadman, Astrophys. J. 157, 1023 (1969).

20-164. Kenty, C., J. Chem. Phys. 23, 1555 (1955).

20-165. Cermak, V., J. Chem. Phys. 44, 1318 (1966).

20-166. Young, R.A., G. Black, and T.G. Slanger, J. Chem. Phys. 50, 303 (1969).

20-167. Young, R.A., and G.A. St. John, J.Chem. Phys. 48, 895 (1968).

20-168. Thrush, B.A., J. Chem. Phys. 47, 3691 (1967).

20-169. Wray, K., J. Chem. Phys. 44, 623 (1966).

20-170. Ajello, J., J. Chem. Phys. 53, 1156 (1970).

20-171. Aarts, J.F.M., and F.J. DeHeer, Physica 52, 45 (1971).

20-172. Holland, R.F., J. Chem. Phys. 51, 3940 (1969).

20-173. Finn, T.G., and J.P. Doering, J. Chem. Phys. 64, 4490 (1976).

20-174. Cermak, V., J. Chem. Phys. 43, 4527 (1965).

20-175. Saha, M.N., Proc. Roy. Soc. (London), A160, 155 (1937).

20-176. Wulf, O.R., and L.S. Deming, J. Geophys. Res. 43, 283 (1938).

20-177. Lee, A.R., and N.P. Carleton, Phys. Letts. 27A, 195 (1968).

20-178. Shemansky, D.E., T.M. Donahue, and E.C. Zipf, J. Quant. Spectry. Radiative Transfer 20, 905 (1972).

20-179. Borst, W.L., and E.C. Zipf, Phys. Rev. A1, 834 (1970).

20-180. McConkey, J.W., J.M. Woolsey, and D.J. Burns, Planet. Space Sci. 15, 1332 (1967).

20-181. Srivastava, B.N., and I.M. Mirza, Trans. Am. Geophys. Union 48, 73 (1967).

20-182. Hirsh, M.N., E. Poss, and P.N. Eisner, Phys. Rev. A1, 1615 (1970).

20-183. Dashchenko, A.I., I.P. Zapesochnyi, and A.I. Imre, Opt. & Spectrosc. 35, 562 (1973).

20-184. Crandall, D.H., et al., Phys. Rev. A9, 2545 (1974).

20-185. McLean, E.A., A.W. Ali, J.A. Stamper, and S.O. Dean, Phys. Letts. A38, 209 (1972).

20-186. Brocklehurst, B., and F.A. Downing, J. Chem. Phys. 46, 2976 (1967).

20-187. Davidson, G., and R. O'Neil, American Science and Engineering Co., Report AFCRL-67-0277 (1968).

20-188. Wallace, L., and M.B. McElroy, Planet. Space Sci. 14, 677 (1966).

20-189. Sharp, W.E., Jr., J. Geophys. Res. 79, 1569 (1974).

20-190. Omholt, A., J. Atm. Terrestr. Phys. 10, 320 (1957).

20-191. Hunten, D.M., Ann. Geophys. 14, 167 (1958).

20-192. Stebbings, R.F., B.R. Turner, and J.A. Rutherford, J. Geophys. Res. 71, 771 (1966).

20-193. Glosik, J., et al., J. Phys. B11, 3365 (1978).

20-194. Vallance Jones, A., Space Sci. Rev. 11, 776 (1971).

20-195. Vallance Jones, A., Space Sci. Rev. 12, 258 (1971).

20-196. Wallace, L., and A.L. Broadfoot, Planet. Space Sci. 17, 975 (1969).

20-197. Holland, R.F., and W.B. Maier II, J. Chem. Phys. 56, 5229 (1972); Erratum, Ibid. 58, 2672 (1973), and references contained therein.

20-198. Cartwright, D.C., W.R. Pendleton, Jr., and L.D. Weaver, J. Geophys. Res. 80, 651 (1975).

20-199. Mitchell, K.B., J. Chem. Phys. 53, 1795 (1970).

20-200. Gray, D.D., T.D. Roberts, and J.L. Morack, J. Chem. Phys. 57, 4190 (1972).

20-201. Gilmore, F.R., Rand Corp., Report RM-4034-1-PR (1966).

20-202. McGowan, J.W., et al., Phys. Rev. Letts. 14, 620 (1964).

20-203. Fite, W.L., and R.T. Brackmann, Proc. Sixth Intl. Conf. Ionization Gases, North-Holland Publishing Co., New York (1963); Vol. 1, p. 21.

20-204. Fineman, M.A., et al., Proc. Fourth Intl. Conf. Phys. Electron Atomic Collisions, Science Bookcrafters, Inc., New York (1965); p. 425.

20-205. Michels, H.H., United Technologies Research Center, Report AFWL-TR-73-288 (1974).

20-206. Kley, D., G.M. Lawrence, and E.J. Stone, J. Chem. Phys. 66, 4157 (1977).

20-207. Michels, H.H., H.J. Kolker, and G. Peterson, Proc. High Altitude Nuclear Effects Symp., Stanford Res. Inst. (1971).

20-208. Seaton, M.J., in Reference 20-1; p. 289.

20-209. Smith, K., R.J.W. Henry, and P.G. Burke, Phys. Rev. 157, 51 (1967).

20-210. Henry, R.J.W., P.G. Burke, and A.L. Sinfailan, Phys. Rev. 178, 218 (1969).

20-211. Ormonde, S., K. Smith, B.W. Torres, and A.R. Davies, Phys. Rev. A8, 262 (1973).

20-212. Berrington, K.A., P.G. Burke, and W.D. Robb, J. Phys. B8, 2500 (1975).

20-213. Ali, A.W., Naval Research Lab., Memo Report 3371 (1976).

20-214. Ali, A.W., Naval Research Lab., Memo Report 3165 (1975).

20-215. Rush, D.W., W.E. Sharp, and P.B. Hays, J. Geophys. Res. 80, 13 (1975).

20-216. Winters, H.F., J. Chem. Phys. 44, 1472 (1966).

20-217. Wells, W.C., W.L. Borst, and E.C. Zipf, Phys. Rev. A14, 695 (1976).

20-218. Zipf, E.C., and R.W. McLaughlin, Planet. Space Sci. 26, 449 (1978).

20-219. Lin, C.L., and F. Kaufman, J. Chem. Phys. 55, 3760 (1971).

20-220. Slanger, T.G., B.J. Wood, and G. Black, J. Geophys. Res. 76, 8430 (1971).

20-221. Black, G., T.G. Slanger, G. St. John, and R.A. Young, J. Chem. Phys. 51, 116 (1969).

20-222. Davenport, J. E., T.G. Slanger, and G. Black, J. Geophys. Res. 81, [illegible] (1976).

20-223. Rush, D.W., A.I. Stewart, P.B. Hays, and J.H. Hoffman, J. Geophys. Res. 80, 2300 (1975).

20-224. Henry, R.J.W., Astrophys. J. 161, 1153 (1970).

20-225. Saraph, H.E., M.J. Seaton, and J. Shemming, Proc. Roy. Soc. (London) 89, 27 (1966).

20-226. Dalgarno, A., and M.B. McElroy, Planet. Space Sci. 14, 1321 (1966).

20-227. Gilpin, R.H., H.I. Schiff, and K.H. Welge, J. Chem. Phys. 55, 1087 (1971).

20-228. Schulz, G.J., and J.T. Dowell, Phys. Rev. 128, 174 (1962).

20-229. Spence, D., and G.J. Schulz, Phys. Rev. A2, 1802 (1970).

20-230. Hyman, E., Naval Research Lab., private communication (1971).

20-231. Cosby, P. and T. Moran, J. Chem. Phys. 52, 6157 (1970).

20-232. Stebbings, R.F., et al., General Atomic Division (General Dynamics Corp.), Report DASA 1708 (1965).

20-233. Fite, W.L., R.T. Brackmann, and W.R. Henderson, Proc. Fourth Intl. Conf. Phys. Electron Atomic Collisions, Science Bookcrafters, Inc., New York (1965); p. 100.

20-234. O'Malley, T.F., Phys. Rev. 155, 59 (1967).

20-235. Chen, J.C.Y., and J.L. Preacher, Phys. Rev. 163, 103 (1967).

20-236. Kovacs, M.A., and M.A. Mack, Appl. Phys. Letts. 20, 487 (1972).

20-237. Kiefer, J.H., and R.W. Lutz, Eleventh Symp. (Intl.) on Combustion, The Combustion Institute, Pittsburgh (1967); p. 67.

20-238. Bauer, S.H., and S.C. Tsang, Phys. Fluids 6, 182 (1963).

20-239. Vallance Jones, A., and R.L. Gattinger, Planet. Space Sci. 11, 961 (1963).

20-240. Evans, W.F., D.M. Hunten, E.J. Llewellyn, and A. Vallance Jones, J. Geophys. Res. 73, 2885 (1968).

20-241. Jones, I.T.N., and R.P. Wayne, J. Chem. Phys. 51, 3617 (1969).

20-242. Hampson, R., et al, J. Phys. Chem. Reference Data 2, 267 (1973).

20-243. Fluegge, R.A., and D. Headrick, Cornell Aeronautical Lab., Report DASA 2551 (1970).

20-244. Trajmar, S., D.C. Cartwright, and W. Williams, Phys. Rev. A4, 1482 (1971).

20-245. Julienne, P.S., and M. Krause, J. Res. Natl. Bur. Stds. 76A, 661 (1972).

20-246. Ali, A.W., Naval Research Lab., Memo Report 3732 (1978).

20-247. Swider, W., J. Geophys. Res. 79, 3221 (1974).

20-248. Evans, W.F.J., E.J. Llewellyn, and A. Vallance Jones, Ann. Geophys. 26, 167 (1970).

20-249. Evans, W.F.J., E.J. Llewellyn, and A. Vallance Jones, J. Geophys. Res. 77, 4899 (1972).

20-250. Wood, H.C., Ph.D. Thesis, University of Saskatchewan (1972).

20-251. Trozzolo, A.M., Ed., Intl. Conf. Singlet Molecular Oxygen and Its Role in Environmental Sciences, Ann. N.Y. Acad. Sci. 171, Art. 1 (1970).

20-252. Clark, I.D., and R.P. Wayne, Proc. Roy. Soc. (London) A314, 111 (1969).

20-253. Winer, A., and K. Bayes, J. Phys. Chem. 70, 302 (1966).

20-254. Clark, I.D., and R.P. Wayne, Chem. Phys. Letts. 3, 93 (1969).

20-255. Findlay, F., C. Fortin, and D. Snelling, Chem. Phys. Letts. 3. 204 (1969).

20-256. Steer, R.P., R.A. Ackerman, and J.N. Pitts, Jr., J. Chem. Phys. 51, 843 (1969).

20-257. Clark, I.D., and R.P. Wayne, Chem. Phys. Letts. 3, 405 (1969).

20-258. McNeal, R.J., and G.R. Cook, J. Chem. Phys. 47, 5385 (1967).

20-259. Megill, L.R., and J.B. Hasted, Planet. Space Sci. 13, 339 (1965).

20-260. Kummler, R.H., and M.H. Bortner, General Electric Co., TIS Report R67SD20 (1967).

20-261. Fehsenfeld, F.C., D.L. Albritton, J.A. Burt, and H.I. Schiff, Can J. Chem. 47, 1783 (1969).

20-262. Kummler, R.H., and M.H. Bortner, in Reference 20-251; p. 237.

20-263. Noxon, J., J. Geophys. Res. 75, 1879 (1970).

20-264. Megill, L.R., A. Despain, D. Baker, and K. Baker, J. Geophys. Res. 75, 4775 (1970).

20-265. Schiff, H.I., J. Haslett, and L.R. Megill, J. Geophys. Res. 75, 4363 (1970).

20-266. Arnold, S.J., N. Finlayson, and E.A. Ogryzlo, J. Chem. Phys. 44, 2529 (1966).

20-267. Young, R.A., and G. Black, J. Chem. Phys. 42, 3740 (1965).

20-268. Derwent, R.G., and B.A. Thrush, Trans. Faraday Soc. 67, 2036 (1971).

20-269. Young, R.A., G. Black, and T.G. Slanger, J. Chem. Phys. 49, 4758 (1968).

20-270. Noxon, J., J. Chem. Phys. 52, 1852 (1970).

20-271. Wallace, L., and J.W. Chamberlain, Planet. Space Sci. 2, 60 (1959).

20-272. Seaton, M.J., J. Atm. Terrestr. Phys. 4, 295 (1953).

20-273. Vallance Jones, A., and R.L. Gattinger, J. Geophys. Res. 79, 4821 (1974).

20-274. Becker, J.H., W. Groth, and U. Schurath, Chem. Phys. Letts. 8, 259 (1971).

20-275. Wallace, L., and D.M. Hunten, J. Geophys. Res. 73, 4813 (1968).

20-276. Chamberlain, J.W., Astrophys. J. 121, 277 (1955).

20-277. Degen, V., J. Geophys. Res. 77, 6213 (1972).

20-278. Young, R.A., and G. Black, J. Chem. Phys. 44, 3741 (1966).

20-279. Trajmar, S., W. Williams, and A. Kuppermann, J. Chem. Phys. 56, 3759 (1972).

20-280. Watanabe, K., Adv. Geophys. 5, 153 (1958).

20-281. Mehr, F.J., and M.A. Biondi, Phys. Rev. 181, 264 (1969), and references cited therein.

20-282. Zipf, E.C., Jr., Bull. Am. Phys. Soc. 12, 225 (1967).

20-283. Zipf, E.C., Jr., Bull. Am. Phys. Soc. 15, 418 (1970).

20-284. Thomas, L.D., and R.K. Nisbet, Phys. Rev. A11, 170 (1975).

20-285. Carleton, N.P., F.J. LeBlanc, and O. Oldenberg, Bull. Am Phys. Soc. 11, 503 (1966).

20-286. McGrath, W.D., and J.J. McGarvey, Planet. Space Sci. 15, 427 (1967).

20-287. Garvin, D., Chemical Kinetics Data Survey IV, Natl. Bur. Stds., NBSIR-73-203 (1973).

20-288. Hunt, B.G., J. Geophys. Res. 71, 1385 (1966).

20-289. Hampson, J., Canadian Armament Research and Development Establishment T.N. 1627/64 (1964).

20-290. Paraskevopoulos, G.M., and R.J. Cvetanovic, Chem. Phys. Letts. 9, 603 (1971).

20-291. Garvin, D., and R. Hampson, Proc. Second Conf. Climatic Impact Assessment Program, A. Broderick, Ed., Dept. of Transportation Report DOT-TSC-OST, 73-4 (1973).

20-292. Crutzen, P.J., J. Geophys. Res. 76, 7311 (1971).

20-293. Hesstvedt, E., Geophys. Norveg. 27, 1 (1967).

20-294. Anderson, J., Ph.D. Dissertation, University of Colorado (1970).

20-295. Nicolet, M., in Reference 20-291.

20-296. Kummler, R.H., M.H. Bortner, and T. Baurer, Envir. Sci. Tech. 3, 248 (1969).

20-297. Kummler, R.H., and T. Baurer, J. Geophys. Res. 78, 5306 (1973).

20-298. Chemeides, W., and J.C.G. Walker, J. Geophys. Res. 78, 8751 (1973).

20-299. Schofield, K., J. Photochem. 9, 55 (1978).

20-300. Chapman, S., Proc. Roy. Soc. (London) A132, 353 (1931).

20-301. Barth, C.A., and A.F. Hildenbrandt, J. Geophys. Res. 66, 985 (1961).

20-302. Donahue, T.M., B. Guenther, and R.J. Thomas, J. Geophys. Res. 78, 6662 (1973).

20-303. Slanger, T.G., and G. Black, Planet. Space Sci. 25, 79 (1977).

20-304. Witt, C., J. Stegman, B.H. Solheim, and E.J. Llewellyn, Planet. Space Sci. 27, 341 (1979).

20-305. Felder, W., and R.A. Young, J. Chem. Phys. 56, 6028 (1972).

20-306. Schaeffer, R.C., P.D. Feldman, and E.C. Zipf, J. Geophys. Res. 77, 6828 (1972).

20-307. Hays, P.B., and W.E. Sharp, J. Geophys. Res. 78, 1153 (1973).

20-308. Lawrence, G.M., and M.J. McEwan, J. Geophys. Res. 78, 8314 (1973).

20-309. Evans, W.F.J., and A. Vallance Jones, Can. J. Phys. 43, 697 (1965).

20-310. Slanger, T.G., B.J. Wood, and G. Black, Chem. Phys. Letts. 17, 401 (1972).

20-311. Atkinson, R., and K.H. Welge, J. Chem. Phys. 57, 3689 (1972).

20-312. Stuhl, F., and K.H. Welge, Can J. Chem. 47, 1870 (1969).

20-313. Dalgarno, A., R.J.W. Henry, and A.L. Stewart, Planet. Space Sci. 12, 235 (1964).

20-314. Stebbings, R.F., in Advances in Atomic and Molecular Physics, Vol. 4, D.R. Bates and I. Estermann, Eds., Academic Press, New York (1968); p. 299.

20-315. Czyzak, S.J., et al., Mon. Not. Roy. Astron. Soc. 148, 361 (1970).

20-316. Ali, A.W., Appl. Optics 12, 2243 (1973).

20-317. Walker, J.C.G., et al., J. Geophys. Res. 80, 1026 (1975).

20-318. Vegard, L., Nature 144, 1089 (1939).

20-319. Eather, R.H., Revs. Geophys. 5, 207 (1967).

20-320. McNeal, R.J., and J.H. Birely, Revs. Geophys. Space Phys. 11, 633 (1973).

20-321. Birely, J.H., and P.A. Johnson, Geophys. Res. Letts. 1, 113 (1974).

20-322. Birely, J.H., Phys. Rev. A10, 550 (1974).

20-323. McNeal, R.J., and D.C. Clark, J. Geophys. Res. 74, 5065 (1969).

20-324. Hoffman, J.M., G.J. Lockwood, and G.H. Miller, Phys. Rev. A11, 841 (1975).

20-325. DeHeer, F.J., and J.F.M. Aarts, Physica 48, 620 (1970).

20-326. Dahlberg, D.A., D.K. Anderson, and I.E. Dayton, Phys. Rev. 164, 20 (1967).

20-327. Dufay, M., J. Desesquelles, M. Druetta, and M. Eidelsberg, Ann. Geophys. 22, 614 (1966).

20-328. Robinson, J.M., and H.B. Gilbody, Proc. Phys. Soc. 92, 589 (1967).

20-329. Moore, J.H., J. Geophys. Res. 77, 5567 (1972).

20-330. Park, J.T., F.D. Schowengerdt, and D.R. Schoonover, Phys. Rev. A3, 679 (1971).

20-331. Hughes, R.H., and D.K.W. Ng, Phys. Rev. 136, A1222 (1964).

20-332. Edgar, B.C., H.S. Porter, and A.E.S. Green, Planet. Space Sci. 23, 787 (1975).

20-333. Hunten, D.M., Space Sci. Rev. 6, 493 (1967).

20-334. Narcisi, R.S., Ann. Geophys. 22, 224 (1966).

20-335. Narcisi, R.S., and A.D. Bailey, J. Geophys. Res. 70, 3687 (1965).

20-336. Narcisi, R.S., C.R. Philbrick, M.A. MacLeod, and N.W. Rosenberg, EOS, Trans. Am. Geophys. Union 53, 462 (1972).

20-337. Narcisi, R.S., in Physics and Chemistry of Upper Atmospheres, B.M. McCormac, Ed., Reidel Publishing Co., Boston (1973); p. 171.

20-338. Kvifte, G., in Reference 20-337; p. 158.

20-339. Fogel, M.Ya., Sov. Phys.-Usp. 3, 390 (1960).

20-340. Layton, J.K., J. Chem. Phys. 47, 1869 (1967).

20-341. Moiseiwitsch, B., and S. Smith, Revs. Mod. Phys. 40, 238 (1968).

20-342. McGowan, J.W., J.F. Williams, and E.K. Corley, Phys. Rev. A180, 132 (1969).

20-343. Fite, W.L., R.F. Stebbings, and R.T. Brackmann, Phys. Rev. 116, 356 (1959).

20-344. Lichten, W., and S. Schulz, Phys. Rev. 116, 1132 (1959).

20-345. Lichten, W., Phys. Rev. Letts. 6, 12 (1961).

20-346. Hils, D., H. Kleinpoppen, and H. Koschmieder, Proc. Phys. Soc. 89, 35 (1966).

20-347. Zapesochnyi, I.P., and L.L. Shimon, Optics & Spectrosc. 19, 268 (1965).

20-348. Holt, H.K., and R. Krotkov, Phys. Rev. 144, 82 (1966).

20-349. Ingraham, J.C., and S.C. Brown, Phys. Rev. 138, A1015 (1965).

20-350. Phelps, A.V., Phys. Rev. 99, 1307 (1955).

20-351. Chaney, E.L., and L.G. Christophorou, J. Chem. Phys. 51, 883 (1969).

20-352. Garvin, D., and R. Hampson, Natl. Bur. Stds., Report NBSIR 74-430 (1974).

20-353. Basco, N., and R.R.W. Norrish, Disc. Faraday Soc. 33, 99 (1962).

20-354. March, R., S. Furnival, and H.I. Schiff, Photochem. Photobiol. 4, 971 (1965).

20-355. Anlauf, K., D. Maylotte, J. Polanyi, and R. Bernstein, J. Chem. Phys. 51, 5716 (1969).

20-356. Polanyi, J., and D. Tardy, J. Chem. Phys. 51, 5717 (1969).

20-357. Polanyi, J.C., Appl. Optics 10, 1717 (1971), and many other articles on specific reactions in the same issue.

20-358. McFarland, M., et al., J. Chem. Phys. 59, 6620 (1973).

20-359. King, A.B., and C. Gatz, J. Chem. Phys. 37, 1566 (1962).

20-360. Kenty, C., J. Chem. Phys. 37, 1567 (1962).

20-361. Broida, H.P., J. Chem. Phys. 36, 444 (1962).

20-362. Cher, M., and C.S. Hollingsworth, Can. J. Chem. 47, 1937 (1969).

20-363. Fehsenfeld, F.C., A.L. Schmeltekopf, D.B. Dunkin, and E.E. Ferguson, ESSA Technical Report ERL 135-AL3 (1969).

20-364. Pradel, P., et al., Phys. Rev. A10, 797 (1974).

20-365. Bauer, E., and M. Salkoff, J. Chem. Phys. 33, 1202 (1960).

20-366. Setser, D.W., and B.A. Thrush, Proc. Roy. Soc. (London) A288, 275 (1965).

20-367. Carabetta, R.A., and W.E. Kaskan, Eleventh Symp. (Intl.) on Combustion, The Combustion Institute, Pittsburgh (1967); p. 321.

20-368. Bates, D.R., Earth is a Planet, University of Chicago Press, Chicago (1960); p. 576.

20-369. Belles, F.E., and M.R. Lauver, J. Chem. Phys. 40, 415 (1964).

20-370. Ali, A.W., and W.W. Jones, Naval Research Lab., Memo Report 3015 (1975).

The following additional references contain new and more current information on some of the excitation processes discussed in this chapter.

20-371. Zipf, E.C., P.J. Epsy and C.F. Boyle, "The Excitation and Collisional Deactivation of Metastable N(^{2}P) Atoms in Auroras," J. Geophys. Res. 85, 687 (1980).

20-372. Wakiya, K., "Differential and Integral Cross-sections for the Electron Impact Excitation of O_2. I - Optically Allowed Transitions from the Ground State," J. Phys. B: Atom. Mole. Physics 11, 3913 (1978).

20-373. Wakiya, K., "Differential and Integral Cross-sections for the Electron Impact Excitation of O_2. II - Optically Forbidden Transitions from the Ground State," J. Phys. B: Atom. Mole. Phys. 11, 3931 (1978).

20-374. Linder, F., and H. Schmidt, "Experimental Study of Low Energy e-O_2 Collision Processes," Z. Naturforsch 26a, 1617 (1971).

DISTRIBUTION LIST

DEPARTMENT OF DEFENSE

Assist to the Sec of Def, Atomic Energy
ATTN: Exec Assist

Defense Intell Agency
ATTN: RTS-2B

Defense Nuclear Agency
ATTN: RAAE
ATTN: RAAE, K. Schwartz
ATTN: RAAE, P. Crowley
4 cys ATTN: STTI-CA

Defense Tech Info Ctr
12 cys ATTN: DD

Field Command, DNA, Det 2
Lawrence Livermore National Lab
ATTN: FC-1

Field Command, Defense Nuclear Agency
ATTN: FCPR
ATTN: FCTT, W. Summa
ATTN: FCTXE

Interservice Nuc Wpns School
ATTN: TTV

Joint Strat Tgt Planning Staff
ATTN: JPPFD

Under Secy of Def for Rsch & Engrg
ATTN: Strat & Space Sys (OS)

DEPARTMENT OF THE ARMY

Atmospheric Sci Lab, US Army Elect R&D Command
ATTN: DELAS-EO, F. Niles
ATTN: DELAS-EO-ME, K. Ballard
ATTN: DELAS-EO-MO, M. Heaps
ATTN: DELAS-EO-MO, R. Olsen

BMD Advanced Technology Ctr
ATTN: ATC-O, W. Davies
ATTN: BMDATC-D, M. Capps

Harry Diamond Laboratories
ATTN: DELHD-NW-P
ATTN: DELHD-TA-L

US Army Ballistic Rsch Lab
ATTN: DRDAR-BLB, J. Batteh
ATTN: DRDAR-BLB, M. Kregel

US Army Foreign Science & Tech Ctr
ATTN: DRXST-SD-3

US Army Nuc & Chem Agcy
ATTN: Library

US Army Rsch Office
ATTN: R. Mace

US Army TRADOC Sys Analysis Actvy
ATTN: ATAA-PL

DEPARTMENT OF THE ARMY (Continued)

US Army White Sands Missile Range
ATTN: STEWS-TE-AN, A. De La Paz
ATTN: STEWS-TE-AN, J. Meason
ATTN: STEWS-TE-AN, R. Hays

USA Missile Command
ATTN: DRSMI-RPR
ATTN: Redstone Scientific Info Ctr

DEPARTMENT OF THE NAVY

Naval Intelligence Support Ctr
ATTN: Doc Control

Naval Ocean Systems Ctr
ATTN: Code 4471, Tech Lib
ATTN: Code 532, R. Pappert
ATTN: Code 532i, I. Rothmuller

Naval Postgraduate School
ATTN: Code 1424, Library
ATTN: Code 61 MN, E. Milne

Naval Research Laboratory
ATTN: Code 1434, E. Brancato
ATTN: Code 2000, J. Brown
ATTN: Code 2627, Tech Lib
ATTN: Code 4700, W. Ali
ATTN: Code 4720, J. Davis
ATTN: Code 4780, D. Strobel
ATTN: Code 6700, T. Coffey
ATTN: Code 7127, C. Johnson
ATTN: Code 7557, J. Davis

Naval Surface Wpns Ctr
ATTN: Code F31
ATTN: Code F46, D. Hudson
ATTN: Code R41, D. Land
ATTN: Code X211, Tech Lib

Nuclear Wpns Tng Gp, Pacific
ATTN: Nuc Warfare Dept

Office of Naval Rsch
ATTN: Code 412, B. Junker

Space & Naval Warfare Systems Cmd
ATTN: ELEX 09I

DEPARTMENT OF THE AIR FORCE

Air Force Technical Applications Ctr
ATTN: STINFO Ofc/TF

Air Force Wpns Lab
ATTN: SUL

Air University Library
ATTN: AUL-LSE

Ballistic Missile Ofc/DAA
ATTN: ENSN

DEPARTMENT OF THE AIR FORCE (Continued)

Air Force Geophysics Laboratory
ATTN: CA, A. Stair
ATTN: LKB, E. Murad
ATTN: LKB, T. Keneshea
ATTN: LKB, W. Swider, Jr.
ATTN: LKD, C. Philbrick
ATTN: LKO, R. Huffman
ATTN: LKO, R. Van Tassel
ATTN: LS, R. Murphy
ATTN: LSI, W. Blumberg
ATTN: LSP, J. Paulson
ATTN: LYD, K. Champion
ATTN: OP, J. Garing
ATTN: OPR, F. Del Greco
ATTN: OPR, H. Gardiner
ATTN: OPR, R. O'Neill
ATTN: PHG, F. Innes
ATTN: SULL

Foreign Technology Div
ATTN: NIIS, Library
ATTN: WE

Rome Air Development Ctr
ATTN: OCD, J. Simons
ATTN: OCS, V. Coyne

Space Division
ATTN: YGJ

Strategic Air Command
ATTN: INAO

USAFETAC
ATTN: CBTL

DEPARTMENT OF ENERGY

Dept of Energy
Office of Military Appl, GTN
ATTN: OMA, F. Hughes

Dept of Energy
Combustion Division
ATTN: PETC, F. Spencer

OTHER GOVERNMENT AGENCIES

Albany Metallurgy Rsch Ctr
ATTN: E. Abshire

Pittsburgh Mining & Safety Rsch Ctr
ATTN: J. Murphy

Central Intell Agcy
ATTN: OSWR/NED

National Bureau of Standards
ATTN: A. Phelps
ATTN: G. Dunn
ATTN: G. Reid
ATTN: P. Bender
ATTN: S. Leone
ATTN: S. Smith

National Oceanic & Atmospheric Admin
ATTN: Assist Administrator, RD
ATTN: J. Townsend, Jr.

OTHER GOVERNMENT AGENCIES (Continued)

National Bureau of Standards
Attention Sec Ofc for
ATTN: J. Cooper
ATTN: L. Gevantman
ATTN: M. Krauss
ATTN: R. Hampson, Jr.
ATTN: R. Levine
ATTN: S. Abramowitz

National Oceanic & Atmospheric Admin
ATTN: Reference Div

National Oceanic & Atmospheric Admin
ATTN: D. Albritton
ATTN: E. Ferguson
ATTN: F. Fehsenfeld
ATTN: W. Spjeldvik

Transportation Rsch Sys Ctr
ATTN: F. Marmo

Federal Aviation Admin
ATTN: A. Broderick
ATTN: J. Rogers
ATTN: W. Smith

NASA, Goddard Space Flight Ctr
ATTN: A. Aikin
ATTN: Code 620, H. Taylor
ATTN: Code 625, J. Heppner
ATTN: Code 625, M. Sugiura
ATTN: J. Vette
ATTN: Tech Library

NASA, George C. Marshall Space Flight Ctr
ATTN: W. Roberts

NASA, Johnson Space Ctr
ATTN: Code JM6, Tech Lib

NASA, Ames Research Ctr
ATTN: W. Starr
3 cys ATTN: N-245-3, R. Whitten

NASA Headquarters
ATTN: E. Schmerling
ATTN: R. Schiffer

National Science Foundation
ATTN: A. Grobecker
ATTN: Div of Atmos Sci, R. McNeal

FOREIGN AGENCIES

University of Birmingham
ATTN: Space Physics Dept

Max-Planck Institute for Aeronomomic
3 cys ATTN: K. Schlegel

Meteorological Ofc
ATTN: J. Harris

S.D. MacKnight
ATTN: S. MacKnight

UK Atomic Wpns Rsch Establishment
5 cys ATTN: P. Flynn

FOREIGN AGENCIES (Continued)

UAR Gp, Aerospace Div
ATTN: K. Lloyd

University College, Wales
ATTN: N. Twiddy

University of Liverpool
ATTN: J. Moruzzi
2 cys ATTN: J. Craggs

York University
ATTN: A. Cunningham
ATTN: M. Bloom
2 cys ATTN: H. Schiff

OTHER

Government Publications Library
ATTN: J. Winkler

Harvard University
ATTN: Library

DEPARTMENT OF ENERGY CONTRACTORS

EG&G, Inc
ATTN: P. Lucero

University of California
Lawrence Livermore National Lab
ATTN: L-325, G. Haugan

Los Alamos National Laboratory
ATTN: MS B245, O. Judd
ATTN: MS 212, W. Barfield
ATTN: MS 560, W. Hughes
ATTN: MS 664, J. Zinn
ATTN: MS 668, H. Hoerlin
ATTN: MS670, J. Malik

Sandia National Laboratories
ATTN: Org 1250, W. Brown
ATTN: Org 4231, T. Wright

DEPARTMENT OF DEFENSE CONTRACTORS

Aero-Chem Rsch Labs, Inc
ATTN: A. Fontijn
ATTN: H. Calcote

Aerodyne Rsch, Inc
ATTN: C. Kolb
ATTN: F. Bien
ATTN: Librarian, B. Duston
ATTN: M. Camac
ATTN: M. Faist

Aerospace Corp
ATTN: H. Mayer
ATTN: H. Wang
ATTN: J. Reinheimer
ATTN: J. Straus
ATTN: Library
ATTN: M. Whitson
ATTN: N. Cohen
ATTN: R. Cohen

AVCO Everett Rsch Lab, Inc
ATTN: C. Von Rosenberg, Jr.

DEPARTMENT OF DEFENSE CONTRACTORS (Continued)

Bell Telephone Labs, Inc
ATTN: L. Lanzerotti

Berkeley Rsch Associates, Inc
ATTN: C. Prettie
ATTN: J. Workman

R.E. Beverly III
ATTN: R. Beverly III

The Trustees of Boston College
ATTN: Dept of Chemistry, D. McFadden
ATTN: Science Library, F. McElroy

University of California at San Diego
ATTN: D. Miller

University of California at Santa Barbara
ATTN: M. Steinberg

California Institute of Technology
ATTN: V. Anicich

Ca'-pan Corp
ATTN: C. Treanor
ATTN: Library
ATTN: W. Wurster

Chem Data Rsch
ATTN: K. Schofield

University of Colorado
ATTN: V. Bierbaum

University of Denver
ATTN: Sec Officer for D. Murcray
ATTN: Security Officer for B. Van Zyl

EOS Technologies, Inc
ATTN: B. Gabbard
ATTN: W. Lelevier

Epsilon Labs, Inc
ATTN: C. Accardo

ESL, Inc
ATTN: W. Bell

General Dynamics Corp
ATTN: Convair Rsch Library

General Electric Co
ATTN: J. Peden
ATTN: P. Zavitsanos
ATTN: Tech Info Ctr for L. Chasen

General Electric Co
ATTN: J. Schroeder

General Rsch Corp
ATTN: R. Rein

General Rsch Corp
ATTN: T. Zakrzewski

HSS, Inc
ATTN: D. Hansen
ATTN: M. Shuler

DEPARTMENT OF DEFENSE CONTRACTORS (Continued)

University of Illinois
ATTN: C. Sechrist
ATTN: S. Bowhill

Information Science, Inc
ATTN: W. Dudziak

Institute for Defense Analyses
ATTN: E. Bauer
ATTN: H. Wolfhard

IRT Corp
ATTN: D. Vroom
ATTN: J. Rutherford
ATTN: R. Neynaber
ATTN: R. Overmyer

JAYCOR
ATTN: D. Higgins

JAYCOR
ATTN: H. Levine

Johns Hopkins University
ATTN: J. Kaufman

Kaman Sciences Corp
ATTN: W. Rich

Kaman Sciences Corp
ATTN: E. Conrad

Kaman Tempo
ATTN: B. Gambill
ATTN: DASIAC
2 cys ATTN: T. Baurer
2 cys ATTN: M. Bortner

Kaman Tempo
ATTN: DASIAC

KMS Fusion, Inc
ATTN: Library

Lockheed Missiles & Space Co, Inc
ATTN: B. McCormac
ATTN: J. Evans
ATTN: J. Kumer
ATTN: J. Reagan
ATTN: M. Walt
ATTN: R. Sears
ATTN: T. James

University of Lowell
ATTN: G. Best

University of Maryland
ATTN: Chemistry Dept, J. Vanderslice

University of Massachusetts
ATTN: H. Sakai

University of Minnesota
ATTN: M. Hirsch

National Academy of Sciences
ATTN: E. Dyer
ATTN: J. Sievers
ATTN: National Materials Advisory Bd

DEPARTMENT OF DEFENSE CONTRACTORS (Continued)

Mission Rsch Corp
ATTN: C. Longmire
ATTN: D. Archer
ATTN: F. Guigliano
ATTN: M. Messier
ATTN: M. Scheibe
ATTN: N. Carron
ATTN: P. Fischer
ATTN: R. Armstrong
ATTN: R. Bogusch
ATTN: R. Christian
ATTN: R. Hendrick
ATTN: R. Kilb
ATTN: R. Stoeckly
ATTN: Tech Lib
ATTN: W. White

Mitre Corp
ATTN: J. Freedman

Mitre Corp
ATTN: A. Schneider

New Technology, Inc
ATTN: D. Divis

State University of New York at Buffalo
ATTN: G. Brink

Nichols Rsch Corp, Inc
ATTN: R. Tippets

Pacific-Sierra Research Corp
ATTN: E. Field, Jr.
ATTN: H. Brode, Chairman SAGE

Panametrics, Inc
ATTN: B. Sellers

Pennsylvania State University
ATTN: J. Nisbet
ATTN: L. Hale

Photometrics, Inc
ATTN: I. Kofsky

Physical Science Lab
ATTN: W. Berning

Physical Sciences, Inc
ATTN: G. Caledonia
ATTN: K. Wray
ATTN: R. Taylor

University of the Commonwealth Pittsburgh
ATTN: F. Kaufman
ATTN: M. Biondi
ATTN: W. Fite

R&D Associates
ATTN: F. Gilmore
ATTN: H. Ory
ATTN: R. Lindgren
ATTN: R. Turco

R&D Associates
ATTN: B. Yoon
ATTN: J. Rosengren
ATTN: R. Davidson

DEPARTMENT OF DEFENSE CONTRACTORS (Continued)

Radiation Rsch Associates, Inc
ATTN: N. Schaeffer

Rand Corp
ATTN: C. Crain
ATTN: P. Davis

Rand Corp
ATTN: B. Bennett

Science Applications Intl Corp
ATTN: B. Myers
ATTN: D. Hamlin

Science Applications Intl Corp
ATTN: R. Johnston

SRI International
ATTN: A. Peterson
ATTN: D. Eckstrom
ATTN: D. Hildenbrand
ATTN: D. Huestis
ATTN: E. Kindermann
ATTN: F. Smith
ATTN: G. Black
ATTN: J. Moseley
ATTN: J. Peterson
ATTN: R. Hake, Jr.
ATTN: R. Leadabrand
ATTN: R. Vidmar
ATTN: T. Slanger
ATTN: V. Wickwar
ATTN: W. Chesnut

Technology International Corp
ATTN: W. Boquist

DEPARTMENT OF DEFENSE CONTRACTORS (Continued)

University of Texas System
ATTN: J. Browne

TRW Electronics & Defense Sector
ATTN: J. Frichtenicht
ATTN: N. Utterback
ATTN: R. Watson
ATTN: Tech Info Ctr

Utah State University
ATTN: D. Baker
ATTN: K. Baker, Dir Atmos & Space Sci
ATTN: Security Officer

VisiDyne, Inc
ATTN: J. Carpenter

Wayne State University
ATTN: P. Rol
ATTN: R. Kummler

Western Rsch Corp
ATTN: R. Hunter

Westinghouse Electric Corp
ATTN: P. Chantry

William Marsh Rice University
ATTN: R. Stebbings

William Marsh Rice University
ATTN: J. Chamberlain

Kaman Sciences Corp
ATTN: T. Stephens